NONLINEAR FREQUENCY CONVERSION PROCESSES IN ONE-DIMENSIONAL PHOTONIC BAND-GAP STRUCTURES

SURAWUT WICHARN

A THESIS SUBMITTED IN FULFILLMENT

OF THE REQUIREMENT FOR THE DEGREE OF

DOCTOR OF PHILOSOPHY IN APPLIED PHYSICS

FACULTY OF SCIENCE

KING MONGKUT'S INSTITUTE OF TECHNOLOGY LADKRABANG

2014

KMITL-2014-SC-D-030-001

หัวข้อวิทยานิพนธ์ กระบวนการเปลี่ยนความถี่แบบไม่เป็นเชิงเส้นในโครงสร้างแถบช่องว่างทางแสงชนิดหนึ่งมิติ
นักศึกษา นายสุรวุฒิ วิจารณ์
รหัสประจำตัว 53650102
ปริญญา ปรัชญาดุษฎีบัณฑิต
สาขาวิชา ฟิสิกส์ประยุกต์
พ.ศ. 2557
อาจารย์ที่ปรึกษา ดร.ประธาน บุรณศิริ

บทคัดย่อ

วิทยานิพนธ์ฉบับนี้นำเสนอการจำลองแบบกระบวนการแปลงความถี่ไม่เป็นเชิงเส้น ได้แก่ การขยายเชิงแสงแบบพาราเมตริก และการสร้างความถี่ฮาร์มอนิกอันดับที่สาม ภายในโครงสร้างแถบช่องว่างทางแสงชนิดหนึ่งมิติ ในขั้นแรกชุดของสมการคัปเปิลโหมดซึ่งประกอบด้วยสัมประสิทธิ์ไม่เป็นเชิงเส้นอันดับสูงและสอดคล้องกับกระบวนการแปลงความถี่ทั้งสองชนิดถูกสร้างขึ้นมาด้วยระเบียบวิธีวิเคราะห์แบบหลายสเกล โดยความยาวคลื่นของพัลส์ขาเข้าที่ใช้ในการกระตุ้นให้เกิดปรากฏการณ์การแปลงความถี่จะถูกเลือกให้ตรงกับตำแหน่งขอบแถบช่องว่างทางแสงทางด้านความถี่ต่ำเพื่อทำให้เกิดปรากฏการณ์ดังกล่าวได้ดีขึ้น ในการสังเกตการเกิดปรากฏการณ์การแปลงความถี่ภายในโครงสร้างแถบช่องว่างทางแสงนั้นได้เลือกใช้ระเบียบวิธีสปลิท-สเต็ป ฟูเรียร์ เพื่อจำลองแบบการสร้างพัลส์ขาออกที่ถูกแปลงความถี่ภายในกระบวนการนี้ ผลการจำลองแบบถูกแบ่งออกเป็นสองส่วนด้วยกัน โดยในส่วนแรกเป็นผลการจำลองแบบสำหรับกระบวนการขยายเชิงแสงแบบพาราเมตริก ผลการจำลองแบบแสดงให้เห็นว่าความเข้มพัลส์ขาออกของพัลส์สัญญาณและพัลส์ไอเดลอร์นั้นมีค่าเพิ่มขึ้นในลักษณะฟังก์ชันเอ็กซ์โพเนนเชียลตามจำนวนชั้นของสารไดอิเล็กตริกที่ประกอบขึ้นเป็นโครงสร้างแถบช่องว่างทางแสง ในขณะเดียวกันการปรับความถี่ของคลื่นกระตุ้นมีผลกระทบโดยตรงกับความเข้มของทั้งพัลส์สัญญาณและไอเดลอร์ เนื่องจากการเพิ่มปรากฏการณ์ไม่เป็นเชิงเส้นด้วยตำแหน่งขอบแถบช่องว่างทางแสงนั้นจะบรรลุผลต่อเมื่อกำหนดค่าพารามิเตอร์การปรับความถี่ที่เหมาะสมเพียงค่าเดียวเท่านั้น นอกจากนี้ทั้งอัตราการขยายเชิงแสงของคลื่นสัญญาณและประสิทธิภาพการแปลงความถี่ของคลื่นไอเดลอร์ยังมีค่าขึ้นกับสเปกตรัมแบนด์วิธของพัลส์กระตุ้น โดยสเปกตรัมแบนด์วิธดังกล่าวต้องมีค่าน้อยกว่าแบนด์วิธของพีกของขอบโครงสร้างแถบช่องว่างทางแสงเพื่อสามารถกระตุ้นให้เกิดกระบวนการแปลงความถี่ที่มีประสิทธิภาพสูงสุด และอีกทั้งประสิทธิภาพการแปลงความถี่ยังขึ้นอยู่กับความเข้มของพัลส์กระตุ้นและสัญญาณขาเข้าอีกด้วย ส่วนที่สองเป็นผลการจำลองแบบของการสร้างความถี่ฮาร์มอนิกอันดับที่สาม ในส่วนนี้ความเข้มขาออกของพัลส์

ความถี่ฮาร์มอนิกอันดับที่สามในทิศไปด้านหน้าและย้อนกลับ รวมทั้งประสิทธิภาพการแปลงความถี่ถูกคำนวณด้วยระเบียบวิธีเชิงตัวเลข ผลลัพธ์แสดงให้เห็นว่าการเพิ่มความยาวของโครงสร้างและค่าพารามิเตอร์การปรับความถี่ที่เหมาะสมสามารถช่วยสร้างพัลส์ความถี่ฮาร์มอนิกอันดับที่สามได้อย่างมีประสิทธิภาพ นอกจากนี้พลังงานความถี่ฮาร์มอกนิกอันดับที่สามรวมที่ได้จากโครงสร้างแถบช่องว่างทางแสงซึ่งมีค่าขึ้นกับแบนด์วิธของพัลส์กระตุ้นยังมีค่ามากกว่าพลังงานขาออกจากโครงผลึกไม่เป็นเชิงเส้น ประสิทธิภาพการแปลงความถี่ที่ดีนั้นเกิดขึ้นเมื่อแบนด์วิธของพัลส์กระตุ้นแคบกว่าพีกการส่งผ่านของตำแหน่งขอบแถบช่องว่างทางแสง อีกทั้งค่าประสิทธิภาพสูงสุดของพัลส์ความถี่ฮาร์มอนิกอันดับที่สามในทิศไปด้านหน้ายังพบว่ามีค่ามากกว่าของพัลส์ความถี่เดียวกันในทิศย้อนกลับ

คำสำคัญ : การขยายสัญญาณเชิงแสง, การสร้างแสงความถี่ฮาร์มอนิกอันดับที่สาม, โครงสร้างแถบช่องว่างทางแสง, การวิเคราะห์แบบหลายสเกล, ระเบียบวิธีสปลิท-สเต็ป ฟูเรียห์

Thesis Title	Nonlinear frequency conversion processes in one-dimensional photonic band-gap structures
Student	Sarawut Wicharn
Student ID	53650102
Degree	Doctor of Philosophy
Program	Applied Physics
Year	2014
Thesis Advisor	Dr. Prathan Buranasiri

ABSTRACT

In this thesis, the nonlinear frequency conversion processes such as, optical parametric amplification and third-harmonic generation, in one-dimensional photonic band-gap structure has been computationally investigated. First, the multiple-scale method have been introduced to derive a new set of coupled-mode equations for finite structure including higher-order nonlinear terms. The wavelength of pump fields for both processes have been determined to be wavelength at the low frequency band-edge of the transmission spectrum, which is illustrated by using transfer matrix method, for achieving the band-edge enhancement. These frequency conversion processes have been modeled by using the split-step Fourier method. The modeling results have been divided into two parts. The first part is the numerical results of optical parametric amplification. These results have shown that the output intensities of signal and idler have exponential growth respect to the layer number of photonic band-gap structure. Meanwhile, the detuning parameter for pump field directly affects the intensities of both pulses due to a band-edge enhancement that might be achieved from only an optimal value of this parameter. Moreover, both of amplification gain and conversion efficiency of idler pulse have been also depended on pump pulse bandwidth. The pulse, whose frequency bandwidth much less than the relevant band-edge peak, enables highest amplification and conversion efficiency in this medium. Finally, the conversion efficiencies can be also enhanced by increasing the input pump and signal intensities. The second part is the numerical results of third-harmonic generation. In this part, the output intensities of third-harmonic pulses in forward- and backward-directions, and also the conversion efficiencies have been numerically calculated. The results show that the structure length increasing and optimal detuning parameter can generate the efficient third-harmonic pulses. Furthermore, the total energy outputs,

depending on the fundamental-frequency pulse width, may be more than the energy produced by a phase-matched nonlinear crystals. The narrow pulse, whose bandwidth less than band-edge transmission peak, enables high conversion efficiency. The maximum efficiency of the forward component is possibly greater than the efficiency of the backward component.

Keywords : optical parametric amplification, third-harmonic generation, photonic band-gap structure, multiple-scale method, split-step Fourier method

Acknowledgement

The journey to the completion of the Degree of Doctor of Philosophy of Science in Applied Physics is not exclusively my individual effort, but done with many supports and helps from many people. First, I would like to thank Dr. Prathan Buranasiri, who is my advisor for his valuable suggestions and corrections. He is always available when I am requiring his advice. I thank him for introducing me to the research fields of photonic crystals and computational physics, and also guiding me to complete my thesis research. Also, I would like to thank my committee members, Assoc. Prof. Dr. Warawoot Thowladda, Dr. Chesta Rattanaphan, Asst. Prof. Dr. Nopparat Pochai, and Asst. Prof. Dr. Ratchapak Chitaree, for the discussions to improve and refine this thesis. I would like to thank my colleagues at Photon Dynamics Laboratory at Department of Physics, KMITL, namely Dr. Prathan Buranasiri, Mr. Suwan Plaipichit, Mr. Ritthirong Nuan-Sri, Ms. Chantira Boonsri, and all graduate and undergraduate students who have ever worked in this laboratory for their supporting. I would like to thank Prof. Joseph W. Haus, who is the inspiration to work in photonic band-gap structure research field. I have been learned about the properties of photonic band-gap structure and continued my research thesis until finish it by reviewing and understanding his researches. He is very kindness in teaching and suggesting many knowledge about photonic band-gap structures. I would like to truly thank the Science Achievement Scholarship of Thailand (SAST) for the financially supporting me for my Ph.D. studying. I think that I would not be here, get the great opportunity, and finish my Ph.D. degree without them.

Finally, I would like to especially thank my family, i.e. Mr. Niyom Wicharn, Mrs. Suchiporn Wicharn, and Ms. Saowapak Wicharn, and my relatives, who have always supported me in every ways from the first day of this voyage. I would like to thank Ms. Kannaphat Pakdeewiwat, who is always keep her fingers crossed for me so far. I would like to thank my friends for supporting me since first time we met. Finally, I would like to thank and pay the respect to all my teachers, who have ever taught me in my life. For those whose names are not mentioned here, I have not neglected you, and you all know that I will always thank you from the deep of my heart. Thanks.

Surawut Wicharn

February 18, 2014

Table of contents

List of figures

List of tables

Chapter 1

Introduction

1.1 Literature review

Photonic crystals are the periodic nanostructures that affect, control, and manipulate the motion and behavior of photons in the same way that the periodic potentials affect electrons in electronic crystal lattices by defining allowed and forbidden electronic band structure. For photonic crystals that contain regularly repeating regions of high and low refractive index. Photons (or electromagnetic waves) propagate through the structures or not depending on their wavelength. The wavelengths that are allowed to propagate through photonic crystals are called *modes*; groups of allowed modes form bands. The disallowed bands of wavelengths are called *photonic band gaps*.

Photonic crystals were firstly studied by Lord Rayleigh in 1887 [1]. In his studying, the one-dimensional photonic crystals in the form of periodic multilayer dielectric stacks (i.e. Bragg mirror) were studied extensively. He had showed that these structures have a one-dimensional photonic band gaps, a spectral range of large reflectivity, or stop-bands. A hundred years later, during in 1987, the two physicist such that Eli Yablonovitch and Sajeev John were trying to study the novel optical phenomena in higher (two- and three-) dimension periodic structures. Yablonovitch was investigating whether the spontaneous emission of excited atoms placed inside dielectric cavities could rigorously be suppressed [2]. Meanwhile, John was instead occupied with a more fundamental challenge: whether systematic observation of Anderson localization (the absence of wave transport in a disordered medium) could be achieved by using classical electromagnetic waves in non-dissipative systems [3]. They both realized that their investigations could be completed if a suitably designed three dimensional periodic dielectric structures were used, such that a full electromagnetic band gap (a frequency region where no modes, regardless of their polarization, are allowed) opens up in the photon dispersion relation.

Now focusing on the simplest systems, the one-dimensional photonic crystals (1D-PCs) or the photonic band gap (PBG) structures. These structures have been theoretically and experimentally studied in

many topics over the past few years and the effects from these structures can be extended to describe the same effects in higher-dimension structures. This kind of periodic structure are compact and could be easily fabricated in the experimental works. Almost researches on PBG structures have been already in widespread use in the form of thin-film optics with applications ranging from low and high reflection coatings on lenses and mirrors to color changing. They are also used in a diverse range of applications; from reflective coatings to enhancing the efficiency of LEDs [4], high-reflecting omni-directional mirrors [5], low-loss-waveguides [6] to highly reflective mirrors in certain laser cavities (for example, VCSEL) [7]. The mentioned application samples of PBG structures always used the high-reflectivity property of photonic band gap, which is the linear optics regime. To go further in optical community, the PBG structures have been applied to nonlinear optics regime for enhancing the nonlinear optical effects and developing the various new PBG devices.

There are many nonlinear optical applications and devices based on PBG structures. For examples, in 1994, Scalora et al have numerically studied about the pulse propagation near the band-edge of the PBG structure with a spatial gradient in the linear refractive index, together with a nonlinear medium response. They found that such a structure can result in unidirectional pulse propagation. This behavior constitutes the operational mechanism for a passive optical diode [8]. In the same year, they also numerically investigated nonlinear propagation of ultra-short pulses near the band edge. They demonstrated that this nonlinear mechanism can induce pulse reshaping and pulse generation. This phenomenon has important new applications in both optical limiting and optical switching [9]. Meanwhile, Dowling et al demonstrated that at near the band edge of a PBG structure the photon group velocity approaches zero. This effect implies an exceedingly long optical path length in the structure. If an active medium was present, the optical path length increased near the photonic band edge can lead to a better than fourfold enhancement of gain. This new effect has important applications to photonic band-edge laser [10]. Two years later, in 1996, Scalora et al, again, examined optical pulse propagation through a PBG structure at the photonic band-edge transmission resonance. They theoretically predicted and experimentally demonstrate an approximate energy, momentum, and form invariance of the transmitted pulse, as well as large group refractive index up to 13.5 and then group velocity was simultaneously slowed. From these results, the PBG structure could be applied to a true-time delay line in optical communication systems [11].

The other application of PBG structure in nonlinear optics regime is nonlinear frequency conversions, i.e. sum-frequency generation (parametric up-conversion), difference-frequency generation (parametric down-conversion), second-harmonic generation, third-harmonic generation, and parametric amplification and oscillation, have been widely studied. The PBG structure plays an important role in nonlinear frequency conversion because the phase-matching problem in nonlinear bulk medium. The examples of nonlinear frequency conversion in PBG structures are second-harmonic generation in pulse regime by Scalora et al in 1997 [19]. They presented the numerical study of second-harmonic generation and showed that their structure could generate short second-harmonic pulses whose energy and power levels may be 2-3 orders of magnitude larger than energy and power of equivalent length of a phase-matched bulk medium. In 2000, the parametric down-conversion for efficient infrared generating in the PBG structure by Centini et al [20]. They used the effective index method to obtain the phase-matched nonlinear generation of infrared radiation. And then the conversion efficiencies were predicted when assuming $\chi^{(2)}$ values of order 100 pm/V and pump intensities of order 100 MW/cm^2.

To achieve the efficient converted-frequency signal from the nonlinear medium. The phase-mismatch Δk that occurs from the sums of wave-vector of interacting waves inside the medium should be zero. But this condition is very difficult to achieve because the material dispersion problem. And consequently the conversion efficiency from bulk medium is quite low. So, this problem should be solved by many technique for improving the efficiency of nonlinear frequency conversion and the PBG structure would be a good option. The phase-matching multi-wave interactions for nonlinear frequency conversion by periodic structures was first discussed by Armstrong et al [12] and by Bloembergen and Sievers [13]. Armstrong et al [12] proposed the three types of phase-matching of efficient harmonic generation. Among them, it was proposed the type of phase-matching which is called *quasi-phase-matching*; the nonlinear susceptibility changes sign, but the linear properties of the medium are the same. Generally, the coherence length is orders of magnitude longer than the fundamental-frequency wavelength. The quasi-phase-matching theoretically preceded birefringent phase matching, but it was not experimentally feasible until recently, when periodic poling of the domains in a ferroelectric crystal was developed [14-17]. Due to the coherence length of quasi-phase-matching is usually longer than the wavelength, so the structure length should be the order of millimeter

or centimeter range. This is a disadvantage of this technique. Unless the quasi-phase-matching, the example techniques, which have been usually used to improve the nonlinear frequency conversion phenomena in the PBG structure, is the using of PBG dispersion characteristics. In 2001, Tarasishin et al have proposed the technique of matching phase and group velocities to improve the second-harmonic generation in the PBG structure [21]. The PBG dispersion characteristics have been combined the phase-matching to compute the group velocities of pump and second-harmonic pulses. By using this technique, the designed PBG structure could give the second-harmonic conversion efficiency is about 20 times greater than the efficiency from quasi-phase-matched medium. Similarly, Yan-qing Lu et al have proposed the use of a nonlinear PBG structure to generate coherent microwave radiation through the optical rectification effect, in 2002 [22]. They have used the PBG dispersion characteristics in order to solve the phase matching problem. Then, they compared the results from the PBG structure with the traditional electron-beam-induced microwaves system. They concluded that the new microwave generation source is economical, compact, and stable. According to the two examples, the nonlinear effect improving technique by using the PBG dispersion characteristics is a good option, but the PBG structures in these cases also have the structure length in order of millimeter for achieving high conversion efficiency.

Besides the both techniques, there is a technique that introduced to enhance the nonlinear optical effects in the PBG structure. The name of the technique is *band-edge enhancement*. This technique is based on the local field enhancement mechanism that is available by choosing the pump or fundamental-frequency fields to the low frequency or long wavelength band-edge of the principle band-gap. The local-field phenomenon involves resonant field enhancement and increased the photon density or equivalently the slow group velocity of the optical waves [19]. The combination of this technique with the nonlinear effects could provide great flexibility in the design of new devices for nonlinear frequency generation. In 1997, the band-edge enhancement had been proposed to enhance the pulsed second-harmonic generation in the multilayered PBG structure by Scalora et al [19]. They have tuned the pump field wavelength to the low frequency band-edge. Moreover, they have also chosen the pulse bandwidth to be smaller than the band-edge peak bandwidth for avoiding the pulse dispersion and allowing the local-field to build-up inside the PBG structure. They found that the total second-harmonic energy output for the PBG sample becomes about 500 times greater than

the total energy output for phase-matched bulk medium with equivalent structure length. In 1999, Centini et al have investigated the highly efficient parametric amplification in the PBG structure. They have combined the band-edge enhancement and phase-matching through anomalous dispersion to provide the conversion efficiencies orders of magnitude larger than quasi-phase-matching [23]. And they also suggests that the enhancement technique is valid for multilayered structures with large index contrast like the PBG structure. Next, in 2004, the band-edge enhancement has been also used to improve the nonlinear frequency conversion in the PBG structure by Haus et al [24]. They have used the local-field enhancement in the structure to design the tunable terahertz (THz) generation device based on the PBG geometry. The two driving fields have been tuned to near the band-edge position. The first one has been fixed to be at the long wavelength band-edge position and the second one has been detuned around the band-edge position to generate the THz field by using the difference frequency generation. Finally, the enhancement values of nonlinear effects in arbitrary conditions have been compared.

1.2 Motivation

Recently, the researches on conversion efficiency improving of nonlinear frequency conversions in the low-index contrast periodic structures, i.e. uniform, chirped, and tilted fiber Bragg gratings, have been numerically examined and widely studied. But, the conversion efficiency improving of nonlinear frequency conversions in the high-index contrast periodic structures like the multilayered PBG structures haven't been completed and haven't been widely studied [19]. According to the above literature reviews, the almost nonlinear effects, which have been examined and investigated, are the second-order nonlinear effects e.g. the second-harmonic generation, optical rectification, parametric-down conversion. These nonlinear frequency conversion effects have been generated in the PBG structures with second-order $\chi^{(2)}$ nonlinearity. So, the improving third-order nonlinear effects in the PBG structure with third-order $\chi^{(3)}$ nonlinearity should be interested to study and investigate their behaviors. The frequency conversions based on $\chi^{(3)}$ nonlinearity have been widely investigated in optical fibers [25-26], grating fibers [27], microstructure fibers [28], micro-ring resonator [29] and silicon photonic structures [30]. But, the investigation of frequency conversion in high-index contrast structure like PBG structure has been rarely examined. So, this thesis is devoted to an analysis of the nonlinear frequency conversions such that optical parametric amplification and third-harmonic generation in

one-dimensional PBG structures with third-order $\chi^{(3)}$ nonlinearity. The band-edge enhancement has been chosen to enhance both nonlinear effects in the PBG structure corresponding with the suggestion of the Centini et al work [23]. The PBG structures are composed of two alternating dielectric layers and their periodic length has been chosen to be on the order of the fundamental harmonic wavelength [18] for creating the structures in micron scales. The nonlinear frequency conversions in the structure have been analyzed by using the multiple-scale method, and then derive the new complete set of nonlinear coupled-mode equations including additional nonlinear terms, which are related to Fourier components of the spatially varying nonlinear coefficient and performing the nonlinear deep gratings inside the structures. And then, the output amplitudes of these frequency conversions have been numerically modeled with split-step Fourier method, which takes into account counter-propagating waves [31]. Finally, the amplification gain and conversion efficiency for optical parametric amplification would be calculated and indicate the physical factors that affect to both of gain and conversion efficiency. Meanwhile, the conversion efficiency of third-harmonic generation would be also calculated and also indicate the factors that affect to the conversion efficiency.

1.3 Objectives of thesis

After the primarily study, we have set the scope of our study in this thesis to just numerically investigate the nonlinear frequency conversion phenomena in photonic band-gap structures with high-index contrast. In addition, we also have demonstrated that the nonlinear phenomena can be improved with the structures by calculating the amplification gains and conversion efficiencies. Then, the goal of this thesis are set to the following tasks.

1) To study the enhancement principle of nonlinear frequency conversion phenomena; optical parametric amplification and third-harmonic generation, by using the optical properties of photonic band-gap structure.
2) To simulate the nonlinear frequency conversion phenomena; optical parametric amplification and third-harmonic generation, in one-dimensional photonic band-gap structures with third-order nonlinearity by using the numerical methods.

3) To develop the MATLAB programing code, for modeling nonlinear frequency conversion phenomena, based on the split-step Fourier method that is suitable for computing with personal computer or laptop.

1.4 Overview of thesis

This thesis is organized into five chapters, named as follows:

Chapter 1: Introduction

Chapter 2: Mathematical methods

Chapter 3: Optical parametric amplification in PBG structure

Chapter 4: Third-harmonic generation in PBG structure

Chapter 5: Conclusions

The brief details of each thesis chapters are shown as below.

Chapter 1 gives the literature review on photonic crystals and their applications, and nonlinear optics in photonic crystals. This chapter also gives the motivation, objectives, and overview of this thesis.

Chapter 2 briefly describes about the mathematical methods, which are used in this thesis i.e. transfer matrix method, multiple-scale method, and split-step Fourier transform. First, the transfer matrix method which is used to calculate the transmission curves of the PBG structures. In addition, the band-edge position, which is used to enhance the considered nonlinear effects in the PBG structure, could be indicated from the given transmission curves. The second method is the multiple-scale method. This method would be used for higher-order perturbation problems that require several time and length scales. This would be done by expanding the independent variables in terms of a perturbation parameter. Thus, a single problem would be simplified by being broken down into several processes, each occurring at a difference scale, and each being independently treated. And the split-step Fourier method has been used to solve the nonlinear wave equations. The nonlinear wave equations have been solved by setting the approximated solution in symmetrized split-step operators and appropriate boundary conditions.

Chapter 3 describes the details of the optical parametric amplification in the PBG structure. First, the PBG structure designing and how to choose the interacting wavelengths of this effect are introduced. Then, the derivation of coupled-mode equations, which correspond this nonlinear effect, have been done. After that, these coupled-mode equations have been solved by the split-step Fourier method to obtain the amplified signal and generated idler amplitudes. Finally, the output amplitudes have been used to calculate the amplification gain and conversion efficiency.

Chapter 4 describes the details of the third-harmonic generation in the PBG structure. First, the PBG structure designing and how to choose the fundamental-frequency and third-harmonic wavelength of this effect are introduced. Then, the derivation of coupled-mode equations, which correspond this nonlinear effect, have been done. After that, these coupled-mode equations have been solved by the split-step Fourier method to obtain the output third-harmonic amplitudes in forward and backward directions. Finally, the output amplitudes have been used to calculate the third-harmonic conversion efficiencies.

Chapter 5 gives the conclusions of this thesis and the suggestions for future works.

Chapter 2

Mathematical Methods

In this chapter, the useful mathematical methods are introduced in more details. Since, this thesis is based on the numerical investigation, so the mathematical methods are required to solve the interesting problems. The mathematical methods which are used in this study consisting of the transfer matrix method, multiple-scale method, and split-step Fourier method. The detail of each methods are presented in subsection as below.

2.1 Transfer matrix method

The light propagating through a periodic structure like PBG material could be differently considered when compare with light propagating through free-space or homogeneous material. There are many analytical and numerical methods to investigate the light propagation behaviors in the linear [32-33] and nonlinear [34-35] stratified structures. A well-known numerical method that use to compute the output wave from PBG structure is the transfer matrix method (TMM). This method is based on the calculation the output wave for a single thin film material by treating the medium as a black-box when knowing the input wave. The single thin film effect could be related to the composite effect of stratified media, by accumulation of each single thin film effect. The output wave has been easily obtained by using matrix multiplication. TMM could be deployed to study optical properties i.e. transmittance, reflectance, and absorbance; in symmetric multilayered structures [36], nonlinear multilayered structures [37], and Fibonacci multilayered structures [38], etc. In this section, the TMM is used to plot the transmission spectrum of our PBG structure, which is composed of two alternating dielectric layers with different $\chi^{(3)}$ in each layer in the linear optics regime (low intensity). In addition, indicating the position of band-edge has been considered because of the wavelength of incident wave would be tuned to this position for enhancing nonlinear effect in the PBG structure [18-19, 23-24]. This enhancement technique is known as the band-edge enhancement. So, the TMM also is an important step of the procedure of designing the optimal PBG structures for both OPA and THG.

Firstly, the Maxwell's equations in particular materials is shown as:

$$\nabla \cdot \mathbf{D} = 0, \tag{2-1a}$$

$$\nabla \cdot \mathbf{B} = 0, \tag{2-1b}$$

$$\nabla \times \mathbf{E} = -\frac{\partial \mathbf{B}}{\partial t}, \tag{2-1c}$$

$$\nabla \times \mathbf{H} = -\frac{\partial \mathbf{D}}{\partial t}, \tag{2-1d}$$

where $\mathbf{E} = \mathbf{E}(z,t)$ and $\mathbf{H} = \mathbf{H}(z,t)$ are the respective electric field (V/m) and magnetic field (A/m) amplitudes, and $\mathbf{D} = \mathbf{D}(z,t)$ and $\mathbf{B} = \mathbf{B}(z,t)$ are the electric displacement (C/m^2) and magnetic flux (Wb/m^2 or T), respectively. Also, in arbitrary materials, we know that $\mathbf{D} = \varepsilon\mathbf{E}$ and $\mathbf{B} = \mu\mathbf{H}$, where ε is the electric permittivity (F/m) and μ is the magnetic permeability (H/m) of material. By using Eq. (2-1c), Eq. (2-1d), and the relation $\mathbf{B} = \mu\mathbf{H}$ and then the obtaining result is given as:

$$\nabla \times \nabla \times \mathbf{E} = -\mu \frac{\partial^2 \mathbf{D}}{\partial t^2}. \tag{2-2}$$

Then, the Eq. (2-2) could be expanded by using the vector identity $\nabla \times \nabla \times \mathbf{A} = \nabla(\nabla \cdot \mathbf{A}) - \nabla^2 \mathbf{A}$ as:

$$\nabla \times \nabla \times \mathbf{E} = \nabla(\nabla \cdot \mathbf{E}) - \nabla^2 \mathbf{E} = -\mu \frac{\partial^2 \mathbf{D}}{\partial t^2},$$

$$\frac{1}{\varepsilon}\nabla(\nabla \cdot \mathbf{D}) - \nabla^2 \mathbf{E} = -\mu \frac{\partial^2 \mathbf{D}}{\partial t^2}. \tag{2-3}$$

Generally, the electric displacement is related to the electric field through the permittivity of a medium and it can be expressed as:

$$\mathbf{D} = \varepsilon\mathbf{E}. \tag{2-4}$$

For the case of linear medium with linear polarization $\mathbf{P} = \chi^{(1)}\mathbf{E}$, the linear electric displacement is obtained:

$$\mathbf{D}_L = \varepsilon_0\mathbf{E} + \mathbf{P} = \varepsilon_0(1 + \chi^{(1)})\mathbf{E} = \varepsilon_L\mathbf{E} \tag{2-5}$$

In reality, the polarization field is more complicated and it can be expanded in Taylor series to obtain:

$$\mathbf{P} = \chi^{(1)}\mathbf{E} + \chi^{(2)}\mathbf{E}\mathbf{E} + \chi^{(3)}\mathbf{E}\mathbf{E}\mathbf{E} + \ldots \tag{2-6}$$

The first term in Eq. (2-6) is the polarization in linear optics regime and the second and the third terms are the polarization in nonlinear optics regime, respectively. In this case, the third-order nonlinearity is only considered. So, the electric displacement in medium with third-order nonlinearity can be expressed as:

$$\begin{aligned}\mathbf{D} &= \varepsilon_0\left(1+\chi^{(1)}\mathbf{E}+\chi^{(3)}\mathbf{EEE}\right)\\ &= \varepsilon_0\left(1+\chi^{(1)}\right)\mathbf{E}+\varepsilon_0\chi^{(3)}\mathbf{EEE}\\ &= \varepsilon_L\mathbf{E}+\varepsilon_{NL}\mathbf{E}\\ &= \mathbf{D}_L+\mathbf{D}_{NL}\end{aligned}$$

$$\mathbf{D}=\mathbf{D}_L+\mathbf{D}_{NL}, \tag{2-7}$$

where $\chi^{(1)}$ is the linear susceptibility (dimensionless) and $\chi^{(3)}$ is the third-order nonlinear susceptibility (m^2/V^2). Note that the subscripts "*L*" and "*NL*" represent linear and nonlinear, respectively. From Eq. (2-1a) that shows $\nabla\cdot\mathbf{D}=0$ and using the general form of electric displacement as in Eq. (2-7), so Eq. (2-3) becomes:

$$-\nabla^2\mathbf{E}=-\mu\frac{\partial^2\mathbf{D}_L}{\partial t^2}-\mu\frac{\partial^2\mathbf{D}_{NL}}{\partial t^2}=-\mu\varepsilon_L\frac{\partial^2\mathbf{E}}{\partial t^2}-\mu\frac{\partial^2\mathbf{D}_{NL}}{\partial t^2}. \tag{2-8}$$

According to the plane wave solution for monochromatic wave propagating in the z-direction, the electric field can be written in the product of electric field amplitude, which is function of z, and its phasor. So, the electric field can be expressed as $\mathbf{E}(z,t)=\tilde{\mathbf{E}}(z)e^{-i\omega t}$. Since, the nonlinear electric displacement is depend on electric field, so it can be expressed as $\mathbf{D}_{NL}(z,t)=\tilde{\mathbf{D}}_{NL}(z)e^{-i\omega t}$. Therefore the derivatives of electric field and electric displacement are $\frac{\partial^2\mathbf{E}}{\partial t^2}=-\omega^2\tilde{\mathbf{E}}(z)e^{-i\omega t}=-\omega^2\mathbf{E}$ and $\frac{\partial^2\mathbf{D}_{NL}}{\partial t^2}=-\omega^2\tilde{\mathbf{D}}_{NL}(z)e^{-i\omega t}=-\omega^2\mathbf{D}_{NL}$. These identities are substituted into Eq. (2-8) as:

$$-\nabla^2\mathbf{E}=\omega^2\mu\varepsilon_L\mathbf{E}+\omega^2\mu\mathbf{D}_{NL}. \tag{2-9}$$

Note that $k=\omega\sqrt{\mu\varepsilon_L}$ and $k=k_0n=k_0\sqrt{\varepsilon_L}$ for $\mu=1$ in non-magnetic material, where the subscript "0" represents free space. So, Eq. (2-9) will be updated and rearranged as:

$$\nabla^2\mathbf{E}+k_0^2\varepsilon_L\mathbf{E}=-k_0^2\mathbf{D}_{NL}. \tag{2-10}$$

According to Eq. (2-10), the nonlinear electric displacement [60] could be expressed as:

$$\mathbf{D}_{NL} = \varepsilon_0 \chi^{(3)} \left[A\mathbf{E}(\mathbf{E}\cdot\mathbf{E}^*) + B\mathbf{E}^*(\mathbf{E}\cdot\mathbf{E}) \right], \tag{2-11}$$

where A and B are nonlinear constants. Both nonlinear constants are obtained from the tensor nature of the third-order nonlinear susceptibility [60]. In one-dimensional case of two counter-propagating waves inside the PBG structure, the electric field could be written as:

$$\mathbf{E}(z) = \mathbf{E}_f e^{ikz} + \mathbf{E}_b e^{-ikz}, \tag{2-12}$$

and its corresponding second-order derivative with respect to z is expressed as:

$$\nabla^2\mathbf{E} = \frac{\partial^2\mathbf{E}}{\partial z^2} = \frac{\partial^2\mathbf{E}_f}{\partial z^2}e^{ikz} + 2ik\frac{\partial\mathbf{E}_f}{\partial z}e^{ikz} - k^2\mathbf{E}_f e^{ikz} + \frac{\partial^2\mathbf{E}_b}{\partial z^2}e^{-ikz} - 2ik\frac{\partial\mathbf{E}_b}{\partial z}e^{-ikz} - k^2\mathbf{E}_b e^{-ikz}, \tag{2-13}$$

where the subscripts "*f*" and "*b*" represent the forward- and backward-direction of wave propagation.

Now, the slowly varying amplitude approximation has been proposed such that $\left|\frac{\partial^2\mathbf{E}_f}{\partial z^2}\right| << \left|ik\frac{\partial\mathbf{E}_f}{\partial z}\right|$ and $\left|\frac{\partial^2\mathbf{E}_b}{\partial z^2}\right| << \left|ik\frac{\partial\mathbf{E}_b}{\partial z}\right|$. So, the two second-order derivative terms in Eq. (2-13) could be neglected. Finally, the equation is given as:

$$\nabla^2\mathbf{E} = 2ik\frac{\partial\mathbf{E}_f}{\partial z}e^{ikz} - k^2\mathbf{E}_f e^{ikz} - 2ik\frac{\partial\mathbf{E}_b}{\partial z}e^{-ikz} - k^2\mathbf{E}_b e^{-ikz}. \tag{2-14}$$

For compact notation, let $\mathbf{E}_+ = \mathbf{E}_f e^{ikz}$ and $\mathbf{E}_- = \mathbf{E}_b e^{-ikz}$, so that:

$$\nabla^2\mathbf{E} = 2ik\frac{\partial\mathbf{E}_+}{\partial z} - k_0^2\varepsilon_L\mathbf{E}_+ - 2ik\frac{\partial\mathbf{E}_-}{\partial z} - k_0^2\varepsilon_L\mathbf{E}_-. \tag{2-15}$$

Then, the nonlinear electric displacement $\mathbf{D}_{NL}$ could be expanded by using these compact notations as:

$$\begin{aligned}\mathbf{D}_{NL} = \varepsilon_0\chi^{(3)}\Big[& A(\mathbf{E}_+(\mathbf{E}_+\cdot\mathbf{E}_+^* + \mathbf{E}_-\cdot\mathbf{E}_-^*)) + A(\mathbf{E}_-(\mathbf{E}_+\cdot\mathbf{E}_+^* + \mathbf{E}_-\cdot\mathbf{E}_-^*)) \\ & + A\mathbf{E}_+\mathbf{E}_+\cdot\mathbf{E}_-^* + A\mathbf{E}_+\mathbf{E}_-\cdot\mathbf{E}_+^* + A\mathbf{E}_-\mathbf{E}_+\cdot\mathbf{E}_-^* + A\mathbf{E}_-\mathbf{E}_-\cdot\mathbf{E}_+^* \\ & + B\mathbf{E}_+^*\mathbf{E}_+\cdot\mathbf{E}_+ + 2B\mathbf{E}_+^*\mathbf{E}_+\cdot\mathbf{E}_- + B\mathbf{E}_+^*\mathbf{E}_-\cdot\mathbf{E}_- \\ & + B\mathbf{E}_-^*\mathbf{E}_+\cdot\mathbf{E}_+ + 2B\mathbf{E}_-^*\mathbf{E}_+\cdot\mathbf{E}_- + B\mathbf{E}_-^*\mathbf{E}_-\cdot\mathbf{E}_-\Big].\end{aligned} \tag{2-16}$$

The terms with phase component e^{ikz} and e^{-ikz} will be kept but the terms, which cannot satisfy phase-matching i.e. $A\mathbf{E}_+\mathbf{E}_+\cdot\mathbf{E}_-^*$, $A\mathbf{E}_-\mathbf{E}_-\cdot\mathbf{E}_+^*$, $B\mathbf{E}_+^*\mathbf{E}_-\cdot\mathbf{E}_-$, and $B\mathbf{E}_-^*\mathbf{E}_+\cdot\mathbf{E}_+$ will be neglected. Next, the Eq. (2-15) and Eq. (2-16) are substituted into Eq. (2-10) as:

$$\begin{aligned}2ik\frac{\partial\mathbf{E}_+}{\partial z}-2ik\frac{\partial\mathbf{E}_-}{\partial z}-k_0^2\varepsilon_L(\mathbf{E}_++\mathbf{E}_-)+k_0^2\varepsilon_L(\mathbf{E}_++\mathbf{E}_-)=-k_0^2\varepsilon_0\chi^{(3)}\Big[&A(\mathbf{E}_+(\mathbf{E}_+\cdot\mathbf{E}_+^*+\mathbf{E}_-\cdot\mathbf{E}_-^*))\\&+A(\mathbf{E}_-(\mathbf{E}_+\cdot\mathbf{E}_+^*+\mathbf{E}_-\cdot\mathbf{E}_-^*))\\&+A\mathbf{E}_+\mathbf{E}_-\cdot\mathbf{E}_+^*+A\mathbf{E}_-\mathbf{E}_+\cdot\mathbf{E}_-^*+B\mathbf{E}_+^*\mathbf{E}_+\cdot\mathbf{E}_+\\&+2B\mathbf{E}_+^*\mathbf{E}_+\cdot\mathbf{E}_-+2B\mathbf{E}_-^*\mathbf{E}_+\cdot\mathbf{E}_-+B\mathbf{E}_-^*\mathbf{E}_-\cdot\mathbf{E}_-\Big],\end{aligned}$$

$$\begin{aligned}2ik_0\sqrt{\varepsilon_L}\frac{\partial\mathbf{E}_+}{\partial z}-2ik_0\sqrt{\varepsilon_L}\frac{\partial\mathbf{E}_-}{\partial z}=-k_0^2\varepsilon_0\chi^{(3)}\Big[&A(\mathbf{E}_+(\mathbf{E}_+\cdot\mathbf{E}_+^*+\mathbf{E}_-\cdot\mathbf{E}_-^*))+A(\mathbf{E}_-(\mathbf{E}_+\cdot\mathbf{E}_+^*+\mathbf{E}_-\cdot\mathbf{E}_-^*))+A\mathbf{E}_+\mathbf{E}_-\cdot\mathbf{E}_+^*\\&+A\mathbf{E}_-\mathbf{E}_+\cdot\mathbf{E}_-^*+B\mathbf{E}_+^*\mathbf{E}_+\cdot\mathbf{E}_++2B\mathbf{E}_+^*\mathbf{E}_+\cdot\mathbf{E}_-+2B\mathbf{E}_-^*\mathbf{E}_+\cdot\mathbf{E}_-+B\mathbf{E}_-^*\mathbf{E}_-\cdot\mathbf{E}_-\Big].\end{aligned}$$

(2-17)

Then, collecting the equation with the terms for e^{ikz} or e^{-ikz}, the coupled equation will be given as:

$$2ik_0\sqrt{\varepsilon_L}\frac{\partial\mathbf{E}_+}{\partial z}=-k_0^2\varepsilon_0\chi^{(3)}\Big[A(\mathbf{E}_+(\mathbf{E}_+\cdot\mathbf{E}_+^*+\mathbf{E}_-\cdot\mathbf{E}_-^*))+A\mathbf{E}_-\mathbf{E}_+\cdot\mathbf{E}_-^*+B\mathbf{E}_+^*\mathbf{E}_+\cdot\mathbf{E}_++2B\mathbf{E}_-^*\mathbf{E}_+\cdot\mathbf{E}_-\Big],$$

(2-18a)

and

$$-2ik_0\sqrt{\varepsilon_L}\frac{\partial\mathbf{E}_-}{\partial z}=-k_0^2\varepsilon_0\chi^{(3)}\Big[A(\mathbf{E}_-(\mathbf{E}_+\cdot\mathbf{E}_+^*+\mathbf{E}_-\cdot\mathbf{E}_-^*))+A\mathbf{E}_+\mathbf{E}_-\cdot\mathbf{E}_+^*+2B\mathbf{E}_+^*\mathbf{E}_+\cdot\mathbf{E}_-+B\mathbf{E}_-^*\mathbf{E}_-\cdot\mathbf{E}_-\Big].$$

(2-18b)

In fact that the linear polarization has been divided into two cases i.e. TE (s-polarized) and TM (p-polarized). The diagram for TE polarization is illustrated in Fig. 2.1. Note that x and y are the transverse directions, and z is the propagation direction.

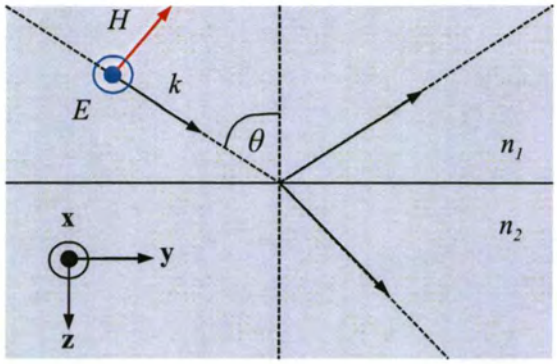

Figure 2.1 The diagram of wave propagation in TE case.

For TE case: $E_{\pm x} \neq 0$, $E_{\pm z} \neq 0$, and $E_{\pm y} = 0$ due to wave propagates in x-z plane. Let $\phi = \chi^{(3)}(A+B)$ and $\varepsilon_L = \varepsilon_0$, then Eq. (2-18) could be extended as:

$$2ik_0\sqrt{\varepsilon_0}\frac{\partial E_{+x}}{\partial z} = -k_0^2\varepsilon_0\phi E_{+x}(|E_{+x}|^2 + 2|E_{-x}|^2), \tag{2-19a}$$

and

$$-2ik_0\sqrt{\varepsilon_0}\frac{\partial E_{-x}}{\partial z} = -k_0^2\varepsilon_0\phi E_{-x}(2|E_{+x}|^2 + |E_{-x}|^2). \tag{2-19b}$$

Rearranging Eq. (2-19) as:

$$\frac{\partial E_{+x}}{\partial z} = \frac{ik_0\phi\sqrt{\varepsilon_0}}{2}(|E_{+x}|^2 + 2|E_{-x}|^2)E_{+x}, \tag{2-20a}$$

and

$$\frac{\partial E_{-x}}{\partial z} = -\frac{ik_0\phi\sqrt{\varepsilon_0}}{2}(2|E_{+x}|^2 + |E_{-x}|^2)E_{-x}. \tag{2-20b}$$

Note that $(|E_{+x}|^2 + 2|E_{-x}|^2)$ and $(2|E_{+x}|^2 + |E_{-x}|^2)$ are constants. Then, Eq. (2-20) will be ordinary differential equations and could be easily solved as:

$$E_{+x} = E_{+x0}\exp\left[\frac{ik_0\phi\sqrt{\varepsilon_0}}{2}(|E_{+x}|^2 + 2|E_{-x}|^2)z\right], \tag{2-21a}$$

and

$$E_{-x} = E_{-x0}\exp\left[-\frac{ik_0\phi\sqrt{\varepsilon_0}}{2}(2|E_{+x}|^2+|E_{-x}|^2)z\right], \tag{2-21b}$$

where E_{+x0} and E_{-x0} are the initial fields. Eq. (2-21) will be substituted into Eq. (2-12) and then:

$$E_x(z) = E_{+x}(z)e^{ik_0\sqrt{\varepsilon_0}z} + E_{-x}(z)e^{-ik_0\sqrt{\varepsilon_0}z},$$

$$E_x(z) = E_{+x0}e^{\frac{ik_0\phi\sqrt{\varepsilon_0}}{2}(|E_{+x}|^2+2|E_{-x}|^2)z}e^{ik_0\sqrt{\varepsilon_0}z} + E_{-x0}e^{-\frac{ik_0\phi\sqrt{\varepsilon_0}}{2}(2|E_{+x}|^2+|E_{-x}|^2)z}e^{-ik_0\sqrt{\varepsilon_0}z},$$

$$E_x(z) = A_+e^{ik_+z} + A_-e^{-ik_-z}, \tag{2-22}$$

where $k_+ = k_0\sqrt{\varepsilon_0}\left[1+\frac{\phi}{2}(|E_{+x}|^2+2|E_{-x}|^2)\right]$, $k_- = k_0\sqrt{\varepsilon_0}\left[1+\frac{\phi}{2}(2|E_{+x}|^2+|E_{-x}|^2)\right]$, $A_+ = E_{+x0}$, and $A_- = E_{-x0}$.

From Maxwell's equation as Eq. (2-1c); $\nabla\times\mathbf{E} = -\frac{\partial\mathbf{B}}{\partial t} = -\frac{i\omega}{c}\mathbf{H}$ and $k_0 = \frac{\omega}{c}$, where c is the light speed in free-space. Therefore, this Maxwell's equation will be:

$$\frac{\partial E_x}{\partial z} = ik_+A_+e^{ik_+z} - ik_-A_-e^{-ik_-z} = -ik_0H_y. \tag{2-23}$$

The tangential component (along y-direction) $H_y = |H|\cos\theta$ will be written as:

$$-H_y = \frac{k_+}{k_0}A_+e^{ik_+z} - \frac{k_-}{k_0}A_-e^{-ik_-z}. \tag{2-24}$$

Eq. (2-22) and Eq. (2-24) could be expressed in matrix form as:

$$\begin{bmatrix} E_x \\ -H_y \end{bmatrix}_{z=0} = \begin{bmatrix} 1 & 1 \\ \frac{k_+}{k_0} & -\frac{k_-}{k_0} \end{bmatrix}\begin{bmatrix} A_+ \\ A_- \end{bmatrix}, \tag{2-25a}$$

and

$$\begin{bmatrix} E_x \\ -H_y \end{bmatrix}_{z=L} = \begin{bmatrix} e^{ik_+L} & e^{-ik_-L} \\ \frac{k_+}{k_0}e^{ik_+L} & -\frac{k_-}{k_0}e^{-ik_-L} \end{bmatrix}\begin{bmatrix} A_+ \\ A_- \end{bmatrix}, \tag{2-25b}$$

where L is the medium length. The left-hand side of Eq. (2-25) distinguish the input and output fields, respectively. Both equations will be combined into one for expressing the output field in term of the input field as:

$$\begin{bmatrix} E_x \\ -H_y \end{bmatrix}_{z=L} = \frac{k_0}{k_+ + k_-} \begin{bmatrix} \frac{k_-}{k_0} e^{ik_+L} + \frac{k_+}{k_0} e^{-ik_-L} & e^{ik_+L} - e^{-ik_-L} \\ \frac{k_+ k_-}{k_0}(e^{ik_+L} - e^{-ik_-L}) & \frac{k_+}{k_0} e^{ik_+L} + \frac{k_-}{k_0} e^{-ik_-L} \end{bmatrix} \begin{bmatrix} E_x \\ -H_y \end{bmatrix}_{z=0}. \quad (2\text{-}26)$$

Let $\bar{M} = \frac{k_0}{k_+ + k_-} \begin{bmatrix} \frac{k_-}{k_0} e^{ik_+L} + \frac{k_+}{k_0} e^{-ik_-L} & e^{ik_+L} - e^{-ik_-L} \\ \frac{k_+ k_-}{k_0}(e^{ik_+L} - e^{-ik_-L}) & \frac{k_+}{k_0} e^{ik_+L} + \frac{k_-}{k_0} e^{-ik_-L} \end{bmatrix}$ is a transfer matrix for a single film layer.

Therefore, the characteristic matrix M for the stratified structure could be determined as:

$$M = \prod_{j=1}^{N} \bar{M}_j(L_j), \quad (2\text{-}27)$$

where N is the number of layer. Here, the transmission and reflection coefficients [64-65] could be directly obtained from the transfer matrix in Eq. (2-27) as:

$$t = M_{11} - \frac{M_{12} M_{21}}{M_{22}}, \quad (2\text{-}28a)$$

and

$$r = -\frac{M_{21}}{M_{22}}, \quad (2\text{-}28b)$$

where the notation M_{ij} is the matrix element for row i and column j of transfer matrix M.

Now, the schematic of the one-dimensional PBG structure is depicted in Fig. 2.2. The first and second layers have thickness of a and b, respectively. And the periodic length of PBG structure could be defined as: $\Lambda = a + b$.

Figure 2.2 The schematic of the one-dimensional PBG structure.

By using this method following Eq. (2-26) and (2-27), and $\phi = 0$, i.e. for low intensity where there is only linear optic regime, the transmission spectrum, which respect to wavelength, is illustrated in Fig. 2.3. The sample PBG structure is 20-periods structure and composed of two alternating layers which each layer thicknesses are $a = 100$ nm and $b = 200$ nm, and each refractive indices are $n_1 = 2$ and $n_2 = 1$.

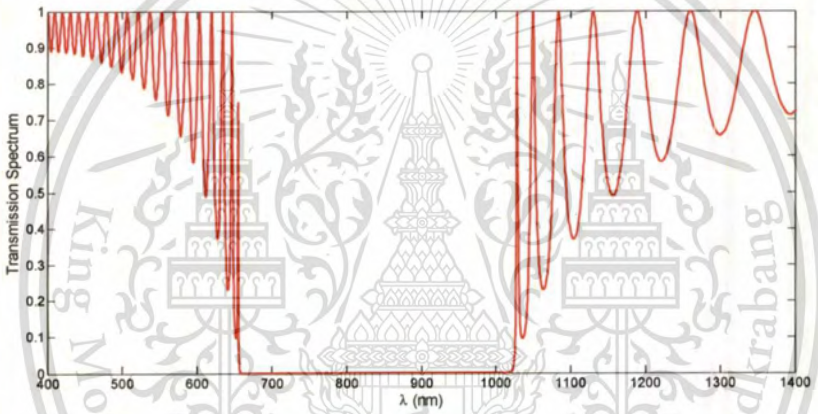

Figure 2.3 The transmission spectrum of the sample 20-periods PBG structure for normal incident angle.

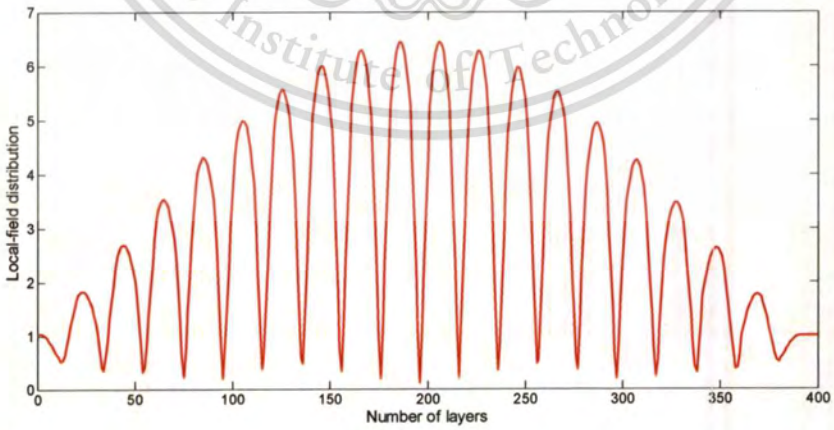

(a)

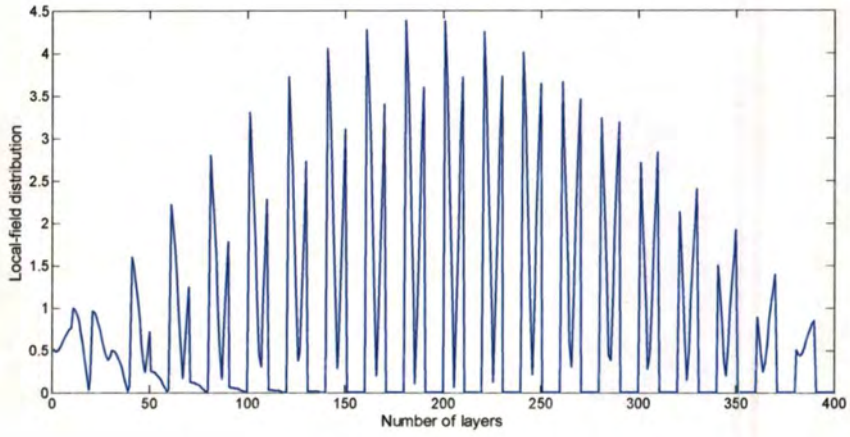

(b)

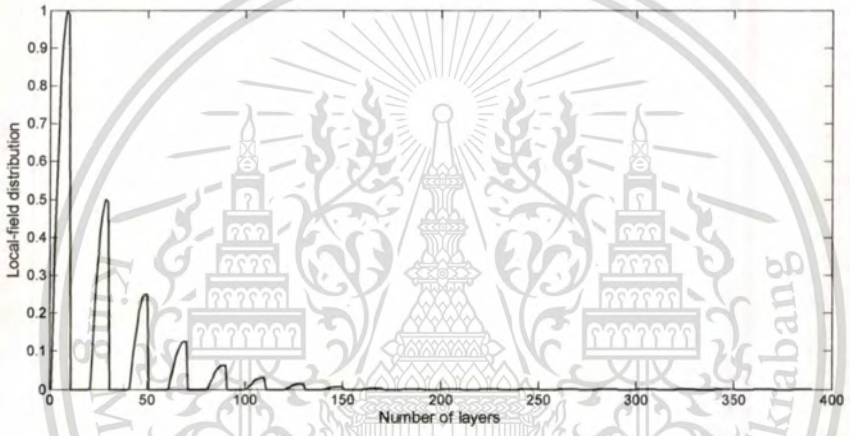

(c)

Figure 2.4 The local electric field distribution at (a) long wavelength band-edge position; (b) short wavelength band-edge position; and (c) other position.

From the calculated results, the transmission curve of this sample structure has obtained as shown in Fig. 2.3. The transmission spectrum and its features are strongly influenced by (i) the number of periods, (ii) layer thickness, and (iii) material dispersion [19]. For example, increasing (decreasing) the number of layers sharpens the band-edge, and increases (decreases) the number of transmission resonances between gaps, causing an effective shift of each resonance. By changing layer thickness could also cause frequency shifts in the location of the band-gaps and transmission resonances. At low intensity, the transmission curve only depends on the linear optics effect. But at high intensity, the transmission curve has been effected by both the

linear and nonlinear optics effects, and with higher the intensity, stronger the dominance of the nonlinear effect. Next, the effect of laser tuning to the band-edge of the photonic band-gap is consider. First, the Fig 2.4 (a) shows the local-field distribution inside PBG structure when laser is tuned to the long wavelength band-edge. At this wavelength, the field is resonance and dramatically increased in the field amplitude inside the structure. Second, as show in Fig. 2.4 (b), the laser wavelength is tuned to the short wavelength band-edge of band-gap. At this wavelength, the local-field is also resonance as first case, but the field amplitude is lower than the field amplitude at the lower band-edge. So, the field at long wavelength band-edge should be efficient for enhancing nonlinear effect in the PBG structure when compare to the field at short wavelength band-edge. Finally, when the laser wavelength is tuned to the other wavelength except both band-edges, the local-field is not resonance and also exponentially rapidly decreased as shown in Fig. 2.4 (c). Therefore, the best option to enhance the nonlinear effect in PBG structure is tuning the input laser wavelength to the long wavelength band-edge of the photonic band-gap.

2.2 Multiple-scale method

In order to model the nonlinear optical phenomena e.g. third-harmonic generation and optical parametric amplification in the PBG structure, we need to consider the wave equation that describe electromagnetic waves behavior in the structure. Depending on the PBG structure, the wave equation can be expressed in different form where each form corresponds to a unique scenario with different boundary and initial conditions. Since, the wave equation in this case can be nonlinear, and ordinary analytical method may not have any possible solution. One method to get around this problem is applying the perturbation method. The concept is to perturb the wave equation with nonlinear source term by a small factor, and expecting to reduce the nonlinearity, enough so that the problem can be solved analytically. Meanwhile the solution of the perturbed form provide a close similarity to the actual solution.

Here, the discussing perturbation method is the multiple-scale method (MSM) [56-57]. The MSM would be used for higher-order perturbation problems that require several time and length scales. This would be done by expanding the independent variables in terms of an expansion parameter. These new coordinates are considered independent of each other. Thus, a single problem would be simplified by being broken down

into several processes, each occurring at a difference scale, and each being independently treated. The advantage of this method over other perturbation techniques is its ability to seek a uniform perturbation expansion by using the systematic elimination of secularly growing forcing terms that enter at the higher perturbation orders [18, 40-41].

Let us consider the scalar wave equation with nonlinear polarization term, which is given by:

$$\frac{\partial^2 E}{\partial z^2} - \frac{1}{c^2}\frac{\partial^2 D_L}{\partial t^2} = \frac{4\pi}{c^2}\frac{\partial^2 P_{NL}}{\partial t^2}, \tag{2-29}$$

where $E(z,t)$ is the electric field, $D_L(z,t)$ is the linear electric displacement, $P_{NL}(z,t)$ is the nonlinear polarization, c is the speed of light in vacuum, z is the propagation direction, and t is the time variable.

Then, the needed perturbation series will be set up for this method. First, the electric displacement is described as:

$$\begin{aligned} D_L(z,t) &= \int_{-\infty}^{t} \varepsilon(z,t-t')E(z,t')dt' \\ &= \varepsilon(z,t) \otimes E(z,t), \end{aligned} \tag{2-30}$$

where $\otimes$ denotes a convolution operation and The function $\varepsilon(z,t)$ is dielectric function which has periodicity in z-direction and the medium is dispersive. Let the Fourier transform in time domain of D_L and ε are $\hat{D}_L$ and $\hat{\varepsilon}$, respectively. Thus, the Fourier transformed Eq. (2-30) is:

$$\hat{D}_L(z,\omega) = \hat{\varepsilon}(z,\omega)\hat{E}(z,\omega), \tag{2-31}$$

where ω is the angular frequency variable, and note that the Fourier transformed dielectric function $\hat{\varepsilon}$ is complex function. Now, it is expanded in Taylor series expansion as:

$$\hat{\varepsilon}(z,\omega) = \sum_{n=0}^{\infty} \hat{\varepsilon}^{(n)}(0)\omega^n. \tag{2-32}$$

Then, substituting Eq. (2-32) into Eq. (2-31), we obtain:

$$\hat{D}_L(z,\omega) = \sum_{n=0}^{\infty} \hat{\varepsilon}^{(n)}(0)\omega^n \hat{E}(z,\omega). \tag{2-33}$$

Next, this relation should be introduced to simplify our analysis,

$$\frac{\partial}{\partial t}e^{i(kz-\omega t)} = -i\omega e^{i(kz-\omega t)}.$$

In other words; $$\frac{\partial}{\partial t} \Rightarrow -i\omega \text{ or } \omega \Rightarrow i\frac{\partial}{\partial t}.$$

Taking the inverse Fourier transform to both sides of Eq. (2-33) and then replacing ω with $i\partial/\partial t$, so we get:

$$\int_{-\infty}^{\infty} \hat{D}_L(z,\omega)e^{i\omega}d\omega = \int_{-\infty}^{\infty}\sum_{n=0}^{\infty}\hat{\varepsilon}^{(n)}(0)\left(i\frac{\partial}{\partial t}\right)^n \hat{E}(z,\omega)e^{i\omega}d\omega. \tag{2-34}$$

Next, the term, which is not dependent on the angular frequency ω, can be pulled out from the integral as:

$$\begin{aligned} D_L(z,t) &= \sum_{n=0}^{\infty}\hat{\varepsilon}^{(n)}(0)\left(i\frac{\partial}{\partial t}\right)^n \int_{-\infty}^{\infty}\hat{E}(z,\omega)e^{i\omega}d\omega \\ &= \left[\sum_{n=0}^{\infty}\hat{\varepsilon}^{(n)}(0)\left(i\frac{\partial}{\partial t}\right)^n\right]E(z,t), \\ &= \hat{\varepsilon}(z,i\frac{\partial}{\partial t})E(z,t), \end{aligned} \tag{2-35}$$

such that $\hat{\varepsilon}(z,i\frac{\partial}{\partial t}) = \sum_{n=0}^{\infty}\hat{\varepsilon}^{(n)}(0)\left(i\frac{\partial}{\partial t}\right)^n$.

Now, the MSM perturbation variables have been introduced [18, 40-41] as:

$$z = z_0 + \mu z_1 + \mu^2 z_2 + \ldots = \sum_{n=0}^{\infty}\mu^n z_n, \tag{2-36a}$$

$$t = t_0 + \mu t_1 + \mu^2 t_2 + \ldots = \sum_{n=0}^{\infty}\mu^n t_n, \tag{2-36b}$$

where μ is the perturbation parameter which is unity at the end of analysis. So, the corresponding second-order derivative of Eq. (2-36) can be given as:

$$\frac{\partial^2}{\partial z^2} = \frac{\partial^2}{\partial z_0^2} + 2\mu\frac{\partial}{\partial z_0}\frac{\partial}{\partial z_1} + 2\mu^2\frac{\partial}{\partial z_0}\frac{\partial}{\partial z_2} + \ldots, \tag{2-37a}$$

$$\frac{\partial^2}{\partial t^2} = \frac{\partial^2}{\partial t_0^2} + 2\mu\frac{\partial}{\partial t_0}\frac{\partial}{\partial t_1} + 2\mu^2\frac{\partial}{\partial t_0}\frac{\partial}{\partial t_2} + \ldots. \tag{2-37b}$$

Next, the angular frequency ω^n or simplified form $i\partial/\partial t$ can be expanded in similar fashion as Eq. (2-37) as:

$$\omega^n = \left(i\frac{\partial}{\partial t}\right)^n = \left(i\frac{\partial}{\partial t_0}\right)^n + n\mu\left(i\frac{\partial}{\partial t_1}\right)\left(i\frac{\partial}{\partial t_0}\right)^{n-1} + (n-1)\mu^2\left(i\frac{\partial}{\partial t_2}\right)\left(i\frac{\partial}{\partial t_0}\right)^{n-2} + \ldots. \qquad (2\text{-}38)$$

Due to the dielectric function is complex so; $\hat{\varepsilon}(z, i\frac{\partial}{\partial t}) = \hat{\varepsilon}_{\mathrm{Re}}(z, i\frac{\partial}{\partial t}) + i\mu\hat{\varepsilon}_{\mathrm{Im}}(z, i\frac{\partial}{\partial t})$, where the subscripts Re and Im represent real and imaginary parts of complex dielectric function, respectively. Then Eq. (2-38) is substituted into the Taylor series expansion of $\hat{\varepsilon}(z, i\frac{\partial}{\partial t})$. So we have:

$$\begin{aligned}\hat{\varepsilon}(z, i\frac{\partial}{\partial t}) &= \sum_{n=0}^{\infty}(\hat{\varepsilon}_{\mathrm{Re}}^{(n)} + i\mu\hat{\varepsilon}_{\mathrm{Im}}^{(n)})(0)\left[\left(i\frac{\partial}{\partial t_0}\right)^n + n\mu\left(i\frac{\partial}{\partial t_1}\right)\left(i\frac{\partial}{\partial t_0}\right)^{n-1} + \ldots\right] \\ &= \sum_{n=0}^{\infty}\hat{\varepsilon}_{\mathrm{Re}}^{(n)}(0)\left(i\frac{\partial}{\partial t_0}\right)^n + i\mu\sum_{n=0}^{\infty}\hat{\varepsilon}_{\mathrm{Im}}^{(n)}(0)\left(i\frac{\partial}{\partial t_0}\right)^n + \sum_{n=0}^{\infty}n\mu\hat{\varepsilon}_{\mathrm{Re}}^{(n)}(0)\left(i\frac{\partial}{\partial t_1}\right)\left(i\frac{\partial}{\partial t_0}\right)^{n-1} + \ldots \\ &= \hat{\varepsilon}_{\mathrm{Re}}\left(i\frac{\partial}{\partial t_0}\right) + i\mu\hat{\varepsilon}_{\mathrm{Im}}\left(i\frac{\partial}{\partial t_0}\right) + i\mu\frac{\partial}{\partial t_1}\hat{\varepsilon}'_{\mathrm{Re}}\left(i\frac{\partial}{\partial t_0}\right) + \ldots,\end{aligned} \qquad (2\text{-}39a)$$

where $\hat{\varepsilon}'_{\mathrm{Re}}\left(i\frac{\partial}{\partial t_0}\right) = \sum_{n=0}^{\infty}n\hat{\varepsilon}_{\mathrm{Re}}^{(n)}(0)\left(i\frac{\partial}{\partial t_0}\right)^{n-1}$ and the prime denotes the derivative with respect to the angular frequency of the function. At the fast scale $z = z_0$, the Fourier series expansion of dielectric function $\hat{\varepsilon}(z_0, \omega)$ along the longitudinal direction is given as:

$$\hat{\varepsilon}(z_0, i\frac{\partial}{\partial t}) = \sum_{\ell=-\infty}^{\infty}\hat{\varepsilon}_\ell e^{i\ell\frac{2\pi}{\Lambda}z_0}, \qquad (2\text{-}39b)$$

where Λ is the periodic length of PBG structure and $\hat{\varepsilon}_\ell$ is the Fourier coefficient of complex dielectric function. If $\ell = 0$, the zeroth-order Fourier coefficient in Eq. (2-39b) have been obtained, and it correspond to the zeroth terms of $\partial/\partial t_0$ in the perturbation series in Eq. (2-39a) such that;

$$\hat{\varepsilon}_0\left(i\frac{\partial}{\partial t}\right) \approx \hat{\varepsilon}_{\mathrm{Re}}\left(i\frac{\partial}{\partial t_0}\right) + i\mu\hat{\varepsilon}_{\mathrm{Im}}\left(i\frac{\partial}{\partial t_0}\right) + i\mu\frac{\partial}{\partial t_1}\hat{\varepsilon}'_{\mathrm{Re}}\left(i\frac{\partial}{\partial t_0}\right).$$

Hence, the Eq. (2-39a) has been combined with Eq. (2-39b) and then the completed form of complex dielectric function of the structure can be expressed as:

$$\hat{\varepsilon}\left(z_0, i\frac{\partial}{\partial t}\right) = \hat{\varepsilon}_{\mathrm{Re}}\left(i\frac{\partial}{\partial t_0}\right) + i\mu\hat{\varepsilon}_{\mathrm{Im}}\left(i\frac{\partial}{\partial t_0}\right) + i\mu\frac{\partial}{\partial t_1}\hat{\varepsilon}'_{\mathrm{Re}}\left(i\frac{\partial}{\partial t_0}\right) + \mu\sum_{\substack{\ell=-\infty \\ \ell\neq 0}}^{\infty}\Delta\hat{\varepsilon}_\ell e^{i\ell\frac{2\pi}{\Lambda}z_0}, \qquad (2\text{-}40)$$

where the delta symbol are added to distinguish between the zeroth-order Fourier coefficient $\hat{\varepsilon}_0\left(z_0, \frac{\partial}{\partial t}\right)$ and the higher-order Fourier coefficient terms, respectively. The higher-order Fourier coefficient term $\Delta\hat{\varepsilon}_\ell$ has been showed the modulated dielectric function of the PBG structure.

Now, let consider the nonlinear polarization term P_{NL} in Eq. (2-39). This term is described as:

$$P_{NL} = \mu\chi^{(3)}E^3(z,t), \qquad (2\text{-}41)$$

where $\chi^{(3)}$ is the third-order nonlinearity. The third-order nonlinearity can be expanded in Fourier series like the complex dielectric function because this value will be modulated by the periodicity of PBG structure. Its Fourier series is given by:

$$\chi^{(3)}(z_0,t) = \sum_{\ell=-\infty}^{\infty}\chi_\ell^{(3)}e^{i\ell\frac{2\pi}{\Lambda}z_0}. \qquad (2\text{-}42)$$

Similarly, the electric field is also expanded in powers of the perturbation parameter as:

$$E(z,t) = E_0 + \mu E_1 + \mu^2 E_2 + \ldots, \qquad (2\text{-}43a)$$

and then expand E^3 to the first-order accuracy as:

$$E^3(z,t) \approx (E_0 + \mu E_1) = E_0^3 + 3\mu E_0^2 E_1 + 3\mu^2 E_0 E_1^2 + \mu^3 E_1^3. \qquad (2\text{-}43b)$$

Now, the perturbation series in Eq. (2-35), (2-37), and Eq. (2-40) to (2-43) are substituted into the wave equation in Eq. (2-29) to perturb this equation by using MSM. Then we obtain:

$$\left(\frac{\partial^2}{\partial z_0^2}+2\mu\frac{\partial}{\partial z_0}\frac{\partial}{\partial z_1}\right)(E_0+\mu E_1)$$
$$-\frac{1}{c^2}\left[\hat{\varepsilon}_{\mathrm{Re}}\left(i\frac{\partial}{\partial t_0}\right)+i\mu\hat{\varepsilon}_{\mathrm{Im}}\left(i\frac{\partial}{\partial t_0}\right)+i\mu\frac{\partial}{\partial t_1}\hat{\varepsilon}'_{\mathrm{Re}}\left(i\frac{\partial}{\partial t_0}\right)+\mu\sum_{\substack{\ell=-\infty\\ \ell\neq 0}}^{\infty}\Delta\hat{\varepsilon}_\ell e^{i\ell\frac{2\pi}{\Lambda}z_0}\right]\left(\frac{\partial^2}{\partial t_0^2}+2\mu\frac{\partial}{\partial t_0}\frac{\partial}{\partial t_1}\right)(E_0+\mu E_1)$$
$$=\frac{4\pi}{c^2}\left(\frac{\partial^2}{\partial t_0^2}+2\mu\frac{\partial}{\partial t_0}\frac{\partial}{\partial t_1}\right)\left(\mu\sum_{\ell=-\infty}^{\infty}\chi_\ell^{(3)}e^{i\ell\frac{2\pi}{\Lambda}z_0}\right)\left(E_0^3+3\mu E_0^2E_1\right).$$

(2-44)

After that, Eq. (2-44) have been expanded and then neglected any terms that contain μ^2 or higher-order because of minuscule contribution for this analysis. The result of expanding of Eq. (2-44) is:

$$\frac{\partial^2E_0}{\partial z_0^2}+\mu\frac{\partial^2E_1}{\partial z_0^2}+2\mu\frac{\partial}{\partial z_0}\frac{\partial E_0}{\partial z_1}$$
$$-\frac{1}{c^2}\left[\hat{\varepsilon}_{\mathrm{Re}}\left(i\frac{\partial}{\partial t_0}\right)\frac{\partial^2E_0}{\partial t_0^2}+i\mu\hat{\varepsilon}_{\mathrm{Im}}\left(i\frac{\partial}{\partial t_0}\right)\frac{\partial^2E_0}{\partial t_{0\ 0}^2}+i\mu\frac{\partial}{\partial t_1}\hat{\varepsilon}'_{\mathrm{Re}}\left(i\frac{\partial}{\partial t_0}\right)\frac{\partial^2E_0}{\partial t_0^2}+\mu\sum_{\substack{\ell=-\infty\\ \ell\neq 0}}^{\infty}\Delta\hat{\varepsilon}_\ell\frac{\partial^2E_0}{\partial t_0^2}e^{i\ell\frac{2\pi}{\Lambda}z_0}\right.$$
$$\left.+\hat{\varepsilon}_{\mathrm{Re}}\left(i\frac{\partial}{\partial t_0}\right)2\mu\frac{\partial}{\partial t_0}\frac{\partial E_0}{\partial t_1}+\hat{\varepsilon}_{\mathrm{Re}}\left(i\frac{\partial}{\partial t_0}\right)\mu\frac{\partial^2E_1}{\partial t_0^2}\right]$$
$$=\frac{4\pi}{c^2}\left(\frac{\partial^2}{\partial t_0^2}\mu\sum_{\ell=-\infty}^{\infty}\chi_\ell^{(3)}e^{i\ell\frac{2\pi}{\Lambda}z_0}E_0^3\right).$$

(2-45)

Now, each terms that contain parameter μ^0 have been grouped together. Then the first grouped equation is shown as:

$$\frac{\partial^2E_0}{\partial z_0^2}-\frac{1}{c^2}\left[\hat{\varepsilon}_r\left(i\frac{\partial}{\partial t_0}\right)\frac{\partial^2E_0}{\partial t_0^2}\right]=0,$$

(2-46a)

Similarly, the terms that contain parameter μ^1 have been grouped together as well. The second grouped equation is shown as:

$$\frac{\partial^2 E_1}{\partial z_0^2}-\frac{1}{c^2}\hat{\varepsilon}_{\mathrm{Re}}\left(i\frac{\partial}{\partial t_0}\right)\frac{\partial^2 E_1}{\partial t_0^2}$$
$$-\frac{i}{c^2}\hat{\varepsilon}_{\mathrm{Im}}\left(i\frac{\partial}{\partial t_0}\right)\frac{\partial^2 E_0}{\partial t_0^2}+2\frac{\partial}{\partial z_0}\frac{\partial E_0}{\partial z_1}-\frac{2}{c^2}\hat{\varepsilon}_{\mathrm{Re}}\left(i\frac{\partial}{\partial t_0}\right)\frac{\partial}{\partial t_0}\frac{\partial E_0}{\partial t_1} \tag{2-46b}$$
$$-\frac{i}{c^2}\hat{\varepsilon}'_{\mathrm{Re}}\left(i\frac{\partial}{\partial t_0}\right)\frac{\partial}{\partial t_1}\frac{\partial^2 E_0}{\partial t_0^2}-\frac{1}{c^2}\sum_{\substack{\ell=-\infty\\ \ell\neq 0}}^{\infty}\Delta\hat{\varepsilon}_\ell\frac{\partial^2 E_0}{\partial t_0^2}e^{i\ell\frac{2\pi}{\Lambda}z_0}=\frac{4\pi}{c^2}\left(\frac{\partial^2}{\partial t_0^2}\sum_{\ell=-\infty}^{\infty}\chi_\ell^{(3)}e^{i\ell\frac{2\pi}{\Lambda}z_0}E_0^3\right).$$

Next step, let L be an operator defined as:

$$L=L_0+\mu L_1+\mu^2 L_2+\ldots, \tag{2-47}$$

and then let L be an operator on the electric field, then we obtain:

$$\begin{aligned}LE&=(L_0+\mu L_1+\mu^2 L_2+\ldots)(E_0+\mu E_1+\mu^2 E_2+\ldots)\\&=L_0E_0+\mu(L_0E_1+L_1E_0)+\ldots.\end{aligned} \tag{2-48}$$

Now, the terms with μ^0 in Eq. (2-48) similar to Eq. (2-46a). Here, the lowest order equation $(O(1))$ is obtained as:

$$L_0E_0=\left[\frac{\partial^2}{\partial z_0^2}-\frac{1}{c^2}\left[\hat{\varepsilon}_{\mathrm{Re}}\left(i\frac{\partial}{\partial t_0}\right)\frac{\partial^2}{\partial t_0^2}\right]\right]E_0=0. \tag{2-49}$$

Similarly, the term with μ^0 in Eq. (2-48) similar to Eq. (2-46b). For convenient, the secular terms in perturbation series are removed by setting $L_0E_1+L_1E_0=0$. Since, Eq. (2-49) is a classical wave equation with nonlinear source term, the solution of E_0 could be easily obtained. So, we can let the relation $L_0E_1=L_1E_0=0$. Now, the first-order equation $(O(\mu))$ is obtained as:

$$\begin{aligned}L_1E_0=\Bigg\{&2\frac{\partial}{\partial z_0}\frac{\partial}{\partial z_1}-\frac{i}{c^2}\hat{\varepsilon}_{\mathrm{Im}}\left(i\frac{\partial}{\partial t_0}\right)\frac{\partial^2}{\partial t_0^2}-\frac{2}{c^2}\hat{\varepsilon}_{\mathrm{Re}}\left(i\frac{\partial}{\partial t_0}\right)\frac{\partial}{\partial t_0}\frac{\partial}{\partial t_1}\\&-\frac{i}{c^2}\hat{\varepsilon}'_{\mathrm{Re}}\left(i\frac{\partial}{\partial t_0}\right)\frac{\partial}{\partial t_1}\frac{\partial^2}{\partial t_0^2}-\frac{1}{c^2}\sum_{\substack{\ell=-\infty\\ \ell\neq 0}}^{\infty}\Delta\hat{\varepsilon}_\ell\frac{\partial^2}{\partial t_0^2}e^{i\ell\frac{2\pi}{\Lambda}z_0}\Bigg\}E_0=\frac{4\pi}{c^2}\left(\frac{\partial^2}{\partial t_0^2}\sum_{\ell=-\infty}^{\infty}\chi_\ell^{(3)}e^{i\ell\frac{2\pi}{\Lambda}z_0}E_0^3\right).\end{aligned} \tag{2-50}$$

The equation (2-50) could be solve analytically for obtaining the plane wave solution that corresponds to the considering nonlinear effect e.g. optical parametric amplification in the chapter 3 and third-

harmonic generation in the chapter 4. After that, the solution of E_0 is substituted into Eq. (2-50) for deriving the set of coupled-mode equations of the nonlinear effect. Finally, the obtained coupled-mode equations would be solved numerically by using the split-step Fourier method. The detail of split-step Fourier method would be shown in the section 2.3 and the numerical results for optical parametric amplification and third-harmonic generation would be shown in the chapter 3 and 4 respectively.

2.3 Split-step Fourier method

The coupled-mode equations, which have been obtained from MSM procedure, for optical parametric amplification and third-harmonic are difficult to have an analytical method. Since, the equations are maintain many nonlinear terms and hard to be solved analytically by ordinary methods. Hence, the numerical methods will play an important role and be a good option to approximate the general solution for these problems. Numerical methods may vary in terms of the demand of computational power and time, memory space, storage space, and coding complexity etc. With the progressive advancement of the computer in the present, the nonlinear differential equations can be numerically computed at high speeds. Some numerical techniques and methods that need enormous memory and waste the computational time are not the good ways in efficient computing. Therefore, a key factor which has been considered when applying a numerical method is that it has to be user friendly in terms of coding with the given computational power and time.

Recently, many numerical methods have been introduced to model the physical phenomena e.g. heat transfer, fluid dynamics, and electromagnetic scattering. For example, the finite difference method, finite element method [42], finite-difference time-domain method [43], and split-step Fourier method [31]. Each method has its own advantage and compatibility with different physical problems. For example, the finite difference method can easily be implemented with the finite difference representation of heat or wave equations; the finite element method is a good option for modeling heat transfer, stress and strain in complex structure, and fluid diffusion; the finite-difference time-domain method is usually used for computational electrodynamics with cover a wide frequency range with a single simulation run, and treat nonlinear material properties in a natural way [44]; and the split-step Fourier method is computational technique, which has been used in optical communication system, with the introduction of speedy algorithm of Fast Fourier Transform

(FFT). Here, we see that the finite-difference time domain method being used to provide solution in both space and time and can be applied to nonlinear problems in optical waveguides [45-46] and photonic crystal structures [47]. This method is perhaps the most accurate, but it often suffer from huge computational requirements in both memory and time that limit its range of practical applicability in the design actual structures. Similarly, the split-step Fourier method has been usually used to model the light propagation in the optical communication devices such the graded-index fibers [48]. But in this work, we have been looking for a numerical method that allows us to model the nonlinear optical phenomena in the one-dimensional photonic band-gap structures, easily code in MATLAB language, and run computing routine on laptop or personal computers.

In preliminary, we need to understand the principle of the split-step Fourier method. We begin with considering a first-order differential equation which can be written in the form, given as:

$$\frac{\partial \psi(t)}{\partial t} = \left[\hat{S} + \hat{D}\right](t)\psi(t), \tag{2-51}$$

where ψ, $\hat{S}$, and $\hat{D}$ are function of time (t), and $\hat{S}$ and $\hat{D}$ are the operators which operate on ψ [31, 58-59]. The Eq. (2-51) is solved, and the result becomes:

$$\psi(t_1) = \psi(t) + \int_t^{t_1}\left[\hat{S} + \hat{D}\right](t')\psi(t')dt'$$

$$\psi(t_1) = \psi(t) + \int_t^{t_1}\left[\hat{S} + \hat{D}\right](t')\psi(t')dt' + \int_t^{t_1}\int_t^{t'}\left[\hat{S} + \hat{D}\right](t')\left[\hat{S} + \hat{D}\right](t'')\psi(t'')dt'.$$

This process has been continued and the general result is:

$$\psi(t_1) = \mathbf{T}\left(\exp\left(\int_t^{t_1}\left[\hat{S} + \hat{D}\right]dt'\right)\right)\psi(t),$$

where there are $\mathbf{T}$ orders product of the operator $\left[\hat{S} + \hat{D}\right](t')$. For the first-order product $\mathbf{T} = 1$ and $t_1 = t + \Delta t$, the first-order result become:

$$\psi(t + \Delta t) = \exp\left[(\hat{S} + \hat{D})\Delta t\right]\psi(t). \tag{2-52}$$

Eq. (2-52) inform us that given an input $\psi(t)$, and knowing the operators $\hat{S}$ and $\hat{D}$, this equation can be computed for $\psi(t + \Delta t)$ with a small incremental time step Δt. Note that $\hat{S}$ is a propagation operator, and $\hat{D}$

is a diffraction operator, such that $\hat{S}$ causes the optical wave to move forward or backward when going through the optical medium and $\hat{D}$ causes the wave reshaping. In addition, note that small Δt give the better computing accuracy.

Then, Eq. (2-52) could be rewritten in the form of split-step operators, where the exponential in this equation is split into multiple exponentials, such that:

$$\psi(t+\Delta t) = \exp\left[\hat{S}\frac{\Delta t}{2}\right]\exp\left[\hat{D}\Delta t\right]\exp\left[\hat{S}\frac{\Delta t}{2}\right]\psi(t). \tag{2-53}$$

This expression is accurate to the second-order in Δt. Clarity, if the term $\exp(\hat{S})$, $\exp(\hat{D})$, and $\exp(\hat{D}+\hat{S})$ could be expanded by using power series, and then they are given by:

$$\exp\left[\hat{S}\Delta t\right] = I + \hat{S}\Delta t + \frac{\hat{S}^2\Delta t^2}{2!} + \frac{\hat{S}^3\Delta t^3}{3!} + \ldots, \tag{2-54a}$$

$$\exp\left[\hat{D}\Delta t\right] = I + \hat{D}\Delta t + \frac{\hat{D}^2\Delta t^2}{2!} + \frac{\hat{D}^3\Delta t^3}{3!} + \ldots, \tag{2-54b}$$

and

$$\begin{aligned}\exp\left[(\hat{S}+\hat{D})\Delta t\right] &= I + (\hat{S}+\hat{D})\Delta t + \frac{(\hat{S}+\hat{D})^2\Delta t^2}{2!} + \frac{(\hat{S}+\hat{D})^3\Delta t^3}{3!} + \ldots \\ &= I + (\hat{S}+\hat{D})\Delta t + \left(\frac{\hat{S}^2+\hat{S}\hat{D}+\hat{D}\hat{S}+\hat{D}^2}{2!}\right)\Delta t^2 + \ldots.\end{aligned} \tag{2-54c}$$

From the split-step approximation, we obtain:

$$\begin{aligned}\psi(t+\Delta t) &= \left(I + \frac{\hat{S}\Delta t}{2} + \frac{1}{2}\frac{\hat{S}^2\Delta t^2}{2^2} + \ldots\right)\left(I + \hat{D}\Delta t + \frac{\hat{D}^2\Delta t^2}{2} + \ldots\right)\left(I + \frac{\hat{S}\Delta t}{2} + \frac{1}{2}\frac{\hat{S}^2\Delta t^2}{2^2} + \ldots\right)\psi(t) \\ &\approx \left[I + (\hat{S}+\hat{D})\Delta t + \left(\frac{\hat{S}^2+\hat{S}\hat{D}+\hat{D}\hat{S}+\hat{D}^2}{2!}\right)\Delta t^2 + \ldots\right]\psi(t).\end{aligned} \tag{2-54d}$$

Note that this is equivalent at order Δt^2 to the expansion in split-step approximation. The important advantage of the split-step Fourier method is that the $\hat{S}$ operator step forward half time step, while $\hat{D}$ operator step forward one full time step, and finally the $\hat{S}$ operator step forward the remaining half time step in one computational time step. Hence, for the $\hat{S}$ operator, it seems like we pick a smaller time step of $\Delta t/2$.

Note that if $\hat{S}$ and $\hat{D}$ are non-commuting matrices, the approximation may not be exact. However, if $\hat{S}$ and $\hat{D}$ are diagonal matrices, they will always commute and the approximation becomes exact. More precisely, the approximation is also exact if $\hat{S}$ and $\hat{D}$ commute with the commutator $[\hat{S},\hat{D}]$.

Since, this numerical method is based on the Fourier transform, so the Fourier properties can give insight to the split-step Fourier method, given as:

$$\mathbb{F}^{-1}\{\psi(\varpi)e^{-i\varpi_s x_s}\} = \psi(x - x_s), \tag{2-55a}$$

and

$$\mathbb{F}\{\psi(x)H(x)\} = \psi(\varpi) \otimes H(\varpi), \tag{2-55b}$$

where x is the spatial variable, ϖ is the frequency variable, x_s and ϖ_s are the respective spatial shift and phase shift, and $\mathbb{F}$ and $\mathbb{F}^{-1}$ are the Fourier transform and inverse Fourier transform operations, respectively. According to Eq. (2-54a), if $\psi(x)$ is Fourier transformed and multiplied by a phase shift $e^{-i\varpi_s x_s}$. This result shows a forward spatial shift after the inverse Fourier transform operation, i.e. causing the wave to move forward. According to Eq. (2-54b), the multiplication of $\psi(x)$ and $H(x)$ in spatial domain correspond to the convolution between $\psi(\varpi)$ and $H(\varpi)$ in the frequency domain, either way, the multiplication or convolution is going to create a new function that is a byproduct of multiplying or convolving ψ and H. Therefore, the wave could be reshaped and diffracted.

Chapter 3

Optical parametric amplification in PBG structure

3.1 Background theory of optical parametric amplification

The third-order parametric processes generally concern with the interaction among four optical waves and include the phenomena such as third-harmonic generation, four-wave mixing, and optical parametric amplification [60-61, 63]. Especially, optical parametric amplification (OPA) has been widely studied in optical fibers and in investigation of the wavelength and dense wavelength division multiplexing (WDM and DWDM) systems [62]. The OPA phenomenon is really a photon-photon scattering process, during which two photons from a high intensity beam, called pump beam, scatter through third-order nonlinearity of a medium to generate two correlated photons, called signal and idler photons, respectively [62]. Its main features could be understood by considering the third-order polarization term, which is given as [60-63]:

$$\mathbf{P}_{NL} = \varepsilon_0 \chi^{(3)} \mathbf{EEE}, \tag{3-1}$$

where $\mathbf{E}$ is the electric field and $\mathbf{P}_{NL}$ is the induced nonlinear polarization. Four optical waves oscillating at frequencies ω_1, ω_2, ω_3, and ω_4 are considered in this case and their polarizations are assumed to be linear polarization along the x axis. The total electric field could be written as:

$$\mathbf{E} = \left\{ \sum_{j=1}^{4} \frac{1}{2} E_j \exp[i(k_j z - \omega_j t)] + c.c. \right\} \hat{\mathbf{x}}, \tag{3-2}$$

where $k_j = n_j \omega_j / c$, n_j is the refractive index, $c = 3 \times 10^8$ m/s is the light speed in vacuum, and all four waves are assumed to be propagating in z direction. After substituting Eq. (3-2) into Eq. (3-1), the nonlinear polarization could be expressed as:

$$\mathbf{P}_{NL} = \left\{ \sum_{j=1}^{4} P_j \exp[i(k_j z - \omega_j t)] + c.c. \right\} \hat{\mathbf{x}}. \tag{3-3}$$

We find that P_j for j = 1, 2, 3, and 4 consists of a large number of terms involving the products of three electric fields. For example, P_4 could be expressed as:

$$P_4 = \frac{3}{8}\varepsilon_0\chi^{(3)}\{(2|E_1|^2 + 2|E_2|^2 + 2|E_3|^2 + |E_4|^2)E_4 + 2E_1E_2E_3^* \exp[(k_1 + k_2 - k_3 - k_4)z - (\omega_1 + \omega_2 - \omega_3 - \omega_4)t] + ...\}. \quad (3\text{-}4)$$

The term proportion to E_4 in Eq. (3-4) is responsible for self-phase modulation (SPM) and cross-phase modulation (XPM) effects, respectively. The last remaining term is responsible for OPA phenomenon. Efficient OPA occurs only if the relative phase of exponential term nearly vanish. In quantum mechanical view point, the two photons at frequencies ω_1 and ω_2 are annihilated with a simultaneous creation of two photons at frequencies ω_3 and ω_4. The conservation of four photon energy for this case can be expressed as:

$$\hbar\omega_1 + \hbar\omega_2 = \hbar\omega_3 + \hbar\omega_4,$$

$$\omega_1 + \omega_2 = \omega_3 + \omega_4. \quad (3\text{-}5)$$

The phase-matching requirement for this process to occur is that $\Delta k_{OPA} = 0$, where

$$\Delta k_{OPA} = k_1 + k_2 - k_3 - k_4 = (n_1\omega_1 + n_2\omega_2 - n_3\omega_3 - n_4\omega_4)/c. \quad (3\text{-}6)$$

In the particular case in which $\omega_1 = \omega_2$, this is a partially degenerate case of OPA and has been widely studied in optical fibers [62-63]. Now, the Eq. (3-5) and Eq. (3-6) could be expressed for the partially degenerate OPA process as below

$$2\omega_1 = \omega_3 + \omega_4, \quad (3\text{-}7)$$

and then

$$\Delta k_{OPA} = 2k_1 - k_3 - k_4 = (2n_1\omega_1 - n_3\omega_3 - n_4\omega_4)/c. \quad (3\text{-}8)$$

According to Eq. (3-7), the frequencies ω_1, ω_3, and ω_4 represent the frequency of pump, signal, and idler waves, respectively. The wavelength of signal and idler photons are close to pump wavelengths. The quantum mechanical picture and frequency spectrum of the partial degenerate OPA phenomenon are shown in Fig. 3.1(a) and (b), respectively.

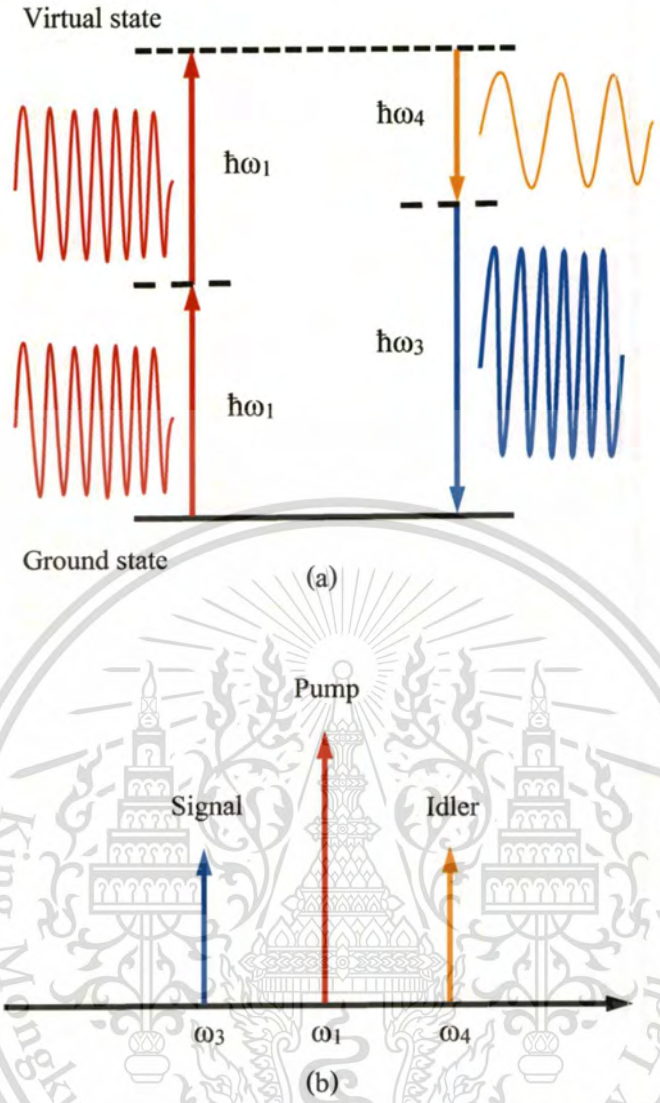

Figure 3.1. (a) Geometry of photon interaction of the OPA in which the input signal wave is amplified and an idler wave is generated by the breakup of two degenerate pump wave. (b) The frequency spectrum of OPA.

3.2 The derivation of coupled-mode equations for optical parametric amplification

According to the Eq. (2-45), the plane-wave solution for this equation which corresponds to OPA process and has the form of classical linear wave equation. This plane-wave solution can be expressed as the sum of electric field amplitudes in forward- and backward-direction with a frequency ω_1, ω_3, and ω_4. The solution is:

$$E_0 = A_{f1}e^{i(k_1 z_0 - \omega_1 t_0)} + A_{b1}e^{-i(k_1 z_0 + \omega_1 t_0)} + A_{f3}e^{i(k_3 z_0 - \omega_3 t_0)} + A_{b3}e^{-i(k_3 z_0 + \omega_3 t_0)} + A_{f4}e^{i(k_4 z_0 - \omega_4 t_0)} + A_{b4}e^{-i(k_4 z_0 + \omega_4 t_0)} + c.c., \quad (3\text{-}9)$$

where the amplitudes; $A_{f1,3,4} = A_{f1,3,4}(z_1, t_1)$ and $A_{b1,3,4} = A_{b1,3,4}(z_1, t_1)$, the subscript f and b refer to the forward- and backward-direction, and the subscript 1, 3, and 4 refer to pump, signal, and idler waves, respectively. In addition, their wave numbers are obtained from chromatic dispersion properties of a homogeneous medium, so that $k_1^2 = \omega_1^2 \hat{\varepsilon}_{\mathrm{Re}}(\omega_1)/c^2$, $k_3^2 = \omega_3^2 \hat{\varepsilon}_{\mathrm{Re}}(\omega_3)/c^2$, and $k_4^2 = \omega_4^2 \hat{\varepsilon}_{\mathrm{Re}}(\omega_4)/c^2$. In this analysis the phase mismatch is also treated as small i.e. $\mu\Delta k_{OPA} = 2k_1 - k_3 - k_4$. Note that $\mu\Delta k_{OPA} z_0 = \Delta k_{OPA} z_1$. The large phase mismatch has been avoided because that would lead to an asymptotic regime beyond four-wave mixing.

Now, the first-order equation as shown in Eq. (2-46) is considered. The right side of this equation is consisted of the E_0^3 term. As we see in Eq. (3-4), the expansion of E_0^3 is absolutely needed. Now, for compact notation, let

$$\mathrm{F}_1 = A_{f1}e^{i(k_1 z_0 - \omega_1 t_0)}, \mathrm{B}_1 = A_{b1}e^{-i(k_1 z_0 + \omega_1 t_0)},$$

$$\mathrm{F}_3 = A_{f3}e^{i(k_3 z_0 - \omega_3 t_0)}, \mathrm{B}_3 = A_{b3}e^{-i(k_3 z_0 + \omega_3 t_0)},$$

$$\mathrm{F}_4 = A_{f4}e^{i(k_4 z_0 - \omega_4 t_0)}, \mathrm{B}_4 = A_{b4}e^{-i(k_4 z_0 + \omega_4 t_0)}.$$

Here, we expand $E_0^3 = (\mathrm{F}_1 + \mathrm{B}_1 + \mathrm{F}_3 + \mathrm{B}_3 + \mathrm{F}_4 + \mathrm{B}_4 + \mathrm{F}_1^* + \mathrm{B}_1^* + \mathrm{F}_3^* + \mathrm{B}_3^* + \mathrm{F}_4^* + \mathrm{B}_4^*)^3$, and we will obtain 1728 terms but only 132 of them are useful because of their phases correspond to the wave-vector mismatch of OPA phenomenon. The expansion of useful terms is shown in Table 3.1, 3.2, and 3.3 where each terms are included the corresponding phase information.

Table 3.1: The expansion of E_0^3 for ω_1 component

Multiplicity	Term	Phase
1	$F_1F_1^*F_1$	$\exp[i(k_1z_0-\omega_1t_0)]$
2	$B_1B_1^*F_1$	$\exp[i(k_1z_0-\omega_1t_0)]$
2	$F_3F_3^*F_1$	$\exp[i(k_1z_0-\omega_1t_0)]$
2	$B_3B_3^*F_1$	$\exp[i(k_1z_0-\omega_1t_0)]$
2	$F_4F_4^*F_1$	$\exp[i(k_1z_0-\omega_1t_0)]$
2	$B_4B_4^*F_1$	$\exp[i(k_1z_0-\omega_1t_0)]$
2	$F_1F_1^*B_1$	$\exp[-i(k_1z_0+\omega_1t_0)]$
1	$B_1B_1^*B_1$	$\exp[-i(k_1z_0+\omega_1t_0)]$
2	$F_3F_3^*B_1$	$\exp[-i(k_1z_0+\omega_1t_0)]$
2	$B_3B_3^*B_1$	$\exp[-i(k_1z_0+\omega_1t_0)]$
2	$F_4F_4^*B_1$	$\exp[-i(k_1z_0+\omega_1t_0)]$
2	$B_4B_4^*B_1$	$\exp[-i(k_1z_0+\omega_1t_0)]$
1	$F_1B_1^*F_1$	$\exp[i(3k_1z_0-\omega_1t_0)]$
1	$B_1F_1^*B_1$	$\exp[-i(3k_1z_0+\omega_1t_0)]$
2	$F_3B_3^*F_1$	$\exp[i((2k_3+k_1)z_0-\omega_1t_0)]$
2	$F_3B_3^*B_1$	$\exp[i((2k_3-k_1)z_0-\omega_1t_0)]$
2	$F_4B_4^*F_1$	$\exp[i((2k_4+k_1)z_0-\omega_1t_0)]$
2	$F_4B_4^*B_1$	$\exp[i((2k_4-k_1)z_0-\omega_1t_0)]$
2	$B_3F_3^*F_1$	$\exp[-i((2k_3-k_1)z_0+\omega_1t_0)]$
2	$B_3F_3^*B_1$	$\exp[-i((2k_3+k_1)z_0+\omega_1t_0)]$
2	$B_4F_4^*F_1$	$\exp[-i((2k_4-k_1)z_0+\omega_1t_0)]$
2	$B_4F_4^*B_1$	$\exp[-i((2k_4+k_1)z_0+\omega_1t_0)]$
2	$F_3F_1^*F_4$	$\exp[i((k_3+k_4-k_1)z_0-\omega_1t_0)]$
2	$B_3B_1^*B_4$	$\exp[-i((k_3+k_4-k_1)z_0+\omega_1t_0)]$

Table 3.2: The expansion of E_0^3 for ω_3 component

Multiplicity	Term	Phase
2	$F_1F_1^*F_3$	$\exp[i(k_3z_0-\omega_3t_0)]$
2	$B_1B_1^*F_3$	$\exp[i(k_3z_0-\omega_3t_0)]$
1	$F_3F_3^*F_3$	$\exp[i(k_3z_0-\omega_3t_0)]$
2	$B_3B_3^*F_3$	$\exp[i(k_3z_0-\omega_3t_0)]$
2	$F_4F_4^*F_3$	$\exp[i(k_3z_0-\omega_3t_0)]$
2	$B_4B_4^*F_3$	$\exp[i(k_3z_0-\omega_3t_0)]$
2	$F_1F_1^*B_3$	$\exp[-i(k_3z_0+\omega_3t_0)]$
2	$B_1B_1^*B_3$	$\exp[-i(k_3z_0+\omega_3t_0)]$
2	$F_3F_3^*B_3$	$\exp[-i(k_3z_0+\omega_3t_0)]$
1	$B_3B_3^*B_3$	$\exp[-i(k_3z_0+\omega_3t_0)]$
2	$F_4F_4^*B_3$	$\exp[-i(k_3z_0+\omega_3t_0)]$
2	$B_4B_4^*B_3$	$\exp[-i(k_3z_0+\omega_3t_0)]$
2	$F_1B_1^*F_3$	$\exp[i((2k_1+k_3)z_0-\omega_3t_0)]$
2	$B_1F_1^*B_3$	$\exp[-i((2k_1+k_3)z_0+\omega_3t_0)]$
1	$F_3B_3^*F_3$	$\exp[i(3k_3z_0-\omega_3t_0)]$
2	$F_1B_1^*B_3$	$\exp[i((2k_1-k_3)z_0-\omega_3t_0)]$
2	$F_4B_4^*F_3$	$\exp[i((2k_4+k_3)z_0-\omega_3t_0)]$
2	$F_4B_4^*B_3$	$\exp[i((2k_4-k_3)z_0-\omega_3t_0)]$
2	$B_1F_1^*F_3$	$\exp[-i(2k_1-k_3)z_0+\omega_3t_0)]$
1	$B_3F_3^*B_3$	$\exp[-i(3k_3z_0+\omega_3t_0)]$
2	$B_4F_4^*F_3$	$\exp[-i(2k_4-k_3)z_0+\omega_3t_0)]$
2	$B_4F_4^*B_3$	$\exp[-i(2k_4+k_3)z_0+\omega_3t_0)]$
2	$F_1F_4^*F_1$	$\exp[i(2k_1-k_4)z_0-\omega_3t_0)]$
2	$B_1B_4^*B_1$	$\exp[-i(2k_1-k_4)z_0+\omega_3t_0)]$

Table 3.3: The expansion of E_0^3 for ω_4 component

Multiplicity	Term	Phase
2	$F_1F_1^*F_4$	$\exp[i(k_4z_0-\omega_4t_0)]$
2	$B_1B_1^*F_4$	$\exp[i(k_4z_0-\omega_4t_0)]$
2	$F_3F_3^*F_4$	$\exp[i(k_4z_0-\omega_4t_0)]$
2	$B_3B_3^*F_4$	$\exp[i(k_4z_0-\omega_4t_0)]$
1	$F_4F_4^*F_4$	$\exp[i(k_4z_0-\omega_4t_0)]$
2	$B_4B_4^*F_4$	$\exp[i(k_4z_0-\omega_4t_0)]$
2	$F_1F_1^*B_4$	$\exp[-i(k_4z_0+\omega_4t_0)]$
2	$B_1B_1^*B_4$	$\exp[-i(k_4z_0+\omega_4t_0)]$
2	$F_3F_3^*B_4$	$\exp[-i(k_4z_0+\omega_4t_0)]$
2	$B_3B_3^*B_4$	$\exp[-i(k_4z_0+\omega_4t_0)]$
2	$F_4F_4^*B_4$	$\exp[-i(k_4z_0+\omega_4t_0)]$
1	$B_4B_4^*B_4$	$\exp[-i(k_4z_0+\omega_4t_0)]$
2	$F_1B_1^*F_4$	$\exp[i((2k_1+k_4)z_0-\omega_4t_0)]$
2	$B_1F_1^*B_4$	$\exp[-i((2k_1+k_4)z_0+\omega_4t_0)]$
1	$F_4B_4^*F_4$	$\exp[i(3k_4z_0-\omega_4t_0)]$
2	$F_1B_1^*B_4$	$\exp[i((2k_1-k_4)z_0-\omega_4t_0)]$
2	$F_3B_3^*F_4$	$\exp[i((2k_1+k_4)z_0-\omega_4t_0)]$
2	$F_3B_3^*B_4$	$\exp[i((2k_3-k_4)z_0-\omega_4t_0)]$
2	$B_1F_1^*F_4$	$\exp[-i(2k_1-k_4)z_0+\omega_4t_0)]$
2	$B_3F_3^*B_4$	$\exp[-i((2k_3+k_4)z_0+\omega_4t_0)]$
2	$B_3F_3^*F_4$	$\exp[-i(2k_3-k_4)z_0+\omega_4t_0)]$
1	$B_4F_4^*B_4$	$\exp[-i(3k_4z_0+\omega_4t_0)]$
2	$F_1F_3^*F_1$	$\exp[i(2k_1-k_3)z_0-\omega_4t_0)]$
2	$B_1B_3^*B_1$	$\exp[-i(2k_1-k_3)z_0+\omega_4t_0)]$

The interested term are separated into three tables for terms of pump ω_1 component, terms of signal ω_3 component and terms of idler ω_4 component. After that, the interested terms are substituted into the Eq. (2-46) for all frequency components. First, we obtain the equation for pump ω_1 component:

$$\left[2\frac{\partial^2}{\partial z_0 \partial z_1}-\frac{i}{c^2}\hat{\varepsilon}_{\mathrm{Im}}\left(i\frac{\partial}{\partial t_0}\right)\frac{\partial^2}{\partial t_0^2}-\frac{2}{c^2}\hat{\varepsilon}_{\mathrm{Re}}\left(i\frac{\partial}{\partial t_0}\right)\frac{\partial^2}{\partial t_0 \partial t_1}\right.$$
$$\left.-\frac{i}{c^2}\frac{\partial^2}{\partial t_0^2}\hat{\varepsilon}'_{\mathrm{Re}}\left(i\frac{\partial}{\partial t_0}\right)\frac{\partial}{\partial t_1}-\frac{1}{c^2}\sum_{\substack{\ell=-\infty \\ \ell\neq 0}}^{\infty}\Delta\hat{\varepsilon}_\ell\frac{\partial^2}{\partial t_0^2}e^{i\ell\frac{2\pi}{\Lambda}z_0}\right](\mathrm{F_1}+\mathrm{B_1})$$
$$=\frac{4\pi}{c^2}\left(\frac{\partial^2}{\partial t_0^2}\sum_{\ell=-\infty}^{\infty}\chi_\ell^{(3)}e^{i\ell\frac{2\pi}{\Lambda}z_0}\right)(\mathrm{F_1F_1^*F_1}+\mathrm{B_1B_1^*F_1}+\mathrm{F_3F_3^*F_1}+\mathrm{B_3B_3^*F_1}+\mathrm{F_4F_4^*F_1}+\mathrm{B_4B_4^*F_1}$$
$$+\mathrm{F_1F_1^*B_1}+\mathrm{B_1B_1^*B_1}+\mathrm{F_3F_3^*B_1}+\mathrm{B_3B_3^*B_1}+\mathrm{F_4F_4^*B_1}+\mathrm{B_4B_4^*B_1}$$
$$+\mathrm{F_1B_1^*F_1}+\mathrm{B_1F_1^*B_1}+\mathrm{F_3B_3^*F_1}+\mathrm{F_3B_3^*B_1}+\mathrm{F_4B_4^*F_1}+\mathrm{F_4B_4^*B_1}$$
$$+\mathrm{B_3F_3^*F_1}+\mathrm{B_3F_3^*B_1}+\mathrm{B_4F_4^*F_1}+\mathrm{B_4F_4^*B_1}+\mathrm{F_3F_1^*F_4}+\mathrm{B_3B_1^*B_4}).$$
(3-10a)

Next, we obtain the equation for signal ω_3 component:

$$\left[2\frac{\partial^2}{\partial z_0 \partial z_1}-\frac{i}{c^2}\hat{\varepsilon}_{\mathrm{Im}}\left(i\frac{\partial}{\partial t_0}\right)\frac{\partial^2}{\partial t_0^2}-\frac{2}{c^2}\hat{\varepsilon}_{\mathrm{Re}}\left(i\frac{\partial}{\partial t_0}\right)\frac{\partial^2}{\partial t_0 \partial t_1}\right.$$
$$\left.-\frac{i}{c^2}\frac{\partial^2}{\partial t_0^2}\hat{\varepsilon}'_{\mathrm{Re}}\left(i\frac{\partial}{\partial t_0}\right)\frac{\partial}{\partial t_1}-\frac{1}{c^2}\sum_{\substack{\ell=-\infty \\ \ell\neq 0}}^{\infty}\Delta\hat{\varepsilon}_\ell\frac{\partial^2}{\partial t_0^2}e^{i\ell\frac{2\pi}{\Lambda}z_0}\right](\mathrm{F_3}+\mathrm{B_3})$$
$$=\frac{4\pi}{c^2}\left(\frac{\partial^2}{\partial t_0^2}\sum_{\ell=-\infty}^{\infty}\chi_\ell^{(3)}e^{i\ell\frac{2\pi}{\Lambda}z_0}\right)(\mathrm{F_1F_1^*F_3}+\mathrm{B_1B_1^*F_3}+\mathrm{F_3F_3^*F_3}+\mathrm{B_3B_3^*F_3}+\mathrm{F_4F_4^*F_3}+\mathrm{B_4B_4^*F_3}$$
$$+\mathrm{F_1F_1^*B_3}+\mathrm{B_1B_1^*B_3}+\mathrm{F_3F_3^*B_3}+\mathrm{B_3B_3^*B_3}+\mathrm{F_4F_4^*B_3}+\mathrm{B_4B_4^*B_3}$$
$$+\mathrm{F_3B_3^*F_3}+\mathrm{B_3F_3^*B_3}+\mathrm{F_1B_1^*F_3}+\mathrm{B_1F_1^*B_3}+\mathrm{F_1B_1^*B_3}+\mathrm{F_4B_4^*F_3}$$
$$+\mathrm{F_4B_4^*B_3}+\mathrm{B_1F_1^*F_3}+\mathrm{B_4F_4^*F_3}+\mathrm{B_4F_4^*B_3}+\mathrm{F_1F_4^*F_1}+\mathrm{B_1B_4^*B_1}).$$
(3-10b)

Finally, we obtain the equation for idler ω_4 component:

$$\left[2\frac{\partial^2}{\partial z_0 \partial z_1}-\frac{i}{c^2}\hat{\varepsilon}_{\mathrm{Im}}\left(i\frac{\partial}{\partial t_0}\right)\frac{\partial^2}{\partial t_0^2}-\frac{2}{c^2}\hat{\varepsilon}_{\mathrm{Re}}\left(i\frac{\partial}{\partial t_0}\right)\frac{\partial^2}{\partial t_0 \partial t_1}\right.$$
$$\left.-\frac{i}{c^2}\frac{\partial^2}{\partial t_0^2}\hat{\varepsilon}'_{\mathrm{Re}}\left(i\frac{\partial}{\partial t_0}\right)\frac{\partial}{\partial t_1}-\frac{1}{c^2}\sum_{\substack{\ell=-\infty \\ \ell\neq 0}}^{\infty}\Delta\hat{\varepsilon}_\ell\frac{\partial^2}{\partial t_0^2}e^{i\ell\frac{2\pi}{\Lambda}z_0}\right](\mathrm{F}_4+\mathrm{B}_4)$$
$$=\frac{4\pi}{c^2}\left(\frac{\partial^2}{\partial t_0^2}\sum_{\ell=-\infty}^{\infty}\chi_\ell^{(3)}e^{i\ell\frac{2\pi}{\Lambda}z_0}\right)(\mathrm{F}_1\mathrm{F}_1^*\mathrm{F}_4+\mathrm{B}_1\mathrm{B}_1^*\mathrm{F}_4+\mathrm{F}_3\mathrm{F}_3^*\mathrm{F}_4+\mathrm{B}_3\mathrm{B}_3^*\mathrm{F}_4+\mathrm{F}_4\mathrm{F}_4^*\mathrm{F}_4+\mathrm{B}_4\mathrm{B}_4^*\mathrm{F}_4 \quad (3\text{-}10c)$$
$$+\mathrm{F}_1\mathrm{F}_1^*\mathrm{B}_4+\mathrm{B}_1\mathrm{B}_1^*\mathrm{B}_4+\mathrm{F}_3\mathrm{F}_3^*\mathrm{B}_4+\mathrm{B}_3\mathrm{B}_3^*\mathrm{B}_4+\mathrm{F}_4\mathrm{F}_4^*\mathrm{B}_4+\mathrm{B}_4\mathrm{B}_4^*\mathrm{B}_4$$
$$+\mathrm{F}_4\mathrm{B}_4^*\mathrm{F}_4+\mathrm{B}_4\mathrm{F}_4^*\mathrm{B}_4+\mathrm{F}_1\mathrm{B}_1^*\mathrm{F}_4+\mathrm{B}_1\mathrm{F}_1^*\mathrm{B}_4+\mathrm{F}_1\mathrm{B}_1^*\mathrm{B}_4+\mathrm{F}_3\mathrm{B}_3^*\mathrm{F}_4$$
$$+\mathrm{F}_3\mathrm{B}_3^*\mathrm{B}_4+\mathrm{B}_1\mathrm{F}_1^*\mathrm{F}_4+\mathrm{B}_3\mathrm{F}_3^*\mathrm{B}_4+\mathrm{B}_3\mathrm{F}_3^*\mathrm{F}_4+\mathrm{F}_1\mathrm{F}_3^*\mathrm{F}_1+\mathrm{B}_1\mathrm{B}_3^*\mathrm{B}_1).$$

The Eq. (3-10a), (3-10b), and Eq. (3-10c) can be simplified and then removed $e^{-i\omega_1 t_0}$, $e^{-i\omega_3 t_0}$, and $e^{-i\omega_4 t_0}$ which are common to both sides of each equations. We obtain:

$$\left[2ik_1\frac{\partial A_{f1}}{\partial z_1}+\frac{i\omega_1^2\hat{\varepsilon}_{\mathrm{Im}}}{c^2}A_{f1}+\frac{2}{c^2}i\omega_1\hat{\varepsilon}_{\mathrm{Re}}\frac{\partial A_{f1}}{\partial t_1}+\frac{i}{c^2}\omega_1^2\hat{\varepsilon}'_{\mathrm{Re}}\frac{\partial A_{f1}}{\partial t_1}-\frac{\omega_1^2}{c^2}\sum_{\substack{\ell=-\infty \\ \ell\neq 0}}^{\infty}\Delta\hat{\varepsilon}_\ell A_{f1}e^{i\ell\frac{2\pi}{\Lambda}z_0}\right]e^{ik_1z_0}$$
$$\left[-2ik_1\frac{\partial A_{b1}}{\partial z_1}+\frac{i\omega_1^2\hat{\varepsilon}_{\mathrm{Im}}}{c^2}A_{b1}+\frac{2}{c^2}i\omega_1\hat{\varepsilon}_{\mathrm{Re}}\frac{\partial A_{b1}}{\partial t_1}+\frac{i}{c^2}\omega_1^2\hat{\varepsilon}'_{\mathrm{Re}}\frac{\partial A_{b1}}{\partial t_1}-\frac{\omega_1^2}{c^2}\sum_{\substack{\ell=-\infty \\ \ell\neq 0}}^{\infty}\Delta\hat{\varepsilon}_\ell A_{b1}e^{i\ell\frac{2\pi}{\Lambda}z_0}\right]e^{-ik_1z_0}$$
$$=-\frac{4\pi\omega_1^2}{c^2}\left(\sum_{\ell=-\infty}^{\infty}\chi_\ell^{(3)}e^{i\ell\frac{2\pi}{\Lambda}z_0}\right)\left[(|A_{f1}|^2+2|A_{b1}|^2+2|A_{f3}|^2+2|A_{b3}|^2+2|A_{f4}|^2+2|A_{b4}|^2)A_{f1}e^{ik_1z_0}\right.$$
$$+(2|A_{f1}|^2+|A_{b1}|^2+2|A_{f3}|^2+2|A_{b3}|^2+2|A_{f4}|^2+2|A_{b4}|^2)A_{b1}e^{-ik_1z_0}+A_{f1}^2A_{b1}^*e^{3ik_1z_0}+A_{b1}^2A_{f1}^*e^{-3ik_1z_0}$$
$$+2A_{f3}A_{b3}^*A_{f1}e^{i(2k_3+k_1)z_0}+2A_{f3}A_{b3}^*A_{b1}e^{i(2k_3-k_1)z_0}+2A_{f4}A_{b4}^*A_{f1}e^{i(2k_4+k_1)z_0}+2A_{f4}A_{b4}^*A_{b1}e^{i(2k_4-k_1)z_0}$$
$$+2A_{b3}A_{f3}^*A_{f1}e^{-i(2k_3-k_1)z_0}+2A_{b3}A_{f3}^*A_{b1}e^{-i(2k_3+k_1)z_0}+2A_{b4}A_{f4}^*A_{f1}e^{-i(2k_4-k_1)z_0}+2A_{b4}A_{f4}^*A_{b1}e^{-i(2k_4+k_1)z_0}$$
$$\left.+2A_{f3}A_{f1}^*A_{f4}e^{i(k_3-k_1+k_4)z_0}+2A_{b3}A_{b1}^*A_{b4}e^{-i(k_3-k_1+k_4)z_0}\right]. \quad (3\text{-}11a)$$

$$\left[2ik_3\frac{\partial A_{f3}}{\partial z_1}+\frac{i\omega_3^2\hat{\varepsilon}_{\mathrm{Im}}}{c^2}A_{f3}+\frac{2}{c^2}i\omega_3\hat{\varepsilon}_{\mathrm{Re}}\frac{\partial A_{f3}}{\partial t_1}+\frac{i}{c^2}\omega_3^2\hat{\varepsilon}'_{\mathrm{Re}}\frac{\partial A_{f3}}{\partial t_1}-\frac{\omega_3^2}{c^2}\sum_{\substack{\ell=-\infty\\ \ell\neq 0}}^{\infty}\Delta\hat{\varepsilon}_\ell A_{f3}e^{i\ell\frac{2\pi}{\Lambda}z_0}\right]e^{ik_3z_0}$$

$$\left[-2ik_3\frac{\partial A_{b3}}{\partial z_1}+\frac{i\omega_3^2\hat{\varepsilon}_{\mathrm{Im}}}{c^2}A_{b3}+\frac{2}{c^2}i\omega_3\hat{\varepsilon}_{\mathrm{Re}}\frac{\partial A_{b3}}{\partial t_1}+\frac{i}{c^2}\omega_3^2\hat{\varepsilon}'_{\mathrm{Re}}\frac{\partial A_{b3}}{\partial t_1}-\frac{\omega_3^2}{c^2}\sum_{\substack{\ell=-\infty\\ \ell\neq 0}}^{\infty}\Delta\hat{\varepsilon}_\ell A_{b3}e^{i\ell\frac{2\pi}{\Lambda}z_0}\right]e^{-ik_3z_0}$$

$$=-\frac{4\pi\omega_3^2}{c^2}\left(\sum_{\ell=-\infty}^{\infty}\chi_\ell^{(3)}e^{i\ell\frac{2\pi}{\Lambda}z_0}\right)\Big[(2|A_{f1}|^2+2|A_{b1}|^2+|A_{f3}|^2+2|A_{b3}|^2+2|A_{f4}|^2+2|A_{b4}|^2)A_{f3}e^{ik_3z_0}$$
$$+(2|A_{f1}|^2+2|A_{b1}|^2+2|A_{f3}|^2+|A_{b3}|^2+2|A_{f4}|^2+2|A_{b4}|^2)A_{b3}e^{-ik_3z_0}+A_{f3}^2A_{b3}^*e^{3ik_3z_0}+A_{b3}^2A_{f3}^*e^{-3ik_3z_0}$$
$$+2A_{f1}A_{b1}^*A_{f3}e^{i(2k_1+k_3)z_0}+2A_{f1}A_{b1}^*A_{b3}e^{i(2k_1-k_3)z_0}+2A_{f4}A_{b4}^*A_{f3}e^{i(2k_4+k_3)z_0}+2A_{f4}A_{b4}^*A_{b3}e^{i(2k_4-k_3)z_0}$$
$$+2A_{b1}A_{f1}^*A_{b3}e^{-i(2k_1+k_3)z_0}+2A_{b4}A_{f4}^*A_{f3}e^{-i(2k_4-k_3)z_0}+2A_{b4}A_{f4}^*A_{b3}e^{-i(2k_4+k_3)z_0}+2A_{b1}A_{f1}^*A_{f3}e^{-i(2k_1-k_3)z_0}$$
$$+2A_{f1}^2A_{f4}^*e^{i(2k_1-k_4)z_0}+2A_{b1}^2A_{b4}^*e^{-i(2k_1-k_4)z_0}\Big].$$

(3-11b)

$$\left[2ik_4\frac{\partial A_{f4}}{\partial z_1}+\frac{i\omega_4^2\hat{\varepsilon}_{\mathrm{Im}}}{c^2}A_{f4}+\frac{2}{c^2}i\omega_4\hat{\varepsilon}_{\mathrm{Re}}\frac{\partial A_{f4}}{\partial t_1}+\frac{i}{c^2}\omega_4^2\hat{\varepsilon}'_{\mathrm{Re}}\frac{\partial A_{f4}}{\partial t_1}-\frac{\omega_4^2}{c^2}\sum_{\substack{\ell=-\infty\\ \ell\neq 0}}^{\infty}\Delta\hat{\varepsilon}_\ell A_{f4}e^{i\ell\frac{2\pi}{\Lambda}z_0}\right]e^{ik_4z_0}$$

$$\left[-2ik_4\frac{\partial A_{b4}}{\partial z_1}+\frac{i\omega_4^2\hat{\varepsilon}_{\mathrm{Im}}}{c^2}A_{b4}+\frac{2}{c^2}i\omega_4\hat{\varepsilon}_{\mathrm{Re}}\frac{\partial A_{b4}}{\partial t_1}+\frac{i}{c^2}\omega_4^2\hat{\varepsilon}'_{\mathrm{Re}}\frac{\partial A_{b4}}{\partial t_1}-\frac{\omega_4^2}{c^2}\sum_{\substack{\ell=-\infty\\ \ell\neq 0}}^{\infty}\Delta\hat{\varepsilon}_\ell A_{b4}e^{i\ell\frac{2\pi}{\Lambda}z_0}\right]e^{-ik_4z_0}$$

$$=-\frac{4\pi\omega_4^2}{c^2}\left(\sum_{\ell=-\infty}^{\infty}\chi_\ell^{(3)}e^{i\ell\frac{2\pi}{\Lambda}z_0}\right)\Big[(2|A_{f1}|^2+2|A_{b1}|^2+2|A_{f3}|^2+2|A_{b3}|^2+|A_{f4}|^2+2|A_{b4}|^2)A_{f4}e^{ik_4z_0}$$
$$+(2|A_{f1}|^2+2|A_{b1}|^2+2|A_{f3}|^2+|A_{b3}|^2+2|A_{f4}|^2+|A_{b4}|^2)A_{b4}e^{-ik_4z_0}+A_{f4}^2A_{b4}^*e^{3ik_4z_0}+A_{b4}^2A_{f4}^*e^{-3ik_4z_0}$$
$$+2A_{f1}A_{b1}^*A_{f4}e^{i(2k_1+k_4)z_0}+2A_{f1}A_{b1}^*A_{b4}e^{i(2k_1-k_4)z_0}+2A_{f3}A_{b3}^*A_{f4}e^{i(2k_3+k_4)z_0}+2A_{f3}A_{b3}^*A_{b4}e^{i(2k_3-k_4)z_0}$$
$$+2A_{b1}A_{f1}^*A_{f4}e^{-i(2k_1-k_4)z_0}+2A_{b3}A_{f3}^*A_{f4}e^{-i(2k_3-k_4)z_0}+2A_{b3}A_{f3}^*A_{b4}e^{-i(2k_3+k_4)z_0}+2A_{b1}A_{f1}^*A_{f4}e^{-i(2k_1-k_4)z_0}$$
$$+2A_{f1}^2A_{f3}^*e^{i(2k_1-k_3)z_0}+2A_{b1}^2A_{b3}^*e^{-i(2k_1-k_3)z_0}\Big].$$

(3-11c)

Before expanding of Eq. (3-11a), (3-11b), and (3-11c), the effect of $\chi^{(3)}$ need to be examined on each of the terms in square bracket in the right-hand side of Eq. (3-11). According to the band-edge enhancement, the periodic length of PBG structure Λ is chosen to be close to the half of pump and signal wavelengths, then deviation from this condition is: $-2\mu\delta = 2\pi/\Lambda - k_{1,3} \rightarrow k_{1,3} = \pi/\Lambda + (\pi/\Lambda)\mu\delta_{1,3}$,

where $\delta_{1,3} = (\Lambda / \pi)\delta$ and note that $2\mu\delta_{1,3}z_0 = 2\delta_{1,3}z_1$ [18]. For matching of phase for ω_1 component, the phase portion of these terms in Eq. (3-11a) can be matched. Then we obtain the phase-matched condition as table 3.4.

Table 3.4: The phase-matched condition for ω_1 component

$e^{i\ell\frac{2\pi}{\Lambda}z_0}e^{ik_1z_0} = e^{i\left(\ell\frac{2\pi}{\Lambda}+2k_1-k_1\right)z_0} = e^{i\left(\ell\frac{2\pi}{\Lambda}+2\left(\frac{\pi}{\Lambda}+\frac{\pi}{\Lambda}\mu\delta_1\right)\right)z_0}e^{-ik_1z_0}$ $\begin{cases}\text{if } \ell=0; & e^{ik_1z_0}\\ \text{if } \ell=-1; & e^{i\frac{2\pi}{\Lambda}\delta_1z_1}e^{-ik_1z_0}\end{cases}$
$e^{i\ell\frac{2\pi}{\Lambda}z_0}e^{-ik_1z_0} = e^{i\left(\ell\frac{2\pi}{\Lambda}-2k_1+k_1\right)z_0} = e^{i\left(\ell\frac{2\pi}{\Lambda}-2\left(\frac{\pi}{\Lambda}+\frac{\pi}{\Lambda}\mu\delta_1\right)\right)z_0}e^{ik_1z_0}$ $\begin{cases}\text{if } \ell=0; & e^{-ik_1z_0}\\ \text{if } \ell=1; & e^{-i\frac{2\pi}{\Lambda}\delta_1z_1}e^{ik_1z_0}\end{cases}$
$e^{i\ell\frac{2\pi}{\Lambda}z_0}e^{3ik_1z_0} = \begin{cases} e^{i\left(\ell\frac{2\pi}{\Lambda}+2k_1+k_1\right)z_0} = e^{i\left(\ell\frac{2\pi}{\Lambda}+2\left(\frac{\pi}{\Lambda}+\frac{\pi}{\Lambda}\mu\delta_1\right)\right)z_0}e^{ik_1z_0} \rightarrow \text{if } \ell=-1; & e^{i\frac{2\pi}{\Lambda}\delta_1z_1}e^{ik_1z_1} \\ e^{i\left(\ell\frac{2\pi}{\Lambda}+4k_1-k_1\right)z_0} = e^{i\left(\ell\frac{2\pi}{\Lambda}+4\left(\frac{\pi}{\Lambda}+\frac{\pi}{\Lambda}\mu\delta_1\right)\right)z_0}e^{-ik_1z_0} \rightarrow \text{if } \ell=-2; & e^{i\frac{4\pi}{\Lambda}\delta_1z_1}e^{-ik_1z_1}\end{cases}$
$e^{i\ell\frac{2\pi}{\Lambda}z_0}e^{-3ik_1z_0} = \begin{cases} e^{i\left(\ell\frac{2\pi}{\Lambda}-2k_1-k_1\right)z_0} = e^{i\left(\ell\frac{2\pi}{\Lambda}-2\left(\frac{\pi}{\Lambda}+\frac{\pi}{\Lambda}\mu\delta_1\right)\right)z_0}e^{-ik_1z_0} \rightarrow \text{if } \ell=1; & e^{-i\frac{2\pi}{\Lambda}\delta_1z_1}e^{-ik_1z_1} \\ e^{i\left(\ell\frac{2\pi}{\Lambda}-4k_1+k_1\right)z_0} = e^{i\left(\ell\frac{2\pi}{\Lambda}-4\left(\frac{\pi}{\Lambda}+\frac{\pi}{\Lambda}\mu\delta_1\right)\right)z_0}e^{ik_1z_0} \rightarrow \text{if } \ell=2; & e^{-i\frac{4\pi}{\Lambda}\delta_1z_1}e^{ik_1z_1}\end{cases}$
$e^{i\ell\frac{2\pi}{\Lambda}z_0}e^{i(2k_3+k_1)z_0} = e^{i\left(\ell\frac{2\pi}{\Lambda}+2\left(\frac{\pi}{\Lambda}+\frac{\pi}{\Lambda}\mu\delta_3\right)+k_1\right)z_0} \rightarrow \ell=-1; \quad e^{i\frac{2\pi}{\Lambda}\mu\delta_3z_0}e^{ik_1z_0}$
$e^{i\ell\frac{2\pi}{\Lambda}z_0}e^{i(2k_3-k_1)z_0} = e^{i\left(\ell\frac{2\pi}{\Lambda}+2\left(\frac{\pi}{\Lambda}+\frac{\pi}{\Lambda}\mu\delta_3\right)-k_1\right)z_0} \rightarrow \ell=-1; \quad e^{i\frac{2\pi}{\Lambda}\mu\delta_3z_0}e^{-ik_1z_0}$
$e^{i\ell\frac{2\pi}{\Lambda}z_0}e^{i(2k_4+k_1)z_0} = e^{i\left(\ell\frac{2\pi}{\Lambda}+4\left(\frac{\pi}{\Lambda}+\frac{\pi}{\Lambda}\mu\delta_1\right)-2\left(\frac{\pi}{\Lambda}+\frac{\pi}{\Lambda}\mu\delta_3\right)-2\mu\Delta k_{OPA}+k_1\right)z_0} \rightarrow \ell=-1; \quad e^{i\frac{2\pi}{\Lambda}\mu\delta_4z_0}e^{ik_1z_0}$
$e^{i\ell\frac{2\pi}{\Lambda}z_0}e^{i(2k_4-k_1)z_0} = e^{i\left(\ell\frac{2\pi}{\Lambda}+4\left(\frac{\pi}{\Lambda}+\frac{\pi}{\Lambda}\mu\delta_1\right)-2\left(\frac{\pi}{\Lambda}+\frac{\pi}{\Lambda}\mu\delta_3\right)-2\mu\Delta k_{OPA}-k_1\right)z_0} \rightarrow \ell=-1; \quad e^{i\frac{2\pi}{\Lambda}\mu\delta_4z_0}e^{-ik_1z_0}$
$e^{i\ell\frac{2\pi}{\Lambda}z_0}e^{-i(2k_3+k_1)z_0} = e^{i\left(\ell\frac{2\pi}{\Lambda}-2\left(\frac{\pi}{\Lambda}+\frac{\pi}{\Lambda}\mu\delta_3\right)-k_1\right)z_0} \rightarrow \ell=1; \quad e^{-i\frac{2\pi}{\Lambda}\mu\delta_3z_0}e^{-ik_1z_0}$
$e^{i\ell\frac{2\pi}{\Lambda}z_0}e^{-i(2k_3-k_1)z_0} = e^{i\left(\ell\frac{2\pi}{\Lambda}-2\left(\frac{\pi}{\Lambda}+\frac{\pi}{\Lambda}\mu\delta_3\right)+k_1\right)z_0} \rightarrow \ell=1; \quad e^{-i\frac{2\pi}{\Lambda}\mu\delta_3z_0}e^{ik_1z_0}$
$e^{i\ell\frac{2\pi}{\Lambda}z_0}e^{-i(2k_4+k_1)z_0} = e^{i\left(\ell\frac{2\pi}{\Lambda}-4\left(\frac{\pi}{\Lambda}+\frac{\pi}{\Lambda}\mu\delta_1\right)+2\left(\frac{\pi}{\Lambda}+\frac{\pi}{\Lambda}\mu\delta_3\right)+2\mu\Delta k_{OPA}-k_1\right)z_0} \rightarrow \ell=1; \quad e^{-i\frac{2\pi}{\Lambda}\mu\delta_4z_0}e^{-ik_1z_0}$
$e^{i\ell\frac{2\pi}{\Lambda}z_0}e^{-i(2k_4-k_1)z_0} = e^{i\left(\ell\frac{2\pi}{\Lambda}-4\left(\frac{\pi}{\Lambda}+\frac{\pi}{\Lambda}\mu\delta_1\right)+2\left(\frac{\pi}{\Lambda}+\frac{\pi}{\Lambda}\mu\delta_3\right)+2\mu\Delta k_{OPA}+k_1\right)z_0} \rightarrow \ell=1; \quad e^{-i\frac{2\pi}{\Lambda}\mu\delta_4z_0}e^{ik_1z_0}$
$e^{i\ell\frac{2\pi}{\Lambda}z_0}e^{i(k_3-k_1+k_4)z_0} = e^{i\left(\ell\frac{2\pi}{\Lambda}+2k_1-\mu\Delta k_{OPA}-k_1\right)z_0}\begin{cases}\ell=0; & e^{-i\mu\Delta k_{OPA}z_0}e^{ik_1z_0}\end{cases}$
$e^{i\ell\frac{2\pi}{\Lambda}z_0}e^{-i(k_3-k_1+k_4)z_0} = e^{i\left(\ell\frac{2\pi}{\Lambda}-2k_1+\mu\Delta k_{OPA}+k_1\right)z_0} = \begin{cases}\ell=0; & e^{i\mu\Delta k_{OPA}z_0}e^{-ik_1z_0}\end{cases}$

For matching of phase for ω_3 component, the phase portion of these terms in Eq. (3-11b) can be matched. Then we obtain the phase-matched condition as table 3.5.

Table 3.5: The phase-matched condition for ω_3 component

$e^{i\ell\frac{2\pi}{\Lambda}z_0}e^{ik_3z_0} = e^{i\left(\ell\frac{2\pi}{\Lambda}+2k_3-k_3\right)z_0} = e^{i\left(\ell\frac{2\pi}{\Lambda}+2\left(\frac{\pi}{\Lambda}+\frac{\pi}{\Lambda}\mu\delta_3\right)\right)z_0}e^{-ik_3z_0}\begin{cases}\text{if } \ell=0; & e^{ik_3z_0}\\ \text{if } \ell=-1; & e^{i\frac{2\pi}{\Lambda}\delta_3z_1}e^{-ik_3z_0}\end{cases}$
$e^{i\ell\frac{2\pi}{\Lambda}z_0}e^{-ik_3z_0} = e^{i\left(\ell\frac{2\pi}{\Lambda}-2k_3+k_3\right)z_0} = e^{i\left(\ell\frac{2\pi}{\Lambda}-2\left(\frac{\pi}{\Lambda}+\frac{\pi}{\Lambda}\mu\delta_3\right)\right)z_0}e^{ik_3z_0}\begin{cases}\text{if } \ell=0; & e^{-ik_3z_0}\\ \text{if } \ell=1; & e^{-i\frac{2\pi}{\Lambda}\delta_3z_3}e^{ik_3z_0}\end{cases}$
$e^{i\ell\frac{2\pi}{\Lambda}z_0}e^{3ik_3z_0} = \begin{cases} e^{i\left(\ell\frac{2\pi}{\Lambda}+2k_3+k_3\right)z_0} = e^{i\left(\ell\frac{2\pi}{\Lambda}+2\left(\frac{\pi}{\Lambda}+\frac{\pi}{\Lambda}\mu\delta_3\right)\right)z_0}e^{ik_3z_0} \rightarrow \text{if } \ell=-1; & e^{i\frac{2\pi}{\Lambda}\delta_1z_1}e^{ik_3z_1} \\ e^{i\left(\ell\frac{2\pi}{\Lambda}+4k_3-k_3\right)z_0} = e^{i\left(\ell\frac{2\pi}{\Lambda}+4\left(\frac{\pi}{\Lambda}+\frac{\pi}{\Lambda}\mu\delta_3\right)\right)z_0}e^{-ik_3z_0} \rightarrow \text{if } \ell=-2; & e^{i\frac{4\pi}{\Lambda}\delta_1z_1}e^{-ik_3z_1}\end{cases}$
$e^{i\ell\frac{2\pi}{\Lambda}z_0}e^{-3ik_3z_0} = \begin{cases} e^{i\left(\ell\frac{2\pi}{\Lambda}-2k_3-k_3\right)z_0} = e^{i\left(\ell\frac{2\pi}{\Lambda}-2\left(\frac{\pi}{\Lambda}+\frac{\pi}{\Lambda}\mu\delta_3\right)\right)z_0}e^{-ik_3z_0} \rightarrow \text{if } \ell=1; & e^{-i\frac{2\pi}{\Lambda}\delta_3z_1}e^{-ik_3z_1} \\ e^{i\left(\ell\frac{2\pi}{\Lambda}-4k_3+k_3\right)z_0} = e^{i\left(\ell\frac{2\pi}{\Lambda}-4\left(\frac{\pi}{\Lambda}+\frac{\pi}{\Lambda}\mu\delta_3\right)\right)z_0}e^{ik_3z_0} \rightarrow \text{if } \ell=2; & e^{-i\frac{4\pi}{\Lambda}\delta_3z_1}e^{ik_3z_1}\end{cases}$
$e^{i\ell\frac{2\pi}{\Lambda}z_0}e^{i(2k_1+k_3)z_0} = e^{i\left(\ell\frac{2\pi}{\Lambda}+2\left(\frac{\pi}{\Lambda}+\frac{\pi}{\Lambda}\mu\delta_1\right)+k_3\right)z_0} \rightarrow \ell=-1; \quad e^{i\frac{2\pi}{\Lambda}\mu\delta_1z_0}e^{ik_3z_0}$
$e^{i\ell\frac{2\pi}{\Lambda}z_0}e^{i(2k_1-k_3)z_0} = e^{i\left(\ell\frac{2\pi}{\Lambda}+2\left(\frac{\pi}{\Lambda}+\frac{\pi}{\Lambda}\mu\delta_3\right)-k_3\right)z_0} \rightarrow \ell=-1; \quad e^{i\frac{2\pi}{\Lambda}\mu\delta_1z_0}e^{-ik_3z_0}$
$e^{i\ell\frac{2\pi}{\Lambda}z_0}e^{i(2k_4+k_3)z_0} = e^{i\left(\ell\frac{2\pi}{\Lambda}+4\left(\frac{\pi}{\Lambda}+\frac{\pi}{\Lambda}\mu\delta_1\right)-2\left(\frac{\pi}{\Lambda}+\frac{\pi}{\Lambda}\mu\delta_3\right)-2\mu\Delta k_{OPA}+k_3\right)z_0} \rightarrow \ell=-1; \quad e^{i\frac{2\pi}{\Lambda}\mu\delta_4z_0}e^{ik_3z_0}$
$e^{i\ell\frac{2\pi}{\Lambda}z_0}e^{i(2k_4-k_3)z_0} = e^{i\left(\ell\frac{2\pi}{\Lambda}+4\left(\frac{\pi}{\Lambda}+\frac{\pi}{\Lambda}\mu\delta_1\right)-2\left(\frac{\pi}{\Lambda}+\frac{\pi}{\Lambda}\mu\delta_3\right)-2\mu\Delta k_{OPA}-k_3\right)z_0} \rightarrow \ell=-1; \quad e^{i\frac{2\pi}{\Lambda}\mu\delta_4z_0}e^{-ik_3z_0}$
$e^{i\ell\frac{2\pi}{\Lambda}z_0}e^{-i(2k_1+k_3)z_0} = e^{i\left(\ell\frac{2\pi}{\Lambda}-2\left(\frac{\pi}{\Lambda}+\frac{\pi}{\Lambda}\mu\delta_1\right)-k_3\right)z_0} \rightarrow \ell=1; \quad e^{-i\frac{2\pi}{\Lambda}\mu\delta_1z_0}e^{-ik_3z_0}$
$e^{i\ell\frac{2\pi}{\Lambda}z_0}e^{-i(2k_1-k_3)z_0} = e^{i\left(\ell\frac{2\pi}{\Lambda}-2\left(\frac{\pi}{\Lambda}+\frac{\pi}{\Lambda}\mu\delta_3\right)+k_3\right)z_0} \rightarrow \ell=1; \quad e^{-i\frac{2\pi}{\Lambda}\mu\delta_1z_0}e^{ik_3z_0}$
$e^{i\ell\frac{2\pi}{\Lambda}z_0}e^{-i(2k_4+k_3)z_0} = e^{i\left(\ell\frac{2\pi}{\Lambda}-4\left(\frac{\pi}{\Lambda}+\frac{\pi}{\Lambda}\mu\delta_1\right)+2\left(\frac{\pi}{\Lambda}+\frac{\pi}{\Lambda}\mu\delta_3\right)+2\mu\Delta k_{OPA}-k_3\right)z_0} \rightarrow \ell=1; \quad e^{-i\frac{2\pi}{\Lambda}\mu\delta_4z_0}e^{-ik_3z_0}$
$e^{i\ell\frac{2\pi}{\Lambda}z_0}e^{-i(2k_4-k_3)z_0} = e^{i\left(\ell\frac{2\pi}{\Lambda}-4\left(\frac{\pi}{\Lambda}+\frac{\pi}{\Lambda}\mu\delta_1\right)+2\left(\frac{\pi}{\Lambda}+\frac{\pi}{\Lambda}\mu\delta_3\right)+2\mu\Delta k_{OPA}+k_3\right)z_0} \rightarrow \ell=1; \quad e^{-i\frac{2\pi}{\Lambda}\mu\delta_4z_0}e^{ik_3z_0}$
$e^{i\ell\frac{2\pi}{\Lambda}z_0}e^{i(2k_1-k_4)z_0} = \begin{cases}\ell=0; & e^{i\left(\ell\frac{2\pi}{\Lambda}+\mu\Delta k_{OPA}+k_3\right)z_0} = e^{i\mu\Delta k_{OPA}z_0}e^{ik_3z_0}\end{cases}$
$e^{i\ell\frac{2\pi}{\Lambda}z_0}e^{-i(2k_1-k_4)z_0} = \begin{cases}\ell=0; & e^{i\left(\ell\frac{2\pi}{\Lambda}-\mu\Delta k_{OPA}-k_3\right)z_0} = e^{-i\mu\Delta k_{OPA}z_0}e^{-ik_3z_0}\end{cases}$

For matching of phase for ω_4 component, the phase portion of these terms in Eq. (3-11c) can be matched. Then we obtain the phase-matched condition as table 3.6.

Table 3.6: The phase-matched condition for ω_4 component

$e^{i\ell\frac{2\pi}{\Lambda}z_0}e^{ik_4z_0} = e^{i\left(\ell\frac{2\pi}{\Lambda}+2k_4-k_4\right)z_0} = e^{i\left(\ell\frac{2\pi}{\Lambda}+4\left(\frac{\pi}{\Lambda}+\frac{\pi}{\Lambda}\mu\delta_1\right)-2\left(\frac{\pi}{\Lambda}+\frac{\pi}{\Lambda}\mu\delta_3\right)-2\mu\Delta k_{OPA}\right)z_0}e^{-ik_4z_0} \begin{cases} \ell=0; & e^{ik_4z_0} \\ \ell=-2; & e^{i\frac{2\pi}{\Lambda}\delta_4z_1}e^{-ik_4z_0} \end{cases}$
$e^{i\ell\frac{2\pi}{\Lambda}z_0}e^{-ik_4z_0} = e^{i\left(\ell\frac{2\pi}{\Lambda}-2k_4+k_4\right)z_0} = e^{i\left(\ell\frac{2\pi}{\Lambda}-4\left(\frac{\pi}{\Lambda}+\frac{\pi}{\Lambda}\mu\delta_1\right)+2\left(\frac{\pi}{\Lambda}+\frac{\pi}{\Lambda}\mu\delta_3\right)+2\mu\Delta k_{OPA}\right)z_0}e^{ik_4z_0} \begin{cases} \ell=0; & e^{-ik_4z_0} \\ \ell=2; & e^{-i\frac{2\pi}{\Lambda}\delta_4z_1}e^{ik_4z_0} \end{cases}$
$e^{i\ell\frac{2\pi}{\Lambda}z_0}e^{3ik_4z_0} = \begin{cases} e^{i\left(\ell\frac{2\pi}{\Lambda}+2k_4+k_4\right)z_0} = e^{i\left(\ell\frac{2\pi}{\Lambda}+4\left(\frac{\pi}{\Lambda}+\frac{\pi}{\Lambda}\mu\delta_1\right)-2\left(\frac{\pi}{\Lambda}+\frac{\pi}{\Lambda}\mu\delta_3\right)-2\mu\Delta k_{OPA}\right)z_0}e^{ik_4z_0} \rightarrow \ell=-1; & e^{i\frac{2\pi}{\Lambda}\delta_4z_1}e^{ik_4z_0} \\ e^{i\left(\ell\frac{2\pi}{\Lambda}+4k_4-k_4\right)z_0} = e^{i\left(\ell\frac{2\pi}{\Lambda}+8\left(\frac{\pi}{\Lambda}+\frac{\pi}{\Lambda}\mu\delta_1\right)-4\left(\frac{\pi}{\Lambda}+\frac{\pi}{\Lambda}\mu\delta_3\right)-4\mu\Delta k_{OPA}\right)z_0}e^{-ik_4z_0} \rightarrow \ell=-2; & e^{i\frac{4\pi}{\Lambda}\delta_4z_1}e^{-ik_4z_0} \end{cases}$
$e^{i\ell\frac{2\pi}{\Lambda}z_0}e^{-3ik_4z_0} = \begin{cases} e^{i\left(\ell\frac{2\pi}{\Lambda}-2k_4-k_4\right)z_0} = e^{i\left(\ell\frac{2\pi}{\Lambda}-4\left(\frac{\pi}{\Lambda}+\frac{\pi}{\Lambda}\mu\delta_1\right)+2\left(\frac{\pi}{\Lambda}+\frac{\pi}{\Lambda}\mu\delta_3\right)+2\mu\Delta k_{OPA}\right)z_0}e^{-ik_4z_0} \rightarrow \ell=1; & e^{-i\frac{2\pi}{\Lambda}\delta_4z_1}e^{-ik_4z_0} \\ e^{i\left(\ell\frac{2\pi}{\Lambda}-4k_4+k_4\right)z_0} = e^{i\left(\ell\frac{2\pi}{\Lambda}-8\left(\frac{\pi}{\Lambda}+\frac{\pi}{\Lambda}\mu\delta_1\right)+4\left(\frac{\pi}{\Lambda}+\frac{\pi}{\Lambda}\mu\delta_3\right)+4\mu\Delta k_{OPA}\right)z_0}e^{ik_4z_0} \rightarrow \ell=2; & e^{-i\frac{4\pi}{\Lambda}\delta_4z_1}e^{ik_4z_0} \end{cases}$
$e^{i\ell\frac{2\pi}{\Lambda}z_0}e^{i(2k_1+k_4)z_0} = e^{i\left(\ell\frac{2\pi}{\Lambda}+2\left(\frac{\pi}{\Lambda}+\frac{\pi}{\Lambda}\mu\delta_1\right)+k_4\right)z_0} \rightarrow \ell=-1; \quad e^{i\frac{2\pi}{\Lambda}\mu\delta_1z_0}e^{ik_4z_0}$
$e^{i\ell\frac{2\pi}{\Lambda}z_0}e^{i(2k_3+k_4)z_0} = e^{i\left(\ell\frac{2\pi}{\Lambda}+2\left(\frac{\pi}{\Lambda}+\frac{\pi}{\Lambda}\mu\delta_3\right)+k_4\right)z_0} \rightarrow \ell=-1; \quad e^{i\frac{2\pi}{\Lambda}\mu\delta_3z_0}e^{ik_4z_0}$
$e^{i\ell\frac{2\pi}{\Lambda}z_0}e^{i(2k_3-k_4)z_0} = e^{i\left(\ell\frac{2\pi}{\Lambda}+2\left(\frac{\pi}{\Lambda}+\frac{\pi}{\Lambda}\mu\delta_3\right)-k_4\right)z_0} \rightarrow \ell=-1; \quad e^{i\frac{2\pi}{\Lambda}\mu\delta_3z_0}e^{-ik_4z_0}$
$e^{i\ell\frac{2\pi}{\Lambda}z_0}e^{-i(2k_1+k_4)z_0} = e^{i\left(\ell\frac{2\pi}{\Lambda}-2\left(\frac{\pi}{\Lambda}+\frac{\pi}{\Lambda}\mu\delta_1\right)-k_4\right)z_0} \rightarrow \ell=1; \quad e^{-i\frac{2\pi}{\Lambda}\mu\delta_1z_0}e^{-ik_4z_0}$
$e^{i\ell\frac{2\pi}{\Lambda}z_0}e^{-i(2k_1-k_4)z_0} = e^{i\left(\ell\frac{2\pi}{\Lambda}-2\left(\frac{\pi}{\Lambda}+\frac{\pi}{\Lambda}\mu\delta_1\right)+k_4\right)z_0} \rightarrow \ell=1; \quad e^{-i\frac{2\pi}{\Lambda}\mu\delta_1z_0}e^{ik_4z_0}$
$e^{i\ell\frac{2\pi}{\Lambda}z_0}e^{-i(2k_3+k_4)z_0} = e^{i\left(\ell\frac{2\pi}{\Lambda}-2\left(\frac{\pi}{\Lambda}+\frac{\pi}{\Lambda}\mu\delta_3\right)-k_4\right)z_0} \rightarrow \ell=1; \quad e^{-i\frac{2\pi}{\Lambda}\mu\delta_3z_0}e^{-ik_4z_0}$
$e^{i\ell\frac{2\pi}{\Lambda}z_0}e^{-i(2k_3-k_4)z_0} = e^{i\left(\ell\frac{2\pi}{\Lambda}-2\left(\frac{\pi}{\Lambda}+\frac{\pi}{\Lambda}\mu\delta_3\right)+k_4\right)z_0} \rightarrow \ell=1; \quad e^{-i\frac{2\pi}{\Lambda}\mu\delta_3z_0}e^{ik_4z_0}$
$e^{i\ell\frac{2\pi}{\Lambda}z_0}e^{i(2k_1-k_3)z_0} = \begin{cases} \ell=0; & e^{i\left(\ell\frac{2\pi}{\Lambda}+\mu\Delta k_{OPA}+k_4\right)z_0} = e^{i\mu\Delta k_{OPA}z_0}e^{ik_4z_0} \end{cases}$
$e^{i\ell\frac{2\pi}{\Lambda}z_0}e^{-i(2k_1-k_3)z_0} = \begin{cases} \ell=0; & e^{i\left(\ell\frac{2\pi}{\Lambda}-\mu\Delta k_{OPA}-k_4\right)z_0} = e^{-i\mu\Delta k_{OPA}z_0}e^{-ik_4z_0} \end{cases}$

Note that $z_1 = \mu z_0$. The table 3.4, 3.5 and 3.6 show that how these terms are now phase matched to $e^{\pm ik_1 z_0}$, $e^{\pm ik_3 z_0}$, and $e^{\pm ik_4 z_0}$, the other unselected terms could not satisfy this desired phase match. Since, the unselected terms have low efficiency, and would have a small contribution. Next, using the phase matched results of the selected terms in two tables to expand Eq. (3-11a), (3-11b) and (3-11c) and collecting the terms corresponding to $e^{\pm ik_1 z_0}$, $e^{\pm ik_3 z_0}$, and $e^{\pm ik_4 z_0}$. Then, we obtain the equations for pump, signal, and idler frequency components:

$$
\begin{aligned}
&2ik_1\frac{\partial A_{f1}}{\partial z_1}+\frac{i\omega_1^2\hat{\varepsilon}_{\mathrm{Im}}}{c^2}A_{f1}+\frac{2}{c^2}i\omega_1\hat{\varepsilon}_{\mathrm{Re}}\frac{\partial A_{f1}}{\partial t_1}+\frac{i}{c^2}\omega_1^2\hat{\varepsilon}'_{\mathrm{Re}}\frac{\partial A_{f1}}{\partial t_1}-\frac{\omega_1^2}{c^2}\Delta\hat{\varepsilon}_1 A_{b1}e^{-i\frac{2\pi}{\Lambda}\delta_1 z_1}\\
&=-\frac{4\pi\omega_1^2}{c^2}\Bigg[\chi_0^{(3)}\left(\left(|A_{f1}|^2+2|A_{b1}|^2+2|A_{f3}|^2+2|A_{b3}|^2+2|A_{f4}|^2+2|A_{b4}|^2\right)A_{f1}+2A_{f3}A_{f1}^{*}A_{f4}e^{-i\Delta k_{OPA}z_1}\right)\\
&\quad+\chi_1^{(3)}\Bigg((2|A_{f1}|^2+|A_{b1}|^2+2|A_{f3}|^2+2|A_{b3}|^2+2|A_{f4}|^2+2|A_{b4}|^2)A_{b1}e^{-i\frac{2\pi}{\Lambda}\delta_1 z_1}+2A_{b3}A_{f3}^{*}A_{f1}e^{-i\frac{2\pi}{\Lambda}\delta_3 z_1}+2A_{b4}A_{f4}^{*}A_{f1}e\\
&\quad+\chi_{-1}^{(3)}\left(A_{f1}^2A_{b1}^{*}e^{i\frac{2\pi}{\Lambda}\delta_1 z_1}+2A_{f3}A_{b3}^{*}A_{f1}e^{i\frac{2\pi}{\Lambda}\delta_3 z_1}+2A_{f4}A_{b4}^{*}A_{f1}e^{i\frac{2\pi}{\Lambda}\delta_4 z_1}\right)+\chi_2^{(3)}\left(A_{b1}^2A_{f1}^{*}e^{-i\frac{4\pi}{\Lambda}\delta_1 z_1}\right)\Bigg)\Bigg],
\end{aligned}
\tag{3-12a}
$$

and

$$
\begin{aligned}
&-2ik_1\frac{\partial A_{b1}}{\partial z_1}+\frac{i\omega_1^2\hat{\varepsilon}_{\mathrm{Im}}}{c^2}A_{b1}+\frac{2}{c^2}i\omega_1\hat{\varepsilon}_{\mathrm{Re}}\frac{\partial A_{b1}}{\partial t_1}+\frac{i}{c^2}\omega_1^2\hat{\varepsilon}'_{\mathrm{Re}}\frac{\partial A_{b1}}{\partial t_1}-\frac{\omega_1^2}{c^2}\Delta\hat{\varepsilon}_{-1}A_{f1}e^{i\frac{2\pi}{\Lambda}\delta_1 z_1}\\
&=-\frac{4\pi\omega_1^2}{c^2}\Bigg[\left(\chi_0^{(3)}(2|A_{f1}|^2+|A_{b1}|^2+2|A_{f3}|^2+2|A_{b3}|^2+2|A_{f4}|^2+2|A_{b4}|^2)A_{f1}+2A_{b3}A_{b1}^{*}A_{b4}e^{i\Delta k_{OPA}z_1}\right)\\
&\quad+\chi_{-1}^{(3)}\Bigg((|A_{f1}|^2+2|A_{b1}|^2+2|A_{f3}|^2+2|A_{b3}|^2+2|A_{f4}|^2+2|A_{b4}|^2)A_{f1}e^{i\frac{2\pi}{\Lambda}\delta_1 z_1}+2A_{f3}A_{b3}^{*}A_{b1}e^{i\frac{2\pi}{\Lambda}\delta_3 z_1}+2A_{f4}A_{b4}^{*}A_{b1}e^{i\frac{2\pi}{\Lambda}}\\
&\quad+\chi_1^{(3)}\left(A_{b1}^2A_{f1}^{*}e^{-i\frac{2\pi}{\Lambda}\delta_1 z_1}+2A_{b3}A_{f3}^{*}A_{b1}e^{-i\frac{2\pi}{\Lambda}\delta_3 z_1}+2A_{b4}A_{f4}^{*}A_{b1}e^{-i\frac{2\pi}{\Lambda}\delta_4 z_1}\right)+\chi_{-2}^{(3)}\left(A_{f1}^2A_{b1}^{*}e^{i\frac{4\pi}{\Lambda}\delta_1 z_1}\right)\Bigg)\Bigg],
\end{aligned}
\tag{3-12b}
$$

and

$$2ik_3\frac{\partial A_{f3}}{\partial z_1}+\frac{i\omega_3^2\hat{\varepsilon}_{\mathrm{Im}}}{c^2}A_{f3}+\frac{2}{c^2}i\omega_3\hat{\varepsilon}_{\mathrm{Re}}\frac{\partial A_{f3}}{\partial t_1}+\frac{i}{c^2}\omega_3^2\hat{\varepsilon}'_{\mathrm{Re}}\frac{\partial A_{f3}}{\partial t_1}-\frac{\omega_3^2}{c^2}\Delta\hat{\varepsilon}_1A_{b3}e^{-i\frac{2\pi}{\Lambda}\delta_3z_1}$$
$$=-\frac{4\pi\omega_3^2}{c^2}\Bigg[\chi_0^{(3)}\left((2|A_{f1}|^2+2|A_{b1}|^2+|A_{f3}|^2+2|A_{b3}|^2+2|A_{f4}|^2+2|A_{b4}|^2)A_{f3}+2A_{f1}^2A_{f4}^*e^{i\Delta k_{OPA}z_1}\right)$$
$$+\chi_1^{(3)}\Bigg((2|A_{f1}|^2+2|A_{b1}|^2+2|A_{f3}|^2+|A_{b3}|^2+2|A_{f4}|^2+2|A_{b4}|^2)A_{b3}e^{-i\frac{2\pi}{\Lambda}\delta_3z_1}+2A_{b1}A_{f1}^*A_{f3}e^{-i\frac{2\pi}{\Lambda}\delta_1z_1}+2A_{b4}A_{f4}^*A_{f3}e^{-i\frac{2\pi}{\Lambda}}$$
$$+\chi_{-1}^{(3)}\left(A_{f3}^2A_{b3}^*e^{i\frac{2\pi}{\Lambda}\delta_3z_1}+2A_{f1}A_{b1}^*A_{f3}e^{i\frac{2\pi}{\Lambda}\delta_1z_1}+2A_{f4}A_{b4}^*A_{f3}e^{i\frac{2\pi}{\Lambda}\delta_4z_1}\right)+\chi_2^{(3)}\left(A_{b3}^2A_{f3}^*e^{-i\frac{4\pi}{\Lambda}\delta_3z_1}\right)\Bigg],$$

(3-12c)

and

$$-2ik_3\frac{\partial A_{b3}}{\partial z_1}+\frac{i\omega_3^2\hat{\varepsilon}_{\mathrm{Im}}}{c^2}A_{b3}+\frac{2}{c^2}i\omega_3\hat{\varepsilon}_{\mathrm{Re}}\frac{\partial A_{b3}}{\partial t_1}+\frac{i}{c^2}\omega_3^2\hat{\varepsilon}'_{\mathrm{Re}}\frac{\partial A_{b3}}{\partial t_1}-\frac{\omega_3^2}{c^2}\Delta\hat{\varepsilon}_{-1}A_{f3}e^{i\frac{2\pi}{\Lambda}\delta_3z_1}$$
$$=-\frac{4\pi\omega_3^2}{c^2}\Bigg[\chi_0^{(3)}\left((2|A_{f1}|^2+2|A_{b1}|^2+2|A_{f3}|^2+|A_{b3}|^2+2|A_{f4}|^2+2|A_{b4}|^2)A_{b3}+2A_{b1}^2A_{b4}^*e^{-i\Delta k_{OPA}z_1}\right)$$
$$+\chi_{-1}^{(3)}\Bigg((2|A_{f1}|^2+2|A_{b1}|^2+|A_{f3}|^2+2|A_{b3}|^2+2|A_{f4}|^2+2|A_{b4}|^2)A_{b3}e^{i\frac{2\pi}{\Lambda}\delta_3z_1}+2A_{f1}A_{b1}^*A_{b3}e^{i\frac{2\pi}{\Lambda}\delta_1z_1}+2A_{f4}A_{b4}^*A_{b3}e^{i\frac{2\pi}{\Lambda}\delta_4z_1}$$
$$+\chi_1^{(3)}\left(A_{b3}^2A_{f3}^*e^{-i\frac{2\pi}{\Lambda}\delta_3z_1}+2A_{b1}A_{f1}^*A_{b3}e^{-i\frac{2\pi}{\Lambda}\delta_1z_1}+2A_{b4}A_{f4}^*A_{b3}e^{-i\frac{2\pi}{\Lambda}\delta_4z_1}\right)+\chi_{-2}^{(3)}\left(A_{f3}^2A_{b3}^*e^{i\frac{4\pi}{\Lambda}\delta_3z_1}\right)\Bigg],$$

(3-12d)

and

$$2ik_4\frac{\partial A_{f4}}{\partial z_1}+\frac{i\omega_4^2\hat{\varepsilon}_{\mathrm{Im}}}{c^2}A_{f4}+\frac{2}{c^2}i\omega_4\hat{\varepsilon}_{\mathrm{Re}}\frac{\partial A_{f4}}{\partial t_1}+\frac{i}{c^2}\omega_4^2\hat{\varepsilon}'_{\mathrm{Re}}\frac{\partial A_{f4}}{\partial t_1}-\frac{\omega_4^2}{c^2}\Delta\hat{\varepsilon}_1A_{b4}e^{-i\frac{2\pi}{\Lambda}\delta_4z_1}$$
$$=-\frac{4\pi\omega_4^2}{c^2}\Bigg[\chi_0^{(3)}\left((2|A_{f1}|^2+2|A_{b1}|^2+2|A_{f3}|^2+2|A_{b3}|^2+|A_{f4}|^2+2|A_{b4}|^2)A_{f4}+2A_{f1}^2A_{f3}^*e^{i\Delta k_{OPA}z_1}\right)$$
$$+\chi_1^{(3)}\Bigg((2|A_{f1}|^2+2|A_{b1}|^2+2|A_{f3}|^2+2|A_{b3}|^2+2|A_{f4}|^2+|A_{b4}|^2)A_{b4}e^{-i\frac{2\pi}{\Lambda}\delta_4z_1}+2A_{b3}A_{f3}^*A_{f4}e^{-i\frac{2\pi}{\Lambda}\delta_3z_1}$$
$$+\chi_{-1}^{(3)}\left(2A_{f1}A_{b1}^*A_{f4}e^{i\frac{2\pi}{\Lambda}\delta_1z_1}+2A_{f3}A_{b3}^*A_{f4}e^{i\frac{2\pi}{\Lambda}\delta_3z_1}+A_{f4}^2A_{b4}^*e^{i\frac{2\pi}{\Lambda}\delta_4z_1}\right)+\chi_2^{(3)}\left(2A_{b1}A_{f1}^*A_{f4}e^{-i\frac{2\pi}{\Lambda}\delta_1z_1}+A_{b4}^2A_{f4}^*e^{-i\frac{4\pi}{\Lambda}\delta_4z_1}\right)\Bigg],$$

(3-12e)

and

$$-2ik_4\frac{\partial A_{b4}}{\partial z_1}+\frac{i\omega_4^2\hat{\varepsilon}_{\mathrm{Im}}}{c^2}A_{b4}+\frac{2}{c^2}i\omega_4\hat{\varepsilon}_{\mathrm{Re}}\frac{\partial A_{b4}}{\partial t_1}+\frac{i}{c^2}\omega_4^2\hat{\varepsilon}'_{\mathrm{Re}}\frac{\partial A_{b4}}{\partial t_1}-\frac{\omega_4^2}{c^2}\Delta\hat{\varepsilon}_{-1}A_{f4}e^{i\frac{2\pi}{\Lambda}\delta_4 z_1}$$
$$=-\frac{4\pi\omega_4^2}{c^2}\Big[\chi_0^{(3)}\Big((2|A_{f1}|^2+2|A_{b1}|^2+2|A_{f3}|^2+2|A_{b3}|^2+2|A_{f4}|^2+|A_{b4}|^2)A_{f4}+2A_{b1}^2A_{b3}^*e^{-i\Delta k_{OPA}z_1}\Big)$$
$$+\chi_{-1}^{(3)}\Big((2|A_{f1}|^2+2|A_{b1}|^2+2|A_{f3}|^2+|A_{b3}|^2+|A_{f4}|^2+2|A_{b4}|^2)A_{b4}e^{i\frac{2\pi}{\Lambda}\delta_4 z_1}+2A_{f3}A_{b3}^*A_{b4}e^{i\frac{2\pi}{\Lambda}\delta_3 z_1}\Big)$$
$$+\chi_1^{(3)}\Big(A_{b4}^2A_{f4}^*e^{-i\frac{2\pi}{\Lambda}\delta_4 z_1}+2A_{b1}A_{f1}^*A_{f4}e^{-i\frac{2\pi}{\Lambda}\delta_1 z_1}+2A_{b3}A_{f3}^*A_{b4}e^{-i\frac{2\pi}{\Lambda}\delta_3 z_1}\Big)+\chi_{-2}^{(3)}\Big(2A_{f1}A_{b1}^*A_{b4}e^{i\frac{2\pi}{\Lambda}\delta_1 z_1}+A_{f4}^2A_{b4}^*e^{i\frac{4\pi}{\Lambda}\delta_4 z_1}\Big)\Big].$$

(3-12f)

Now, Eq. (3-12a) and (3-12b) are divided by $2ik_1$, Eq. (3-12c) and (3-12d) are divided by $2ik_3$, and Eq. (3-12e) and (3-12f) are divided by $2ik_4$ and rearranged the terms in the equations. Then, the equations is given as:

$$\frac{\partial A_{f1}}{\partial z_1}+\frac{\omega_1^2\hat{\varepsilon}_{\mathrm{Im}}}{2k_1c^2}A_{f1}+\frac{\omega_1}{k_1c^2}\hat{\varepsilon}_{\mathrm{Re}}\frac{\partial A_{f1}}{\partial t_1}+\frac{\omega_1^2}{2k_1c^2}\hat{\varepsilon}'_{\mathrm{Re}}\frac{\partial A_{f1}}{\partial t_1}+i\frac{\omega_1^2}{2k_1c^2}\Delta\hat{\varepsilon}_1A_{b1}e^{-i\frac{2\pi}{\Lambda}\delta_1 z_1}$$
$$=i\frac{2\pi\omega_1^2}{k_1c^2}\Big[\chi_0^{(3)}\Big((|A_{f1}|^2+2|A_{b1}|^2+2|A_{f3}|^2+2|A_{b3}|^2+2|A_{f4}|^2+2|A_{b4}|^2)A_{f1}+2A_{f3}A_{f1}^*A_{f4}e^{-i\Delta k_{OPA}z_1}\Big)$$
$$+\chi_1^{(3)}\Big((2|A_{f1}|^2+|A_{b1}|^2+2|A_{f3}|^2+2|A_{b3}|^2+2|A_{f4}|^2+2|A_{b4}|^2)A_{b1}e^{-i\frac{2\pi}{\Lambda}\delta_1 z_1}+2A_{b3}A_{f3}^*A_{f1}e^{-i\frac{2\pi}{\Lambda}\delta_3 z_1}+2A_{b4}A_{f4}^*A_{f1}e^{-i\frac{2\pi}{\Lambda}\delta$$
$$+\chi_{-1}^{(3)}\Big(A_{f1}^2A_{b1}^*e^{i\frac{2\pi}{\Lambda}\delta_1 z_1}+2A_{f3}A_{b3}^*A_{f1}e^{i\frac{2\pi}{\Lambda}\delta_3 z_1}+2A_{f4}A_{b4}^*A_{f1}e^{i\frac{2\pi}{\Lambda}\delta_4 z_1}\Big)+\chi_2^{(3)}\Big(A_{b1}^2A_{f1}^*e^{-i\frac{4\pi}{\Lambda}\delta_1 z_1}\Big)\Big],$$

(3-13a)

and

$$-\frac{\partial A_{b1}}{\partial z_1}+\frac{\omega_1^2\hat{\varepsilon}_{\mathrm{Im}}}{2k_1c^2}A_{b1}+\frac{\omega_1}{k_1c^2}\hat{\varepsilon}_{\mathrm{Re}}\frac{\partial A_{b1}}{\partial t_1}+\frac{\omega_1^2}{2k_1c^2}\hat{\varepsilon}'_{\mathrm{Re}}\frac{\partial A_{b1}}{\partial t_1}+i\frac{\omega_1^2}{2k_1c^2}\Delta\hat{\varepsilon}_{-1}A_{f1}e^{i\frac{2\pi}{\Lambda}\delta_1 z_1}$$
$$=i\frac{2\pi\omega_1^2}{k_1c^2}\Big[\Big(\chi_0^{(3)}(2|A_{f1}|^2+|A_{b1}|^2+2|A_{f3}|^2+2|A_{b3}|^2+2|A_{f4}|^2+2|A_{b4}|^2)A_{f1}+2A_{b3}A_{b1}^*A_{b4}e^{i\Delta k_{OPA}z_1}\Big)$$
$$+\chi_{-1}^{(3)}\Big((|A_{f1}|^2+2|A_{b1}|^2+2|A_{f3}|^2+2|A_{b3}|^2+2|A_{f4}|^2+2|A_{b4}|^2)A_{f1}e^{i\frac{2\pi}{\Lambda}\delta_1 z_1}+2A_{f3}A_{b3}^*A_{b1}e^{i\frac{2\pi}{\Lambda}\delta_3 z_1}+2A_{f4}A_{b4}^*A_{b1}e^{i\frac{2\pi}{\Lambda}\delta_4 z_1}\Big)$$
$$+\chi_1^{(3)}\Big(A_{b1}^2A_{f1}^*e^{-i\frac{2\pi}{\Lambda}\delta_1 z_1}+2A_{b3}A_{f3}^*A_{b1}e^{-i\frac{2\pi}{\Lambda}\delta_3 z_1}+2A_{b4}A_{f4}^*A_{b1}e^{-i\frac{2\pi}{\Lambda}\delta_4 z_1}\Big)+\chi_{-2}^{(3)}\Big(A_{f1}^2A_{b1}^*e^{i\frac{4\pi}{\Lambda}\delta_1 z_1}\Big)\Big],$$

(3-13b)

and

$$\frac{\partial A_{f3}}{\partial z_1}+\frac{\omega_3^2\hat{\varepsilon}_{\mathrm{Im}}}{2k_3c^2}A_{f3}+\frac{\omega_3}{k_3c^2}\hat{\varepsilon}_{\mathrm{Re}}\frac{\partial A_{f3}}{\partial t_1}+\frac{\omega_3^2}{2k_3c^2}\hat{\varepsilon}'_{\mathrm{Re}}\frac{\partial A_{f3}}{\partial t_1}+i\frac{\omega_3^2}{2k_3c^2}\Delta\hat{\varepsilon}_1A_{b3}e^{-i\frac{2\pi}{\Lambda}\delta_3z_1}$$
$$=i\frac{2\pi\omega_3^2}{k_3c^2}\Big[\chi_0^{(3)}\Big((2|A_{f1}|^2+2|A_{b1}|^2+|A_{f3}|^2+2|A_{b3}|^2+2|A_{f4}|^2+2|A_{b4}|^2)A_{f3}+2A_{f1}^2A_{f4}^*e^{i\Delta k_{OPA}z_1}\Big)$$
$$+\chi_1^{(3)}\Big((2|A_{f1}|^2+2|A_{b1}|^2+2|A_{f3}|^2+|A_{b3}|^2+2|A_{f4}|^2+2|A_{b4}|^2)A_{b3}e^{-i\frac{2\pi}{\Lambda}\delta_3z_1}+2A_{b1}A_{f1}^*A_{f3}e^{-i\frac{2\pi}{\Lambda}\delta_1z_1}+2A_{b4}A_{f4}^*A_{f3}e^{-i\frac{2\pi}{\Lambda}}$$
$$+\chi_{-1}^{(3)}\Big(A_{f3}^2A_{b3}^*e^{i\frac{2\pi}{\Lambda}\delta_3z_1}+2A_{f1}A_{b1}^*A_{f3}e^{i\frac{2\pi}{\Lambda}\delta_1z_1}+2A_{f4}A_{b4}^*A_{f3}e^{i\frac{2\pi}{\Lambda}\delta_4z_1}\Big)+\chi_2^{(3)}\Big(A_{b3}^2A_{f3}^*e^{-i\frac{4\pi}{\Lambda}\delta_3z_1}\Big)\Big],$$

(3-13c)

and

$$-\frac{\partial A_{b3}}{\partial z_1}+\frac{\omega_3^2\hat{\varepsilon}_{\mathrm{Im}}}{2k_3c^2}A_{b3}+\frac{\omega_3}{k_3c^2}\hat{\varepsilon}_{\mathrm{Re}}\frac{\partial A_{b3}}{\partial t_1}+\frac{\omega_3^2}{2k_3c^2}\hat{\varepsilon}'_{\mathrm{Re}}\frac{\partial A_{b3}}{\partial t_1}+i\frac{\omega_3^2}{2k_3c^2}\Delta\hat{\varepsilon}_{-1}A_{f3}e^{i\frac{2\pi}{\Lambda}\delta_3z_1}$$
$$=i\frac{2\pi\omega_3^2}{k_3c^2}\Big[\chi_0^{(3)}\Big((2|A_{f1}|^2+2|A_{b1}|^2+2|A_{f3}|^2+|A_{b3}|^2+2|A_{f4}|^2+2|A_{b4}|^2)A_{b3}+2A_{b1}^2A_{b4}^*e^{-i\Delta k_{OPA}z_1}\Big)$$
$$+\chi_{-1}^{(3)}\Big((2|A_{f1}|^2+2|A_{b1}|^2+|A_{f3}|^2+2|A_{b3}|^2+2|A_{f4}|^2+2|A_{b4}|^2)A_{b3}e^{i\frac{2\pi}{\Lambda}\delta_3z_1}+2A_{f1}A_{b1}^*A_{b3}e^{i\frac{2\pi}{\Lambda}\delta_1z_1}+2A_{f4}A_{b4}^*A_{b3}e^{i\frac{2\pi}{\Lambda}\delta_4z_1}$$
$$+\chi_1^{(3)}\Big(A_{b3}^2A_{f3}^*e^{-i\frac{2\pi}{\Lambda}\delta_3z_1}+2A_{b1}A_{f1}^*A_{b3}e^{-i\frac{2\pi}{\Lambda}\delta_1z_1}+2A_{b4}A_{f4}^*A_{b3}e^{-i\frac{2\pi}{\Lambda}\delta_4z_1}\Big)+\chi_{-2}^{(3)}\Big(A_{f3}^2A_{b3}^*e^{i\frac{4\pi}{\Lambda}\delta_3z_1}\Big)\Big],$$

(3-13d)

and

$$\frac{\partial A_{f4}}{\partial z_1}+\frac{\omega_4^2\hat{\varepsilon}_{\mathrm{Im}}}{2k_4c^2}A_{f4}+\frac{\omega_4}{k_4c^2}\hat{\varepsilon}_{\mathrm{Re}}\frac{\partial A_{f4}}{\partial t_1}+\frac{\omega_4^2}{2k_4c^2}\hat{\varepsilon}'_{\mathrm{Re}}\frac{\partial A_{f4}}{\partial t_1}+i\frac{\omega_4^2}{2k_4c^2}\Delta\hat{\varepsilon}_1A_{b4}e^{-i\frac{2\pi}{\Lambda}\delta_4z_1}$$
$$=i\frac{2\pi\omega_4^2}{k_4c^2}\Big[\chi_0^{(3)}\Big((2|A_{f1}|^2+2|A_{b1}|^2+2|A_{f3}|^2+2|A_{b3}|^2+|A_{f4}|^2+2|A_{b4}|^2)A_{f4}+2A_{f1}^2A_{f3}^*e^{i\Delta k_{OPA}z_1}\Big)$$
$$+\chi_1^{(3)}\Big((2|A_{f1}|^2+2|A_{b1}|^2+2|A_{f3}|^2+2|A_{b3}|^2+2|A_{f4}|^2+|A_{b4}|^2)A_{b4}e^{-i\frac{2\pi}{\Lambda}\delta_4z_1}+2A_{b3}A_{f3}^*A_{f4}e^{-i\frac{2\pi}{\Lambda}\delta_3z_1}\Big)$$
$$+\chi_{-1}^{(3)}\Big(2A_{f1}A_{b1}^*A_{f4}e^{i\frac{2\pi}{\Lambda}\delta_1z_1}+2A_{f3}A_{b3}^*A_{f4}e^{i\frac{2\pi}{\Lambda}\delta_3z_1}+A_{f4}^2A_{b4}^*e^{i\frac{2\pi}{\Lambda}\delta_4z_1}\Big)+\chi_2^{(3)}\Big(2A_{b1}A_{f1}^*A_{f4}e^{-i\frac{2\pi}{\Lambda}\delta_1z_1}+A_{b4}^2A_{f4}^*e^{-i\frac{4\pi}{\Lambda}\delta_4z_1}\Big)\Big],$$

(3-13e)

and

$$-\frac{\partial A_{b4}}{\partial z_1}+\frac{\omega_4^2\hat{\varepsilon}_{\mathrm{Im}}}{2k_4c^2}A_{b4}+\frac{\omega_4}{k_4c^2}\hat{\varepsilon}_{\mathrm{Re}}\frac{\partial A_{b4}}{\partial t_1}+\frac{\omega_4^2}{2k_4c^2}\hat{\varepsilon}'_{\mathrm{Re}}\frac{\partial A_{b4}}{\partial t_1}+i\frac{\omega_4^2}{2k_4c^2}\Delta\hat{\varepsilon}_{-1}A_{f4}e^{i\frac{2\pi}{\Lambda}\delta_4 z_1}$$
$$=i\frac{2\pi\omega_4^2}{k_4c^2}\Big[\chi_0^{(3)}\left((2|A_{f1}|^2+2|A_{b1}|^2+2|A_{f3}|^2+2|A_{b3}|^2+2|A_{f4}|^2+|A_{b4}|^2)A_{b4}+2A_{b1}^2A_{b3}^*e^{-i\Delta k_{OPA}z_1}\right)$$
$$+\chi_{-1}^{(3)}\left((2|A_{f1}|^2+2|A_{b1}|^2+2|A_{f3}|^2+|A_{b3}|^2+|A_{f4}|^2+2|A_{b4}|^2)A_{f4}e^{i\frac{2\pi}{\Lambda}\delta_4 z_1}+2A_{f3}A_{b3}^*A_{b4}e^{i\frac{2\pi}{\Lambda}\delta_3 z_1}\right)$$
$$+\chi_1^{(3)}\left(A_{b4}^2A_{f4}^*e^{-i\frac{2\pi}{\Lambda}\delta_4 z_1}+2A_{b1}A_{f1}^*A_{f4}e^{-i\frac{2\pi}{\Lambda}\delta_1 z_1}+2A_{b3}A_{f3}^*A_{b4}e^{-i\frac{2\pi}{\Lambda}\delta_3 z_1}\right)+\chi_{-2}^{(3)}\left(2A_{f1}A_{b1}^*A_{b4}e^{i\frac{2\pi}{\Lambda}\delta_1 z_1}+A_{f4}^2A_{b4}^*e^{i\frac{4\pi}{\Lambda}\delta_4 z_1}\right)\Big].$$

(3-13f)

To simplify these coupled equations, some terms in these equations need to be defined as:

the linear absorption is defined as $\alpha_j=\frac{\Lambda\omega_j^2}{\pi k_jc^2}\hat{\varepsilon}_{\mathrm{Im}}(\omega_j)\Rightarrow\frac{\omega_j^2}{2k_1c^2}\hat{\varepsilon}_{\mathrm{Im}}(\omega_j)=\frac{2\pi}{\Lambda}\alpha_j=\bar{\alpha}_j$,

the coupling coefficient is defined as $\kappa_\ell^{(j)}=\frac{\Lambda\omega_j^2}{4\pi k_jc^2}\Delta\hat{\varepsilon}_\ell\Rightarrow-\frac{i\omega_j^2}{2k_jc^2}\Delta\hat{\varepsilon}_\ell(\omega_j)=-i\frac{2\pi}{\Lambda}\kappa_\ell^{(j)}=-i\bar{\kappa}_\ell^{(j)}$,

the inverse of group velocity is defined as $\frac{1}{v_{gj}}=\frac{\partial k_j}{\partial\omega_j}=\frac{1}{2k_jc^2}(2\omega_j\hat{\varepsilon}_{\mathrm{Re}}(\omega_j)+\omega_j^2\hat{\varepsilon}'_{\mathrm{Re}}(\omega_j))$,

and also the nonlinear coefficients are defined as $\eta_\ell^{(j)}=\frac{2\pi\omega_j^2}{k_jc^2}\chi_\ell^{(3)}$, where $j=1,3,4$.

In addition, let the scaled length is $z=(\pi/\Lambda)z_1\Rightarrow\partial z=(\pi/\Lambda)\partial z_1$, and then $\partial z_1=(\Lambda/\pi)\partial z$. Let amplitudes of each frequency components can be as $A_{f_j}=a_{f_j}e^{-i\frac{\pi}{\Lambda}\delta_j z_1}$ and $A_{b_j}=a_{b_j}e^{i\frac{\pi}{\Lambda}\delta_j z_1}$. So the amplitudes with scaled length are $A_{f_j}=a_{f_j}e^{-i\delta_j z}$ and $A_{b_j}=a_{b_j}e^{i\delta_j z}$. If the amplitudes are differentiated respect to scaled length, so we obtain: $\frac{\partial A_{f_j}}{\partial z}=-i\delta_j a_{f_j}e^{-i\delta_j z}+\frac{\partial a_{f_j}}{\partial z}e^{-i\delta_j z}$ and $\frac{\partial A_{b_j}}{\partial z}=i\delta_j a_{b_j}e^{i\delta_j z}+\frac{\partial a_{b_j}}{\partial z}e^{i\delta_j z}$. Similarly, the corresponding time derivatives of all amplitudes are $\frac{\partial A_{f_j}}{\partial t}=\frac{\partial a_{f_j}}{\partial t}e^{-i\delta_j z}$ and $\frac{\partial A_{b_j}}{\partial t}=\frac{\partial a_{b_j}}{\partial t}e^{i\delta_j z}$, where $j=1,3,4$. The detuning parameter for pump and signal pulses are $\delta_1=(\Lambda/\pi)(k_1-\pi/\Lambda)$ and $\delta_3=(\Lambda/\pi)(k_3-\pi/\Lambda)$. And also the detuning parameter for idler is $\delta_4=2\delta_1-\delta_3-(\Lambda/\pi)\Delta k_{OPA}$,

where $\mu\Delta k_{OPA} = 2k_1 - k_3 - k_4$ is the wave-vector mismatch [18]. Then, substituting the above new defined parameters and identities into Eq. (3-13a), (3-13b), (3-13c), (3-13d), (3-13e) and (3-13f), respectively. So, the coupled equations can be further simplified and hence, the scaled coupled equations have been obtained as following:

$$\begin{aligned}
&\frac{\pi}{\Lambda}\left(\frac{\partial a_{f1}}{\partial z} - i\delta_1 a_{f1}\right)e^{-i\delta_1 z} + \frac{\pi}{2\Lambda}\alpha_1 a_{f1}e^{-i\delta_1 z} + \frac{1}{v_{g1}}\frac{\partial a_{f1}}{\partial t_1}e^{-i\delta_1 z} - i\frac{2\pi}{\Lambda}\kappa_1^{(1)}a_{b1}e^{-i\delta_1 z} \\
&= i\eta_0^{(1)}\left((|a_{f1}|^2 + 2|a_{b1}|^2 + 2|a_{f3}|^2 + 2|a_{b3}|^2 + 2|a_{f4}|^2 + 2|a_{b4}|^2)a_{f1}e^{-i\delta_1 z} + 2a_{f3}a_{f1}^{*}a_{f4}e^{-i\delta_1 z}\right) \\
&\quad + i\eta_1^{(1)}\left((2|a_{f1}|^2 + |a_{b1}|^2 + 2|a_{f3}|^2 + 2|a_{b3}|^2 + 2|a_{f4}|^2 + 2|a_{b4}|^2)a_{b1}e^{-i\delta_1 z} + 2a_{b3}a_{f3}^{*}a_{f1}e^{-i\delta_1 z} + 2a_{b4}a_{f4}^{*}a_{f1}e^{-i\delta_1 z}\right) \\
&\quad + i\eta_{-1}^{(1)}\left(a_{f1}^2 a_{b1}^{*}e^{-i\delta_1 z} + 2a_{f3}a_{b3}^{*}a_{f1}e^{-i\delta_1 z} + 2a_{f4}a_{b4}^{*}a_{f1}e^{-i\delta_1 z}\right) + i\eta_2^{(1)}\left(a_{b1}^2 a_{f1}^{*}e^{-i\delta_1 z}\right)\Big],
\end{aligned} \tag{3-14a}$$

$$\begin{aligned}
&-\frac{\pi}{\Lambda}\left(\frac{\partial a_{b1}}{\partial z} + i\delta_1 a_{b1}\right)e^{i\delta_1 z} + \frac{\pi}{2\Lambda}\alpha_1 a_{b1}e^{i\delta_1 z} + \frac{1}{v_{g1}}\frac{\partial a_{b1}}{\partial t_1}e^{i\delta_1 z} - i\frac{2\pi}{\Lambda}\kappa_{-1}^{(1)}a_{f1}e^{i\delta_1 z} \\
&= i\eta_0^{(1)}\left((2|a_{f1}|^2 + |a_{b1}|^2 + 2|a_{f3}|^2 + 2|a_{b3}|^2 + 2|a_{f4}|^2 + 2|a_{b4}|^2)a_{f1}e^{i\delta_1 z} + 2a_{b3}a_{b1}^{*}a_{b4}e^{i\delta_1 z}\right) \\
&\quad + i\eta_{-1}^{(1)}\left((|a_{f1}|^2 + 2|a_{b1}|^2 + 2|a_{f3}|^2 + 2|a_{b3}|^2 + 2|a_{f4}|^2 + 2|a_{b4}|^2)a_{f1}e^{i\delta_1 z} + 2a_{f3}a_{b3}^{*}a_{b1}e^{i\delta_1 z} + 2a_{f4}a_{b4}^{*}a_{b1}e^{i\delta_1 z}\right) \\
&\quad + i\eta_1^{(1)}\left(a_{b1}^2 a_{f1}^{*}e^{i\delta_1 z} + 2a_{b3}a_{f3}^{*}a_{b1}e^{i\delta_1 z} + 2a_{b4}a_{f4}^{*}a_{b1}e^{i\delta_1 z}\right) + i\eta_{-2}^{(1)}\left(a_{f1}^2 a_{b1}^{*}e^{i\delta_1 z}\right)\Big],
\end{aligned} \tag{3-14b}$$

$$\begin{aligned}
&\frac{\pi}{\Lambda}\left(\frac{\partial a_{f3}}{\partial z} - i\delta_3 a_{f3}\right)e^{-i\delta_3 z} + \frac{\pi}{2\Lambda}\alpha_3 a_{f3}e^{-i\delta_3 z} + \frac{1}{v_{g3}}\frac{\partial a_{f3}}{\partial t_1}e^{-i\delta_3 z} - i\frac{2\pi}{\Lambda}\kappa_1^{(3)}a_{b3}e^{-i\delta_3 z} \\
&= i\eta_0^{(3)}\left((2|a_{f1}|^2 + 2|a_{b1}|^2 + |a_{f3}|^2 + 2|a_{b3}|^2 + 2|a_{f4}|^2 + 2|a_{b4}|^2)a_{f3}e^{-i\delta_3 z} + 2a_{f1}^2 a_{f4}^{*}e^{-i\delta_3 z}\right) \\
&\quad + i\eta_1^{(3)}\left((2|a_{f1}|^2 + 2|a_{b1}|^2 + 2|a_{f3}|^2 + |a_{b3}|^2 + 2|a_{f4}|^2 + 2|a_{b4}|^2)a_{b3}e^{-i\delta_3 z} + 2a_{b1}a_{f1}^{*}a_{f3}e^{-i\delta_3 z} + 2a_{b4}a_{f4}^{*}a_{f3}e^{-i\delta_3 z}\right) \\
&\quad + i\eta_{-1}^{(3)}\left(a_{f3}^2 a_{b3}^{*}e^{-i\delta_3 z} + 2a_{f1}a_{b1}^{*}a_{f3}e^{-i\delta_3 z} + 2a_{f4}a_{b4}^{*}a_{f3}e^{-i\delta_3 z}\right) + i\eta_2^{(3)}\left(a_{b3}^2 a_{f3}^{*}e^{-i\delta_3 z}\right)\Big],
\end{aligned} \tag{3-14c}$$

$$-\frac{\pi}{\Lambda}\left(\frac{\partial a_{b3}}{\partial z}+i\delta_3 a_{b3}\right)e^{i\delta_3 z}+\frac{\pi}{2\Lambda}\alpha_3 a_{b3}e^{i\delta_3 z}+\frac{1}{v_{g3}}\frac{\partial a_{b3}}{\partial t_1}e^{i\delta_3 z}-i\frac{2\pi}{\Lambda}\kappa_{-1}^{(3)}a_{f3}e^{i\delta_3 z}$$
$$=i\eta_0^{(3)}\left((2|a_{f1}|^2+2|a_{b1}|^2+2|a_{f3}|^2+|a_{b3}|^2+2|a_{f4}|^2+2|a_{b4}|^2)a_{b3}e^{i\delta_3 z}+2a_{b1}^2a_{b4}^*e^{i\delta_3 z}\right)$$
$$+i\eta_{-1}^{(3)}\left((2|a_{f1}|^2+2|a_{b1}|^2+|a_{f3}|^2+2|a_{b3}|^2+2|a_{f4}|^2+2|a_{b4}|^2)a_{b3}e^{i\delta_3 z}+2a_{f1}a_{b1}^*a_{b3}e^{i\delta_3 z}+2a_{f4}a_{b4}^*a_{b3}e^{i\delta_3 z}\right)$$
$$+i\eta_1^{(3)}\left(a_{b3}^2a_{f3}^*e^{i\delta_3 z}+2a_{b1}a_{f1}^*a_{b3}e^{i\delta_3 z}+2a_{b4}a_{f4}^*a_{b3}e^{i\delta_3 z}\right)+i\eta_{-2}^{(3)}\left(a_{f3}^2a_{b3}^*e^{i\delta_3 z}\right)\Big],$$

(3-14d)

$$\frac{\pi}{\Lambda}\left(\frac{\partial a_{f4}}{\partial z}-i\delta_4 a_{f4}\right)e^{-i\delta_4 z}+\frac{\pi}{2\Lambda}\alpha_4 a_{f4}e^{-i\delta_4 z}+\frac{1}{v_{g4}}\frac{\partial a_{f4}}{\partial t_1}e^{-i\delta_4 z}-i\frac{2\pi}{\Lambda}\kappa_1^{(4)}a_{b4}e^{-i\delta_4 z}$$
$$=i\eta_0^{(4)}\left((2|a_{f1}|^2+2|a_{b1}|^2+2|a_{f3}|^2+2|a_{b3}|^2+|a_{f4}|^2+2|a_{b4}|^2)a_{f4}e^{-i\delta_4 z}+2a_{f1}^2a_{f3}^*e^{-i\delta_4 z}\right)$$
$$+i\eta_1^{(4)}\left((2|a_{f1}|^2+2|a_{b1}|^2+2|a_{f3}|^2+2|a_{b3}|^2+2|a_{f4}|^2+|a_{b4}|^2)a_{b4}e^{-i\delta_4 z}+2a_{b3}a_{f3}^*a_{f4}e^{-i\delta_4 z}\right)$$
$$+i\eta_{-1}^{(4)}\left(2a_{f1}a_{b1}^*a_{f4}e^{-i\delta_4 z}+2a_{f3}a_{b3}^*a_{f4}e^{-i\delta_4 z}+a_{f4}^2a_{b4}^*e^{-i\delta_4 z}\right)+i\eta_2^{(4)}\left(2a_{b1}a_{f1}^*a_{f4}e^{-i\delta_4 z}+a_{b4}^2a_{f4}^*e^{-i\delta_4 z}\right)\Big],$$

(3-14e)

and

$$-\frac{\pi}{\Lambda}\left(\frac{\partial a_{b4}}{\partial z}+i\delta_4 a_{b4}\right)e^{i\delta_4 z}+\frac{\pi}{2\Lambda}\alpha_4 a_{b4}e^{i\delta_4 z}+\frac{1}{v_{g4}}\frac{\partial a_{b4}}{\partial t_1}e^{i\delta_4 z}-i\frac{2\pi}{\Lambda}\kappa_{-1}^{(4)}a_{f4}e^{i\delta_4 z}$$
$$=i\eta_0^{(4)}\left((2|a_{f1}|^2+2|a_{b1}|^2+2|a_{f3}|^2+2|a_{b3}|^2+2|a_{f4}|^2+|a_{b4}|^2)a_{f4}e^{i\delta_4 z}+2a_{f1}^2a_{f3}^*e^{i\delta_4 z}\right)$$
$$+i\eta_{-1}^{(4)}\left((2|a_{f1}|^2+2|a_{b1}|^2+2|a_{f3}|^2+|a_{b3}|^2+|a_{f4}|^2+2|a_{b4}|^2)a_{b4}e^{i\delta_4 z}+2a_{f3}a_{b3}^*a_{b4}e^{i\delta_4 z}\right)$$
$$+i\eta_1^{(4)}\left(a_{b4}^2a_{f4}^*e^{i\delta_4 z}+2a_{b1}a_{f1}^*a_{f4}e^{i\delta_4 z}+2a_{b3}a_{f3}^*a_{b4}e^{i\delta_4 z}\right)+i\eta_{-2}^{(4)}\left(2a_{f1}a_{b1}^*a_{b4}e^{i\delta_4 z}+a_{f4}^2a_{b4}^*e^{i\delta_4 z}\right)\Big].$$

(3-14f)

Finally, the completed form of scaled coupled-mode equation for both pump, signal and idler frequency components have been obtained.

The scaled form of the coupled-mode equations for the pump frequency are:

$$\begin{aligned}
&\frac{\partial a_{f1}}{\partial z_1}+\left(\frac{\bar{\alpha}_1}{2}-i\bar{\delta}_1\right)a_{f1}+\frac{1}{v_{g1}}\frac{\partial a_{f1}}{\partial t_1}-i\bar{\kappa}_1^{(1)}a_{b1}\\
&=i\eta_0^{(1)}\left((|a_{f1}|^2+2|a_{b1}|^2+2|a_{f3}|^2+2|a_{b3}|^2+2|a_{f4}|^2+2|a_{b4}|^2)a_{f1}+2a_{f3}a_{f1}^*a_{f4}\right)\\
&\quad+i\eta_1^{(1)}\left((2|a_{f1}|^2+|a_{b1}|^2+2|a_{f3}|^2+2|a_{b3}|^2+2|a_{f4}|^2+2|a_{b4}|^2)a_{b1}+2a_{b3}a_{f3}^*a_{f1}+2a_{b4}a_{f4}^*a_{f1}\right)\\
&\quad+i\eta_{-1}^{(1)}\left(a_{f1}^2a_{b1}^*+2a_{f3}a_{b3}^*a_{f1}+2a_{f4}a_{b4}^*a_{f1}\right)+i\eta_2^{(1)}\left(a_{b1}^2a_{f1}^*\right)\Big],
\end{aligned}\tag{3-15a}$$

and

$$\begin{aligned}
&-\frac{\partial a_{b1}}{\partial z_1}+\left(\frac{\bar{\alpha}_1}{2}-i\bar{\delta}_1\right)a_{b1}+\frac{1}{v_{g1}}\frac{\partial a_{b1}}{\partial t_1}-i\bar{\kappa}_{-1}^{(1)}a_{f1}\\
&=i\eta_0^{(1)}\left((2|a_{f1}|^2+|a_{b1}|^2+2|a_{f3}|^2+2|a_{b3}|^2+2|a_{f4}|^2+2|a_{b4}|^2)a_{f1}+2a_{b3}a_{b1}^*a_{b4}\right)\\
&\quad+i\eta_{-1}^{(1)}\left((|a_{f1}|^2+2|a_{b1}|^2+2|a_{f3}|^2+2|a_{b3}|^2+2|a_{f4}|^2+2|a_{b4}|^2)a_{f1}+2a_{f3}a_{b3}^*a_{b1}+2a_{f4}a_{b4}^*a_{b1}\right)\\
&\quad+i\eta_1^{(1)}\left(a_{b1}^2a_{f1}^*+2a_{b3}a_{f3}^*a_{b1}+2a_{b4}a_{f4}^*a_{b1}\right)+i\eta_{-2}^{(1)}\left(a_{f1}^2a_{b1}^*\right)\Big].
\end{aligned}\tag{3-15b}$$

The scaled form of the coupled-mode equations for the signal frequency are:

$$\begin{aligned}
&\frac{\partial a_{f3}}{\partial z_1}+\left(\frac{\bar{\alpha}_3}{2}-i\bar{\delta}_3\right)a_{f3}+\frac{1}{v_{g3}}\frac{\partial a_{f3}}{\partial t_1}-i\bar{\kappa}_1^{(3)}a_{b3}\\
&=i\eta_0^{(3)}\left((2|a_{f1}|^2+2|a_{b1}|^2+|a_{f3}|^2+2|a_{b3}|^2+2|a_{f4}|^2+2|a_{b4}|^2)a_{f3}+2a_{f1}^2a_{f4}^*\right)\\
&\quad+i\eta_1^{(3)}\left((2|a_{f1}|^2+2|a_{b1}|^2+2|a_{f3}|^2+|a_{b3}|^2+2|a_{f4}|^2+2|a_{b4}|^2)a_{b3}+2a_{b1}a_{f1}^*a_{f3}+2a_{b4}a_{f4}^*a_{f3}\right)\\
&\quad+i\eta_{-1}^{(3)}\left(a_{f3}^2a_{b3}^*+2a_{f1}a_{b1}^*a_{f3}+2a_{f4}a_{b4}^*a_{f3}\right)+i\eta_2^{(3)}\left(a_{b3}^2a_{f3}^*\right)\Big],
\end{aligned}\tag{3-15c}$$

and

$$\begin{aligned}
&-\frac{\partial a_{b3}}{\partial z_1}+\left(\frac{\bar{\alpha}_3}{2}-i\bar{\delta}_3\right)a_{b3}+\frac{1}{v_{g3}}\frac{\partial a_{b3}}{\partial t_1}-i\bar{\kappa}_{-1}^{(3)}a_{f3}\\
&=i\eta_0^{(3)}\left((2|a_{f1}|^2+2|a_{b1}|^2+2|a_{f3}|^2+|a_{b3}|^2+2|a_{f4}|^2+2|a_{b4}|^2)a_{b3}+2a_{b1}^2a_{b4}^*\right)\\
&\quad+i\eta_{-1}^{(3)}\left((2|a_{f1}|^2+2|a_{b1}|^2+|a_{f3}|^2+2|a_{b3}|^2+2|a_{f4}|^2+2|a_{b4}|^2)a_{b3}+2a_{f1}a_{b1}^*a_{b3}+2a_{f4}a_{b4}^*a_{b3}\right)\\
&\quad+i\eta_1^{(3)}\left(a_{b3}^2a_{f3}^*+2a_{b1}a_{f1}^*a_{b3}+2a_{b4}a_{f4}^*a_{b3}\right)+i\eta_{-2}^{(3)}\left(a_{f3}^2a_{b3}^*\right)\Big].
\end{aligned}\tag{3-15d}$$

Finally, the scaled form of the coupled-mode equations for the idler frequency are:

$$\begin{aligned}
&\frac{\partial a_{f4}}{\partial z_1}+\left(\frac{\bar{\alpha}_4}{2}-i\bar{\delta}_4\right)a_{f4}+\frac{1}{v_{g4}}\frac{\partial a_{f4}}{\partial t_1}-i\bar{\kappa}_1^{(4)}a_{b4}\\
&=i\eta_0^{(4)}\left((2|a_{f1}|^2+2|a_{b1}|^2+2|a_{f3}|^2+2|a_{b3}|^2+|a_{f4}|^2+2|a_{b4}|^2)a_{f4}+2a_{f1}^2a_{f3}^*\right)\\
&\quad+i\eta_1^{(4)}\left((2|a_{f1}|^2+2|a_{b1}|^2+2|a_{f3}|^2+2|a_{b3}|^2+2|a_{f4}|^2+|a_{b4}|^2)a_{b4}+2a_{b3}a_{f3}^*a_{f4}\right)\\
&\quad+i\eta_{-1}^{(4)}\left(2a_{f1}a_{b1}^*a_{f4}+2a_{f3}a_{b3}^*a_{f4}+a_{f4}^2a_{b4}^*\right)+i\eta_2^{(4)}\left(2a_{b1}a_{f1}^*a_{f4}+a_{b4}^2a_{f4}^*\right)\Big],
\end{aligned}\tag{3-15e}$$

and

$$\begin{aligned}
&-\frac{\partial a_{b4}}{\partial z_1}+\left(\frac{\bar{\alpha}_4}{2}-i\bar{\delta}_4\right)a_{b4}+\frac{1}{v_{g4}}\frac{\partial a_{b4}}{\partial t_1}-i\bar{\kappa}_{-1}^{(4)}a_{f4}\\
&=i\eta_0^{(4)}\left((2|a_{f1}|^2+2|a_{b1}|^2+2|a_{f3}|^2+2|a_{b3}|^2+2|a_{f4}|^2+|a_{b4}|^2)a_{f4}+2a_{f1}^2a_{f3}^*\right)\\
&\quad+i\eta_{-1}^{(4)}\left((2|a_{f1}|^2+2|a_{b1}|^2+2|a_{f3}|^2+|a_{b3}|^2+|a_{f4}|^2+2|a_{b4}|^2)a_{b4}+2a_{f3}a_{b3}^*a_{b4}\right)\\
&\quad+i\eta_1^{(4)}\left(a_{b4}^2a_{f4}^*+2a_{b1}a_{f1}^*a_{f4}+2a_{b3}a_{f3}^*a_{b4}\right)+i\eta_{-2}^{(4)}\left(2a_{f1}a_{b1}^*a_{b4}+a_{f4}^2a_{b4}^*\right)\Big].
\end{aligned}\tag{3-15f}$$

The scaled form of coupled-mode equations for all frequency components in Eq. (3-15) have shown that the higher-order nonlinear coefficients ($\ell=\pm1,\pm2$) are the new found terms when comparing with the previous OPA works. These is similar to another version of the coupled-mode equation derived for light propagation through the deep nonlinear grating [49-51].

3.3 Numerical computations for OPA coupled-mode equations

A split-step Fourier method could be used to observe many natural phenomena in wave propagation such as transmission, reflection, and diffraction [31]. Here, the method has been developed to compute the transmission and reflection in both separated [51-52] and same solution space. According to the coupled-mode equations of OPA phenomenon as shown in Eq. (3-15a) to (3-15f). The matrix U is created as interacting amplitude matrix and operators $\hat{L}$, $\hat{K}$, and $\hat{N}$ are the linear operator, coupling operator, and nonlinear operator, respectively. The linear operator contains the spatial derivatives of longitudinal direction, the linear absorption coefficient, and the detuning parameters. This operator has been solved by using the FFT algorithm. Then the coupling operator contains the coupling coefficients. Finally, the nonlinear operator

contains the nonlinear terms which correspond to nonlinear OPA phenomenon. We summarize the detail of each operators in the Appendix B of this thesis. The coupled-mode equations can be rewritten as the ordinary differential equation as:

$$\frac{1}{v_g}\frac{\partial U}{\partial t} = \left[\hat{L} + \hat{K} + \hat{N}\right]U, \tag{3-16}$$

and now, Eq. (3-16) could be related to Eq. (2-47), and the additional operators in Eq. (3-16) could be noticed. Easily, the split-step formalism could be applied to Eq. (3-16) for obtaining the symmetrized split-step form [53] given as:

$$U(t+\Delta t) = \exp\left[v_g \frac{\Delta t}{2}\hat{L}\right]\exp\left[v_g \frac{\Delta t}{2}\hat{K}\right]\exp\left[v_g \Delta t\hat{N}\right]\exp\left[v_g \frac{\Delta t}{2}\hat{K}\right]\exp\left[v_g \frac{\Delta t}{2}\hat{L}\right]U(t). \tag{3-17}$$

Note that the Eq. (3-17) is only possible if the operators $\hat{L}$, $\hat{K}$, and $\hat{N}$ all commute. According to the operator $\hat{L}$ and $\hat{K}$ are diagonal matrices but $\hat{N}$ is not diagonal matrix because of including both diagonal and off-diagonal elements. So, the operator $\hat{N}$ could be manipulated different from the other by rewriting this operator as: $\hat{N} = \mathrm{diag}(\hat{N}) + (\hat{N} - \mathrm{diag}(\hat{N})) = \hat{N}_d + \hat{N}_{od}$ where the subscript "*d*" and "*od*" refer to diagonal and off-diagonal [52]. Now, operator $\hat{N}$ becomes the sum of two diagonal matrices. The approximated exponential of

$$\begin{aligned}
\exp\left[\hat{N}\Delta t\right] &= \exp\left[(\hat{N}_d + \hat{N}_{od})\Delta t\right] \\
&= \left(I + (\hat{N}_d + \hat{N}_{od})\Delta t + \frac{(\hat{N}_d + \hat{N}_{od})^2\Delta t^2}{2!} + \ldots\right) \\
&= \left(I + \hat{N}_d\Delta t + \frac{\hat{N}_d^2\Delta t^2}{2!} + \ldots\right) + \left(\hat{N}_{od}\Delta t + \frac{(\hat{N}_d\hat{N}_{od} + \hat{N}_{od}\hat{N}_d + \hat{N}_{od}^2)\Delta t^2}{2!} + \ldots\right) \\
&\approx \exp\left[\hat{N}_d\Delta t\right] + \hat{N}_{od}\Delta t,
\end{aligned} \tag{3-18}$$

where the higher-order term of $\hat{N}_{od}$ could be neglected in the expansion.

A rapid and easy way to check if the numerical method is stable is to make sure the law of energy conservation is achieved in every computational step. That is to say if the initial total energy of the wave is a certain quantity, then after every time step, this amount of energy stays the same. For this thesis, the errors of

energy conservation should not exceed 1%. But in case of considering material absorption, then the energy quantity may decrease as the wave propagates. In an unstable system, the energy quantity could numerically increase, and eventually causing the overflow problem. A flow chart of SSFM algorithm and a sample of the MATLAB code for modeling OPA phenomenon in PBG structure are shown in the appendix E.

3.4 Modeling

3.4.1 The PBG structure for optical parametric amplification process

In this section, the example of PBG structure is assumed to be consisted of 120 layers, which are alternating half-wave/eight-wave thin films. So that the thicknesses of two dielectric layers are a = 351 nm and b = 100 nm when the reference wavelength is 1,489 nm. Then, the transmission spectrum of the PBG structure has been calculated by using the TMM and calculated results is illustrated as Fig. 3.2 (a). Furthermore, the wavelength at the long-wavelength edge of photonic band-gap has been especially interested due to maximum resonance occurs at this position, which is called a "band-edge resonance" [18-20, 23-24, 65]. The local-field of band-edge wavelength distribute inside PBG structure is shown as Fig. 3.2 (b). From previous literatures [54], the photon density was high at band-edge position and then it is possible to enhance the nonlinear effect in the PBG structure. So in this modeling, the wavelength of pump field has been implicitly fixed at band-edge, about 1,550 nm, and continuously tuning the wavelength of signal field around the maximum transmission at the band-edge for obtaining the idler pulse [24]. Therefore the signal wavelength is chosen to be 1,555 nm and then the idler wavelength must be 1,545 nm, consequently. The sample PBG structure composed of chalcogenide-glass layer pair (As_2Se_3/As_2S_3) [70]. Chalcogenides are chosen because of their known large nonlinear optical coefficients [68-69]. The choice of materials for the sample PBG structure could be tabulated as Table 3.7.

Table 3.7: The choice of material for the sample PBG structure [70]

Optical parameter/Material layer	**Layer a**	**Layer b**
Refractive index	$n_a = 2.12$	$n_b = 1.85$
Third-order susceptibility	$\chi_a^{(3)} = 2.9\times10^{-19}$ m^2/V^2	$\chi_b^{(3)} = 4.2\times10^{-20}$ m^2/V^2
Layer thickness	$a = \lambda_0 / 2n_a = 351$ nm	$b = \lambda_0 / 8n_b = 100$ nm

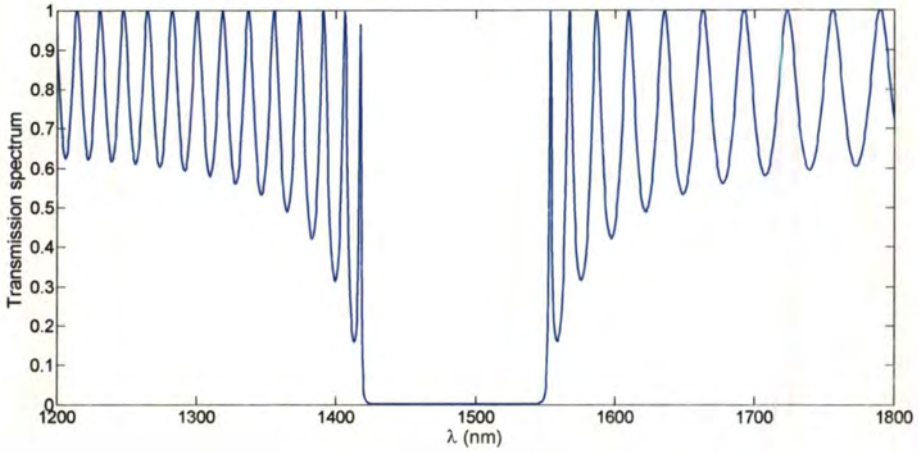

(a)

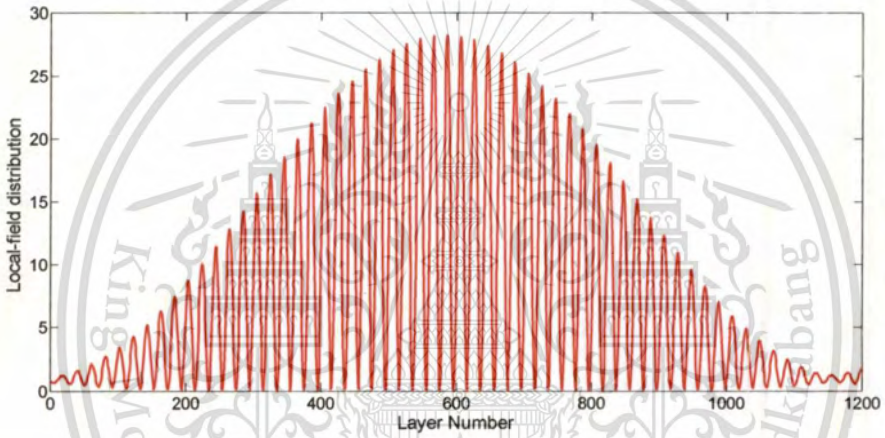

(b)

Figure 3.2 (a) The transmission spectrum of half-wave/eight-wave PBG structure which composed of 120 dielectric layers. (b) The local-field distributions (of λ_1 = 1,550 nm) inside PBG structure when band-edge resonance is satisfied.

3.4.2 Boundary and initial conditions

For solving CMEs with the SSFM, the appropriated boundary and initial conditions, which correspond to parametric interaction process, have been applied to the two ends of the sample PBG structure with the length *L*. In computational space, the left boundary condition for calculation at $z = 0$ could be defined as:

$$E_{f,pump}(0,t) = a_{f1}(0,t),$$
$$E_{f,signal}(0,t) = a_{f3}(0,t), \tag{3-19a}$$

and the right boundary condition at $z = L$ could be defined as:

$$\frac{\partial}{\partial z} E_{b,pump}(L,t) = 0,$$
$$\frac{\partial}{\partial z} E_{b,signal}(L,t) = 0. \tag{3-19b}$$

Finally, the initial condition for this modeling is:

$$E_f(z,0) = a_{f1}(z,0) + a_{f3}(z,0)$$
$$E_b(z,0) = 0 \tag{3-20}$$

for all $0 \le z \le L$. In this case, the pump and signal fields have been launched to the left-hand side of the PBG structure only and all other field amplitudes are zero.

3.4.3 Modeling results

The optical pulse propagation and OPA phenomenon have been modeled by using SSFM where the incident optical (input pump and signal) pulses are the one-dimensional Gaussian pulses, expressed similarly as:

$$a_{f1}(z,0) = a_{10} e^{\frac{(z-z_0)^2}{\sigma_{z1}^2}},$$
$$a_{f3}(z,0) = a_{30} e^{\frac{(z-z_0)^2}{\sigma_{z3}^2}}, \tag{3-21}$$

where a_{10} and a_{30} are the peak magnitudes of the initial pump and signal pulses, z is the spatial variables, and σ_z^2 is the variance of the Gaussian pulse in the corresponding direction. In the numerical modeling, the incident pulses need to be placed far enough away from the PBG structure for avoiding the overlap of the leading tail on the structure before the commencement of the pulse propagation. This problem could be solved by shifting the pulse center by a distance z_0. The Gaussian pump pulse could be tuned inside or outside the photonic band-gap. However, we are interesting in maximizing the nonlinear effect like an OPA process inside the PBG structure, so the laser detuning has been intentionally adjusted to the long-wavelength band-edge of the transmission spectrum as illustrated in Fig. 3.2 (a).

For the PBG structure, the choice of parameter values, which are used in the SSFM, is tabulated in Table 3.8.

Table 3.8: The parameter values that used in the SSFM modeling

Parameter	Pump	Signal	Idler
Absorption coefficient	$\bar{\alpha}_1 = 0$	$\bar{\alpha}_3 = 0$	$\bar{\alpha}_4 = 0$
Group velocity	$v_{g1} = 0.496c$	$v_{g3} = 0.507c$	$v_{g4} = 0.497c$
Detuning parameter	$\bar{\delta}_1 = 0.1462$	$\bar{\delta}_3 = 0.1425$	$\bar{\delta}_4 = 0.1499$
Coupling coefficient	$\bar{\kappa}_1^{(1)} = \bar{\kappa}_{-1}^{(1)} = 0.0421$	$\bar{\kappa}_1^{(3)} = \bar{\kappa}_{-1}^{(3)} = 0.0420$	$\bar{\kappa}_1^{(4)} = \bar{\kappa}_{-1}^{(4)} = 0.0422$
Nonlinear coefficient	$\eta_0^{(1)} = 0.2999$ $\eta_1^{(1)} = -0.0458 - 0.0333i$ $\eta_{-1}^{(1)} = -0.0458+0.0333\text{i}$ $\eta_2^{(1)} = -0.0142+0.0436\text{i}$ $\eta_{-2}^{(1)} = -0.0142+0.0436\text{i}$	$\eta_0^{(3)} = 0.2989$ $\eta_1^{(3)} = -0.0457 - 0.0332i$ $\eta_{-1}^{(3)} = -0.0457+0.0332\text{i}$ $\eta_2^{(3)} = -0.0141 - 0.0434i$ $\eta_{-2}^{(3)} = -0.0141 + 0.0434i$	$\eta_0^{(4)} = 0.3009$ $\eta_1^{(4)} = -0.0460 - 0.0092i$ $\eta_{-1}^{(4)} = -0.0460+0.0092\text{i}$ $\eta_2^{(4)} = -0.0142 - 0.0166i$ $\eta_{-2}^{(4)} = -0.0142+0.0166i$

Note: The calculation method of nonlinear coefficients is shown in the appendix A. And the $c = 3 \times 10^8$ m/s.

In this modeling, the total propagating length (dimensionless unit) in the z axis spans from -20π to 20π, the total time step (dimensionless unit) is $t = 400$, and the incremental of each step is $\Delta t = 0.1$. At initial state, the input pump and signal intensities are respective 4.5 and 0.011 GW/cm^2. The plots of OPA in PBG structure modeling are depicted in Fig. 3.3. The forward propagating optical pulses and the backward propagating optical pulses are in the same computational space. Each snapshot, as shown in Fig. 3.3 (a), (b), and (c), has been immediately captured when the time steps are 0, 200, and 400, respectively. The rectangular black bar in each figure denotes the PBG structure.

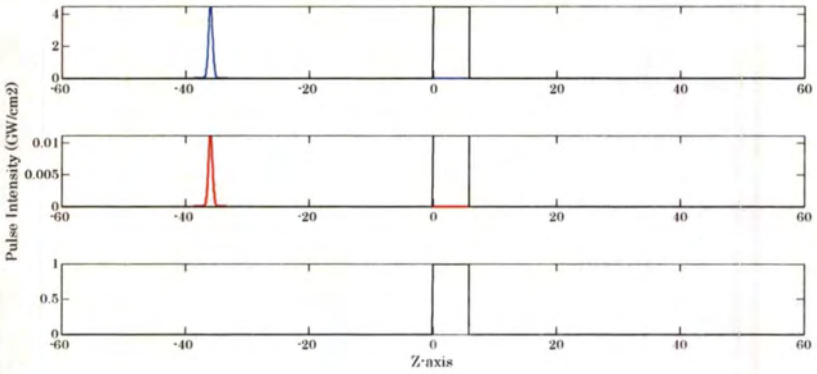

(a) $t = 0$

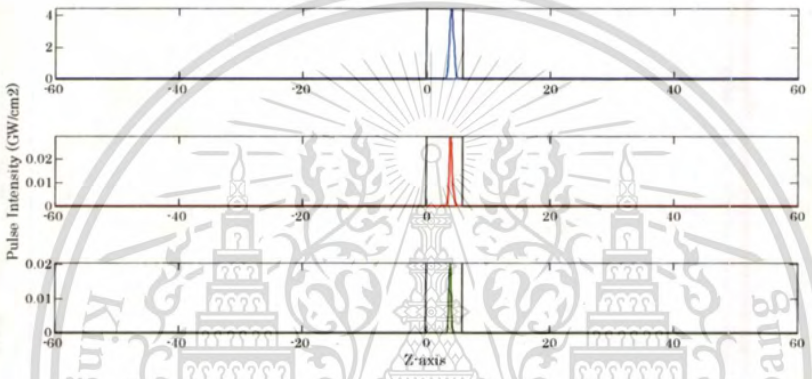

(b) $t = 200$

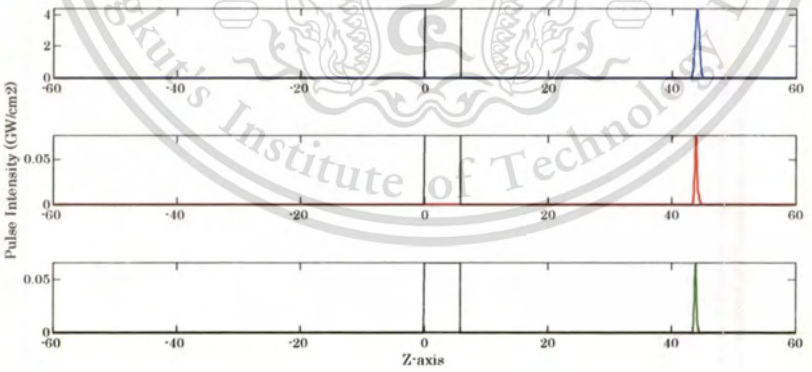

(c) $t = 400$

Figure 3.3 The snapshot of the OPA process in a PBG structure (black bar) where the pump, signal, and idler pulses are represented by the blue line (top plot of each snapshot), red line (middle plot of each snapshot), and

green line (bottom plot of each snapshot), respectively. Figures 3.3 (a)-(c) are immediately captured when total time step are 0, 200, and 400, respectively.

The parametric interaction of the input pump pulse and the signal pulse inside the PBG structure has created an idler pulse, whose frequency obtained from the difference of pump and signal frequencies. The generated idler pulse co-propagates with the pump and signals pulses, while the signal pulse has been amplified corresponding to the OPA process. In this modeling results, backward-propagating pulses have low intensities such that the intensities of these backward-propagating pulses of pump, signal, and idler are 0.006, 0.0025, and 0.0015 GW/cm^2, respectively, and they are greatly distorted. So, the propagation of backward pulses have not been shown in Fig 3.3. For this example, since the group velocity of each frequency component is different and then the signal pulse is noticed, as the leading pulse due to its fastest group velocity. The slowest pulse is pump pulse because the wavelength of this pulse was chosen at the band-edge position in Fig 3.2 (a). So the effective refractive index, due to this wavelength, of our structure has large value, consequently, the group velocity has been reduced [55]. Then, the slow-light effect has been noticed. But the wavelengths of signal and idler components are not at a transmission maximum, so their group velocities are larger than the group velocity of the pump pulse. In addition, the pulses have been simultaneously compressed because of the slow light effect near the band-edge as previous mentioned.

The strength of OPA effect has been enhanced by increasing the number of pair layers into stack. Consequently, the magnitudes of both forward-propagating signal and idler pulse amplitude are increased as shown in Fig 3.4. This figure shows both amplitudes of the amplified signal (a) and the generated idler (b) pulses have exponentially growth with the structure length. The signal pulse retains its initial phase and is simply amplified by the nonlinear interaction, whereas the generated idler pulse has a phase that depends both on the pump and signal pulses.

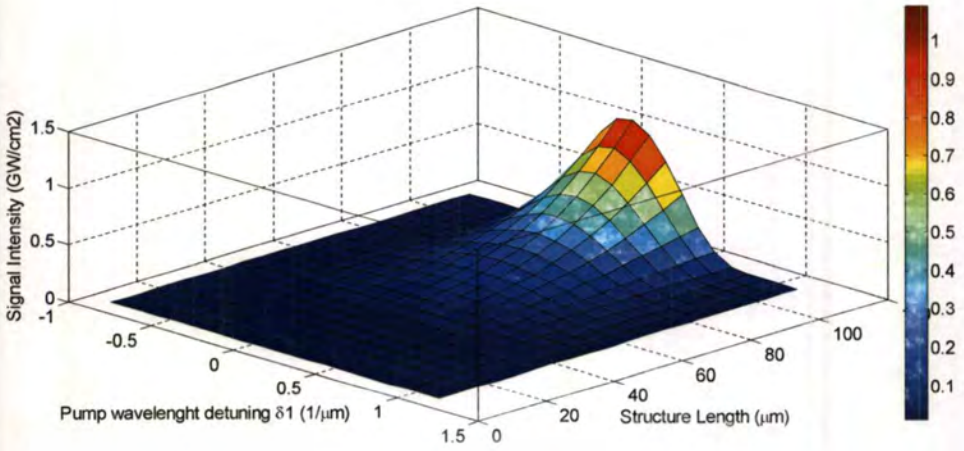

(a)

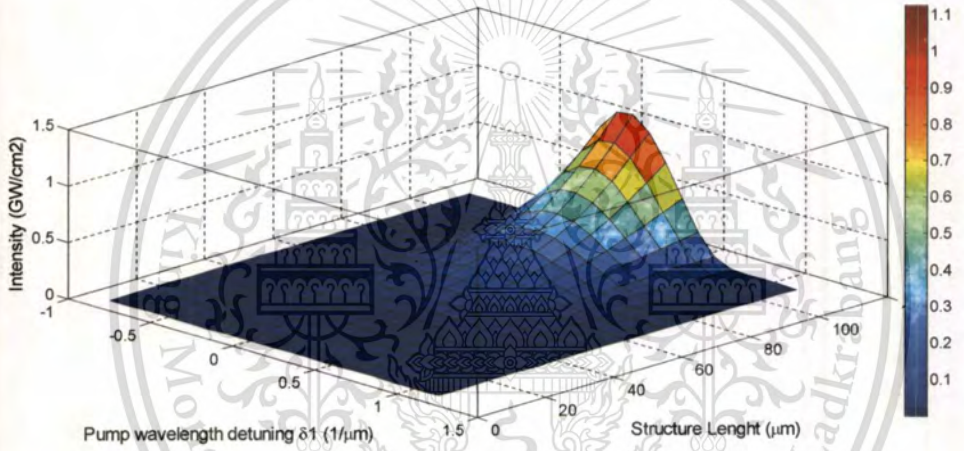

(b)

Fig. 3.4 The output intensity of signal (a) and idler (b) pulses which both depend on pump detuning parameter (δ_1) and total structure length (L)

Furthermore, the effect of output intensity of signal and idler pulses and detuning parameter between wave-vector of pump pulse and grating wave-vector have been also shown in Fig. 3.4. The maximum intensity of amplified signal 3.4 (a) and generated idler 3.4 (b) pulses are obtained when optimal detuning parameter of pump pulse (δ_1) is 0.1462. Both output signal and idler intensities were decreased by decreasing or increasing of pump detuning parameter, with changing wavelength of pump pulse or periodic

length of structure (Λ), because this detuning parameter have been affected directly to band-edge phase matching condition.

Here, the signal gain (G_s) which is calculated by using the ratio of forward-propagating output and input signal power and can be expressed as following [62-63]:

$$G_s = \frac{\left|a_{f3}(L)\right|^2}{\left|a_{f3}(0)\right|^2}. \tag{3-22}$$

And the conversion efficiency for idler pulse generation can be determined by the ratio of the generated idler power to the input pump power and can be expressed as following [62-63]:

$$C.E. = \frac{\left|a_{f4}(L)\right|^2}{\left|a_{f1}(0)\right|^2}. \tag{3-23}$$

The signal gain illustration has been shown in Fig. 3.5 (a) when pulse widths of the signal pulse are 16, 8, and 4-ps, respectively, and intensities of the input pump and signal pulses are 4.50 and 0.0112 GW/cm^2, respectively. Similarly, conversion efficiency for idler pulse generation can be illustrated as shown in figure 3.5 (b) with same initial condition.

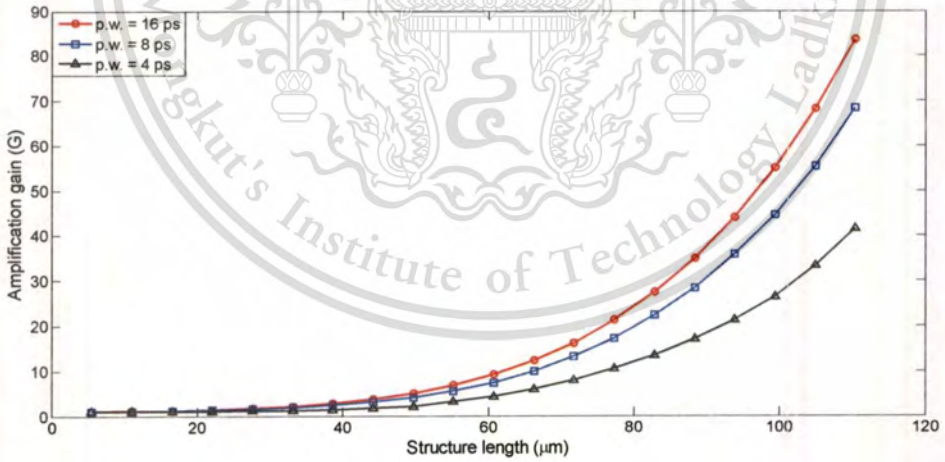

(a)

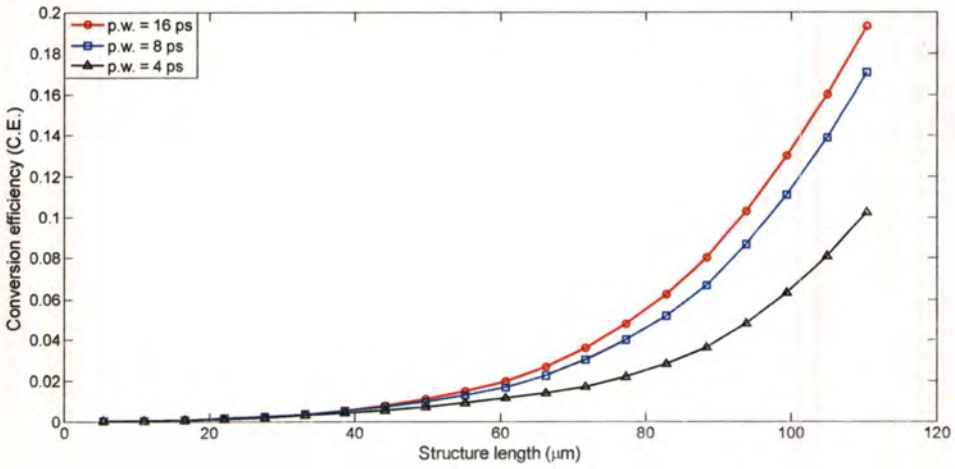

(b)

Figure 3.5 (a) The amplification gain of the signal pulse when pulse widths are 16 (red line), 8 (blue line), and 4 (black line) ps, respectively, which is respected to the structure length. (b) The conversion efficiency of idler pulse generation when pulse width are 16 (red line), 8 (blue line), and 4 (black line) ps, respectively, is respected to the structure length.

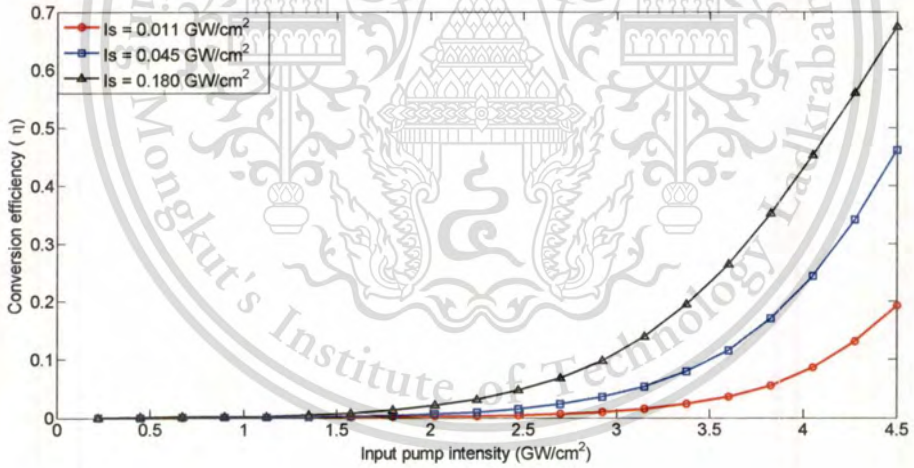

Figure 3.6 The conversion efficiency of idler pulse generation for PBG structure respect to input pump intensity when input signal intensity is 0.011 (red), 0.045 (blue), and 0.180 (black) GW/cm^2 with medium length is 101.5 μm.

The relationship between signal gain, and conversion efficiency of idler pulse and number of layers (medium length) have been shown in Fig. 3.5. The signal gain and conversion efficiency have exponentially

growth with medium length. When the periodic structure lengths are larger than about 50 μm, both gain and conversion efficiency for each pulse width has been obviously separated and continued to exponentially increase. The effects of input broaden pump pulse to both gain and conversion efficiency has been investigated as well. As shown in Fig. 3.5, both gain and conversion efficiency is reduced when the pulse width of input pulses is large. In our calculation, the pump pulse width was varied from 4, 8, and 16-ps but the pulse width of signal pulse was fixed at 8-ps. Since, we are dealing with the pulse propagation through the PBG structure, so the spectrum frequency bandwidth of picosecond pump pulse should be less than the bandwidth of the first transmission resonance (about 1 nm) where the pump wavelength is tuned to this location. So, the pulse width that corresponds to band-edge resonance peak bandwidth (1 nm) is 8-ps. And the condition that the bandwidth of pulse equal to bandwidth of band-edge resonance peak can be called *quasi-monochromatic* [19]. Therefore, the higher amplification gain and conversion efficiency have been obtained from the case that pump pulse width is about 16-ps. In the other hand, the amplification gain and conversion efficiency would be decreased when the pump pulse width is decreased to 4-ps because of the pulse dispersion in the structure.

The conversion efficiency can be enhanced by the pump pulse intensity. Fig. 3.6 shows the conversion efficiency for several sets of input pump and signal intensities. From the figure, there are two interesting aspects. First, there are same threshold input pump intensities for several input signal intensities, which leads to the maximum conversion efficiency. The threshold input pump intensity is 1.62 GW/cm^2 when input signal intensities are 0.011, 0.045, and 0.180 GW/cm2, respectively. Finally, the conversion efficiency is increasing with the input pump intensity and the input signal intensities. The maximum conversion efficiencies in each case are 19.24, 46.15, and 67.52%, respectively; when number of layer of PBG structure is about 101.5 μm.

Chapter 4

Third-harmonic generation via PBG structure

4.1 Background theory of third-harmonic generation

The third-harmonic generation (THG) has been widely studied in any nonlinear medium such as nonlinear crystals and optical fibers. THG phenomenon is really a photon-photon scattering process, during which three photons with frequency ω from a high intensity beam, called fundamental-frequency (FF) beam, are annihilated when scattering through third-order nonlinear medium and then a photon with frequency 3ω, called third-harmonic (TH) frequency, is created simultaneously. Its main features could be understood by considering the third-order polarization term, which is given as [60-61, 66-67]:

$$\mathbf{P}_{NL} = \varepsilon_0 \chi^{(3)} \mathbf{EEE}, \tag{4-1}$$

where $\mathbf{E}$ is the electric field and $\mathbf{P}_{NL}$ is the induced nonlinear polarization. Three optical waves oscillating at frequencies ω and a wave oscillating at 3ω are considered in this case and their polarizations are assumed to be linear polarization along the x axis. The electric field could be written as:

$$\mathbf{E} = \frac{1}{2}\left\{ E \exp[i(k_1 z - \omega t)] + E^* \exp[-i(k_1 z - \omega t)] \right\} \hat{\mathbf{x}}, \tag{4-2}$$

where $k_1 = n_1 \omega / c$, and n_1 is the refractive index at FF frequency, $c = 3\times10^8$ m/s is the light speed in vacuum, and all waves are assumed to be propagating in z direction. After substituting Eq. (4-2) into Eq. (4-1), the nonlinear polarization could be expressed as:

$$\mathbf{P}_{NL} = \frac{1}{8}\varepsilon_0 \chi^{(3)} \left\{ \left(3|E|^2 \exp[i(k_1 z - \omega t)] + c.c. \right) + \left(E^3 \exp[i(k_3 z - 3\omega t)] + c.c. \right) \right\} \hat{\mathbf{x}}, \tag{4-3}$$

where $k_3 = n_3(3\omega)/c$, and n_3 is the refractive index at TH frequency. We find that the P_{NL} consists of two terms involving the products of FF and TH fields. For example, the nonlinear polarization of TH field P_3 could be expressed as:

$$P_3 = \frac{1}{8}\varepsilon_0 \chi^{(3)} \left[E^3 \exp(ik_3 z - 3\omega t) + c.c. \right]. \tag{4-4}$$

The term proportion to E^3 in Eq. (4-4) is the energy transfer term and responsible for THG process. Efficient THG phenomenon occurs only if the relative phase of exponential term nearly vanish. In quantum mechanical view point, the three photons at frequency ω are annihilated with a simultaneous creation of a photon at frequency 3ω. The conservation of four photon energy for this case can be expressed as:

$$\hbar\omega + \hbar\omega + \hbar\omega = \hbar 3\omega,$$

$$\omega + \omega + \omega = 3\omega. \tag{4-5}$$

The phase-matching requirement for this phenomenon to occur is that $\Delta k_{THG} = 0$, where

$$\begin{aligned} \Delta k_{THG} &= k_3 - 3k_1 \\ &= \left[n_3(3\omega) - 3n_1\omega \right] / c. \end{aligned} \tag{4-6}$$

According to Eq. (4-6), the frequencies ω and 3ω represent the frequency of FF and TH waves, respectively. The quantum mechanical picture and frequency spectrum of the THG process are shown in Fig. 4.1(a) and (b), respectively.

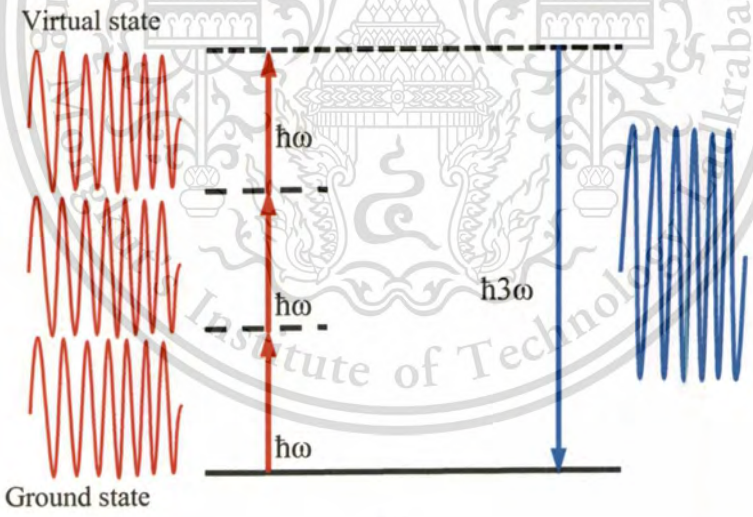

(a)

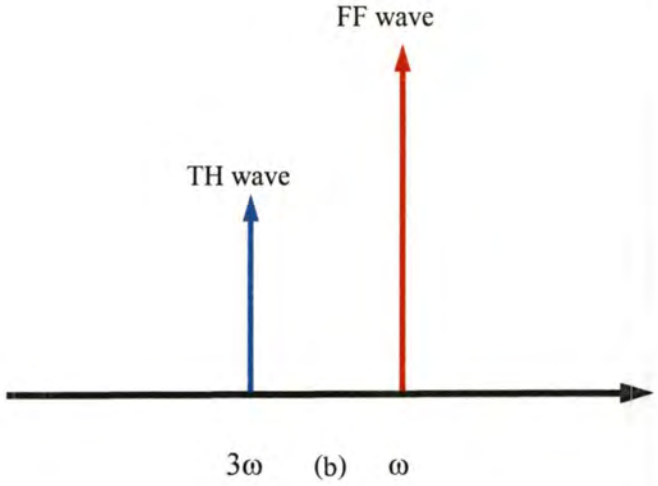

Figure 4.1. (a) Geometry of photon interaction of the THG in which the input FF photons is annihilated and a TH photon is simultaneously created. (b) The frequency spectrum of this THG.

4.2 The derivation of coupled-mode equations for third-harmonic generation

According to Eq. (2-45), this equation has the form of classical linear wave equation. The plane-wave solution of this equation, which corresponds to THG phenomenon, could be expressed as the sum of electric field amplitudes in forward- and backward-direction with a frequency ω and 3ω. The solution is expressed as:

$$E_0 = A_{f1}e^{i(k_1 z_0 - \omega t_0)} + A_{b1}e^{-i(k_1 z_0 + \omega t_0)} + A_{f3}e^{i(k_3 z_0 - 3\omega t_0)} + A_{b3}e^{-i(k_3 z_0 + 3\omega t_0)} + c.c., \qquad (4\text{-}7)$$

where the amplitudes; $A_{f1,3} = A_{f1,3}(z_1, t_1)$ and $A_{b1,3} = A_{b1,3}(z_1, t_1)$, the subscript f and b refer to the forward- and backward-direction, and the subscript 1 and 3 refer to FF and TH waves, respectively. In addition, the wave numbers (k_1, k_3) are obtained from chromatic dispersion properties of a homogeneous medium, so that $k_1^2 = \omega^2 \hat{\varepsilon}_{\mathrm{Re}}(\omega)/c^2$ and $k_3^2 = (3\omega)^2 \hat{\varepsilon}_{\mathrm{Re}}(3\omega)/c^2$. In this analysis, the phase mismatch is also treated as small i.e. $\mu\Delta k_{TH} = (k_3 - 3k_1)$. Note that $\mu\Delta k_{TH} z_0 = \Delta k_{TH} z_1$. The large phase mismatch has been avoided because that would lead to an asymptotic regime beyond four-wave mixing. Now, the first-order equation as Eq. (2-46) is then considered. The right side of this equation is consisted of the E_0^3 term. As we see in Eq. (3-4), the expansion of E_0^3 is absolutely needed. Now, for compact notation, let

$$\mathrm{F}_1 = A_{f1}e^{i(k_1 z_0 - \omega t_0)}, \mathrm{B}_1 = A_{b1}e^{-i(k_1 z_0 + \omega t_0)},$$

$$F_3 = A_{f3}e^{i(k_3 z_0 - 3\omega t_0)}, B_3 = A_{b3}e^{-i(k_3 z_0 + 3\omega t_0)},$$

Here, we expand $E_0^3 = (F_1+B_1+F_3+B_3+F_1^*+B_1^*+F_3^*+B_3^*)^3$, and we will obtain 512 terms but only 176 of them are useful because of their phases correspond to the wave-vector mismatch of THG phenomenon. The expansion of useful terms is shown in Table 4.1, and 4.2 where each terms are included the corresponding phase information.

Table 4.1: The expansion of E_0^3 for fundamental frequency component

Multiplicity	Term	Phase
3	$F_1F_1^*F_1$	$\exp[i(k_1z_0 - \omega t_0)]$
3	$F_1B_1^*F_1$	$\exp[i(3k_1z_0 - \omega t_0)]$
3	$B_1^*B_1^*F_3$	$\exp[i((2k_1 + k_3)z_0 - \omega t_0)]$
3	$B_1^*B_1^*B_3$	$\exp[i((2k_1 - k_3)z_0 - \omega t_0)]$
3	$B_1B_1^*B_1$	$\exp[-i(k_1z_0 + \omega t_0)]$
3	$B_1F_1^*B_1$	$\exp[-i(3k_1z_0 + \omega t_0)]$
3	$F_1^*F_1^*F_3$	$\exp[-i((2k_1 - k_3)z_0 + \omega t_0)]$
3	$F_1^*F_1^*B_3$	$\exp[-i((2k_1 + k_3)z_0 + \omega t_0)]$
6	$B_1B_1^*F_1$	$\exp[i(k_1z_0 - \omega t_0)]$
6	$F_3F_3^*F_1$	$\exp[i(k_1z_0 - \omega t_0)]$
6	$B_3B_3^*F_1$	$\exp[i(k_1z_0 - \omega t_0)]$
6	$F_1^*B_1^*F_3$	$\exp[i(k_3z_0 - \omega t_0)]$
6	$F_3B_3^*F_1$	$\exp[i((2k_3 + k_1)z_0 - \omega t_0)]$
6	$F_3^*B_3F_1$	$\exp[-i((2k_3 - k_1)z_0 + \omega t_0)]$
6	$F_1F_1^*B_1$	$\exp[-i(k_1z_0 + \omega t_0)]$
6	$F_3F_3^*B_1$	$\exp[-i(k_1z_0 + \omega t_0)]$
6	$B_3B_3^*B_1$	$\exp[-i(k_1z_0 + \omega t_0)]$
6	$F_1^*B_1^*B_3$	$\exp[-i(k_3z_0 + \omega t_0)]$
6	$B_1B_3F_3^*$	$\exp[-i((2k_3 + k_1)z_0 + \omega t_0)]$
6	$B_1F_3B_3^*$	$\exp[i((2k_3 - k_1)z_0 + \omega t_0)]$

Table 4.2: The expansion of E_0^3 for third-harmonic frequency component

Multiplicity	Term	Phase
1	$F_1F_1F_1$	$\exp[i(3k_1z_0-3\omega t_0)]$
1	$B_1B_1B_1$	$\exp[-i(3k_1z_0+3\omega t_0)]$
3	$F_3F_3^*F_3$	$\exp[i(k_3z_0-3\omega t_0)]$
3	$B_3B_3^*B_3$	$\exp[-i(k_3z_0+3\omega t_0)]$
3	$F_1F_1B_1$	$\exp[i(k_1z_0-3\omega t_0)]$
3	$F_3F_3B_3^*$	$\exp[i(3k_3z_0-3\omega t_0)]$
3	$B_1B_1F_1$	$\exp[-i(k_1z_0+3\omega t_0)]$
3	$B_3B_3F_3^*$	$\exp[-i(3k_3z_0+3\omega t_0)]$
6	$F_1F_1^*F_3$	$\exp[i(k_3z_0-3\omega t_0)]$
6	$B_1B_1^*F_3$	$\exp[i(k_3z_0-3\omega t_0)]$
6	$B_3B_3^*F_3$	$\exp[i(k_3z_0-3\omega t_0)]$
6	$F_1F_1^*B_3$	$\exp[-i(k_3z_0+3\omega t_0)]$
6	$B_1B_1^*B_3$	$\exp[-i(k_3z_0+3\omega t_0)]$
6	$F_3F_3^*B_3$	$\exp[-i(k_3z_0+3\omega t_0)]$
6	$F_1B_1^*F_3$	$\exp[i((2k_1+k_3)z_0-3\omega t_0)]$
6	$B_1F_1^*F_3$	$\exp[-i((2k_1-k_3)z_0+3\omega t_0)]$
6	$F_1B_1^*B_3$	$\exp[i((2k_1-k_3)z_0-3\omega t_0)]$
6	$B_1F_1^*B_3$	$\exp[-i((2k_1+k_3)z_0+3\omega t_0)]$

The interested term are separated into two tables for terms of FF component and terms of TH component. After that, the interested terms are substituted into Eq. (2-46) for both frequency components. First, we obtain the equation for FF component:

$$\left[-\frac{i}{c^2}\hat{\varepsilon}_{\mathrm{Im}}\left(i\frac{\partial}{\partial t_0}\right)\frac{\partial^2}{\partial t_0^2}+2\frac{\partial^2}{\partial z_0\partial z_1}-\frac{2}{c^2}\hat{\varepsilon}_{\mathrm{Re}}\left(i\frac{\partial}{\partial t_0}\right)\frac{\partial^2}{\partial t_0\partial t_1}\right.$$

$$\left.-\frac{i}{c^2}\frac{\partial^2}{\partial t_0^2}\hat{\varepsilon}'_{\mathrm{Re}}\left(i\frac{\partial}{\partial t_0}\right)\frac{\partial}{\partial t_1}-\frac{1}{c^2}\sum_{\substack{\ell=-\infty\\ \ell\neq 0}}^{\infty}\Delta\hat{\varepsilon}_\ell\frac{\partial^2}{\partial t_0^2}e^{i\ell\frac{2\pi}{\Lambda}z_0}\right](\mathrm{F_1}+\mathrm{B_1})$$

$$=\frac{4\pi}{c^2}\left(\frac{\partial^2}{\partial t_0^2}\sum_{\ell=-\infty}^{\infty}\chi_\ell^{(3)}e^{i\ell\frac{2\pi}{\Lambda}z_0}\right)(\mathrm{F_1F_1^*F_1}+\mathrm{B_1B_1^*F_1}+\mathrm{F_3F_3^*F_1}+\mathrm{B_3B_3^*F_1}+\mathrm{F_1F_1^*B_1}+\mathrm{B_1B_1^*B_1} \qquad (4\text{-}8a)$$

$$+\mathrm{F_3F_3^*B_1}+\mathrm{B_3B_3^*B_1}+\mathrm{F_1B_1^*F_1}+\mathrm{B_1F_1^*B_1}+\mathrm{F_1B_1^*F_3}+\mathrm{F_1B_1^*B_3}+\mathrm{F_1^*F_1^*F_3}$$

$$+\mathrm{F_1^*F_1^*B_3}+\mathrm{B_1^*B_1^*F_3}+\mathrm{B_1^*B_1^*B_3}+\mathrm{F_3B_3^*F_1}+\mathrm{F_3^*B_3F_1}+\mathrm{B_1B_3F_3^*}+\mathrm{B_1F_3B_3^*}).$$

Next, we obtain the equation for TH component:

$$\left[-\frac{i}{c^2}\hat{\varepsilon}_{\mathrm{Im}}\left(i\frac{\partial}{\partial t_0}\right)\frac{\partial^2}{\partial t_0^2}+2\frac{\partial^2}{\partial z_0\partial z_1}-\frac{2}{c^2}\hat{\varepsilon}_{\mathrm{Re}}\left(i\frac{\partial}{\partial t_0}\right)\frac{\partial^2}{\partial t_0\partial t_1}\right.$$

$$\left.-\frac{i}{c^2}\frac{\partial^2}{\partial t_0^2}\hat{\varepsilon}'_{\mathrm{Re}}\left(i\frac{\partial}{\partial t_0}\right)\frac{\partial}{\partial t_1}-\frac{1}{c^2}\sum_{\substack{\ell=-\infty\\ \ell\neq 0}}^{\infty}\Delta\hat{\varepsilon}_\ell\frac{\partial^2}{\partial t_0^2}e^{i\ell\frac{2\pi}{\Lambda}z_0}\right](\mathrm{F_3}+\mathrm{B_3})$$

$$=\frac{4\pi}{c^2}\left(\frac{\partial^2}{\partial t_0^2}\sum_{\ell=-\infty}^{\infty}\chi_\ell^{(3)}e^{i\ell\frac{2\pi}{\Lambda}z_0}\right)(\mathrm{F_1F_1^*F_3}+\mathrm{B_1B_1^*F_3}+\mathrm{F_3F_3^*F_3}+\mathrm{B_3B_3^*F_3}+\mathrm{F_1F_1^*B_3}+\mathrm{B_1B_1^*B_3} \qquad (4\text{-}8b)$$

$$+\mathrm{F_3F_3^*B_3}+\mathrm{B_3B_3^*B_3}+\mathrm{F_1F_1F_1}+\mathrm{B_1B_1B_1}+\mathrm{F_1F_1B_1}+\mathrm{B_1B_1F_1}$$

$$+\mathrm{F_3F_3B_3^*}+\mathrm{B_3B_3F_3^*}+\mathrm{F_1B_1^*F_3}+\mathrm{F_1B_1^*B_3}+\mathrm{B_1F_1^*F_3}+\mathrm{B_1F_1^*B_3}).$$

The Eq. (4-8a) and Eq. (4-8b) can be simplified and then removed $e^{-i\omega t_0}$ and $e^{-i3\omega t_0}$ which are common to both sides of each equations. We obtain:

$$\left[2ik_1\frac{\partial A_{f1}}{\partial z_1}+\frac{i\omega^2\hat{\varepsilon}_{\mathrm{Im}}}{c^2}A_{f1}+\frac{2}{c^2}i\omega\hat{\varepsilon}_{\mathrm{Re}}\frac{\partial A_{f1}}{\partial t_1}+\frac{i}{c^2}\omega^2\hat{\varepsilon}'_{\mathrm{Re}}\frac{\partial A_{f1}}{\partial t_1}-\frac{\omega^2}{c^2}\sum_{\substack{\ell=-\infty\\ \ell\neq 0}}^{\infty}\Delta\hat{\varepsilon}_\ell A_{f1}e^{i\ell\frac{2\pi}{\Lambda}z_0}\right]e^{ik_1z_0}$$

$$\left[-2ik_1\frac{\partial A_{b1}}{\partial z_1}+\frac{i\omega^2\hat{\varepsilon}_{\mathrm{Im}}}{c^2}A_{b1}+\frac{2}{c^2}i\omega\hat{\varepsilon}_{\mathrm{Re}}\frac{\partial A_{b1}}{\partial t_1}+\frac{i}{c^2}\omega^2\hat{\varepsilon}'_{\mathrm{Re}}\frac{\partial A_{b1}}{\partial t_1}-\frac{\omega^2}{c^2}\sum_{\substack{\ell=-\infty\\ \ell\neq 0}}^{\infty}\Delta\hat{\varepsilon}_\ell A_{b1}e^{i\ell\frac{2\pi}{\Lambda}z_0}\right]e^{-ik_1z_0}$$

$$\begin{aligned}
&=-\frac{4\pi\omega^2}{c^2}\left(\sum_{\ell=-\infty}^{\infty}\chi_\ell^{(3)}e^{i\ell\frac{2\pi}{\Lambda}z_0}\right)\Big[(3|A_{f1}|^2+6|A_{b1}|^2+6|A_{f3}|^2+6|A_{b3}|^2)A_{f1}e^{ik_1z_0}\\
&\quad+(6|A_{f1}|^2+3|A_{b1}|^2+6|A_{f3}|^2+6|A_{b3}|^2)A_{b1}e^{-ik_1z_0}\\
&\quad+3A_{f1}^2A_{b1}^*e^{i3k_1z_0}+3A_{b1}^2A_{f1}^*e^{-i3k_1z_0}+6A_{f1}A_{b1}^*A_{f3}e^{i(2k_1+k_3)z_0}+6A_{f1}A_{b1}^*A_{b3}e^{i(2k_1-k_3)z_0}+3A_{f1}^{*2}A_{f3}e^{-i(2k_1-k_3)z_0}\\
&\quad+3A_{f1}^{*2}A_{b3}e^{-i(2k_1+k_3)z_0}+3A_{b1}^{*2}A_{f3}e^{i(2k_1+k_3)z_0}+3A_{b1}^{*2}A_{b3}e^{i(2k_1-k_3)z_0}+6A_{f3}A_{b3}^*A_{f1}e^{i(2k_3+k_1)z_0}+6A_{f3}^*A_{b3}A_{f1}e^{-i(2k_3-k_1)z_0}\\
&\quad+6A_{b1}A_{b3}A_{f3}^*e^{-i(2k_1+k_1)z_0}+6A_{b1}A_{f3}A_{b3}^*e^{i(2k_3-k_1)z_0}\Big].
\end{aligned}\tag{4-9a}$$

$$\left[2ik_3\frac{\partial A_{f3}}{\partial z_1}+\frac{i(3\omega)^2\hat{\varepsilon}_{\mathrm{Im}}}{c^2}A_{f3}+\frac{2}{c^2}i3\omega\hat{\varepsilon}_{\mathrm{Re}}\frac{\partial A_{f3}}{\partial t_1}+\frac{i}{c^2}(3\omega)^2\hat{\varepsilon}'_{\mathrm{Re}}\frac{\partial A_{f3}}{\partial t_1}-\frac{(3\omega)^2}{c^2}\sum_{\substack{\ell=-\infty\\ \ell\neq 0}}^{\infty}\Delta\hat{\varepsilon}_\ell A_{f3}e^{i\ell\frac{2\pi}{\Lambda}z_0}\right]e^{ik_3z_0}$$

$$\left[-2ik_3\frac{\partial A_{b3}}{\partial z_1}+\frac{i(3\omega)^2\hat{\varepsilon}_{\mathrm{Im}}}{c^2}A_{b3}+\frac{2}{c^2}i3\omega\hat{\varepsilon}_{\mathrm{Re}}\frac{\partial A_{b3}}{\partial t_1}+\frac{i}{c^2}(3\omega)^2\hat{\varepsilon}'_{\mathrm{Re}}\frac{\partial A_{b3}}{\partial t_1}-\frac{(3\omega)^2}{c^2}\sum_{\substack{\ell=-\infty\\ \ell\neq 0}}^{\infty}\Delta\hat{\varepsilon}_\ell A_{b3}e^{i\ell\frac{2\pi}{\Lambda}z_0}\right]e^{-ik_3z_0}$$

$$\begin{aligned}
&=-\frac{4\pi(3\omega)^2}{c^2}\left(\sum_{\ell=-\infty}^{\infty}\chi_\ell^{(3)}e^{i\ell\frac{2\pi}{\Lambda}z_0}\right)\Big[(6|A_{f1}|^2+6|A_{b1}|^2+3|A_{f3}|^2+6|A_{b3}|^2)A_{f3}e^{ik_3z_0}\\
&\quad+(6|A_{f1}|^2+6|A_{b1}|^2+6|A_{f3}|^2+3|A_{b3}|^2)A_{b3}e^{-ik_3z_0}\\
&\quad+A_{f1}^3e^{3ik_1z_0}+A_{b1}^3e^{-3ik_1z_0}+3A_{f1}^2A_{b1}e^{ik_1z_0}+3A_{b1}^2A_{f1}e^{-ik_1z_0}+3A_{f3}^2A_{b3}^*e^{3ik_3z_0}+3A_{b3}^2A_{f3}^*e^{-3ik_3z_0}+6A_{f1}A_{b1}^*A_{f3}e^{i(2k_1+k_3)z_0}\\
&\quad+6A_{f1}A_{b1}^*A_{b3}e^{i(2k_1-k_3)z_0}+6A_{b1}A_{f1}^*A_{f3}e^{-i(2k_1-k_3)z_0}+6A_{b1}A_{f1}^*A_{b3}e^{-i(2k_1+k_3)z_0}\Big].
\end{aligned}\tag{4-9b}$$

Before expanding of Eq. (4-9a) and (4-9b), the effect of $\chi^{(3)}$ need to be examined on each of the terms in square bracket in the right-hand side of Eq. (4-9). According to the band-edge enhancement, the periodic length of PBG structure Λ is chosen to be close to the half of FF wavelengths, then deviation from this condition is: $-2\mu\delta=2\pi/\Lambda-k_1\rightarrow k_1=\pi/\Lambda+(\pi/\Lambda)\mu\delta_1$, where $\delta_1=(\Lambda/\pi)\delta$ and note that

$2\mu\delta_1 z_0 = 2\delta_1 z_1$ [18]. For matching of phase for fundamental frequency component, the phase portion of these terms in Eq. (4-9a) can be matched. Then we obtain the phase-matched condition as table 4.3.

Table 4.3: The phase-matched condition for fundamental frequency component

$e^{i\ell\frac{2\pi}{\Lambda}z_0}e^{ik_1z_0} = e^{i\left(\ell\frac{2\pi}{d}+2k_1-k_1\right)z_0} = e^{i\left(\ell\frac{2\pi}{\Lambda}+2\left(\frac{\pi}{\Lambda}+\frac{\pi}{\Lambda}\mu\delta_1\right)\right)z_0}e^{-ik_1z_0}$ $\begin{cases}\text{if } \ell=0; & e^{ik_1z_0}\\ \text{if } \ell=-1; & e^{i\frac{2\pi}{\Lambda}\delta_1z_1}e^{-ik_1z_0}\end{cases}$
$e^{i\ell\frac{2\pi}{\Lambda}z_0}e^{-ik_1z_0} = e^{i\left(\ell\frac{2\pi}{\Lambda}-2k_1+k_1\right)z_0} = e^{i\left(\ell\frac{2\pi}{\Lambda}-2\left(\frac{\pi}{\Lambda}+\frac{\pi}{\Lambda}\mu\delta_1\right)\right)z_0}e^{ik_1z_0}$ $\begin{cases}\text{if } \ell=0; & e^{-ik_1z_0}\\ \text{if } \ell=1; & e^{-i\frac{2\pi}{\Lambda}\delta_1z_1}e^{ik_1z_0}\end{cases}$
$e^{i\ell\frac{2\pi}{\Lambda}z_0}e^{3ik_1z_0} = \begin{cases} e^{i\left(\ell\frac{2\pi}{\Lambda}+2k_1+k_1\right)z_0} = e^{i\left(\ell\frac{2\pi}{\Lambda}+2\left(\frac{\pi}{\Lambda}+\frac{\pi}{\Lambda}\mu\delta_1\right)\right)z_0}e^{ik_1z_0} \rightarrow \text{if } \ell=-1; & e^{i\frac{2\pi}{\Lambda}\delta_1z_1}e^{ik_1z_1}\\ e^{i\left(\ell\frac{2\pi}{\Lambda}+4k_1-k_1\right)z_0} = e^{i\left(\ell\frac{2\pi}{\Lambda}+4\left(\frac{\pi}{\Lambda}+\frac{\pi}{\Lambda}\mu\delta_1\right)\right)z_0}e^{-ik_1z_0} \rightarrow \text{if } \ell=-2; & e^{i\frac{4\pi}{\Lambda}\delta_1z_1}e^{-ik_1z_1}\end{cases}$
$e^{i\ell\frac{2\pi}{\Lambda}z_0}e^{-3ik_1z_0} = \begin{cases} e^{i\left(\ell\frac{2\pi}{\Lambda}-2k_1-k_1\right)z_0} = e^{i\left(\ell\frac{2\pi}{\Lambda}-2\left(\frac{\pi}{\Lambda}+\frac{\pi}{\Lambda}\mu\delta_1\right)\right)z_0}e^{-ik_1z_0} \rightarrow \text{if } \ell=1; & e^{-i\frac{2\pi}{\Lambda}\delta_1z_1}e^{-ik_1z_1}\\ e^{i\left(\ell\frac{2\pi}{\Lambda}-4k_1+k_1\right)z_0} = e^{i\left(\ell\frac{2\pi}{\Lambda}-4\left(\frac{\pi}{\Lambda}+\frac{\pi}{\Lambda}\mu\delta_1\right)\right)z_0}e^{ik_1z_0} \rightarrow \text{if } \ell=2; & e^{-i\frac{4\pi}{\Lambda}\delta_1z_1}e^{ik_1z_1}\end{cases}$
$e^{i\ell\frac{2\pi}{\Lambda}z_0}e^{ik_3z_0} = \begin{cases} e^{i\left(\ell\frac{2\pi}{\Lambda}+\mu\Delta k_{TH}+2k_1+k_1\right)z_0} = e^{i\left(\ell\frac{2\pi}{\Lambda}+2\left(\frac{\pi}{\Lambda}+\frac{\pi}{\Lambda}\mu\delta_1\right)\right)z_0}e^{i\mu\Delta k_{TH}z_0}e^{ik_1z_0} \rightarrow \text{if } l=-1; & e^{i\frac{2\pi}{\Lambda}\delta_1z_1}e^{i\Delta k_{TH}z_1}e^{ik_1z_1}\\ e^{i\left(\ell\frac{2\pi}{\Lambda}+\mu\Delta k_{TH}+4k_1-k_1\right)z_0} = e^{i\left(\ell\frac{2\pi}{\Lambda}+4\left(\frac{\pi}{\Lambda}+\frac{\pi}{\Lambda}\mu\delta_1\right)\right)z_0}e^{i\mu\Delta k_{TH}z_0}e^{-ik_1z_0} \rightarrow \text{if } l=-2; & e^{i\frac{4\pi}{\Lambda}\delta_1z_1}e^{i\Delta k_{TH}z_1}e^{-ik_1z_1}\end{cases}$
$e^{i\ell\frac{2\pi}{\Lambda}z_0}e^{-ik_3z_0} = \begin{cases} e^{i\left(\ell\frac{2\pi}{\Lambda}-\mu\Delta k_{TH}-2k_1-k_1\right)z_0} = e^{i\left(\ell\frac{2\pi}{\Lambda}-2\left(\frac{\pi}{\Lambda}+\frac{\pi}{\Lambda}\mu\delta_1\right)\right)z_0}e^{-i\mu\Delta k_{TH}z_0}e^{-ik_1z_0} \rightarrow \text{if } \ell=1; & e^{-i\frac{2\pi}{\Lambda}\delta_1z_1}e^{-i\Delta k_{TH}z_1}e^{-ik_1z_1}\\ e^{i\left(\ell\frac{2\pi}{\Lambda}-\mu\Delta k_{TH}-4k_1+k_1\right)z_0} = e^{i\left(\ell\frac{2\pi}{\Lambda}-4\left(\frac{\pi}{\Lambda}+\frac{\pi}{\Lambda}\mu\delta_1\right)\right)z_0}e^{-i\mu\Delta k_{TH}z_0}e^{ik_1z_0} \rightarrow \text{if } \ell=2; & e^{-i\frac{4\pi}{\Lambda}\delta_1z_1}e^{-i\Delta k_{TH}z_1}e^{ik_1z_1}\end{cases}$
$e^{i\ell\frac{2\pi}{\Lambda}z_0}e^{i(2k_3+k_1)z_0} = e^{i\left(\ell\frac{2\pi}{\Lambda}+k_1+2\mu\Delta k_{TH}+6k_1\right)z_0} = e^{i\left(\ell\frac{2\pi}{\Lambda}+6\left(\frac{\pi}{\Lambda}+\frac{\pi}{\Lambda}\mu\delta_1\right)\right)z_0}e^{2i\mu\Delta k_{TH}z_0}e^{ik_1z_0} \rightarrow \text{if } \ell=-3; \quad e^{i\ell\frac{6\pi}{\Lambda}\delta_1z_1}e^{2i\Delta k_{TH}z_1}e^{ik_1z_0}$
$e^{i\ell\frac{2\pi}{\Lambda}z_0}e^{-i(2k_3+k_1)z_0} = e^{i\left(\ell\frac{2\pi}{\Lambda}-k_1-2\mu\Delta k_{TH}-6k_1\right)z_0} = e^{i\left(\ell\frac{2\pi}{\Lambda}-6\left(\frac{\pi}{\Lambda}+\frac{\pi}{\Lambda}\mu\delta_1\right)\right)z_0}e^{-2i\mu\Delta k_{TH}z_0}e^{-ik_1z_0} \rightarrow \text{if } \ell=3; \quad e^{-i\frac{6\pi}{\Lambda}\delta_1z_1}e^{-2i\Delta k_{TH}z_1}e^{-ik_1z_0}$
$e^{i\ell\frac{2\pi}{\Lambda}z_0}e^{i(2k_3-k_1)z_0} = e^{i\left(\ell\frac{2\pi}{\Lambda}-k_1+2\mu\Delta k_{TH}+6k_1\right)z_0} = e^{i\left(\ell\frac{2\pi}{\Lambda}+6\left(\frac{\pi}{\Lambda}+\frac{\pi}{\Lambda}\mu\delta_1\right)\right)z_0}e^{2i\mu\Delta k_{TH}z_0}e^{-ik_1z_0} \rightarrow \text{if } \ell=-3; \quad e^{i\frac{6\pi}{\Lambda}\delta_1z_1}e^{2i\Delta k_{TH}z_1}e^{-ik_1z_0}$
$e^{i\ell\frac{2\pi}{\Lambda}z_0}e^{-i(2k_3-k_1)z_0} = e^{i\left(\ell\frac{2\pi}{\Lambda}+k_1-2\mu\Delta k_{TH}-6k_1\right)z_0} = e^{i\left(\ell\frac{2\pi}{\Lambda}-6\left(\frac{\pi}{\Lambda}+\frac{\pi}{\Lambda}\mu\delta_1\right)\right)z_0}e^{-2i\mu\Delta k_{TH}z_0}e^{ik_1z_0} \rightarrow \text{if } l=3; \quad e^{-i\frac{6\pi}{\Lambda}\delta_1z_1}e^{-2i\Delta k_{TH}z_1}e^{ik_1z_0}$
$e^{i\ell\frac{2\pi}{\Lambda}z_0}e^{i(2k_1-k_3)z_0} = e^{i\ell\frac{2\pi}{\Lambda}z_0}e^{i(2k_1-\mu\Delta k_{TH}-3k_1)z_0} = e^{i\left(\ell\frac{2\pi}{\Lambda}-2\left(\frac{\pi}{\Lambda}+\frac{\pi}{\Lambda}\mu\delta_1\right)\right)z_0}e^{-i\mu\Delta k_{TH}z_0}e^{ik_1z_0} \rightarrow \text{if } \ell=1; \quad e^{-i\frac{2\pi}{\Lambda}\delta_1z_1}e^{-i\Delta k_{TH}z_1}e^{ik_1z_0}$
$e^{i\ell\frac{2\pi}{\Lambda}z_0}e^{-i(2k_1-k_3)z_0} = e^{i\ell\frac{2\pi}{\Lambda}z_0}e^{-i(2k_1-\mu\Delta k_{TH}-3k_1)z_0} = e^{i\left(\ell\frac{2\pi}{\Lambda}+2\left(\frac{\pi}{\Lambda}+\frac{\pi}{\Lambda}\mu\delta_1\right)\right)z_0}e^{i\mu\Delta k_{TH}z_0}e^{-ik_1z_0} \rightarrow \text{if } \ell=-1; \quad e^{i\frac{2\pi}{\Lambda}\delta_1z_1}e^{i\Delta k_{TH}z_1}e^{-ik_1z_0}$

Table 4.3: The phase-matched condition for fundamental frequency component (continue)

$e^{i\ell\frac{2\pi}{\Lambda}z_0}e^{i(2k_1+k_3)z_0}=\begin{cases} e^{i\ell\frac{2\pi}{\Lambda}z_0}e^{i(2k_1+\mu\Delta k_{TH}+3k_1)z_0}=e^{i\left(\ell\frac{2\pi}{\Lambda}+4\left(\frac{\pi}{\Lambda}+\frac{\pi}{\Lambda}\mu\delta_1\right)\right)z_0}e^{i\mu\Delta k_{TH}z_0}e^{ik_1z_0}\rightarrow \text{if } \ell=-2;\quad e^{i\frac{4\pi}{\Lambda}\delta_1 z_1}e^{i\Delta k_{TH}z_1}e^{ik_1z_0} \\ e^{i\ell\frac{2\pi}{\Lambda}z_0}e^{i(2k_1+\mu\Delta k_{TH}+3k_1)z_0}=e^{i\left(\ell\frac{2\pi}{\Lambda}+6\left(\frac{\pi}{\Lambda}+\frac{\pi}{\Lambda}\mu\delta_1\right)\right)z_0}e^{i\mu\Delta k_{TH}z_0}e^{-ik_1z_0}\rightarrow \text{if } \ell=-3;\quad e^{i\frac{6\pi}{\Lambda}\delta_1 z_1}e^{i\Delta k_{TH}z_1}e^{-ik_1z_0} \end{cases}$
$e^{i\ell\frac{2\pi}{\Lambda}z_0}e^{-i(2k_1+k_3)z_0}=\begin{cases} e^{i\ell\frac{2\pi}{\Lambda}z_0}e^{-i(5k_1+\mu\Delta k_{TH})z_0}=e^{i\left(\ell\frac{2\pi}{\Lambda}-4\left(\frac{\pi}{\Lambda}+\frac{\pi}{\Lambda}\mu\delta_1\right)\right)z_0}e^{-i\mu\Delta k_{TH}z_0}e^{-ik_1z_0}\rightarrow \text{if } \ell=2;e^{-i\frac{4\pi}{\Lambda}\delta_1 z_1}e^{-i\Delta k_{TH}z_1}e^{-ik_1z_0} \\ e^{i\ell\frac{2\pi}{\Lambda}z_0}e^{-i(5k_1+\mu\Delta k_{TH})z_0}=e^{i\left(\ell\frac{2\pi}{\Lambda}-6\left(\frac{\pi}{\Lambda}+\frac{\pi}{\Lambda}\mu\delta_1\right)\right)z_0}e^{-i\mu\Delta k_{TH}z_0}e^{ik_1z_0}\rightarrow \text{if } \ell=3;e^{-i\frac{6\pi}{\Lambda}\delta_1 z_1}e^{-i\Delta k_{TH}z_1}e^{ik_1z_0} \end{cases}$

For matching of phase for third-harmonic frequency component, the phase portion of these terms in Eq. (4-9b) can be matched. Then we obtain the phase-matched condition as table 4.4.

Table 4.4: The phase-matched condition for third-harmonic frequency component

$e^{i\ell\frac{2\pi}{\Lambda}z_0}e^{ik_1z_0}=e^{i\left(\ell\frac{2\pi}{\Lambda}+k_3+k_1-\mu\Delta k_{TH}-3k_1\right)z_0}=e^{i\left(\ell\frac{2\pi}{\Lambda}-\mu\Delta k_{TH}-2\left(\frac{\pi}{\Lambda}+\frac{\pi}{\Lambda}\mu\delta_1\right)\right)z_0}e^{ik_3z_0}\begin{cases}\text{if } \ell=1;\quad e^{-i\frac{2\pi}{\Lambda}\delta_1 z_1}e^{-i\Delta k_{TH}z_1}e^{ik_3z_0}\end{cases}$
$e^{i\ell\frac{2\pi}{\Lambda}z_0}e^{-ik_1z_0}=e^{i\left(\ell\frac{2\pi}{\Lambda}+\mu\Delta k_{TH}+3k_1-k_1-k_3\right)z_0}=e^{i\left(\ell\frac{2\pi}{\Lambda}+\mu\Delta k_{TH}+2\left(\frac{\pi}{\Lambda}+\frac{\pi}{\Lambda}\mu\delta_1\right)\right)z_0}e^{-ik_3z_0}\begin{cases}\text{if } \ell=-1;\quad e^{i\frac{2\pi}{\Lambda}\delta_1 z_1}e^{i\Delta k_{TH}z_1}e^{-ik_3z_0}\end{cases}$
$e^{i\ell\frac{2\pi}{\Lambda}z_0}e^{3ik_1z_0}=e^{i\left(\ell\frac{2\pi}{\Lambda}+k_3-\mu\Delta k_{TH}\right)z_0}=e^{i\ell\frac{2\pi}{\Lambda}z_0}e^{-i\mu\Delta k_{TH}z_0}e^{ik_3z_0}\begin{cases}\text{if } \ell=0;\quad e^{-i\Delta k_{TH}z_1}e^{ik_3z_0}\end{cases}$
$e^{i\ell\frac{2\pi}{\Lambda}z_0}e^{-3ik_1z_0}=e^{i\left(\ell\frac{2\pi}{\Lambda}-k_3+\mu\Delta k_{TH}\right)z_0}=e^{i\ell\frac{2\pi}{\Lambda}z_0}e^{i\mu\Delta k_{TH}z_0}e^{-ik_3z_0}\begin{cases}\text{if } \ell=0;\quad e^{i\Delta k_{TH}z_1}e^{-ik_3z_0}\end{cases}$
$e^{i\ell\frac{2\pi}{\Lambda}z_0}e^{ik_3z_0}=e^{i\left(\ell\frac{2\pi}{\Lambda}+2k_3-k_3\right)z_0}=e^{i\left(\ell\frac{2\pi}{\Lambda}+2\mu\Delta k_{TH}+6\left(\frac{\pi}{\Lambda}+\frac{\pi}{\Lambda}\mu\delta_1\right)\right)z_0}e^{-ik_3z_0}\begin{cases}\text{if } \ell=0;\quad e^{ik_3z_0}\\ \text{if } \ell=-3;\quad e^{i\frac{6\pi}{\Lambda}\delta_1 z_1}e^{2i\Delta k_{TH}z_1}e^{-ik_3z_0}=e^{i\frac{\pi}{\Lambda}\delta_3 z_1}e^{-ik_3z_0}\end{cases}$
$e^{i\ell\frac{2\pi}{\Lambda}z_0}e^{-ik_3z_0}=e^{i\left(\ell\frac{2\pi}{\Lambda}-2k_3+k_3\right)z_0}=e^{i\left(\ell\frac{2\pi}{\Lambda}-2\mu\Delta k_{TH}-6\left(\frac{\pi}{\Lambda}+\frac{\pi}{\Lambda}\mu\delta_1\right)\right)z_0}e^{ik_3z_0}\begin{cases}\text{if } \ell=0;\quad e^{-ik_3z_0}\\ \text{if } \ell=3;\quad e^{-i\frac{6\pi}{\Lambda}\delta_1 z_1}e^{-2i\Delta k_{TH}z_1}e^{ik_3z_0}\end{cases}$
$e^{i\ell\frac{2\pi}{\Lambda}z_0}e^{3ik_3z_0}=\begin{cases} e^{i\left(\ell\frac{2\pi}{\Lambda}+2k_3+k_3\right)z_0}=e^{i\left(\ell\frac{2\pi}{\Lambda}+2\mu\Delta k_{TH}+6\left(\frac{\pi}{\Lambda}+\frac{\pi}{\Lambda}\mu\delta_1\right)\right)z_0}e^{ik_3z_0}\begin{cases}\text{if } \ell=-3;\quad e^{i\frac{6\pi}{\Lambda}\delta_1 z_1}e^{2i\Delta k_{TH}z_1}e^{ik_3z_0}\end{cases} \\ e^{i\left(\ell\frac{2\pi}{\Lambda}+4k_3-k_3\right)z_0}=e^{i\left(\ell\frac{2\pi}{\Lambda}+4\mu\Delta k_{TH}+12\left(\frac{\pi}{\Lambda}+\frac{\pi}{\Lambda}\mu\delta_1\right)\right)z_0}e^{-ik_3z_0}\begin{cases}\text{if } \ell=-6;\quad e^{i\frac{12\pi}{\Lambda}\delta_1 z_1}e^{4i\Delta k_{TH}z_1}e^{-ik_3z_0}\end{cases} \end{cases}$
$e^{i\ell\frac{2\pi}{\Lambda}z_0}e^{-3ik_3z_0}=\begin{cases} e^{i\left(\ell\frac{2\pi}{\Lambda}-2k_3-k_3\right)z_0}=e^{i\left(\ell\frac{2\pi}{\Lambda}-2\mu\Delta k_{TH}-6\left(\frac{\pi}{\Lambda}+\frac{\pi}{\Lambda}\mu\delta_1\right)\right)z_0}e^{-ik_3z_0}\begin{cases}\text{if } \ell=3;\quad e^{-i\frac{6\pi}{\Lambda}\delta_1 z_1}e^{-2i\Delta k_{TH}z_1}e^{-ik_3z_0}\end{cases} \\ e^{i\left(\ell\frac{2\pi}{\Lambda}-4k_3+k_3\right)z_0}=e^{i\left(\ell\frac{2\pi}{\Lambda}-4\mu\Delta k_{TH}-12\left(\frac{\pi}{\Lambda}+\frac{\pi}{\Lambda}\mu\delta_1\right)\right)z_0}e^{ik_3z_0}\begin{cases}\text{if } \ell=6;\quad e^{-i\frac{12\pi}{\Lambda}\delta_1 z_1}e^{-4i\Delta k_{TH}z_1}e^{ik_3z_0}\end{cases} \end{cases}$

Table 4.4: The phase-matched condition for third-harmonic frequency component (continue)

$e^{i\ell\frac{2\pi}{\Lambda}z_0}e^{i(2k_1+k_3)z_0} = \begin{cases} e^{i\ell\frac{2\pi}{\Lambda}z_0}e^{i(2k_1+k_3)z_0} = e^{i\left(\ell\frac{2\pi}{\Lambda}+2\left(\frac{\pi}{\Lambda}+\frac{\pi}{\Lambda}\mu\delta_1\right)\right)z_0}e^{ik_3z_0} \rightarrow \text{if } \ell=-1; \quad e^{i\frac{2\pi}{\Lambda}\delta_1 z_1}e^{ik_3z_0} \\ e^{i\ell\frac{2\pi}{\Lambda}z_0}e^{i(2k_1+2k_3-k_3)z_0} = e^{i\left(\ell\frac{2\pi}{\Lambda}+2\mu\Delta k_{TH}+8\left(\frac{\pi}{\Lambda}+\frac{\pi}{\Lambda}\mu\delta_1\right)\right)z_0}e^{-ik_3z_0} \rightarrow \text{if } \ell=-4; \quad e^{i\frac{8\pi}{\Lambda}\delta_1 z_1}e^{2i\Delta k_{TH}z_1}e^{-ik_3z_0} \end{cases}$
$e^{i\ell\frac{2\pi}{\Lambda}z_0}e^{-i(2k_1+k_3)z_0} = \begin{cases} e^{i\ell\frac{2\pi}{\Lambda}z_0}e^{-i(2k_1+k_3)z_0} = e^{i\left(\ell\frac{2\pi}{\Lambda}-2\left(\frac{\pi}{\Lambda}+\frac{\pi}{\Lambda}\mu\delta_1\right)\right)z_0}e^{-ik_3z_0} \rightarrow \text{if } \ell=1; \quad e^{-i\frac{2\pi}{\Lambda}\delta_1 z_1}e^{-ik_3z_0} \\ e^{i\ell\frac{2\pi}{\Lambda}z_0}e^{-i(2k_1+2k_3-k_3)z_0} = e^{i\left(\ell\frac{2\pi}{\Lambda}-2\mu\Delta k_{TH}-8\left(\frac{\pi}{\Lambda}+\frac{\pi}{\Lambda}\mu\delta_1\right)\right)z_0}e^{ik_3z_0} \rightarrow \text{if } \ell=4; \quad e^{-i\frac{8\pi}{\Lambda}\delta_1 z_1}e^{-2i\Delta k_{TH}z_1}e^{ik_3z_0} \end{cases}$
$e^{i\ell\frac{2\pi}{\Lambda}z_0}e^{i(2k_1-k_3)z_0} = \begin{cases} e^{i\ell\frac{2\pi}{\Lambda}z_0}e^{i(2k_1-k_3)z_0} = e^{i\left(\ell\frac{2\pi}{\Lambda}+2\left(\frac{\pi}{\Lambda}+\frac{\pi}{\Lambda}\mu\delta_1\right)\right)z_0}e^{-ik_3z_0} \rightarrow \text{if } \ell=-1; \quad e^{i\frac{2\pi}{\Lambda}\delta_1 z_1}e^{-ik_3z_0} \\ e^{i\ell\frac{2\pi}{\Lambda}z_0}e^{i(2k_1-2k_3+k_3)z_0} = e^{i\left(\ell\frac{2\pi}{\Lambda}-2\mu\Delta k_{TH}-4\left(\frac{\pi}{\Lambda}+\frac{\pi}{\Lambda}\mu\delta_1\right)\right)z_0}e^{ik_3z_0} \rightarrow \text{if } \ell=2; \quad e^{-i\frac{4\pi}{\Lambda}\delta_1 z_1}e^{-2i\Delta k_{TH}z_1}e^{ik_3z_0} \end{cases}$
$e^{i\ell\frac{2\pi}{\Lambda}z_0}e^{-i(2k_1-k_3)z_0} = \begin{cases} e^{i\ell\frac{2\pi}{\Lambda}z_0}e^{-i(2k_1-k_3)z_0} = e^{i\left(\ell\frac{2\pi}{\Lambda}-2\left(\frac{\pi}{\Lambda}+\frac{\pi}{\Lambda}\mu\delta_1\right)\right)z_0}e^{ik_3z_0} \rightarrow \text{if } \ell=1; \quad e^{-i\frac{2\pi}{\Lambda}\delta_1 z_1}e^{ik_3z_0} \\ e^{i\ell\frac{2\pi}{\Lambda}z_0}e^{-i(2k_1-2k_3+k_3)z_0} = e^{i\left(\ell\frac{2\pi}{\Lambda}+2\mu\Delta k_{TH}+4\left(\frac{\pi}{\Lambda}+\frac{\pi}{\Lambda}\mu\delta_1\right)\right)z_0}e^{ik_3z_0} \rightarrow \text{if } \ell=-2; \quad e^{i\frac{4\pi}{\Lambda}\delta_1 z_1}e^{2i\Delta k_{TH}z_1}e^{-ik_3z_0} \end{cases}$

Note that $z_1 = \mu z_0$. The table 4.3 and 4.4 show that how these terms are now phase matched to $e^{\pm ik_1 z_1}$ and $e^{\pm ik_3 z_1}$, the other unselected terms could not satisfy this desired phase match. Since, the unselected terms have low efficiency, and would have a small contribution. Next, using the phase matched results of the selected terms in two tables to expand Eq. (4-9a) and (4-9b) and collecting the terms corresponding to $e^{\pm ik_1 z_1}$ and $e^{\pm ik_3 z_1}$. Then, we obtain the equations for both frequency components:

$$
\begin{aligned}
&2ik_1\frac{\partial A_{f1}}{\partial z_1}+\frac{i\omega^2\hat{\varepsilon}_{\text{Im}}}{c^2}A_{f1}+\frac{2}{c^2}i\omega\hat{\varepsilon}_{\text{Re}}\frac{\partial A_{f1}}{\partial t_1}+\frac{i}{c^2}\omega^2\hat{\varepsilon}'_{\text{Re}}\frac{\partial A_{f1}}{\partial t_1}-\frac{\omega^2}{c^2}\Delta\hat{\varepsilon}_1 A_{b1}e^{-i\frac{2\pi}{\Lambda}\delta_1 z_1} \\
&=-\frac{4\pi\omega^2}{c^2}\Big[\chi_0^{(3)}(3|A_{f1}|^2+6|A_{b1}|^2+6|A_{f3}|^2+6|A_{b3}|^2)A_{f1} \\
&+\chi_1^{(3)}\left((6|A_{f1}|^2+3|A_{b1}|^2+6|A_{f3}|^2+6|A_{b3}|^2)A_{b1}+3A_{b1}^{*2}A_{b3}e^{-i\Delta k_{TH}z_1}\right)e^{-i\frac{2\pi}{\Lambda}\delta_1 z_1} \\
&+\chi_{-1}^{(3)}\left(3A_{f1}^2A_{b1}^*+6A_{f1}^*A_{b1}^*A_{f3}e^{i\Delta k_{TH}z_1}\right)e^{i\frac{2\pi}{\Lambda}\delta_1 z_1} \\
&+\chi_{-2}^{(3)}\left(3A_{b1}^{*2}A_{f3}e^{i\Delta k_{TH}z_1}\right)e^{i\frac{4\pi}{\Lambda}\delta_1 z_1}+\chi_2^{(3)}\left(3A_{b1}^2A_{f1}^*+6A_{f1}^*A_{b1}^*A_{b3}e^{-i\Delta k_{TH}z_1}\right)e^{-i\frac{4\pi}{\Lambda}\delta_1 z_1} \\
&+\chi_{-3}^{(3)}\left(6A_{f3}A_{b3}^*A_{f1}e^{2i\Delta k_{TH}z_1}\right)e^{i\frac{6\pi}{\Lambda}\delta_1 z_1}+\chi_3^{(3)}\left(3A_{f1}^{*2}A_{b3}e^{-i\Delta k_{TH}z_1}+6A_{f3}^*A_{b3}A_{f1}e^{-2i\Delta k_{TH}z_1}\right)e^{-i\frac{6\pi}{\Lambda}\delta_1 z_1}\Big],
\end{aligned}
\tag{4-10a}
$$

and

$$
\begin{aligned}
&-2ik_1\frac{\partial A_{b1}}{\partial z_1}+\frac{i\omega^2\hat{\varepsilon}_{\mathrm{Im}}}{c^2}A_{b1}+\frac{2}{c^2}i\omega\hat{\varepsilon}_{\mathrm{Re}}\frac{\partial A_{b1}}{\partial t_1}+\frac{i}{c^2}\omega^2\hat{\varepsilon}'_{\mathrm{Re}}\frac{\partial A_{b1}}{\partial t_1}-\frac{\omega^2}{c^2}\Delta\hat{\varepsilon}_{-1}A_{f1}e^{i\frac{2\pi}{\Lambda}\delta_1 z_1}\\
&=-\frac{4\pi\omega^2}{c^2}\Big[\chi_0^{(3)}(6|A_{f1}|^2+3|A_{b1}|^2+6|A_{f3}|^2+6|A_{b3}|^2)A_{b1}\\
&+\chi_{-1}^{(3)}\Big((3|A_{f1}|^2+6|A_{b1}|^2+6|A_{f3}|^2+6|A_{b3}|^2)A_{f1}+3A_{f1}^{*2}A_{f3}e^{i\Delta k_{TH}z_1}\Big)e^{i\frac{2\pi}{\Lambda}\delta_1 z_1}\\
&+\chi_1^{(3)}\Big(3A_{b1}^2A_{f1}^*+6A_{f1}^*A_{b1}^*A_{b3}e^{-i\Delta k_{TH}z_1}\Big)e^{-i\frac{2\pi}{\Lambda}\delta_1 z_1}\\
&+\chi_{-2}^{(3)}\Big(3A_{f1}^2A_{b1}^*+6A_{f1}^*A_{b1}^*A_{f3}e^{i\Delta k_{TH}z_1}\Big)e^{i\frac{4\pi}{\Lambda}\delta_1 z_1}+\chi_2^{(3)}\Big(3A_{f1}^{*2}A_{b3}e^{-i\Delta k_{TH}z_1}\Big)e^{-i\frac{4\pi}{\Lambda}\delta_1 z_1}\\
&+\chi_3^{(3)}\Big(6A_{b1}A_{b3}A_{f3}^*e^{-2i\Delta k_{TH}z_1}\Big)e^{-i\frac{6\pi}{\Lambda}\delta_1 z_1}+\chi_{-3}^{(3)}\Big(3A_{b1}^{*2}A_{f3}e^{i\Delta k_{TH}z_1}+6A_{b1}A_{f3}A_{b3}^*e^{2i\Delta k_{TH}z_1}\Big)e^{i\frac{6\pi}{\Lambda}\delta_1 z_1}\Big],
\end{aligned}
\tag{4-10b}
$$

and

$$
\begin{aligned}
&2ik_3\frac{\partial A_{f3}}{\partial z_1}+\frac{i(3\omega)^2\hat{\varepsilon}_{\mathrm{Im}}}{c^2}A_{f3}+\frac{2}{c^2}i3\omega\hat{\varepsilon}_{\mathrm{Re}}\frac{\partial A_{f3}}{\partial t_1}+\frac{i}{c^2}(3\omega)^2\hat{\varepsilon}'_{\mathrm{Re}}\frac{\partial A_{f3}}{\partial t_1}-\frac{(3\omega)^2}{c^2}\Delta\hat{\varepsilon}_1A_{b3}e^{-i\frac{2\pi}{\Lambda}\delta_3 z_1}\\
&=-\frac{4\pi(3\omega)^2}{c^2}\Big[\chi_0^{(3)}\Big((6|A_{f1}|^2+6|A_{b1}|^2+3|A_{f3}|^2+6|A_{b3}|^2)A_{f3}+A_{f1}^3e^{-i\Delta k_{TH}z_1}\Big)\\
&+\chi_1^{(3)}\Big(3A_{f1}^2A_{b1}e^{-i\Delta k_{TH}z_1}+6A_{b1}A_{f1}^*A_{f3}\Big)e^{-i\frac{2\pi}{\Lambda}\delta_1 z_1}+\chi_{-1}^{(3)}\Big(6A_{f1}A_{b1}^*A_{f3}\Big)e^{i\frac{2\pi}{\Lambda}\delta_1 z_1}\\
&+\chi_2^{(3)}\Big(6A_{f1}A_{b1}^*A_{b3}e^{-2i\Delta k_{TH}z_1}\Big)e^{-i\frac{4\pi}{\Lambda}\delta_1 z_1}+\chi_3^{(3)}\Big((6|A_{f1}|^2+6|A_{b1}|^2+6|A_{f3}|^2+3|A_{b3}|^2)A_{b3}e^{-2i\Delta k_{TH}z_1}\Big)e^{-i\frac{6\pi}{\Lambda}\delta_1 z_1}\\
&+\chi_{-3}^{(3)}\Big(3A_{f3}^2A_{b3}^*e^{2i\Delta k_{TH}z_1}\Big)e^{i\frac{6\pi}{\Lambda}\delta_1 z_1}\Big],
\end{aligned}
\tag{4-10c}
$$

and

$$-2ik_3\frac{\partial A_{b3}}{\partial z_1}+\frac{i(3\omega)^2\hat{\varepsilon}_{\mathrm{Im}}}{c^2}A_{b3}+\frac{2}{c^2}i3\omega\hat{\varepsilon}_{\mathrm{Re}}\frac{\partial A_{b3}}{\partial t_1}+\frac{i}{c^2}(3\omega)^2\hat{\varepsilon}'_{\mathrm{Re}}\frac{\partial A_{b3}}{\partial t_1}-\frac{(3\omega)^2}{c^2}\Delta\hat{\varepsilon}_{-1}A_{f3}e^{i\frac{2\pi}{\Lambda}\delta_3 z_1}$$
$$=-\frac{4\pi(3\omega)^2}{c^2}\Big[\chi_0^{(3)}\left((6|A_{f1}|^2+6|A_{b1}|^2+6|A_{f3}|^2+3|A_{b3}|^2)A_{b3}+A_{b1}^3e^{i\Delta k_{TH}z_1}\right)$$
$$+\chi_{-1}^{(3)}\left(3A_{b1}^2A_{f1}e^{-i\Delta k_{TH}z_1}+6A_{f1}A_{b1}^*A_{b3}\right)e^{i\frac{2\pi}{\Lambda}\delta_1 z_1}+\chi_1^{(3)}\left(6A_{b1}A_{f1}^*A_{b3}\right)e^{-i\frac{2\pi}{\Lambda}\delta_1 z_1}$$
$$+\chi_{-2}^{(3)}\left(6A_{b1}A_{f1}^*A_{f3}e^{2i\Delta k_{TH}z_1}\right)e^{i\frac{4\pi}{\Lambda}\delta_1 z_1}+\chi_{-3}^{(3)}(6|A_{f1}|^2+6|A_{b1}|^2+3|A_{f3}|^2+6|A_{b3}|^2)A_{f3}e^{2i\Delta k_{TH}z_1}e^{i\frac{6\pi}{\Lambda}\delta_1 z_1}$$
$$+\chi_3^{(3)}\left(3A_{b3}^2A_{f3}^*e^{2i\Delta k_{TH}z_1}\right)e^{-i\frac{6\pi}{\Lambda}\delta_1 z_1}\Big].$$

(4-10d)

Now, Eq. (4-10a) and (4-10b) are divided by $2ik_1$ and Eq. (4-10c) and (4-10d) are divided by $2ik_3$ and rearranged the terms in the equations. Then, the equations is given as:

$$\frac{\partial A_{f1}}{\partial z_1}+\frac{\omega^2}{2k_1c^2}\hat{\varepsilon}_{\mathrm{Im}}A_{f1}+\frac{\omega}{k_1c^2}\hat{\varepsilon}_{\mathrm{Re}}\frac{\partial A_{f1}}{\partial t_1}+\frac{\omega^2}{2k_1c^2}\hat{\varepsilon}'_{\mathrm{Re}}\frac{\partial A_{f1}}{\partial t_1}-\frac{i\omega^2}{2k_1c^2}\Delta\hat{\varepsilon}_1A_{b1}e^{-i\frac{2\pi}{\Lambda}\delta_1 z_1}$$
$$=\frac{i2\pi\omega^2}{k_1c^2}\Big[\chi_0^{(3)}(3|A_{f1}|^2+6|A_{b1}|^2+6|A_{f3}|^2+6|A_{b3}|^2)A_{f1}$$
$$+\chi_1^{(3)}\left((6|A_{f1}|^2+3|A_{b1}|^2+6|A_{f3}|^2+6|A_{b3}|^2)A_{b1}+3A_{b1}^{*2}A_{b3}e^{-i\Delta k_{TH}z_1}\right)e^{-i\frac{2\pi}{\Lambda}\delta_1 z_1}$$
$$+\chi_{-1}^{(3)}\left(3A_{f1}^2A_{b1}^*+6A_{f1}^*A_{b1}^*A_{f3}e^{i\Delta k_{TH}z_1}\right)e^{i\frac{2\pi}{\Lambda}\delta_1 z_1}$$
$$+\chi_{-2}^{(3)}\left(3A_{b1}^{*2}A_{f3}e^{i\Delta k_{TH}z_1}\right)e^{i\frac{4\pi}{\Lambda}\delta_1 z_1}+\chi_2^{(3)}\left(3A_{b1}^2A_{f1}^*+6A_{f1}^*A_{b1}^*A_{b3}e^{-i\Delta k_{TH}z_1}\right)e^{-i\frac{4\pi}{\Lambda}\delta_1 z_1}$$
$$+\chi_{-3}^{(3)}\left(6A_{f3}A_{b3}^*A_{f1}e^{2i\Delta k_{TH}z_1}\right)e^{i\frac{6\pi}{\Lambda}\delta_1 z_1}+\chi_3^{(3)}\left(3A_{f1}^{*2}A_{b3}e^{-i\Delta k_{TH}z_1}+6A_{f3}^*A_{b3}A_{f1}e^{-2i\Delta k_{TH}z_1}\right)e^{-i\frac{6\pi}{\Lambda}\delta_1 z_1}\Big],$$

(4-11a)

and

$$-\frac{\partial A_{b1}}{\partial z_1}+\frac{\omega^2}{2k_1c^2}\hat{\varepsilon}_{\mathrm{Im}}A_{b1}+\frac{\omega}{k_1c^2}\hat{\varepsilon}_{\mathrm{Re}}\frac{\partial A_{b1}}{\partial t_1}+\frac{\omega^2}{2k_1c^2}\hat{\varepsilon}'_{\mathrm{Re}}\frac{\partial A_{b1}}{\partial t_1}-\frac{i\omega^2}{2k_1c^2}\Delta\hat{\varepsilon}_{-1}A_{f1}e^{i\frac{2\pi}{\Lambda}\delta_1 z_1}$$
$$=\frac{i2\pi\omega^2}{k_1c^2}\Big[\chi_0^{(3)}(6|A_{f1}|^2+3|A_{b1}|^2+6|A_{f3}|^2+6|A_{b3}|^2)A_{b1}$$
$$+\chi_{-1}^{(3)}\left((3|A_{f1}|^2+6|A_{b1}|^2+6|A_{f3}|^2+6|A_{b3}|^2)A_{f1}+3A_{f1}^{*2}A_{f3}e^{i\Delta k_{TH}z_1}\right)e^{i\frac{2\pi}{\Lambda}\delta_1 z_1}$$
$$+\chi_1^{(3)}\left(3A_{b1}^2A_{f1}^*+6A_{f1}^*A_{b1}^*A_{b3}e^{-i\Delta k_{TH}z_1}\right)e^{-i\frac{2\pi}{\Lambda}\delta_1 z_1}$$
$$+\chi_{-2}^{(3)}\left(3A_{f1}^2A_{b1}^*+6A_{f1}^*A_{b1}^*A_{f3}e^{i\Delta k_{TH}z_1}\right)e^{i\frac{4\pi}{\Lambda}\delta_1 z_1}+\chi_2^{(3)}\left(3A_{f1}^{*2}A_{b3}e^{-i\Delta k_{TH}z_1}\right)e^{-i\frac{4\pi}{\Lambda}\delta_1 z_1}$$
$$+\chi_3^{(3)}\left(6A_{b1}A_{b3}A_{f3}^*e^{-2i\Delta k_{TH}z_1}\right)e^{-i\frac{6\pi}{\Lambda}\delta_1 z_1}+\chi_{-3}^{(3)}\left(3A_{b1}^{*2}A_{f3}e^{i\Delta k_{TH}z_1}+6A_{b1}A_{f3}A_{b3}^*e^{2i\Delta k_{TH}z_1}\right)e^{i\frac{6\pi}{\Lambda}\delta_1 z_1}\Big],$$

(4-11b)

$$\frac{\partial A_{f3}}{\partial z_1}+\frac{(3\omega)^2}{2k_3c^2}\hat{\varepsilon}_{\mathrm{Im}}A_{f3}+\frac{3\omega}{k_3c^2}\hat{\varepsilon}_{\mathrm{Re}}\frac{\partial A_{f3}}{\partial t_1}+\frac{(3\omega)^2}{2k_3c^2}\hat{\varepsilon}'_{\mathrm{Re}}\frac{\partial A_{f3}}{\partial t_1}-\frac{i(3\omega)^2}{2k_3c^2}\Delta\hat{\varepsilon}_1A_{b3}e^{i\frac{2\pi}{\Lambda}\delta_3 z_1}$$
$$=\frac{i2\pi(3\omega)^2}{k_3c^2}\Big[\chi_0^{(3)}\left((6|A_{f1}|^2+6|A_{b1}|^2+3|A_{f3}|^2+6|A_{b3}|^2)A_{f3}+A_{f1}^3e^{-i\Delta k_{TH}z_1}\right)$$
$$+\chi_1^{(3)}\left(3A_{f1}^2A_{b1}e^{-i\Delta k_{TH}z_1}+6A_{b1}A_{f1}^*A_{f3}\right)e^{-i\frac{2\pi}{\Lambda}\delta_1 z_1}+\chi_{-1}^{(3)}\left(6A_{f1}A_{b1}^*A_{f3}\right)e^{i\frac{2\pi}{\Lambda}\delta_1 z_1}$$
$$+\chi_2^{(3)}\left(6A_{f1}A_{b1}^*A_{b3}e^{-2i\Delta k_{TH}z_1}\right)e^{-i\frac{4\pi}{\Lambda}\delta_1 z_1}+\chi_3^{(3)}\left((6|A_{f1}|^2+6|A_{b1}|^2+6|A_{f3}|^2+3|A_{b3}|^2)A_{b3}e^{-2i\Delta k_{TH}z_1}\right)e^{-i\frac{6\pi}{\Lambda}\delta_1 z_1}$$
$$+\chi_{-3}^{(3)}\left(3A_{f3}^2A_{b3}^*e^{2i\Delta k_{TH}z_1}\right)e^{i\frac{6\pi}{\Lambda}\delta_1 z_1}\Big],$$

(4-11c)

and

$$-\frac{\partial A_{b3}}{\partial z_1}+\frac{(3\omega)^2}{2k_3c^2}\hat{\varepsilon}_{\mathrm{Im}}A_{b3}+\frac{3\omega}{k_3c^2}\hat{\varepsilon}_{\mathrm{Re}}\frac{\partial A_{b3}}{\partial t_1}+\frac{(3\omega)^2}{2k_3c^2}\hat{\varepsilon}'_{\mathrm{Re}}\frac{\partial A_{b3}}{\partial t_1}-\frac{i(3\omega)^2}{2k_3c^2}\Delta\hat{\varepsilon}_{-1}A_{f3}e^{-i\frac{2\pi}{\Lambda}\delta_3 z_1}$$

$$=\frac{i2\pi(3\omega)^2}{k_3c^2}\Big[\chi_0^{(3)}\Big((6|A_{f1}|^2+6|A_{b1}|^2+6|A_{f3}|^2+3|A_{b3}|^2)A_{b3}+A_{b1}^3e^{i\Delta k_{TH}z_1}\Big)$$

$$+\chi_{-1}^{(3)}\Big(3A_{b1}^2A_{f1}e^{-i\Delta k_{TH}z_1}+6A_{f1}A_{b1}^*A_{b3}\Big)e^{i\frac{2\pi}{\Lambda}\delta_1 z_1}+\chi_1^{(3)}\Big(6A_{b1}A_{f1}^*A_{b3}\Big)e^{-i\frac{2\pi}{\Lambda}\delta_1 z_1}$$

$$+\chi_{-2}^{(3)}\Big(6A_{b1}A_{f1}^*A_{f3}e^{2i\Delta k_{TH}z_1}\Big)e^{i\frac{4\pi}{\Lambda}\delta_1 z_1}+\chi_{-3}^{(3)}(6|A_{f1}|^2+6|A_{b1}|^2+3|A_{f3}|^2+6|A_{b3}|^2)A_{f3}e^{2i\Delta k_{TH}z_1}e^{i\frac{6\pi}{\Lambda}\delta_1 z_1}$$

$$+\chi_3^{(3)}\Big(3A_{b3}^2A_{f3}^*e^{2i\Delta k_{TH}z_1}\Big)e^{-i\frac{6\pi}{\Lambda}\delta_1 z_1}\Big]. \qquad \text{(4-11d)}$$

To simplify these coupled equations, some terms in these equations need to be defined. First, for the coupled-equations of FF components;

the linear absorption is defined as $\alpha_1=\frac{\Lambda\omega^2}{\pi k_1c^2}\hat{\varepsilon}_{\mathrm{Im}}(\omega)\Rightarrow\frac{\omega^2}{2k_1c^2}\hat{\varepsilon}_{\mathrm{Im}}(\omega)=\frac{2\pi}{\Lambda}\bar{\alpha}_1$,

the coupling coefficient is defined as $\kappa_\ell^{(1)}=\frac{\Lambda\omega^2}{4\pi k_1c^2}\Delta\hat{\varepsilon}_\ell\Rightarrow-\frac{i\omega^2}{2k_1c^2}\Delta\hat{\varepsilon}_\ell(\omega)=-i\frac{2\pi}{\Lambda}\bar{\kappa}_\ell^{(1)}$,

the inverse of group velocity is defined as $\frac{1}{v_{g1}}=\frac{\partial k_1}{\partial\omega}=\frac{1}{2k_1c^2}(2\omega\hat{\varepsilon}_{\mathrm{Re}}(\omega)+\omega^2\hat{\varepsilon}'_{\mathrm{Re}}(\omega))$,

and also the nonlinear coefficients are defined as $\eta_\ell^{(1)}=\frac{6\pi\omega^2}{k_1c^2}\chi_\ell^{(3)}$.

Second, for the coupled-equations of TH frequency components;

the linear absorption is defined as $\alpha_3=\frac{\Lambda(3\omega)^2}{\pi k_3c^2}\hat{\varepsilon}_{\mathrm{Im}}(3\omega)\Rightarrow\frac{(3\omega)^2}{2k_3c^2}\hat{\varepsilon}_{\mathrm{Im}}(3\omega)=\frac{2\pi}{\Lambda}\bar{\alpha}_3$,

the coupling coefficient is defined as $\kappa_\ell^{(3)}=\frac{\Lambda(3\omega)^2}{4\pi k_3c^2}\Delta\hat{\varepsilon}_\ell\Rightarrow-\frac{i(3\omega)^2}{2k_3c^2}\Delta\hat{\varepsilon}_\ell(3\omega)=-i\frac{2\pi}{\Lambda}\bar{\kappa}_\ell^{(3)}$,

and the inverse of group velocity is defined as $\frac{1}{v_{g3}}=\frac{\partial k_3}{\partial(3\omega)}=\frac{1}{2k_3c^2}(2(3\omega)\hat{\varepsilon}_{\mathrm{Re}}(3\omega)+(3\omega)^2\hat{\varepsilon}'_{\mathrm{Re}}(3\omega))$,

and also the nonlinear coefficients are defined as $\eta_\ell^{(3)} = \frac{6\pi(3\omega)^2}{k_3 c^2}\chi_\ell^{(3)}$.

In addition, let the scaled length is $z = (\pi/\Lambda)z_1 \Rightarrow \partial z = (\pi/\Lambda)\partial z_1$, and then $\partial z_1 = (\Lambda/\pi)\partial z$. Let amplitudes of each frequency components can be as $A_{f1} = a_{f1}e^{-i\frac{\pi}{\Lambda}\delta_1 z_1}$ and $A_{b1} = a_{b1}e^{i\frac{\pi}{\Lambda}\delta_1 z_1}$, and $A_{f3} = a_{f3}e^{i\frac{\pi}{\Lambda}\delta_3 z_1}$ and $A_{b3} = a_{b3}e^{-i\frac{\pi}{\Lambda}\delta_3 z_1}$. So the amplitudes with scaled length are $A_{f1} = a_{f1}e^{-i\delta_1 z}$ and $A_{b1} = a_{b1}e^{i\delta_1 z}$, and $A_{f3} = a_{f3}e^{i\delta_3 z}$ and $A_{b3} = a_{b3}e^{-i\delta_3 z}$. If the amplitudes are differentiated respect to scaled length, so we obtain: $\frac{\partial A_{f1}}{\partial z} = -i\delta_1 a_{f1}e^{-i\delta_1 z} + \frac{\partial a_{f1}}{\partial z}e^{-i\delta_1 z}$ and $\frac{\partial A_{b1}}{\partial z} = i\delta_1 a_{b1}e^{i\delta_1 z} + \frac{\partial a_{b1}}{\partial z}e^{i\delta_1 z}$, and $\frac{\partial A_{f3}}{\partial z} = i\delta_3 a_{f3}e^{i\delta_3 z} + \frac{\partial a_{f3}}{\partial z}e^{i\delta_3 z}$ and $\frac{\partial A_{b3}}{\partial z} = -i\delta_3 a_{b3}e^{-i\delta_3 z} + \frac{\partial a_{b3}}{\partial z}e^{-i\delta_3 z}$. Similarly, the corresponding time derivatives of all amplitudes are $\frac{\partial A_{f1}}{\partial t} = \frac{\partial a_{f1}}{\partial t}e^{-i\delta_1 z}$ and $\frac{\partial A_{b1}}{\partial t} = \frac{\partial a_{b1}}{\partial t}e^{i\delta_1 z}$, and $\frac{\partial A_{f3}}{\partial t} = \frac{\partial a_{f3}}{\partial t}e^{i\delta_3 z}$ and $\frac{\partial A_{b3}}{\partial t} = \frac{\partial a_{b3}}{\partial t}e^{-i\delta_3 z}$. The detuning parameter for FF wave is $\delta_1 = (\Lambda/\pi)(k_1 - \pi/\Lambda)$. And also the detuning parameter for TH wave is $\delta_3 = (\Lambda/\pi)\Delta k_{THG} - 3\delta_1$, where $\mu\Delta k_{THG} = k_3 - 3k_1$ is the wave-vector mismatch [18]. Then, substituting the above new defined parameters and identities into Eq. (4-11a), (4-11b), (4-11c), and (4-11d), respectively. So, the coupled equations can be further simplified and hence, the scaled coupled equations have been obtained as following:

$$
\begin{aligned}
&\frac{\pi}{\Lambda}\left(\frac{\partial a_{f1}}{\partial z} - i\delta_1 a_{f1}\right)e^{-i\delta_1 z} + \frac{\pi}{2\Lambda}\alpha_1 a_{f1}e^{-i\delta_1 z} + \frac{1}{v_{g1}}\frac{\partial a_{f1}}{\partial t_1}e^{-i\delta_1 z} - i\frac{2\pi}{\Lambda}\kappa_1^{(1)}a_{b1}e^{-i\delta_1 z} \\
&= i\eta_0^{(1)}\left(|a_{f1}|^2 + 2|a_{b1}|^2 + 2|a_{f3}|^2 + 2|a_{b3}|^2\right)a_{f1}e^{-i\delta_1 z} \\
&+ i\eta_1^{(1)}\left((2|a_{f1}|^2 + |a_{b1}|^2 + 2|a_{f3}|^2 + 2|a_{b3}|^2)a_{b1}e^{i\delta_1 z} + a_{b1}^{*2}e^{-i\delta_1 z}a_{b3}e^{-i\delta_3 z}e^{i\Delta k_{THG} z_1}\right)e^{-2i\delta_1 z} \\
&+ i\eta_{-1}^{(1)}\left(a_{f1}^2 a_{b1}^* e^{-3i\delta_1 z} + 2a_{f1}^* a_{b1}^* a_{f3}e^{i\delta_3 z}e^{-i\Delta k_{THG} z_1}\right)e^{2i\delta_1 z} \\
&+ i\eta_{-2}^{(1)}\left(a_{b1}^{*2}a_{f3}e^{-2i\delta_1 z}e^{i\delta_3 z}e^{-i\Delta k_{THG} z_1}\right)e^{4i\delta_1 z} + i\eta_2^{(1)}\left(a_{b1}^2 a_{f1}^* e^{3i\delta_1 z} + 2a_{f1}^* a_{b1}^* a_{b3}e^{-i\delta_3 z}e^{i\Delta k_{THG} z_1}\right)e^{-4i\delta_1 z} \\
&+ i\eta_{-3}^{(1)}\left(2a_{f3}a_{b3}^* a_{f1}e^{-i\delta_1 z}e^{2i\delta_3 z}e^{-2i\Delta k_{THG} z_1}\right)e^{6i\delta_1 z} + i\eta_3^{(1)}\left(a_{f1}^{*2}a_{b3}e^{2i\delta_1 z}e^{-i\delta_3 z}e^{i\Delta k_{THG} z_1} + 2a_{f3}^* a_{b3}a_{f1}e^{-i\delta_1 z}e^{-2i\delta_3 z}e^{2i\Delta k_{THG} z_1}\right)e^{-6i\delta_1 z}
\end{aligned}
\tag{4-12a}
$$

$$-\frac{\pi}{\Lambda}\left(\frac{\partial a_{b1}}{\partial z}e^{i\delta_1 z}+i\delta_1 a_{b1}e^{i\delta_1 z}\right)+\frac{\pi}{2\Lambda}\alpha_1 a_{b1}e^{i\delta_1 z}+\frac{1}{v_{g1}}\frac{\partial a_{b1}}{\partial t_1}e^{i\delta_1 z}-\frac{2\pi}{\Lambda}\kappa_{-1}^{(1)}a_{f1}e^{i\delta_1 z}$$
$$=i\eta_0^{(1)}(2|a_{f1}|^2+|a_{b1}|^2+2|a_{f3}|^2+2|a_{b3}|^2)a_{b1}e^{i\delta_1 z}$$
$$+i\eta_{-1}^{(1)}\left((|a_{f1}|^2+2|a_{b1}|^2+2|a_{f3}|^2+2|a_{b3}|^2)a_{f1}e^{-i\delta_1 z}+a_{f1}^{*2}a_{f3}e^{2i\delta_1 z}e^{i\delta_3 z}e^{-i\Delta k_{THG}z_1}\right)e^{2i\delta_1 z}$$
$$+i\eta_1^{(1)}\left(a_{b1}^2a_{f1}^*e^{3i\delta_1 z}+2a_{f1}^*a_{b1}^*a_{b3}e^{-i\delta_3 z}e^{i\Delta k_{THG}z_1}\right)e^{-2i\delta_1 z}$$
$$+i\eta_{-2}^{(1)}\left(a_{f1}^2a_{b1}^*e^{-3i\delta_1 z}+2a_{f1}^*a_{b1}^*a_{f3}e^{i\delta_3 z}e^{-i\Delta k_{THG}z_1}\right)e^{4i\delta_1 z}+i\eta_2^{(1)}\left(a_{f1}^{*2}a_{b3}e^{2i\delta_1 z}e^{-i\delta_3 z}e^{i\Delta k_{THG}z_1}\right)e^{-4i\delta_1 z}$$
$$+i\eta_3^{(1)}\left(2a_{b1}a_{b3}a_{f3}^*e^{i\delta_1 z}e^{-i\delta_3 z}e^{2i\Delta k_{THG}z_1}\right)e^{-6i\delta_1 z}+i\eta_{-3}^{(1)}\left(a_{b1}^{*2}a_{f3}e^{-2i\delta_1 z}e^{i\delta_3 z}e^{-i\Delta k_{THG}z_1}+2a_{b1}a_{f3}a_{b3}^*e^{i\delta_1 z}e^{2i\delta_3 z}e^{-2i\Delta k_{THG}z_1}\right)e^{6i\delta_1 z},$$

(4-12b)

$$\frac{\pi}{\Lambda}\left(\frac{\partial a_{f3}}{\partial z}+i\delta_3 a_{f3}\right)e^{i\delta_3 z}+\frac{\pi}{2\Lambda}\alpha_3 a_{f3}e^{i\delta_3 z}+\frac{1}{v_{g3}}\frac{\partial a_{f3}}{\partial t_1}e^{i\delta_3 z}-i\frac{2\pi}{\Lambda}\kappa_1^{(3)}a_{b3}e^{i\delta_3 z}$$
$$=i\eta_0^{(3)}\left((2|a_{f1}|^2+2|a_{b1}|^2+|a_{f3}|^2+2|a_{b3}|^2)a_{f3}e^{i\delta_3 z}+a_{f1}^3e^{-3i\delta_1 z}e^{i\Delta k_{THG}z_1}\right)$$
$$+i\eta_1^{(3)}\left(a_{f1}^2a_{b1}e^{-i\delta_1 z}e^{i\Delta k_{THG}z_1}+2a_{b1}a_{f1}^*a_{f3}e^{2i\delta_1 z}e^{i\delta_3 z}\right)e^{-2i\delta_1 z}+i\eta_{-1}^{(3)}\left(2a_{f1}a_{b1}^*a_{f3}e^{-2i\delta_1 z}e^{i\delta_3 z}\right)e^{2i\delta_1 z}$$
$$+i\eta_2^{(3)}\left(2a_{f1}a_{b1}^*a_{b3}e^{-2i\delta_1 z}e^{-i\delta_3 z}e^{2i\Delta k_{THG}z_1}\right)e^{-4i\delta_1 z}+i\eta_3^{(3)}\left((2|a_{f1}|^2+2|a_{b1}|^2+2|a_{f3}|^2+|a_{b3}|^2)a_{b3}e^{-i\delta_3 z}e^{2i\Delta k_{THG}z_1}\right)e^{-6i\delta_1 z}$$
$$+i\eta_{-3}^{(3)}\left(a_{f3}^2a_{b3}^*e^{3i\delta_3 z}e^{-2i\Delta k_{THG}z_1}\right)e^{6i\delta_1 z},$$

(4-12c)

$$-\frac{\pi}{\Lambda}\left(\frac{\partial a_{b3}}{\partial z}-i\delta_3 a_{b3}\right)e^{-i\delta_3 z}+\frac{\pi}{2\Lambda}\alpha_3 a_{b3}e^{-i\delta_3 z}+\frac{1}{v_{g3}}\frac{\partial a_{b3}}{\partial t_1}e^{-i\delta_3 z}-i\frac{2\pi}{\Lambda}\kappa_{-1}^{(3)}a_{f3}e^{-i\delta_3 z}$$
$$=i\eta_0^{(3)}\left((2|a_{f1}|^2+2|a_{b1}|^2+2|a_{f3}|^2\,2|a_{b3}|^2)a_{b3}e^{-i\delta_3 z}+a_{b1}^3e^{3i\delta_1 z}e^{-i\Delta k_{THG}z_1}\right)$$
$$+i\eta_{-1}^{(3)}\left(a_{b1}^2a_{f1}e^{i\delta_1 z}e^{-i\Delta k_{THG}z_1}+2a_{f1}a_{b1}^*a_{b3}e^{-2i\delta_1 z}e^{-i\delta_3 z}\right)e^{2i\delta_1 z}+i\eta_1^{(3)}\left(2a_{b1}a_{f1}^*a_{b3}e^{2i\delta_1 z}e^{-i\delta_3 z}\right)e^{-2i\delta_1 z_1}$$
$$+i\eta_{-2}^{(3)}\left(2a_{b1}a_{f1}^*a_{f3}e^{2i\delta_1 z}e^{i\delta_3 z}e^{-2i\Delta k_{THG}z_1}\right)e^{4i\delta_1 z}+i\eta_{-3}^{(3)}(2|a_{f1}|^2+2|a_{b1}|^2+|a_{f3}|^2+2|a_{b3}|^2)a_{f3}e^{i\delta_3 z}e^{-2i\Delta k_{THG}z_1}e^{6i\delta_1 z}$$
$$+i\eta_3^{(3)}\left(a_{b3}^2a_{f3}^*e^{-3i\delta_3 z}e^{2i\Delta k_{THG}z_1}\right)e^{-6i\delta_1 z}.$$

(4-12d)

Finally, the completed scaled form of coupled-mode equation for both FF and TH frequency components have been obtained. The scaled form of the coupled-mode equations for the FF component are:

$$\frac{\partial a_{f1}}{\partial z_1}+\left(\frac{\bar{\alpha}_1}{2}-i\bar{\delta}_1\right)a_{f1}+\frac{1}{v_{g1}}\frac{\partial a_{f1}}{\partial t_1}+-i\bar{\kappa}_1^{(1)}a_{b1}$$
$$=i\eta_0^{(1)}(|a_{f1}|^2+2|a_{b1}|^2+2|a_{f3}|^2+2|a_{b3}|^2)a_{f1}+i\eta_1^{(1)}\left((2|a_{f1}|^2+|a_{b1}|^2+2|a_{f3}|^2+2|a_{b3}|^2)a_{b1}+a_{b1}^{*2}a_{b3}\right)$$
$$+i\eta_{-1}^{(1)}\left(a_{f1}^2a_{b1}^*+2a_{f1}^*a_{b1}^*a_{f3}\right)+i\eta_{-2}^{(1)}\left(a_{b1}^{*2}a_{f3}\right)+i\eta_2^{(1)}\left(a_{b1}^2a_{f1}^*+2a_{f1}^*a_{b1}^*a_{b3}\right)+i\eta_{-3}^{(1)}\left(2a_{f3}a_{b3}^*a_{f1}\right)$$
$$+i\eta_3^{(1)}\left(a_{f1}^{*2}a_{b3}+2a_{f3}^*a_{b3}a_{f1}\right),$$

(4-13a)

and

$$-\frac{\partial a_{b1}}{\partial z_1}+\left(\frac{\bar{\alpha}_1}{2}-i\bar{\delta}_1\right)a_{b1}+\frac{1}{v_{g1}}\frac{\partial a_{b1}}{\partial t_1}-i\bar{\kappa}_{-1}^{(1)}a_{f1}$$
$$=i\eta_0^{(1)}(2|a_{f1}|^2+|a_{b1}|^2+2|a_{f3}|^2+2|a_{b3}|^2)a_{b1}+i\eta_{-1}^{(1)}\left((|a_{f1}|^2+2|a_{b1}|^2+2|a_{f3}|^2+2|a_{b3}|^2)a_{f1}+a_{f1}^{*2}a_{f3}\right)$$
$$+i\eta_1^{(1)}\left(a_{b1}^2a_{f1}^*+2a_{f1}^*a_{b1}^*a_{b3}\right)+i\eta_{-2}^{(1)}\left(a_{f1}^2a_{b1}^*+2a_{f1}^*a_{b1}^*a_{f3}\right)+i\eta_2^{(1)}\left(a_{f1}^{*2}a_{b3}\right)+i\eta_3^{(1)}\left(2a_{b1}a_{b3}a_{f3}^*\right)$$
$$+i\eta_{-3}^{(1)}\left(a_{b1}^{*2}a_{f3}+2a_{b1}a_{f3}a_{b3}^*\right),$$

(4-13b)

The scaled form of the coupled-mode equations for the TH frequency component are:

$$\frac{\partial a_{f3}}{\partial z_1}+\left(\frac{\bar{\alpha}_3}{2}+i\bar{\delta}_3\right)a_{f3}+\frac{1}{v_{g3}}\frac{\partial a_{f3}}{\partial t_1}-i\bar{\kappa}_1^{(3)}a_{b3}$$
$$=i\eta_0^{(3)}\left((2|a_{f1}|^2+2|a_{b1}|^2+|a_{f3}|^2+2|a_{b3}|^2)a_{f3}+a_{f1}^3\right)+i\eta_1^{(3)}\left(a_{f1}^2a_{b1}+2a_{b1}a_{f1}^*a_{f3}\right)$$
$$+i\eta_{-1}^{(3)}\left(2a_{f1}a_{b1}^*a_{f3}\right)+i\eta_2^{(3)}\left(2a_{f1}a_{b1}^*a_{b3}\right)+i\eta_3^{(3)}(2|a_{f1}|^2+2|a_{b1}|^2+2|a_{f3}|^2+|a_{b3}|^2)a_{b3}$$
$$+i\eta_{-3}^{(3)}\left(a_{f3}^2a_{b3}^*\right),$$

(4-13c)

and

$$-\frac{\partial a_{b3}}{\partial z}+\left(\frac{\bar{\alpha}_3}{2}+i\bar{\delta}_3\right)a_{b3}+\frac{1}{v_{g3}}\frac{\partial a_{b3}}{\partial t_1}-i\bar{\kappa}_{-1}^{(3)}a_{f3}$$
$$=i\eta_0^{(3)}\left((2|a_{f1}|^2+2|a_{b1}|^2+2|a_{f3}|^2\,2|a_{b3}|^2)a_{b3}+a_{b1}^3\right)+i\eta_{-1}^{(3)}\left(a_{b1}^2a_{f1}+2a_{f1}a_{b1}^*a_{b3}\right)$$
$$+i\eta_1^{(3)}\left(2a_{b1}a_{f1}^*a_{b3}\right)+i\eta_{-2}^{(3)}\left(2a_{b1}a_{f1}^*a_{f3}\right)+i\eta_{-3}^{(3)}(2|a_{f1}|^2+2|a_{b1}|^2+|a_{f3}|^2+2|a_{b3}|^2)a_{f3}$$
$$+i\eta_3^{(3)}\left(a_{b3}^2a_{f3}^*\right).$$

(4-13d)

The scaled form of coupled-mode equations for both FF and TH frequency components in Eq. (4-13) have shown that the higher-order nonlinear coefficients ($\ell = \pm 1, \pm 2, \pm 3$) are the new found terms when comparing with the previous works. These is similar to another version of the coupled-mode equation derived for deep nonlinear grating.

4.3 Numerical computations for the coupled-mode equations

A SSFM could be used to observe many natural phenomena in wave propagation such as transmission, reflection, and diffraction. Here, the method has been developed to compute the transmission and reflection in separated solution space. According to the coupled-mode equations of THG phenomena as shown in Eq. (4-13a) to (4-13d). The matrix U is created as interacting amplitude matrix and operators $\hat{L}$, $\hat{K}$, and $\hat{N}$ are the linear operator, coupling operator, and nonlinear operator, respectively. The linear operator contains the spatial derivatives of longitudinal direction, the linear absorption coefficient, and the detuning parameters. This operator has been solved by using the FFT algorithm. Then the coupling operator contains the coupling coefficients. Finally, the nonlinear operator contains the nonlinear terms which correspond to THG phenomenon. We summarize the detail of each operators in the appendices of this thesis. The coupled-mode equations can be rewritten as the ordinary differential equation as:

$$\frac{1}{v_g}\frac{\partial U}{\partial t} = \left[\hat{L} + \hat{K} + \hat{N}\right]U, \tag{4-14}$$

and now, Eq. (4-14) could be related to Eq. (2-47), and the additional operators in Eq. (4-14) could be noticed. Easily, the split-step formalism could be applied to Eq. (4-14) for obtaining the split-step form [53] given as:

$$U(t+\Delta t) = \exp\left[v_g \frac{\Delta t}{2}\hat{L}\right]\exp\left[v_g \frac{\Delta t}{2}\hat{K}\right]\exp\left[v_g \Delta t\hat{N}\right]\exp\left[v_g \frac{\Delta t}{2}\hat{K}\right]\exp\left[v_g \frac{\Delta t}{2}\hat{L}\right]U(t). \tag{4-15}$$

Note that the Eq. (4-15) is only possible if the operators $\hat{L}$, $\hat{K}$, and $\hat{N}$ all commute. According to the operator $\hat{L}$ and $\hat{K}$ are diagonal matrices but $\hat{N}$ is not diagonal matrix because of including both diagonal and off-diagonal elements. So, the operator $\hat{N}$ could be manipulated different from the other by rewriting this operator as: $\hat{N} = \text{diag}(\hat{N}) + (\hat{N} - \text{diag}(\hat{N})) = \hat{N}_d + \hat{N}_{od}$ where the subscript "*d*" and "*od*" refer to diagonal

and off-diagonal. Now, operator $\hat{N}$ becomes the sum of two diagonal matrices. The approximated exponential of

$$\begin{aligned}\exp\left[\hat{N}\Delta t\right] &= \exp\left[(\hat{N}_d + \hat{N}_{od})\Delta t\right] \\ &= \left(I + (\hat{N}_d + \hat{N}_{od})\Delta t + \frac{(\hat{N}_d + \hat{N}_{od})^2 \Delta t^2}{2!} + \ldots\right) \\ &= \left(I + \hat{N}_d \Delta t + \frac{\hat{N}_d^2 \Delta t^2}{2!} + \ldots\right) + \left(\hat{N}_{od}\Delta t + \frac{(\hat{N}_d \hat{N}_{od} + \hat{N}_{od}\hat{N}_d + \hat{N}_{od}^2)\Delta t^2}{2!} + \ldots\right) \\ &\approx \exp\left[\hat{N}_d \Delta t\right] + \hat{N}_{od}\Delta t,\end{aligned} \tag{4-16}$$

where the higher-order term of $\hat{N}_{od}$ could be neglected in the expansion.

A rapid and easy way to check if the numerical method is stable is to make sure the law of energy conservation is achieved in every computational step. That is to say if the initial total energy of the wave is a certain quantity, then after every time step, this amount of energy stays the same. For this thesis, the errors of energy conservation should not exceed 1%. But in case of considering material absorption, then the energy quantity may decrease as the wave propagates. In an unstable system, the energy quantity could numerically increase, and eventually causing the overflow problem. A flow chart of SSFM algorithm and a sample of the MATLAB code for modeling THG phenomenon in PBG structure are shown in the appendix E.

4.4 Modeling

4.4.1 The PBG structure for third-harmonic generation process

In this section, the example of PBG structure is assumed to be consisted of 120 layers, which are alternating quarter-wave thin films. So that the thicknesses of two dielectric layers are a = 175.5 nm and b = 200 nm when the reference wavelength is 1,489 nm. Then, the transmission spectrum of the PBG structure has been calculated by using the TMM and calculated results is illustrated as Fig. 4.2 (a). The FF wavelength is tuned to the first long-wavelength band-edge transmission peak to avoid taking material dispersion into account. The forward and backward TH generation can occur and their wavelength have been found well away from the second long-wavelength band-edge as indicated in Fig. 4.2 (a). So the wavelength of FF and TH signal

are 1,550 nm and 517 nm, respectively. Finally, the choice of materials for the sample PBG structure could be tabulated as Table 4.5. The PBG materials also composed of chalcogenide glass layer-pair (As_2Se_3/As_2S_3) used in the sample PBG structure in chapter 3.

Table 4.5: The choice of material for the sample PBG structure [70]

Optical parameter/Material layer	**Layer a**	**Layer b**
Refractive index	$n_a = 2.12$	$n_b = 1.85$
Third-order susceptibility	$\chi_a^{(3)} = 2.9\times10^{-19}$ m^2/V^2	$\chi_b^{(3)} = 4.2\times10^{-20}$ m^2/V^2
Layer thickness	$a = \lambda_0 / 4n_a = 175.5$ nm	$b = \lambda_0 / 4n_b = 200$ nm

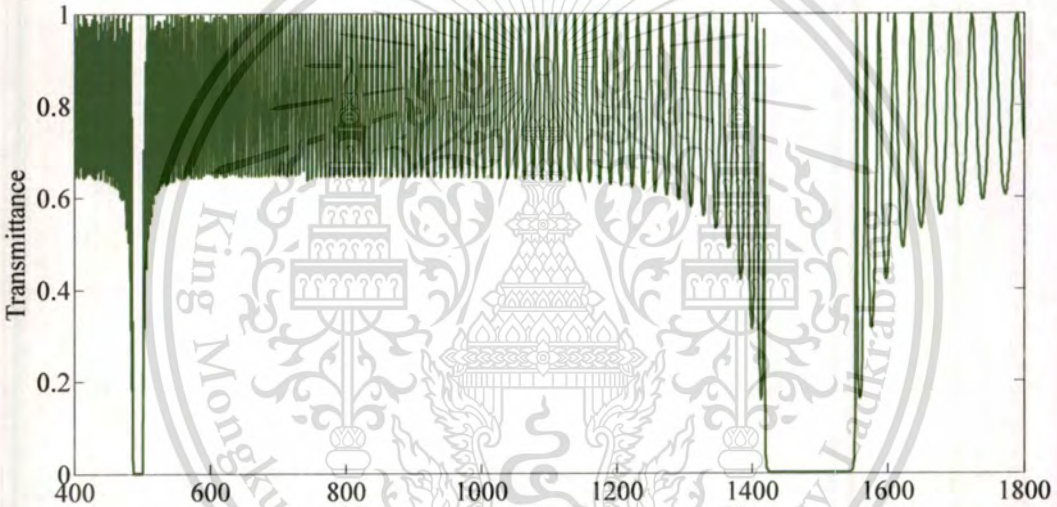

(a)

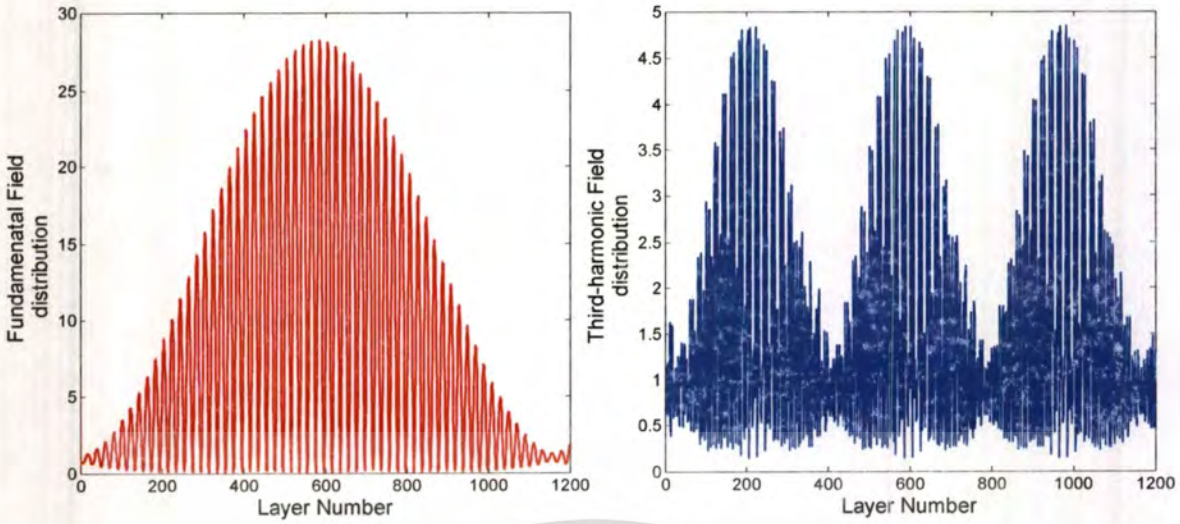

(b)

Figure 4.2 (a) The transmission spectrum of quarter-wave PBG structure which composed of 120 dielectric layers. (b) The local-field distributions (of λ_{ω} = 1,550 nm and $\lambda_{3\omega}$ = 517 nm) inside PBG structure when band-edge resonance is satisfied.

4.4.2 Boundary conditions

For numerically solving CMEs with the SSFM, the appropriated boundary conditions have been applied to the two ends of the sample PBG structure with the length L. In computational space, the left boundary condition for calculation at $z = 0$ and the right boundary condition at $z = L$ could be respective defined as:

$$E_{f,FF}(0,t) = a_{f1}(0,t), \tag{4-17a}$$

$$\frac{\partial}{\partial z} E_{b,FF}(L,t) = 0. \tag{4-17b}$$

Finally, the initial condition for this modeling is:

$$\begin{aligned} E_f(z,0) &= a_{f1}(z,0), \\ E_b(z,0) &= 0, \end{aligned} \tag{4-18}$$

for all $0 \le z \le L$. In this case, the input FF driving field has been launched to the left-hand side of the PBG structure only and all other field amplitudes are initially zero.

4.4.3 Modeling results

The optical pulse propagation and THG phenomenon have been modeled by using SSFM where the incident optical (input FF) pulse is the one-dimensional Gaussian pulses, expressed similarly as:

$$a_{f1}(z,0) = a_{10} e^{-\frac{(z-z_0)^2}{\sigma_{z1}^2}}, \tag{4-19}$$

where a_{10} is the peak magnitudes of the initial FF pulse, z is the spatial variables, and σ_z^2 is the variance of the Gaussian pulse in the corresponding direction. In the numerical modeling, the incident pulse need to be placed far enough away from the PBG structure for avoiding the overlap of the leading tail on the structure before the commencement of the pulse propagation. This problem could be solved by shifting the pulse center by a distance z_0. The Gaussian pump pulse could be tuned inside or outside the photonic band-gap. However, we are interesting in maximizing the nonlinear effect like a THG phenomenon inside the PBG structure, so the detuning parameter of FF pulse has been intentionally adjusted to the long-wavelength band-edge of the transmission spectrum as illustrated in Fig. 4.2 (a). For the PBG structure, the choice of parameter values, which are used in SSFM modeling, is tabulated in Table 4.5.

Table 4.6: The parameter values that used in the SSFM modeling

Parameter	Fundamental frequency	Third-harmonic frequency
Absorption coefficient	$\bar{\alpha}_1 = 0$	$\bar{\alpha}_3 = 0$
Group velocity	$v_{g1} = 0.496c$	$v_{g3} = 0.466c$
Detuning parameter	$\bar{\delta}_1 = 0.1462$	$\bar{\delta}_3 = -0.4405$
Coupling coefficient	$\bar{\kappa}_1^{(1)} = \bar{\kappa}_{-1}^{(1)} = 0.0422$	$\bar{\kappa}_1^{(3)} = \bar{\kappa}_{-1}^{(3)} = 0.1264$
Nonlinear coefficient	$\eta_0^{(1)} = 0.2001$ $\eta_1^{(1)} = 0.0090 - 0.0955i$ $\eta_{-1}^{(1)} = 0.0090 + 0.0955i$ $\eta_2^{(1)} = -0.0089 - 0.0017i$ $\eta_{-2}^{(1)} = -0.0089 + 0.0017i$ $\eta_3^{(1)} = 0.0086 - 0.0296i$ $\eta_{-3}^{(1)} = 0.0086 + 0.0296i$	$\eta_0^{(3)} = 0.5998$ $\eta_1^{(3)} = 0.0271 - 0.2862i$ $\eta_{-1}^{(3)} = 0.0271 + 0.2862i$ $\eta_2^{(3)} = -0.0266 - 0.0051i$ $\eta_{-2}^{(3)} = -0.0266 + 0.0051i$ $\eta_3^{(1)} = 0.0258 - 0.0888i$ $\eta_{-3}^{(1)} = 0.0258 + 0.0888i$

Note: The calculation method of nonlinear coefficients is shown in the appendix A. And the $c = 3 \times 10^8$ m/s.

In this modeling, the total propagating length (dimensionless unit) in the z axis spans from -20π to 20π, the total time step (dimensionless unit) is $t = 400$, and the incremental of each step is $\Delta t = 0.1$. At initial state, the input FF field intensity is 4.5 GW/cm^2. The plots of THG in PBG structure modeling are depicted in Fig. 4.3. The forward- and the backward-propagating optical pulses are in the same computational space. Each snapshot, as shown in Fig. 4.3 (a), (b), and (c), has been immediately captured when the total time steps are 0, 200, and 400, respectively. The rectangular black bar in each figure denotes the PBG structure.

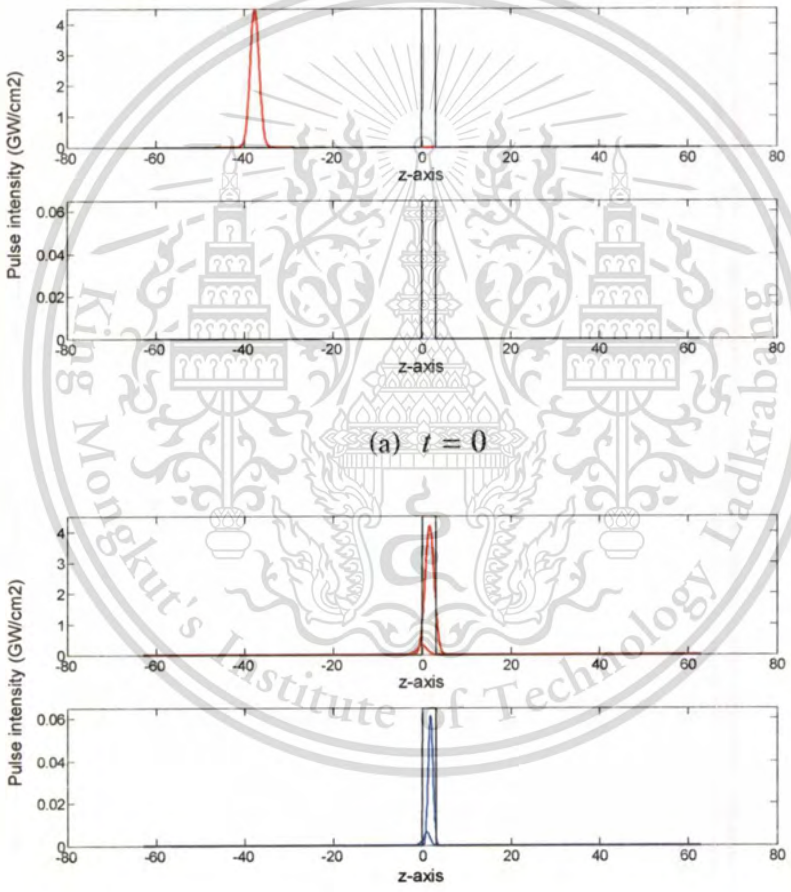

(a) $t = 0$

(b) $t = 200$

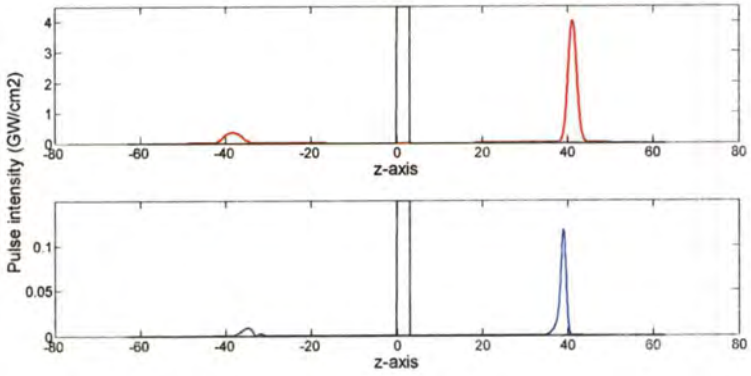

(c) $t = 400$

Figure 4.3 The snapshot of the THG process in a PBG structure (black bar) where the FF, and TH pulses are represented by the red line (top plot of each snapshot), and blue line (bottom plot of each snapshot), respectively. Figures 4.3 (a)-(c) are immediately captured when total time step are 0, 200, and 400, respectively.

Figure 4.3 shows that, the initial 4.5 GW/cm^2-FF pulse with Gaussian-shape is located in outside the PBG structure, corresponding to the boundary and the initial conditions in Eq. (4-17) and (4-18). In the figure, the PBG structure is represented by the black bar that located near the origin and the scaled structure length is about 4.7 (actual length is about 22.5 μm). The initial FF pump pulse is incident from the left as shown in Fig. 4.3 (a), note that the structure scatters output FF pulses and emits TH pulses significantly in both directions as shown in Figs. 4.3 (b) when $t = 200$ and 4.3 (c) when $t = 400$, respectively. The intensity of FF pulse in the forward-direction is about 3.997 GW/cm^2 and decreased after passing through the structure because of energy transferring between the frequency components and conversion to reflected energy. The backward FF pulse is generated from the multi-reflection inside multilayered structure as our PBG structure and its intensity (0.3479 GW/cm^2) is much lower than forward FF pulse due to the choice of transmission maximum for the central FF wavelength which results in a low forward-backward conversion efficiency. Meanwhile, the TH pulses at a time snapshot after the FF pulse has propagated through the PBG structure. The TH pulses in both propagating directions are generated since energy transfer from FF pulse to TH pulses. The output intensities of forward- and backward-TH pulses are about 0.1167 and 0.0089 GW/cm2, respectively. The wavelength for the FF pulse is tuned to the first long-wavelength band-edge transmission

maximum in Fig. 4.2 (a), where the group velocity for this frequency component is slowed to 0.496c. The slow light effect occurred because the dispersion of the effective index of PBG structure at the band-edge is large [55]. Consequently, the longitudinal walk-off between the FF and TH pulses occurs because of the change in the group velocities near the first and second band-edge of photonic band-gap, the group velocities of TH pulse is 0.466c, which is close to the FF pulse group velocity. Therefore, the FF pulses will lead the TH pulses as shown in Figs. 4.3 (b), and 4.3 (c).

The THG phenomenon has been enhanced by increasing the number of pair layers into stack. Consequently, the magnitudes of both forward- and backward-propagating TH pulse amplitudes are increased as shown in Fig 4.4. This figure shows both amplitudes of the forward-TH (a) and the backward-TH (b) pulses have growth with the structure length. Furthermore, the effect of output intensity of TH pulses and detuning parameter between wave-vector of FF pulse and grating wave-vector has been also shown in Fig. 4.4. The maximum intensity of forward-TH 4.4 (a) and backward-TH 4.4 (b) pulses are obtained when optimal detuning parameter of pump FF pulse is 0.0046. Both output TH intensities were decreased by decreasing or increasing of FF detuning parameter, with changing wavelength of FF pulse or periodic length of structure, because this detuning parameter have been affected directly to band-edge phase matching condition.

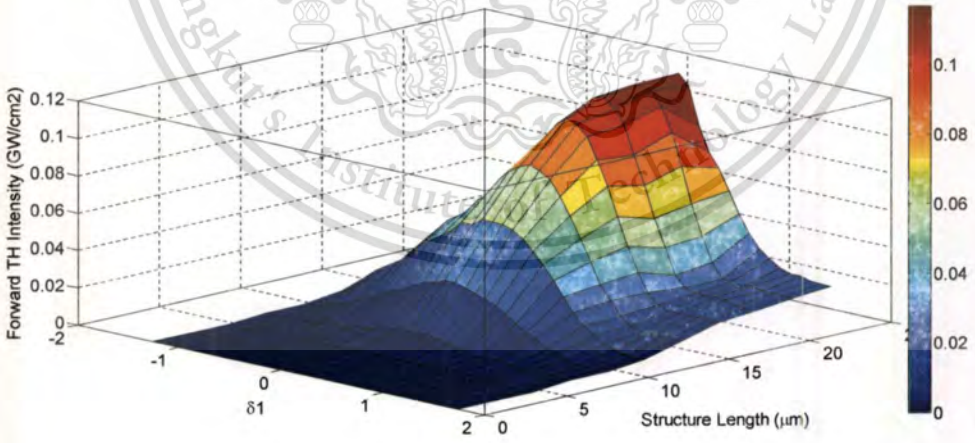

(a)

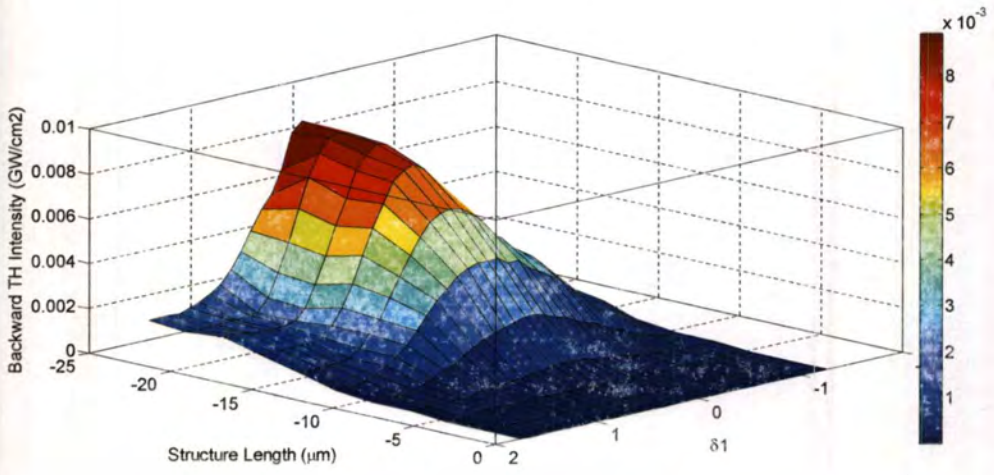

(b)

Fig. 4.4 The output intensity of forward-TH (a) and backward-TH (b) pulses which both depend on pump wave-vector detuning and total structure length (L)

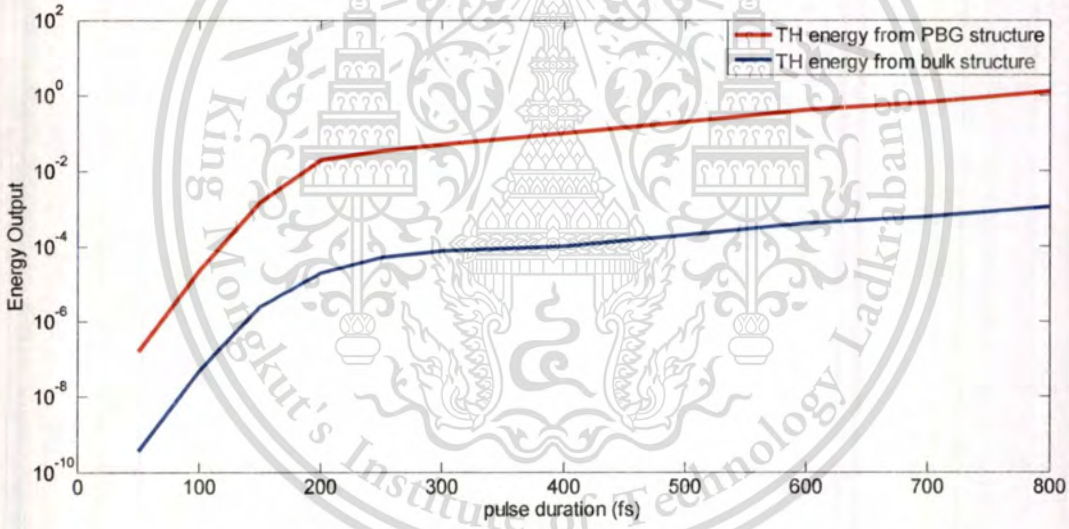

Fig. 4.5 The comparison between the total TH energy output from the PBG structure (red line) and from the phase-matched bulk medium (blue line), as a function of pulse width. The vertical axis is represented in logarithmic scale. The pulse width is given in units of femtosecond (fs). The output energy from PBG structure is greater than the output energy from bulk medium about 1,000 times when the incident pulse width approaches 800-fs.

In Fig. 4.5, the total-energy output (both forward and backward components) is plotted as a function of incident pulse width for a 60-period, 22-μm-thick PBG structure (red line), and 22-μm bulk medium (blue line). For clarity, the graph is plotted on a logarithmic scale. The figure shows that the total-energy output becomes 1,000 times greater for the PBG structure when compared to a phase-matched bulk medium of the same length [61] when pulse width approaches 800-fs. For very short pulses the energy conversion grows rapidly and then slowly increases only when pulse width approaches 800-fs for both cases as shown in Fig. 4.5. The rapid increase of the TH field intensity as the incident pulse width increases, and its subsequent saturation when frequency bandwidth of the pulse begins to be less than band-edge resonance bandwidth is responsible for this phenomenon. When the pulse frequency bandwidth is less than the transmission resonance bandwidth the *quasi-monochromatic* limit is reached. In both regimes, the amplitude of the generated TH pulses is increasing with increasing incident pulse width.

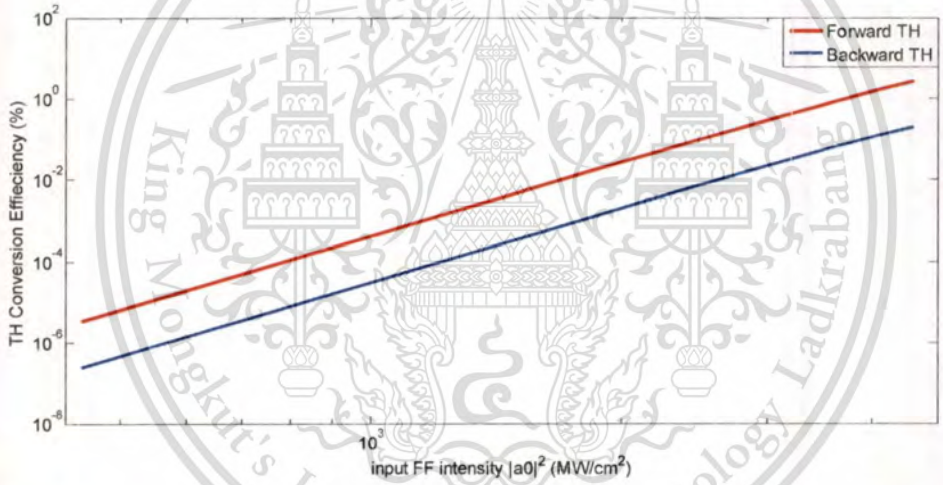

Figure 4.6. The TH conversion efficiency respect to the incident FF pump pulse intensity for forward- and backward-propagating TH pulses. Our calculations show that the conversion efficiency is increasing proportional to the amount of pump passes inside the structure. The maxima of conversion efficiency is achieved when the FF pulse intensity reach to 4.5 GW/cm^2.

Here, the conversion efficiency for TH field generation can be determined by the ratio of the generated forward- and backward-propagating direction TH power to the input FF pump power and can be expressed as following [62-63]:

$$C.E. = \frac{\left|a_{f3}(L)\right|^2}{\left|a_{f1}(0)\right|^2}. \tag{4-20a}$$

and

$$C.E. = \frac{\left|a_{b3}(0)\right|^2}{\left|a_{f1}(0)\right|^2}. \tag{4-20a}$$

The equation (4-20a) and (4-20b) are the mathematical formula for calculating conversion efficiency of forward- and backward-direction TH pulses, respectively. Figure 4.6 plots the conversion efficiency with respect to the power of FF pump field FF for a pulse of 800-fs duration. Figure 4.6 shows that for this PBG structure, the conversion efficiencies achieved is 1.8% for forward TH component and to 0.14 % for backward TH component when the incident FF pump intensity is 4.5 GW/cm^2, yielding a TH intensity of approximately 0.1167 and 0.0089 GW/cm^2, respectively. This figure also shows that the conversion efficiency becomes about 10 times greater for forward-TH pulse than for backward-TH pulse when input FF intensity approaches 4.5 GW/cm^2. As we previously mentioned, the higher conversion efficiencies can be obtained by increasing structure length or number of periods (N), since it increases proportional to N^2 due to the field enhancement inside the structure [19]. Furthermore, according to the set of coupled-mode equations containing with the zeroth-order and higher-order Fourier nonlinear components which depend on the amplitude (or intensity) of the FF pulse, the action of the high intensity FF pulse through the nonlinearity of PBG structure is to further amplify the third-harmonic wave. Consequently, all nonlinear effects, like third-harmonic generation, can be strengthened and the conversion efficiency is directly increased through the additional nonlinear contributions in the PBG structure.

Chapter 5

Conclusions

5.1 Summary of optical parametric amplification phenomenon in PBG structure

In this thesis, the third-order nonlinear optical effects such as optical parametric amplification (OPA) and third-harmonic generation (THG) phenomena in photonic band-gap (PBG) structure have been numerically investigated. The mathematical methods, which have been used in this investigation, are transfer-matrix method (TMM), multiple-scale method (MSM), and split-step Fourier method (SSFM). The more details of each mathematical methods have been shown in chapter 2. The first investigating effect is the OPA effect as in chapter 3. In this chapter, a completed set of coupled-mode equations (CMEs), which correspond to this effect, is derived by using the MSM procedure with phase-matching condition. The derived CMEs have the additional terms including the higher-order nonlinear coefficients. So the set of CMEs is difference from the conventional CMEs in previous OPA works. The PBG structure, for OPA investigating, is designed by optimizing type of two layer materials and their thicknesses. The half-wave/eighth-wave thin film structure is found that being an efficient structure to achieve efficient frequency conversion efficiency. After that, the TMM is used to calculate the transmission spectrum of this PBG structure. By using this method, the input pump wavelength is tuned to long wavelength band-edge of transmission spectrum to make the band-edge resonance inside PBG structure and achieve efficient nonlinear effect, while input signal wavelength is tuned around near band-edge wavelength. After that, SSFM has been proposed to solve these six scaled CMEs with appropriate boundary condition. In this modeling, input Gaussian-shape pump and signal pulses are initially launched into only left-hand side of PBG structure with input intensities 4.50 GW/cm^2 (pump) and 0.0112 GW/cm^2 (signal), respectively.

The modeling results show that idler pulses can be generated by gaining energy from input pump and signal fields, while signal field can be immediately amplified under this nonlinear interaction. The intensity of signal and idler pulses has exponential growth with increasing of number of layers. Meanwhile, these intensities have been directly affected by pump detuning parameter (δ_1) due to band-edge phase matching

condition could be achieved by determining the optimal detuning parameter. From our modelled results, the output intensities would be decreased by increasing and decreasing of detuning parameter from optimal value (0.1462). Then, signal gain and conversion efficiency of idler generation were calculated directly and both exponentially increased with number of layers. The maximum gain is about 83.5 can be achieved when PBG structure composed of 245 layers (~110.5 μm). Furthermore, gain and conversion efficiency have been depended on pulse width of input pump pulse, since phase matching condition can be achieve for short pulse regime more than long pulse regime. Finally, the input pump and signal intensities have been found that there are directly affect to the conversion efficiency. As the calculated result, threshold intensity, for several input signal amplitudes, is 1.62 GW/cm^2 and achieving the maximum efficiency (19.24, 46.15, and 67.52%) when input pump intensity increases until to 4.5 GW/cm^2.

5.2 Summary of third-harmonic generation phenomenon in PBG structure

In summary, THG phenomenon in PBG structure, which has $\chi^{(3)}$ response, has been numerically investigated. To model TH generation in the structure, a completed group of scaled CMEs, which correspond to TH generating effect, has been derived by using the MSM. Strong TH enhancement is found for band-edge phase matching condition. A SSFM has been adopted to solve these four scaled CMEs with appropriate boundary condition. In this section, the PBG structure has been composed of 120 dielectric layers, which are alternating two types of quarter-wave films. So, the total length of this finite structure is about 22 μm. The transmission spectrum of the TMM designed structure has two photonic band-gaps; the second band-gap center wavelength position is shifted to a shorter wavelength from the first band-gap center wavelength by a factor of 3.

In the modeling, the input FF (pump) pulse has a Gaussian-shape and it is initially launched toward the left-hand side of PBG structure with a peak intensity of 4.5 GW/cm^2. The input FF wavelength is chosen at the lower frequency band-edge of the first band-gap about 1,550 nm (to enhance nonlinear effect in the structure based on band-edge enhancement principle). Consequently, the wavelength of TH pulse is about 517 nm. In addition, the spectrum bandwidth of FF pulse should be less than or equal to the spectrum bandwidth of lower band-edge peak (~10 nm) to avoid pulse dispersion in the structure and reflection of the FF pulse

energy; this condition will guarantee that efficient TH generation occurs. For our model the pulse width of the FF pulse which has the desired spectral bandwidth, is 800-fs.

The modeling results show that the TH pulses in forward- and backward-direction can be emitted from the structure by gaining energy from input FF field under the nonlinear interaction. The output intensities of forward and backward TH pulse have been directly affected by FF detuning parameter (δ_1) because the band-edge phase matching condition could be achieved by determining the optimal detuning parameter. From our modeled results, the output TH intensities is decreased by increasing and decreasing of detuning parameter from its optimal value (0.0046). Furthermore, the total-energy output of TH pulses are also depended on the pulse width of FF pulse. The total-energy output is 1,000 times greater for the PBG structure than that of phase-matched bulk medium when pulse width approaches 800-fs. The third-harmonic energy output grows rapidly when FF pulse width is initially small and then approaches 800-fs and then more increases for longer pulse widths. The energy saturates because pulse width corresponds to a spectral width that is smaller than the spectral width of the band-edge transmission peak; in other words the *quasi-monochromatic* limit is reached. TH conversion efficiencies are calculated directly and both are increased with input FF intensity. The maximum conversion efficiencies are about 1.8% for forward TH component and 0.14% for backward TH component, which can be achieved when the input intensity is reached to 4.5 GW/cm^2.

5.3 Future work

Finally, this thesis results have suggest that the PBG structure can be possibly applied and designed for nonlinear frequency conversion processes. Our research is focused on the improvement of mathematical models that show how to enhance the nonlinear frequency conversions in the PBG structure. For future work, first, we would like to re-derive the CMEs for both OPA and THG phenomena by expanding parameters in wave equation and grouping terms with the higher-order perturbation variables e.g. μ^2 and obtaining the $O(\mu^2)$ equation in MSM procedure. Then, the CMEs, which can contain many higher-order Fourier coefficients of nonlinear coefficients, will be obtained. These Fourier coefficients may realize the square wave form of nonlinear grating of PBG structure that is like the nonlinear grating in actual PBG structure.

Finally, we will obtain mathematical model of actual PBG structure which can precisely describe the nonlinear optical phenomena inside the PBG structure. For second future work, we wish to have an opportunity to fabricate and test the nonlinear frequency converter based on PBG structure from this thesis. In near future, we hope that the PBG structure will be widely integrated in the optoelectronic devices and photonic systems. The PBG structure can reduce the size and cost of devices because it can be made with uncomplicated fabrication process.

References

[1] J. W. S. Rayleigh, "On the remarkable phenomenon of crystalline reflexion described by Prof. Stokes", *Phil. Mag* **26**, 256–265 (1888).

[2] E. Yablonovitch, "Inhibited spontaneous emission in solid-state physics and electronics", *Phys. Rev. Lett.* **58**(20), 2059–2062 (1987).

[3] S. John, "Strong localization of photons in certain disordered dielectric superlattices", *Phys. Rev. Lett.* **58**(23), 2486–2489 (1987).

[4] J. Y. Kim, M. K. Kwon, K. S. Lee, S. J. Park, S. H. Kim, and K. D. Lee, "Enhanced light extraction from GaN-based green light-emitting diode with photonic crystal", *Appl. Phys. Lett.* **91**(18), 181109 (2007).

[5] H. H. Guan, P. Han, Y. Q. Yang, Y. P. Li, X. Zhang, and W. T. Zhang, "Omni-directional mirror for visible light based on one-dimensional photonic crystal", *Chin. Opt. Lett.* **9**(7), 071603 (2011).

[6] P. Kaspar, R. Kappeler, H. Jäckel, and C. Hafner, "Toward low-loss photonic crystal waveguides in InP/InGaAsP heterostructures", *Opt. Lett.* **37**(17), 3717-3719 (2012).

[7] B. L. Guana, X. Guob, X. J. Ren, S. Li, and G. D. Shen, "Multiwavelength fabrication of vertical-cavity surface-emitting lasers based on asymmetric one-dimensional photonic crystal", *J. Appl. Phys.* **110**(5), 053101 (2011).

[8] M. Scalora, J. P. Dowling, M. J. Bloemer, C. M. Bowden, "The photonic band edge optical diode", *J. Appl. Phys.* **76**(4), 2023-2026 (1994).

[9] M. Scalora, J. P. Dowling, C. M. Bowden, and M. J. Bloemer, "Optical limiting and switching of ultrashort pulses in nonlinear photonic band- gap materials", *Phys. Rev. Lett.* **73**(10), 1368-1371 (1994).

[10] J. P. Dowling, M. Scalora, M. J. Bloemer and C. M. Bowden, "The photonic band edge laser: A new approach to gain enhancement," *J. Appl. Phys.* **75**(4), 1896-1899 (1994).

[11] M. Scalora, R.J. Flynn, S.B. Reinhardt, R.L. Fork, M.J. Bloemer, M.D. Tocci, C.M. Bowden, H.S. Ledbetter, J.M. Bendickson, J.P. Dowling, and R.P. Leavitt, "Ultrashort pulse propagation at the photonic band edge: Large tunable group delay with minimal distortion and loss," *Phys. Rev. E* **54**(2), 1078–1081 (1996).

[12] J.A. Armstrong, N. Bloembergen, J. Ducuing, and P.S. Pershan, "Interactions between Light Waves in a Nonlinear Dielectric", *Phys. Rev.* **127**(6), 1918 (1962).

[13] N. Bloembergen, A. J. Sievers, "Nonlinear optical properties of periodic laminar structures", *Appl. Phys. Lett.* **17**(11), 483-485 (1970).

[14] M. Yamada, N. Nada, M. Saitoh, and K. Watanabe, "First-order quasi-phase matched LiNbO3 waveguide periodically poled by applying an external field for efficient blue second-harmonic generation", *Appl. Phys. Lett.* **62**(5), 435 (1993).

[15] W. K. Burns, W. McElhanon, and L. Goldberg, "Second harmonic generation in field poled, quasi-phase-matched, bulk $LiNbO_3$", *IEEE Photon. Technol. Lett.* **6**(2), 252 -254(1994).

[16] M. M. Fejer, G. A. Magerl, D. H. Jundt, and R. L. Byers, "Quasi-phase-matched second harmonic generation: tuning and tolerances", *IEEE J. Quantum Electron.* **28**(11), 2631 (1992).

[17] Q. Chen and W. P. Risk, "Periodic poling of $KTiOPO_4$ using an applied electric field", *Electron. Lett.* **30**(18), 1516 (1994).

[18] J. W. Haus, R. Viswanathan, M. Scalora, A. G. Kalocsai, J. D. Cole, and J. Theimer, "Enhanced second-harmonic generation in media with a weak periodicity," *Phys. Rev. A* **57**(3), 2120-2128 (1998).

[19] M. Scalora, M.J. Bloemer, A.S. Manka, J.P. Dowling, C.M. Bowden, R. Viswanathan, and J. W. Haus, "Pulsed second-harmonic generation in nonlinear, one-dimensional, periodic structures," *Phys. Rev. A* **56**(4), 3166-3174 (1997).

[20] M. Centini, M. Scalora, C. Sibilia, M. Bertolotti, M. J. Bloemer, C. M. Bowden, J. W. Haus, "Efficient nonlinear infrared parametric generation on one-dimensional photonic band gap structures," *Opt. Commun.* **189**(1-3), 135–142 (2001).

[21] A. V. Tarasishin, S. A. Magnitskii, and A. M. Zheltikov, "Matching phase and group velocities in second-harmonic generation in finite one-dimensional photonic band-gap structures," *Laser Phys.* **11**(1), 31-38 (2001).

[22] Y. Q. Lu, M. Xiao, and G. J. Salamo, "Coherent microwave generation in a nonlinear photonic crystal," *IEEE J. Quan. Elec.* **28**(5), 481-485 (2002).

[23] M. Centini, C. Sibilia, M. Scalora, V. Rugolo, M. Bertolotti, M. J. Bloemer, and C. M. Bowden, "On the phase matching conditions in applications of one-dimensional photonic band gap structures for nonlinear frequency conversion," *J. Opt. A: Pure Appl. Opt.* **2**, 327-331 (2000).

[24] J. W. Haus, P. Powers, P. Bojja, M. Torres-Cisneros, M. Scalora, M. J. Bloemer, N. Akozbek, and M. A. Meneses-Nava, "Enhanced tunable terahertz generation in photonic band-gap structures," *Laser Phys.* **14**(5), 1-8 (2004).

[25] K. Suizu and K. Kawase, "Terahertz-wave generation in a conventional optical fiber," *Opt. Lett.* **32**(20), 289-291 (2007).

[26] K. Bencheikh, S. Richard, G. Melin, G. Krabshuis, F. Gooijer, and J. A. Levenson, "Phase-matched third-harmonic generation in highly germanium-doped fiber," *Opt. Lett.* **37**(3), 289-291 (2012).

[27] K. Tarnowski, B. Kibler, C. Finot, and W. Urbanczyk, "Quasi-phase-matched third harmonic generation in optical fibers using refractive-index gratings," *IEEE J. Quant. Elec.* **47**(5), 622-628 (2011).

[28] F. Omenetto, A. Efimov, A. Taylor, J. Knight, W. Wadswort, and P. Russel, "Polarization dependent harmonic generation in microstructured fibers," *Opt. Express* **11**(1), 61-67 (2003).

[29] A. C. Turner, M. A. Foster, A. L. Gaeta, and M. Lipson, "Ultra-low power parametric frequency conversion in a silicon microring resonator," *Opt. Express* **16**(7), 4881-4887 (2008).

[30] E. K. Tien, Y. W. Huang, S. M. Gao, Q. Song, F. Qian, S. K. Kalyoncu, and O. Boyraz, "Discrete parametric band conversion in silicon for mid-infrared applications," *Opt. Express* **18**(21), 21981-21989 (2010).

[31] M. Scalora, and M. E. Crenshaw, "A beam propagation method that handles reflections," *Opt. commu.* **108**(4-6), 191-196 (1994).

[32] P. Yeh, A. Yariv, and C. Hong, "Electromagnetic propagation in periodic stratified media. I. General theory," *J. Opt. Soc. Am.* **67**(4), 423-438 (1977).

[33] A. Yariv, and P. Yeh, "Electromagnetic propagation in periodic stratified media. II. Birefringence, phase matching, and x-ray lasers," *J. Opt. Soc. Am.* **67**(4), 438-448 (1977).

[34] J. Danckaert, K. Fobelets, I. Veretennicoff, and R. Reinisch, "Dispersive optical bistability in stratified structures," *Phys. Rev. B* **44**(15), 8214-8225 (1991).

[35] P. Delaye, M. Astic, R. Frey, and G. Roosen, "Transfer-matrix modeling of four-wave mixing at the band edge of a one-dimensional photonic crystal," *J. Opt. Soc. Am. B* **22**(11), 2494-2504 (2005).

[36] M. Pande and S. Gupta, "Nonlinearity-induced resonances and optical multistability with coupled surface plasmons in a symmetric layered structure," *Opt. Lett.* **15**(17), 944-946 (1990).

[37] J. Jose and S. Gupta, "Phase conjugation induced distortion correction and optical multistability in enhanced back scattering in nonlinear layered media," *Opt. Comm.* **145**, 220-226 (1998).

[38] S. Gupta and D. Ray, "Optical multistability in a nonlinear Fibonacci multilayer," *Rapid Comm.* **38**(5), 3628-3631 (1988).

[39] P. Maker, R. Terhune, and C. Savage, "Intensity-dependent changes in the refractive index of liquids," *Phys. Rev. Lett.* **12**, 507-509 (1964).

[40] A. G. Kalocsai, and J. W. Haus, "Nonlinear Schrödinger equation for optical media with quadratic nonlinearity," *Phys. Rev. A* **49**(1), 574–585 (1994).

[41] A. G. Kalocsai, and J. W. Haus, "Asymptotic wave-wave processes beyond cascading in quadratic nonlinear optical materials," *Phys. Rev. E* **52**(3), 3166–3183 (1995).

[42] H. M. Lee and J. C. Wu, "Transmittance spectra in one-dimensional superconductor-dielectric photonic crystal", *J. Appl. Phys.* **107**, 09E149 (2010).

[43] K. Yee, "Numerical solution to initial boundary value problems involving Maxwell's equations in isotropic media," *IEEE Trans. Antennas & Prop.* **14**, 302307 (1966).

[44] A. Bi, K. Wu, C. Wu, and J. Litva, "A new finite-difference time-domain algorithm for solving Maxwell's equation," *IEEE microwave & Guided Wave Lett.* **1**, 382-384 (1991).

[45] S. Chu and S. Chaudhuri, "A finite-difference time-domain method for the design and analysis of guided-wave optical structures," *J. Lightwave Tech.* **7**, 2033-2038 (1989).

[46] W. Huang, S. Chu, A. Goss, and S. Chaudhuri, "A scalar finite-difference time-domain approach to guided-wave optics," *IEEE Photon. Tech. Lett.* **3**, 524-526 (1991).

[47] P. Tran, "All-optical switching with a nonlinear chiral photonic bandgap structure," *J. Opt. Soc. Am. B* **16**, 70-73 (1999).

[48] M. Feit and J. Fleck, Jr., "Light propagation in graded-index optical fibers," *Appl. Opt.* **17**, 3990-3998 (1978).

[49] D. G. Salinas, C. M. de Sterke, and J. E. Sipe, "Coupled-mode equations for deep gratings," *Opt. Commu.* **111**, 105-110 (1994).

[50] C. M. de Sterke, D. G. Salinas, and J. E. Sipe, "Coupled-mode equations for light propagation through deep nonlinear gratings," Phys. Rev. E 54(2), 1969-1989 (1996).

[51] J. W. Haus, B. Y. Soon, M. Scalora, C. Sibilia, and I. V. Mel'nikov, "Coupled equations for Kerr media with periodically modulated linear and nonlinear coefficients," *J. Opt. Soc. Am. B* **19**, 2282-2291 (2002).

[52] J. W. Haus, B. Y. Soon, M. Scalora, M. Bloemer, C. Bowden, C. Sibilia, and A. Zheltikov, "Spatio-temporal instabilities for counter-propagating waves in periodic media," *Opt. Express* **10**, 114-121 (2002).

[53] Z. Toroker and M. Horowitz, "Optimized split-step method for modeling nonlinear pulse propagation in fiber Bragg gratings," *J. Opt. Soc. Am. B* **25**, 448-457 (2008).

[54] J. M. Bendickson and J. P. Dowling, "Analytic expressions for the electromagnetic mode density in finite, one-dimensional, photonic band-gap structures," *Phys. Rev. E* **53**(4), 4107–4121 (1996).

[55] M. Centini, C. Sibilia, M. Scalora, G. D'Aguanno, M. Bertolotti, M. J. Bloemer, C. M. Bowden, and I. Nefedov, "Dispersive properties of finite, one-dimensional photonic band gap structures: applications to nonlinear quadratic interactions," *Phys. Rev. E* **60**(4), 4891–4898 (1999).

[56] J. Kevorkian and J. D. Cole, "Perturbation methods in applied mathematics," Springer-Verlag, New York (1981).

[57] M. J. Ablowitz, "Nonlinear dispersive waves: Asymptotic analysis and solitons," Cambridge University Press, Cambridge (2011).

[58] T. C. Poon and T. G. Kim, "Engineering optics with MATLAB," World Scientific, Singapore (2006).

[59] T. C. Poon and P. P. Banerjee, "Contemporary optical image processing with MATLAB," Elsevier, Amsterdam (2001).

[60] R. Boyd, "Nonlinear optics," Academic Press, California (1995).

[61] T. Schneider, "Nonlinear optics in telecommunications," Springer-Verlag, Berlin (2004).

[62] M. E. Marhic, "Fiber optical parametric amplifiers, oscillations and related devices," Cambridge University Press, Cambridge (2008).

[63] G. P. Agrawal, "Nonlinear fiber optics, 2nd ed.," Academic Press, California (1995).

[64] P. Yeh, "Optical waves in layered media, 2nd ed.," Wiley-Interscience, New Jersey (2005).

[65] A. Lakhtakia, "The handbook of nanotechnology: nanometer structures: theory, modeling, and simulation," Prentice-Hall India, New Delhi (2007).

[66] P. E. Powers, "Fundamentals of nonlinear optics," CRC Press, Florida (2011).

[67] G. I. Stegeman, "Nonlinear optics: Phenomena, materials, and devices," John Wiley, New Jersey (2012).

[68] G. Lenz, J. Zimmermann, T. Katsufuji, M. E. Lines, H. Y. Hwang, S. Spälter, R. E. Slusher, S.-W. Cheong, J.S. Sanghera, and I. D. Aggarwal, "Large Kerr effect in bulk Se-based chalcogenide glasses," *Opt. Lett.* **25**(4), 254-256 (2000).

[69] J. M. Laniel, N. Ho, R. Vallee, and A. Villeneuve, "Nonlinear-refractive-index measurement in As_2S_3 channel waveguides by asymmetric self-phase modulation," *J. Opt. Soc. Am. B* **22**(2), 437-445 (2005).

[70] C. Becker, M. Wegener, S. Wong, and G. von Freyman, "Phase-matched nondegenerate four-wave mixing in one-dimensional photonic crystals," *Appl. Phys.* **89**, 131122 (2006).

Appendix A

In this section, the issue of how to make use of the η nonlinear coefficients would be addressed to change the $\chi^{(3)}$ function and also the duty cycle of the PBG structure. The $\chi^{(3)}$ function could be expanded in the Fourier series form as follow:

$$f(z)=\sum_{s=-\infty}^{\infty}F(s)\exp\left(\frac{2\pi isz}{\Lambda}\right), \tag{A.1a}$$

where

$$F(s)=\frac{1}{\Lambda}\int_0^{\Lambda}f(z)\exp\left(\frac{-2\pi isz}{\Lambda}\right)dz, \tag{A.1b}$$

is represented as Fourier coefficients of $\chi^{(3)}$ function, s is the frequency variable, and Λ is the periodic length of PBG structure. Here, the duty cycle (DC) of the PBG structure is defined as $\mathrm{DC}=(a/\Lambda)\times 100\%$ and $\mathrm{IDC}=\Lambda/a$ is the reciprocal of DC. An example to show how can incorporate η and DC in the PBG structure design would be illustrated. Now, the value of nonlinear coefficient $\eta=\frac{2\pi\omega_1^2}{k_1c^2}\chi^{(3)}$ at ω_1 would be respectively 0.3604 and 0.0578 in the first and second dielectric layers with an arbitrary DC as illustrated in Figure A.1.

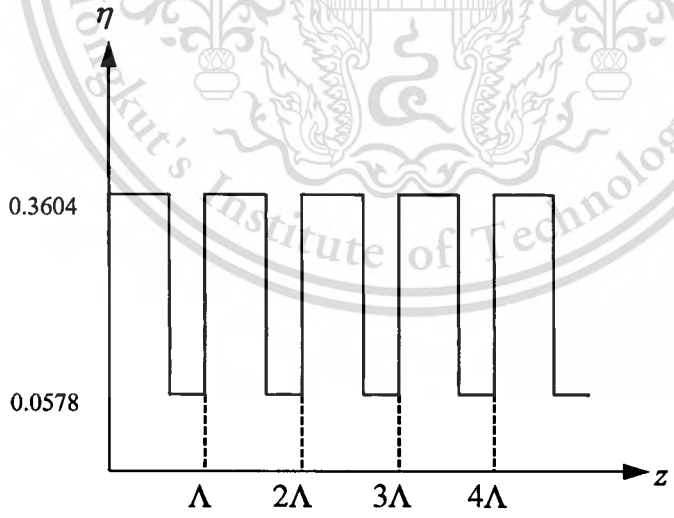

Figure A.1. The schematic of the PBG structure where the η of the first and second dielectric layers are respectively 0.3604 and 0.0578 with arbitrary DC.

The zeroth-order Fourier coefficient could be determined by

$$\begin{aligned}\eta_0 &= \frac{1}{\Lambda}\int_0^{\Lambda/\mathrm{IDC}}(0.3604)dz + \frac{1}{T}\int_{\Lambda/\mathrm{IDC}}^{\Lambda}(0.0578)dz \\ &= \frac{0.3604}{\mathrm{IDC}} + \left(0.0578 - \frac{0.0578}{\mathrm{IDC}}\right),\end{aligned} \tag{A.2a}$$

and the higher-order Fourier coefficients are determined by

$$\begin{aligned}\eta_\ell &= \frac{1}{\Lambda}\int_0^{\Lambda/\mathrm{IDC}}(0.3604)e^{-2\pi i\ell z/\Lambda}dz + \frac{1}{T}\int_{\Lambda/\mathrm{IDC}}^{\Lambda}(0.0578)e^{-2\pi i\ell z/\Lambda}dz \\ &= \left[\frac{0.3604}{-2\pi i\ell}\left(e^{-2\pi i\ell/\mathrm{IDC}} - 1\right)\right] + \left[\frac{0.0578}{-2\pi i\ell}\left(e^{-2\pi i\ell} - e^{-2\pi i\ell/\mathrm{IDC}}\right)\right].\end{aligned} \tag{A.2b}$$

Using the Fourier coefficients determined in Eq. (A.2) with Eq. (A.1a), the nonlinear coefficient η could be synthesized. In this case, the DC is varied as 0, 10, 20... 100 and the computed Fourier coefficients for η_ℓ, where $\ell = 0, \pm 1, \pm 2$ are tabulated in Table A.1.

Table A.1. The Fourier coefficients of η of pump pulse with ω_1

DC	$\eta_0^{(1)}$	$\eta_1^{(1)}$	$\eta_{-1}^{(1)}$	$\eta_2^{(1)}$	$\eta_{-2}^{(1)}$
0	0.0578	0	0	0	0
10	0.0881	0.0283 - 0.0092i	0.0283 + 0.0092i	0.0229 - 0.0166i	0.0229 + 0.0166i
20	0.1183	0.0458 - 0.0333i	0.0458 + 0.0333i	0.0142 - 0.0436i	0.0142 + 0.0436i
30	0.1486	0.0458 - 0.0630i	0.0458 + 0.0630i	-0.0142 - 0.0436i	-0.0142 + 0.0436i
40	0.1789	0.0283 - 0.0871i	0.0283 + 0.0871i	-0.0229 - 0.0166i	-0.0229 + 0.0166i
50	0.2091	0.0000 - 0.0963i	0.0000 + 0.0963i	0	0
60	0.2394	-0.0283 - 0.0871i	-0.0283 + 0.0871i	0.0229 - 0.0166i	0.0229 + 0.0166i
70	0.2696	-0.0458 - 0.0630i	-0.0458 + 0.0630i	0.0142 - 0.0436i	0.0142 + 0.0436i
80	0.2999	-0.0458 - 0.0333i	-0.0458 + 0.0333i	-0.0142 - 0.0436i	-0.0142 + 0.0436i
90	0.3302	-0.0283 - 0.0092i	-0.0283 + 0.0092i	-0.0229 - 0.0166i	-0.0229 + 0.0166i
100	0.3604	0	0	0	0

Table A.2. The Fourier coefficients of η of signal pulse with ω_3

DC	$\eta_0^{(3)}$	$\eta_1^{(3)}$	$\eta_{-1}^{(3)}$	$\eta_2^{(3)}$	$\eta_{-2}^{(3)}$
0	0.0576	0	0	0	0
10	0.0878	0.0282 - 0.0092i	0.0282 + 0.0092i	0.0228 - 0.0166i	0.0228 + 0.0166i
20	0.1180	0.0457 - 0.0332i	0.0457 + 0.0332i	0.0141 - 0.0434i	0.0141 + 0.0434i
30	0.1481	0.0457 - 0.0628i	0.0457 + 0.0628i	-0.0141 - 0.0434i	-0.0141 + 0.0434i
40	0.1783	0.0282 - 0.0868i	0.0282 + 0.0868i	-0.0228 - 0.0166i	-0.0228 + 0.0166i
50	0.2085	0.0000 - 0.0960i	0.0000 + 0.0960i	0	0
60	0.2386	-0.0282 - 0.0868i	-0.0282 + 0.0868i	0.0228 - 0.0166i	0.0228 + 0.0166i
70	0.2688	-0.0457 - 0.0628i	-0.0457 + 0.0628i	0.0141 - 0.0434i	0.0141 + 0.0434i
80	0.2989	-0.0457 - 0.0332i	-0.0457 + 0.0332i	-0.0141 - 0.0434i	-0.0141 + 0.0434i
90	0.3291	-0.0282 - 0.0092i	-0.0282 + 0.0092i	-0.0228 - 0.0166i	-0.0228 + 0.0166i
100	0.3593	0	0	0	0

Table A.3. The Fourier coefficients of η of idler pulse with ω_4

DC	$\eta_0^{(4)}$	$\eta_1^{(4)}$	$\eta_{-1}^{(4)}$	$\eta_2^{(4)}$	$\eta_{-2}^{(4)}$
0	0.0580	0	0	0	0
10	0.0884	0.0284 - 0.0092i	0.0284 + 0.0092i	0.0230 - 0.0167i	0.0230 + 0.0167i
20	0.1187	0.0460 - 0.0334i	0.0460 + 0.0334i	0.0142 - 0.0437i	0.0142 + 0.0437i
30	0.1491	0.0460 - 0.0632i	0.0460 + 0.0632i	-0.0142 - 0.0437i	-0.0142 + 0.0437i
40	0.1794	0.0284 - 0.0874i	0.0284 + 0.0874i	-0.0230 - 0.0167i	-0.0230 + 0.0167i
50	0.2098	0.0000 - 0.0966i	0.0000 + 0.0966i	0	0
60	0.2402	-0.0284 - 0.0874i	-0.0284 + 0.0874i	0.0230 - 0.0167i	0.0230 + 0.0167i
70	0.2705	-0.0460 - 0.0632i	-0.0460 + 0.0632i	0.0142 - 0.0437i	0.0142 + 0.0437i
80	0.3009	-0.0460 - 0.0334i	-0.0460 + 0.0334i	-0.0142 - 0.0437i	-0.0142 + 0.0437i
90	0.3312	-0.0284 - 0.0092i	-0.0284 + 0.0092i	-0.0230 - 0.0167i	-0.0230 + 0.0167i
100	0.3616	0	0	0	0

Note that the Fourier coefficients for η could be always computed to obtain more than 5 coefficients. But if we need to incorporate more than 5 Fourier coefficients for better synthesis accuracy, we may need to re-derive the coupled-mode equations to accommodate the extra coefficients. This addition will increase the coding complexity, together with increment of computational time and memory usage. Therefore, with consideration of the exchange between the number of Fourier coefficients and synthesis accuracy, we believe that the 5 Fourier coefficients for η synthesis is adequate for academic investigation of parametric amplification in the PBG structure.

Appendix B

By using the Eq. (A.2a) and (A.2b), the nonlinear coefficients for FF and TH frequencies can be obtained like in appendix A. In this case, the DC is varied as 0, 10, 20... 100 and the computed Fourier coefficients for η_ℓ, where $\ell = 0, \pm 1, \pm 2, \pm 3$ are tabulated in Table B.1.

Table B.1. The Fourier coefficients of η of fundamental-frequency pulse with ω

DC	$\eta_0^{(1)}$	$\eta_{\pm 1}^{(1)}$	$\eta_{\pm 2}^{(1)}$	$\eta_{\pm 3}^{(1)}$
0	0.0578	0	0	0
10	0.0881	0.0283 ∓ 0.0092i	0.0229 ∓ 0.0166i	0.0153 ∓ 0.0210i
20	0.1183	0.0458 ∓ 0.0333i	0.0142 ∓ 0.0436i	-0.0094 ∓ 0.0290i
30	0.1486	0.0458 ∓ 0.0630i	-0.0142 ∓ 0.0436i	-0.0094 ∓ 0.0031i
40	0.1789	0.0283 ∓ 0.0871i	-0.0229 ∓ 0.0166i	0.0153 ∓ 0.0111i
50	0.2091	0.0000 ∓ 0.0963i	0	0.0000 ∓ 0.0321i
60	0.2394	-0.0283 ∓ 0.0871i	0.0229 ∓ 0.0166i	-0.0153 ∓ 0.0111i
70	0.2696	-0.0458 ∓ 0.0630i	0.0142 ∓ 0.0436i	0.0094 ∓ 0.0031
80	0.2999	-0.0458 ∓ 0.0333i	-0.0142 ∓ 0.0436i	0.0094 ∓ 0.0290i
90	0.3302	-0.0283 ∓ 0.0092i	-0.0229 ∓ 0.0166i	-0.0153 ∓ 0.0210i
100	0.3604	0	0	0

The computed Fourier coefficients for η_ℓ, where $\ell = 0, \pm 1, \pm 2, \pm 3$ are tabulated in Table B.2.

Table B.2. The Fourier coefficients of η of third-harmonic frequency pulse with 3ω

DC	$\eta_0^{(3)}$	$\eta_{\pm 1}^{(3)}$	$\eta_{\pm 2}^{(3)}$	$\eta_{\pm 3}^{(3)}$
0	0.1734	0	0	0
10	0.2641	0.0849 ∓ 0.0276i	0.0687 ∓ 0.0499i	0.0458 ∓ 0.0630i
20	0.3548	0.1373 ∓ 0.0998i	0.0424 ∓ 0.1306i	-0.0283 ∓ 0.0871i
30	0.4455	0.1373 ∓ 0.1890i	-0.0424 ∓ 0.1306i	-0.0283 ∓ 0.0092i
40	0.5362	0.0849 ∓ 0.2612i	-0.0687 ∓ 0.0499i	0.0458 ∓ 0.0333i
50	0.6270	0.0000 ∓ 0.2888i	0	0.0000 ∓ 0.0963i
60	0.7177	-0.0849 ∓ 0.2612i	0.0687 ∓ 0.0499i	-0.0458 ∓ 0.0333i
70	0.8084	-0.1373 ∓ 0.1890i	0.0424 ∓ 0.1306i	0.0283 ∓ 0.0092i
80	0.8991	-0.1373 ∓ 0.0998i	-0.0424 ∓ 0.1306i	0.0283 ∓ 0.0871i
90	0.9899	-0.0849 ∓ 0.0276i	-0.0687 ∓ 0.0499i	-0.0458 ∓ 0.0630i
100	1.0806	0	0	0

Note that the Fourier coefficients for η could be always computed to obtain more than 7 coefficients for FF and TH components. But if we need to incorporate more than 7 Fourier coefficients for better synthesis accuracy, we may need to re-derive the coupled-mode equations to accommodate the extra coefficients. But this additional terms will increase the coding complexity, together with increment of computational time and memory usage. Therefore, with consideration of the exchange between the number of Fourier coefficients and synthesis accuracy, we believe that the 7 Fourier coefficients for η synthesis is adequate for academic investigation of third-harmonic generation in the PBG structure.

Appendix C

The matrix of pulse amplitude, which contains amplitude of each pump, signal, and idler pulses in forward- and backward-direction has been shown as following equation:

$$U = \begin{bmatrix} a_{f1} & a_{b1} & a_{f3} & a_{b3} & a_{f4} & a_{b4} \end{bmatrix}^T . \tag{C1}$$

In split-step algorithm, the linear and nonlinear parameters have been defined as linear and nonlinear operators. The linear operator is split into two operators such as propagating and coupling operators and their matrix elements have been shown as following

$$\hat{L} = \begin{bmatrix} -\frac{\partial}{\partial z} + i\bar{\delta}_1 & 0 & 0 & 0 & 0 & 0 \\ 0 & \frac{\partial}{\partial z} + i\bar{\delta}_1 & 0 & 0 & 0 & 0 \\ 0 & 0 & -\frac{\partial}{\partial z} + i\bar{\delta}_3 & 0 & 0 & 0 \\ 0 & 0 & 0 & \frac{\partial}{\partial z} + i\bar{\delta}_3 & 0 & 0 \\ 0 & 0 & 0 & 0 & -\frac{\partial}{\partial z} + i\bar{\delta}_4 & 0 \\ 0 & 0 & 0 & 0 & 0 & \frac{\partial}{\partial z} + i\bar{\delta}_4 \end{bmatrix}, \tag{C2}$$

$$\hat{K} = \begin{bmatrix} 0 & i\bar{\kappa}_{+1}^{(1)} & 0 & 0 & 0 & 0 \\ i\bar{\kappa}_{-1}^{(1)} & 0 & 0 & 0 & 0 & 0 \\ 0 & 0 & 0 & i\bar{\kappa}_{+1}^{(3)} & 0 & 0 \\ 0 & 0 & i\bar{\kappa}_{-1}^{(3)} & 0 & 0 & 0 \\ 0 & 0 & 0 & 0 & 0 & i\bar{\kappa}_{+1}^{(4)} \\ 0 & 0 & 0 & 0 & i\bar{\kappa}_{-1}^{(4)} & 0 \end{bmatrix}. \tag{C3}$$

Finally, the nonlinear operator which includes diagonal and off-diagonal elements could be written in matrix form as propagating and coupling operators as shown in following:

$$\hat{N}=\begin{bmatrix} N_{11} & N_{12} & 0 & 0 & 0 & 0 \\ N_{21} & N_{22} & 0 & 0 & 0 & 0 \\ 0 & 0 & N_{33} & N_{34} & 0 & 0 \\ 0 & 0 & N_{43} & N_{44} & 0 & 0 \\ 0 & 0 & 0 & 0 & N_{55} & N_{56} \\ 0 & 0 & 0 & 0 & N_{65} & N_{66} \end{bmatrix}, \tag{C4}$$

where the diagonal matrix elements are:

$$N_{11}=i\eta_0^{(1)}\left[\left|a_{f1}\right|^2+2\left|a_{b1}\right|^2+2\left|a_{f3}\right|^2+2\left|a_{b3}\right|^2+2\left|a_{f4}\right|^2+2\left|a_{b4}\right|^2+2a_{b3}a_{f4}\frac{a_{f1}^*}{a_{f1}}\right] \tag{C4.1}$$
$$+i\eta_1^{(1)}\left[2a_{b3}a_{f3}^*+2a_{b4}a_{f4}^*\right]+i\eta_{-1}^{(1)}\left[a_{f1}a_{b1}^*+2a_{f3}a_{b3}^*+2a_{f4}a_{b4}^*\right],$$

$$N_{22}=i\eta_0^{(1)}\left[2\left|a_{f1}\right|^2+\left|a_{b1}\right|^2+2\left|a_{f3}\right|^2+2\left|a_{b3}\right|^2+2\left|a_{f4}\right|^2+2\left|a_{b4}\right|^2+2a_{b3}a_{b4}\frac{a_{b1}^*}{a_{b1}}\right] \tag{C4.2}$$
$$+i\eta_{-1}^{(1)}\left[2a_{f3}a_{b3}^*+2a_{f4}a_{b4}^*\right]+i\eta_1^{(1)}\left[a_{b1}a_{f1}^*+2a_{b3}a_{f3}^*+2a_{b4}a_{f4}^*\right],$$

$$N_{33}=i\eta_0^{(3)}\left[2\left|a_{f1}\right|^2+2\left|a_{b1}\right|^2+\left|a_{f3}\right|^2+2\left|a_{b3}\right|^2+2\left|a_{f4}\right|^2+2\left|a_{b4}\right|^2+2a_{f1}^2\frac{a_{f4}^*}{a_{f4}}\right] \tag{C4.3}$$
$$+i\eta_1^{(3)}\left[2a_{b1}a_{f1}^*+2a_{b4}a_{f4}^*\right]+i\eta_{-1}^{(3)}\left[2a_{f1}a_{b1}^*+a_{f3}a_{b3}^*+2a_{f4}a_{b4}^*\right],$$

$$N_{44}=i\eta_0^{(3)}\left[2\left|a_{f1}\right|^2+2\left|a_{b1}\right|^2+2\left|a_{f3}\right|^2+\left|a_{b3}\right|^2+2\left|a_{f4}\right|^2+2\left|a_{b4}\right|^2+2a_{b1}^2\frac{a_{b4}^*}{a_{b4}}\right] \tag{C4.4}$$
$$+i\eta_{-1}^{(3)}\left[2a_{f1}a_{b1}^*+2a_{f4}a_{b4}^*\right]+i\eta_1^{(3)}\left[2a_{b1}a_{f1}^*+a_{b3}a_{f3}^*+2a_{b4}a_{f4}^*\right],$$

$$N_{55}=i\eta_0^{(4)}\left[2\left|a_{f1}\right|^2+2\left|a_{b1}\right|^2+2\left|a_{f3}\right|^2+2\left|a_{b3}\right|^2+\left|a_{f4}\right|^2+2\left|a_{b4}\right|^2+2a_{f1}^2\frac{a_{f3}^*}{a_{f3}}\right] \tag{C4.5}$$
$$+i\eta_1^{(4)}\left[2a_{b1}a_{f1}^*+2a_{b3}a_{f3}^*\right]+i\eta_{-1}^{(4)}\left[2a_{f1}a_{b1}^*+2a_{f3}a_{b3}^*+a_{f4}a_{b4}^*\right],$$

$$N_{66}=i\eta_0^{(4)}\left[2\left|a_{f1}\right|^2+2\left|a_{b1}\right|^2+2\left|a_{f3}\right|^2+2\left|a_{b3}\right|^2+2\left|a_{f4}\right|^2+\left|a_{b4}\right|^2+2a_{b1}^2\frac{a_{b3}^*}{a_{b3}}\right] \tag{C4.6}$$
$$+i\eta_{-1}^{(4)}\left[2a_{f1}a_{b1}^*+2a_{f3}a_{b3}^*\right]+i\eta_1^{(4)}\left[2a_{b1}a_{f1}^*+2a_{b3}a_{f3}^*+a_{b4}a_{f4}^*\right],$$

And off-diagonal matrix elements are:

$$N_{12} = i\eta_1^{(1)}\left[2|a_{f1}|^2 + |a_{b1}|^2 + 2|a_{f3}|^2 + 2|a_{b3}|^2 + 2|a_{f4}|^2 + 2|a_{b4}|^2\right] + i\eta_2^{(1)}\left[a_{b1}a_{f1}^*\right], \quad \text{(C4.7)}$$

$$N_{21} = i\eta_{-1}^{(1)}\left[|a_{f1}|^2 + 2|a_{b1}|^2 + 2|a_{f3}|^2 + 2|a_{b3}|^2 + 2|a_{f4}|^2 + 2|a_{b4}|^2\right] + i\eta_{-2}^{(1)}\left[a_{f1}a_{b1}^*\right], \quad \text{(C4.8)}$$

$$N_{34} = i\eta_1^{(3)}\left[2|a_{f1}|^2 + 2|a_{b1}|^2 + 2|a_{f3}|^2 + |a_{b3}|^2 + 2|a_{f4}|^2 + 2|a_{b4}|^2\right] + i\eta_2^{(3)}\left[a_{b3}a_{f3}^*\right], \quad \text{(C4.9)}$$

$$N_{43} = i\eta_{-1}^{(3)}\left[2|a_{f1}|^2 + 2|a_{b1}|^2 + |a_{f3}|^2 + 2|a_{b3}|^2 + 2|a_{f4}|^2 + 2|a_{b4}|^2\right] + i\eta_{-2}^{(3)}\left[a_{f3}a_{b3}^*\right], \quad \text{(C4.10)}$$

$$N_{56} = i\eta_1^{(4)}\left[2|a_{f1}|^2 + 2|a_{b1}|^2 + 2|a_{f3}|^2 + 2|a_{b3}|^2 + 2|a_{f4}|^2 + |a_{b4}|^2\right] + i\eta_2^{(4)}\left[a_{b4}a_{f4}^*\right], \quad \text{(C4.11)}$$

$$N_{65} = i\eta_{-1}^{(4)}\left[2|a_{f1}|^2 + 2|a_{b1}|^2 + 2|a_{f3}|^2 + 2|a_{b3}|^2 + |a_{f4}|^2 + 2|a_{b4}|^2\right] + i\eta_{-2}^{(4)}\left[a_{f4}a_{b4}^*\right], \quad \text{(C4.12)}$$

Appendix D

The matrix of pulse amplitude, which contains amplitude of each fundamental-frequency and third-harmonic frequency pulses in forward- and backward-direction has been shown as following equation:

$$U = \begin{bmatrix} a_{f1} & a_{b1} & a_{f3} & a_{b3} \end{bmatrix}^T . \tag{D1}$$

In split-step algorithm, the linear and nonlinear parameters have been defined as linear and nonlinear operators. The linear operator is split into two operators such as propagating and coupling operators and their matrix elements have been shown as following

$$\hat{L} = \begin{bmatrix} -\frac{\partial}{\partial z} + i\bar{\delta}_1 & 0 & 0 & 0 \\ 0 & \frac{\partial}{\partial z} + i\bar{\delta}_1 & 0 & 0 \\ 0 & 0 & -\frac{\partial}{\partial z} + i\bar{\delta}_3 & 0 \\ 0 & 0 & 0 & \frac{\partial}{\partial z} + i\bar{\delta}_3 \end{bmatrix}, \tag{D2}$$

$$\hat{K} = \begin{bmatrix} 0 & i\bar{\kappa}_{+1} & 0 & 0 \\ i\bar{\kappa}_{-1} & 0 & 0 & 0 \\ 0 & 0 & 0 & i\bar{\kappa}_{+3} \\ 0 & 0 & i\bar{\kappa}_{-3} & 0 \end{bmatrix}. \tag{D3}$$

Finally, the nonlinear operator which includes diagonal and off-diagonal elements could be written in matrix form as propagating and coupling operators as shown in following:

$$\hat{N} = \begin{bmatrix} N_{11} & N_{12} & 0 & 0 \\ N_{21} & N_{22} & 0 & 0 \\ 0 & 0 & N_{33} & N_{34} \\ 0 & 0 & N_{43} & N_{44} \end{bmatrix}, \tag{D4}$$

where the diagonal matrix elements are:

$$N_{11} = i\eta_0^{(1)}\left[|a_{f1}|^2 + 2|a_{b1}|^2 + 2|a_{f3}|^2 + 2|a_{b3}|^2\right] + i\eta_{-1}^{(1)}\left[a_{f1}a_{b1}^* + \frac{2a_{f1}^*a_{b1}^*a_{f3}}{a_{f1}}\right] + i\eta_{-2}^{(1)}\left[\frac{a_{b1}^{*2}a_{f3}}{a_{f1}}\right] + i\eta_3^{(1)}\left[2a_{f3}^*a_{b3} + \frac{a_{f1}^{*2}a_{b3}}{a_{f1}}\right] + i\eta_{-3}^{(1)}\left[2a_{f3}a_{b3}^*\right], \quad \text{(D5.1)}$$

$$N_{22} = i\eta_0^{(1)}\left[2|a_{f1}|^2 + |a_{b1}|^2 + 2|a_{f3}|^2 + 2|a_{b3}|^2\right] + i\eta_1^{(1)}\left[a_{b1}a_{f1}^* + \frac{2a_{f1}^*a_{b1}^*a_{b3}}{a_{b1}}\right] + i\eta_2^{(1)}\left[\frac{a_{f1}^{*2}a_{b3}}{a_{b1}}\right] + i\eta_{-3}^{(1)}\left[2a_{f1}a_{b3}^* + \frac{a_{b1}^{*2}a_{f3}}{a_{b1}}\right] + i\eta_3^{(1)}\left[2a_{b3}a_{f3}^*\right], \quad \text{(D5.2)}$$

$$N_{33} = i\eta_0^{(3)}\left[\left(2|a_{f1}|^2 + 2|a_{b1}|^2 + |a_{f3}|^2 + 2|a_{b3}|^2\right) + \frac{1}{3}\frac{a_{f1}^3}{a_{f3}}\right] + i\eta_1^{(3)}\left[\frac{a_{f1}^2a_{b1}}{a_{f3}} + 2a_{b1}a_{f1}^*\right] + i\eta_{-1}^{(3)}\left[2a_{f1}a_{b1}^*\right] + i\eta_{-3}^{(3)}\left[a_{f3}a_{b3}^*\right], \quad \text{(D5.3)}$$

$$N_{44} = i\eta_0^{(3)}\left[\left(2|a_{f1}|^2 + 2|a_{b1}|^2 + 2|a_{f3}|^2 + |a_{b3}|^2\right) + \frac{1}{3}\frac{a_{b1}^3}{a_{b3}}\right] + i\eta_{-1}^{(3)}\left[\frac{a_{b1}^2a_{f1}}{a_{b3}} + 2a_{f1}a_{b1}^*\right] + i\eta_1^{(3)}\left[2a_{b1}a_{f1}^*\right] + i\eta_3^{(3)}\left[a_{b3}a_{f3}^*\right]. \quad \text{(D5.4)}$$

And off-diagonal matrix elements are:

$$N_{12} = i\eta_1^{(1)}\left[\left(2|a_{f1}|^2 + |a_{b1}|^2 + 2|a_{f3}|^2 + 2|a_{b3}|^2\right) + \frac{a_{b1}^{*2}a_{b3}}{a_{b1}}\right] + i\eta_2^{(1)}\left[a_{b1}a_{f1}^* + \frac{2a_{f1}^*a_{b1}^*a_{b3}}{a_{b1}}\right], \quad \text{(D5.5)}$$

$$N_{21} = i\eta_{-1}^{(1)}\left[\left(|a_{f1}|^2 + 2|a_{b1}|^2 + 2|a_{f3}|^2 + 2|a_{b3}|^2\right) + \frac{a_{f1}^{*2}a_{f3}}{a_{f1}}\right] + i\eta_{-2}^{(1)}\left[a_{f1}a_{b1}^* + \frac{2a_{f1}^*a_{b1}^*a_{f3}}{a_{f1}}\right], \quad \text{(D5.6)}$$

$$N_{34} = i\eta_2^{(1)}\left[2a_{b1}a_{f1}^*\right] + i\eta_3^{(3)}\left[2|a_{f1}|^2 + 2|a_{b1}|^2 + 2|a_{f3}|^2 + |a_{b3}|^2\right], \quad \text{(D5.7)}$$

$$N_{43} = i\eta_{-2}^{(1)}\left[2a_{f1}a_{b1}^*\right] + i\eta_{-3}^{(3)}\left[2|a_{f1}|^2 + 2|a_{b1}|^2 + |a_{f3}|^2 + 2|a_{b3}|^2\right]. \quad \text{(D5.8)}$$

Appendix E

The split-step Fourier method (SSFM)

The flow chart of SSFM algorithm in its simplest form is shown in Fig. E1.

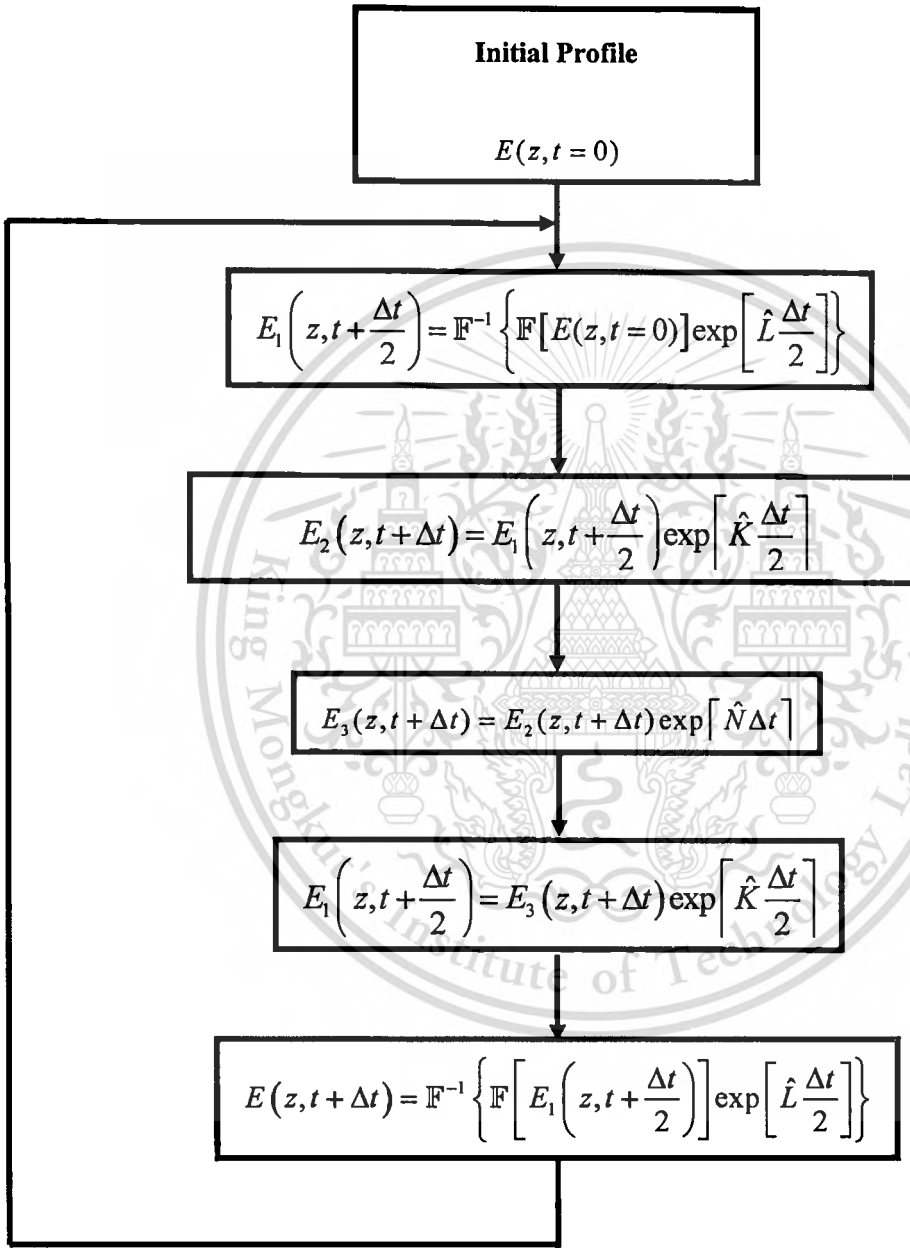

Figure E.1. The flow chart of SSFM algorithm.

Table E1 MATLAB code example for simulating the optical parametric amplification (OPA) in one-dimensional photonic band-gap (1D-PBG) structure

```
tic
clc; clear;
%Input Data
tt = 400;
%Define amplitude, nonlinear coefficient, linear coupling coefficient, and detuning parameter for pump, signal, and idler waves.
%Pump wave
Amp1 = 1.0;
Kappa1 = 0.0421;
Delta1 = 0.1462;
vg1 = 0.4924;
%Signal wave
Amp2 = 0.05;
Kappa2 = 0.0420;
Delta2 = -0.0426;
vg2 = 0.4649;
%Idler wave
Amp3 = 0.0;
Kappa3 = 0.0422;
Delta3 = -0.0364;
vg3 = 0.4655;
%parameters for the strengths of each nonlinear coefficient
Chi3 = 1.0;
gamma0 = 0.2932;
gamma1 = -0.0477 - 0.0333i; gamman1 = -0.0477 + 0.0333i;
gamma2 = -0.0089 - 0.0436i; gamman2 = -0.0089 + 0.0436i;
%Setting total point number, propagation length, step size, total thickness
```

```
n = 4*512;
n2 = n/2;
Z0 = 20*pi;
Z = linspace(-Z0,Z0,n);
dz = Z0/n;
dz2 = dz/2;
D = 200;
L = dz*D;
sigmaz = 1;
%Setting time interval and time increment
dt = 0.1;
dt2 = dt/2.;
TT = dt*tt;
T = linspace(0,TT,n);
%Setting wavenumber vectors
z = 0:1/n:1-1/n;
kz = 2*pi*(0:n-1);
kz = [kz(1:(n/2+1)) -kz(n/2:-1:2)];
Kz = kz/Z0;
%Coupling coefficient matrix
Kappa1 = zeros(1,n); Kappa2 = zeros(1,n); Kappa3 = zeros(1,n);
%Detuning coefficient matrix
delta1 = zeros(1,n); delta2 = zeros(1,n); delta3 = zeros(1,n);
%matrix used in the solution
Ddelta1 = ones(1,n); Ddelta2 = ones(1,n); Ddelta3 = ones(1,n);
%Nonlinearity coefficient matrix
chi3 = zeros(1,n);
for i3 = 1:D
    %Pump wave
```

```
        kappa1(1,n2+i3) = Kappa1;
        delta1(1,n2+i3) = Delta1;
        Ddelta1(1,n2+i3) = exp(1i*delta1(1,n2+i3)*vg1*dt2);
        chi3(1,n2+i3) = Chi3;
        %Signal wave
        kappa2(1,n2+i3) = Kappa2;
        delta2(1,n2+i3) = Delta2;
        Ddelta2(1,n2+i3) = exp(1i*delta_2(1,n2+i3)*vg2*dt2);
        chi3(1,n2+i3) = Chi3;
        %Idler wave
        kappa3(1,n2+i3) = Kappa3;
        delta3(1,n2+i3) = Delta3;
        Ddelta3(1,n2+i3) = exp(1i*delta3(1,n2+i3)*vg3*dt2);
        chi3(1,n2+i3) = Chi3;
end
%Define linear operator
%Pump wave
uaf1 = -1i*vg1*Kz; uab1 = +1i*vg1*Kz;
Uf1 = exp(uaf1*dt2); Ub1 = exp(uab1*dt2);
%Signal wave
uaf2 = -1i*vg2*Kz; uab2 = +1i*vg2*Kz;
Uf2 = exp(uaf2*dt2); Ub2 = exp(uab2*dt2);
%Idler wave
uaf3 = -1i*vg3*Kz; uab3 = +1i*vg3*Kz;
Uf3 = exp(uaf3*dt2); Ub3 = exp(uab3*dt2);
%longitudinal mode
zt = Z0*(z-0.2)/sigmaz;
%Pump wave
Afinit1 = Amp1*exp(-zt.^2); Abinit1 = zeros(1,n);
```

```
Af1 = Afinit1; Ab1 = Abinit1;
Phif1 = angle(Af1); Phib1 = angle(Ab1);
%Signal wave
Afinit2 = Amp2*exp(-zt.^2); Abinit2 = zeros(1,n);
Af2 = Afinit2; Ab2 = Abinit2;
Phif2 = angle(Af2); Phib2 = angle(Ab2);
%Idler wave
Afinit3 = zeros(1,n); Abinit3 = zeros(1,n);
Af3 = Afinit3; Ab3 = Abinit3;
Phif3 = angle(Af3); Phib3 = angle(Ab3);
%Conservation of energy test
E(1) = sum(sum((abs(Af1).^2+abs(Ab1).^2+abs(Af2).^2+abs(Ab2).^2+abs(Af3).^2+abs(Ab3).^2)))*(Z0/n);
%Define Nonlinear Operator
%Pump wave
ck1 = cos(kappa1*vg1*dt2); sk1 = sin(kappa1*vg1*dt2);
Phif1 = angle(Af1); Phib1 = angle(Ab1);
%Signal wave
ck2 = cos(kappa2*vg2*dt2); sk2 = sin(kappa2*vg2*dt2);
Phif2 = angle(Af2); Phib2 = angle(Ab2);
%Idler wave
ck3 = cos(kappa3*vg3*dt2); sk3 = sin(kappa3*vg3*dt2);
Phif3 = angle(Af3); Phib3 = angle(Ab3);
for jj = 1:tt
    %exp(Ldt/2)
    A1f1 = ifft2(Uf1.*fft2(Af1)); A1b1 = ifft2(Ub1.*fft2(Ab1));
    A1f2 = ifft2(Uf2.*fft2(Af2)); A1b2 = ifft2(Ub2.*fft2(Ab2));
    A1f3 = ifft2(Uf3.*fft2(Af3)); A1b3 = ifft2(Ub3.*fft2(3));
    %exp(Kdt/2)
    A2f1 = Ddelta1.*(ck1.*A1f1+1i*sk1.*A1b1); A2b1 = Ddelta1.*(ck1.*A1b1+1i*sk1.*A1f1);
```

```
A2f2 = Ddelta2.*(ck2.*A1f2+1i*sk2.*A1b2); A2b2 = Ddelta2.*(ck2.*A1b2+1i*sk2.*A1f2);
A2f3 = Ddelta3.*(ck3.*A1f3+1i*sk3.*A1b3); A2b3 = Ddelta3.*(ck3.*A1b3+1i*sk3.*A1f3);
%exp(Ndt)
A3f1=A2f1.*exp((1i*(chi3.*(gamma0*(abs(Af1).^2 + 2*abs(Ab1).^2 + 2*abs(Af2).^2 +2*abs(Ab2).^2
+ 2*abs(Af3).^2 + 2*abs(Ab3).^2)) + gamma1*(2*Ab2.*conj(Af2) + 2*Ab3.*conj(Af3))
+ gamman1*(Af1.*conj(Ab1) + 2*Af2.*conj(Ab2) + 2*Af3.*conj(Ab3))))*vg1*dt)
+ (1i*chi3.*(gamma0*(5.5*Af2.*Af3.*conj(Af1))))*vg1*dt
+ A2b1.*((1i*(chi3.*(gamma1*(2*abs(Af1).^2 + abs(Ab1).^2
+ 2*abs(Af2).^2 + 2*abs(Ab2).^2 + 2*abs(Af3).^2 + 2*abs(Ab3).^2))
+ gamma2*((Ab_pp.^2).*conj(Af_pp).*exp(1i*2.*Phif_pp)))))*vg1*dt;
A3b1=A2b1.*exp((1i*(chi3.*(gamma0*(2*abs(Af1).^2 + abs(Ab1).^2 + 2*abs(Af2).^2+2*abs(Ab2).^2
+2*abs(Af3).^2 + 2*abs(Ab3).^2)) + gamman1*(2*Af2.*conj(Ab2) + 2*Af3.*conj(Ab3))
+ gamma1*(Ab1.*conj(Af1) + 2*Ab2.*conj(Af2) + 2*Ab3.*conj(Af3))))*vg1*dt)
+ (1i*chi3.*(gamma0*(5.5*Ab2.*Ab3.*conj(Ab1))))*vg1*dt
+ A2f1.*((1i*(chi3.*(gamman1*(abs(Af1).^2 + 2*abs(Ab1).^2
+ 2*abs(Af1).^2 + 2*abs(Ab2).^2 + 2*abs(Af3).^2 + 2*abs(Ab3).^2))
+ gamman2*((Af1.^2).*conj(Ab1).*exp(-1i*2.*Phib1)))))*vg1*dt;
A3f2=A2f2.*exp((1i*(chi3.*(gamma0*(2*abs(Af1).^2 + 2*abs(Ab1).^2 + abs(Af2).^2 +2*abs(Ab2).^2
+ 2*abs(Af3).^2 + 2*abs(Ab3).^2)) + gamma1*(2*Ab1.*conj(Af1) + 2*Ab3.*conj(Af3))
+ gamman1*(2*Af1.*conj(Ab1) + Af2.*conj(Ab2) + 2*Af3.*conj(Ab3))))*vg2*dt)
+ (1i*chi3.*(gamma0*(2*(Af1.^2).*conj(Af3))))*vg2*dt...
+ A2b2.*((1i*(chi3.*(gamma1*(2*abs(Af1).^2 + 2*abs(Ab1).^2
+ 2*abs(Af2).^2 + abs(Ab2).^2 + 2*abs(Af3).^2 + 2*abs(Ab3).^2))
+ gamma2*((Ab2.^2).*conj(Af2).*exp(-1i*2.*Phif2)))))*vg2*dt;
A3b2=A2b2.*exp((1i*(chi3.*(gamma0*(2*abs(Af1).^2 + 2*abs(Ab1).^2 + 2*abs(Af2).^2
+ abs(Ab2).^2 +2*abs(Af3).^2 + 2*abs(Ab3).^2)) + gamman1*(2*Af1.*conj(Ab1)+2*Af3.*conj(Ab3))
+ gamma1*(2*Ab1.*conj(Af1) + Ab2.*conj(A2f2) + 2*Ab3.*conj(Af3))))*vg2*dt)
+ (1i*chi3.*(gamma0*(2*(Ab1).^2.*conj(Ab3))))*vg2*dt
+ A2f2.*((1i*(chi3.*(gamman1*(2*abs(Af1).^2 + 2.*abs(Ab1).^2
```

```
+ abs(Af2).^2 + 2*abs(Ab2).^2 + 2*abs(Af3).^2 + 2*abs(Ab3).^2))
+ gamman2*((Af2.^2).*conj(Ab2).*exp(-1i*2.*Phib2)))))*vg2*dt;
A3f3=A2f3.*exp((1i*(chi3.*(gamma0*(2*abs(Af1).^2 + 2*abs(Ab1).^2 + 2*abs(Af2).^2
+ 2*abs(Ab2).^2 +abs(Af3).^2 +2*abs(Ab3).^2)) + gamma1*(2*Ab1.*conj(Af1)+2*Ab2.*conj(Af2))
+ gamman1*(2*Af1.*conj(Ab1) + 2*Af2.*conj(Ab2) + Af3.*conj(Ab3))))*vg3*dt)
+ (1i*chi3.*(gamma0*(2*(Af1.^2).*conj(Af2))))*vg3*dt
+ A2b3.*((1i*(chi3.*(gamma1*(2*abs(Af1).^2 + 2*abs(Ab1).^2
+ 2*abs(Af2).^2 + 2*abs(Ab2).^2 + 2*abs(Af3).^2 + abs(Ab3).^2))
+ gamma2*((Ab3.^2).*conj(Af3).*exp(-1i*2.*Phif3)))))*vg3*dt;
A3b3=A2b3.*exp((1i*(chi3.*(gamma0*(2*abs(Af1).^2 + 2*abs(Ab1).^2 +2*abs(Af2).^2
+ 2*abs(Ab2).^2 + 2*abs(Af3).^2 +abs(Ab3).^2)) +gamman1*(2*Af1.*conj(Ab1) +2*Af2.*conj(Ab2))
+ gamma1*(2*Ab1.*conj(Af1) + 2*Ab2.*conj(Af2) + Ab3.*conj(Af3))))*vg3*dt)
+ (1i*chi3.*(gamma0*(2*(Ab1).^2.*conj(Ab2))))*vg3*dt
+ A2f3.*((1i*(chi3.*(gamman1*(2*abs(Af1).^2 + 2.*abs(Ab1).^2
+2*abs(Af2).^2 + 2*abs(Ab2).^2 + abs(Af3).^2 + 2*abs(Ab3).^2))
+ gamman2*((Af3.^2).*conj(Ab3).*exp(-1i*2.*Phib3)))))*vg3*dt;
%exp(Kdt/2)
A1f1 = Ddelta1.*(ck1.*A3f1+1i*sk1.*A3b1); A1b1 = Ddelta1.*(ck1.*A3b1+1i*sk1.*A3f1);
A1f2 = Ddelta2.*(ck2.*A3f2+1i*sk2.*A3b2); A1b2 = Ddelta2.*(ck2.*A3b2+1i*sk2.*A3f2);
A1f3 = Ddelta3.*(ck3.*A3f3+1i*sk3.*A3b3); A1b3 = Ddelta3.*(ck3.*A3b3+1i*sk3.*A3f3);
%exp(Ldt/2)
Af1 = ifft2(Uf1.*fft2(A1f1)); Ab1 = ifft2(Ub1.*fft2(A1b1));
Af2 = ifft2(Uf2.*fft2(A1f2)); Ab2 = ifft2(Ub2.*fft2(A1b2));
Af3 = ifft2(Uf3.*fft2(A1f3)); Ab3 = ifft2(Ub3.*fft2(A1b3));
%updating and capturing fields at the boundaries
Phif1 = angle(Af1); Phib1 = angle(Ab1);
Phif2 = angle(Af2); Phib2 = angle(Ab2);
Phif3 = angle(Af3); Phib3 = angle(Ab3);
```

```
%Register the conservation of the energy (first conservation law)
E(jj+1)=sum(sum((abs(Af1).^2+abs(Ab1).^2+abs(Af2).^2+abs(Ab2).^2+abs(Af3).^2+abs(Ab3).^2)))*(Z0/n);
end
%storing data
If1 = abs(Af1).^2; Ib1 = abs(Ab1).^2;
If2 = abs(Af2).^2; Ib2 = abs(Ab2).^2;
If3 = abs(Af3).^2; Ib3 = abs(Ab3).^2;
toc
```

Table E2 MATLAB code example for simulating the third-harmonic generation (THG) in one-dimensional photonic band-gap (1D-PBG) structure

```
tic
clc; clear;
%Input Data
tt = 400; %total time steps
%Define amplitude, nonlinear coefficient, linear coupling coefficient, and detuning parameter for fundamental
%and third-harmonic waves.
Chi3 = 0.5;
%Fundamental field
Amp1 = 0.1;
Kappa1 = 0.3271;
Delta1 = 0.0046;
vg1 = 0.492;
%Third-harmonic field
Amp3 = 0.0;
Kappa3 = 0.9820;
Delta3 = -0.0117;
vg3 = 0.466;
%parameters for the strengths of each nonlinear coefficient
g10 = 0.209507; g30 = 0.628947;
g11 = 0.0095 - 0.1000i; g31 = 0.0284 - 0.3002i;
g1n1 = 0.0095 + 0.1000i; g3n1 = 0.0284 + 0.3002i;
g12 = -0.0093 - 0.0018i; g32 = -0.0279 - 0.0053i;
g1n2 = -0.0093 + 0.0018i; g3n2 = -0.0279 + 0.0053i;
g13 = 0.0090 - 0.0310i; g33 = 0.0270 - 0.0931i;
g1n3 = 0.0090 + 0.0310i; g3n3 = 0.0270 + 0.0931i;
%Setting number of modes, propagation length, and step size
%total point number
```

```
n = 2048;
n2 = n/2;
Z0 = 20*pi;
Z = linspace(-Z0,Z0,n);
dz = Z0/n;
dz2 = dz/2;
D = 50;
L = dz*D;
%Setting longitudinal pulse width
sigmaz = 1.0;
%Setting time interval and time increment
dt = 0.1;
dt2 = dt/2.;
TT = dt*tt;
T = linspace(0,TT,n);
%Setting wavenumber vectors
z = 0:1/n:1-1/n;
kz = 2*pi*(0:n-1);
kz = [kz(1:(n/2+1)) -kz(n/2:-1:2)];
Kz = kz/Z0;
%Coupling coefficient matrix
kappa1 = zeros(1,n); kappa3 = zeros(1,n);
%Detuning coefficient matrix
delta1 = zeros(1,n); delta3 = zeros(1,n);
Ddelta1 = ones(1,n); Ddelta3 = ones(1,n);
%Nonlinearity coefficient matrix
chi3 = zeros(1,n);
for i3 = 1:D
    %Fundamental field
```

```
    kappa1(1,n2+i3) = Kappa1;
    delta1 (1,n2+i3) = Delta1;
    Ddelta1(1,n2+i3) = exp(1i*delta1(1,n2+i3)*vg1*dt2);
    chi3(1,n2+i3) = Chi3;
    %Third-harmonic field
    kappa3(1,n2+i3) = Kappa3;
    delta3(1,n2+i3) = Delta3;
    Ddelta3(1,n2+i3) = exp(1i*delta3(1,n2+i3)*vg3*dt2);
    chi3(1,n2+i3) = Chi3;
end
%Define linear operator
%FF pulse
uaf1 = -1i*vg1*Kz; uab1 = +1i*vg1*Kz;
Uf1 = exp(uaf1*dt2); Ub1 = exp(uab1*dt2);
%TH pulse
uaf3 = -1i*vg3*Kz; uab3 = +1i*vg3*Kz;
Uf3 = exp(uaf3*dt2); Ub3 = exp(uab3*dt2);
%longitudinal mode
zt = Z0*(z-0.2)/sigmaz;
%Fundamental field
Afinit1 = Amp1*exp(-zt.^2); Abinit1 = zeros(1,n);
Af1 = Afinit1; Ab1 = Abinit1;
Phif1 = angle(Af1); Phib1 = angle(Ab1);
%Third-harmonic field
Afinit3 = zeros(1,n); Abinit3 = zeros(1,n);
Af3 = Afinit3; Ab3 = Abinit3;
Phif3 = angle(Af3); Phib3 = angle(Ab3);
%Conservation of energy test
E(1) = sum(sum((abs(Af1).^2 + abs(Ab1).^2 + abs(Af3).^2 + abs(Ab3).^2)))*(Z0/n);
```

```
%Define Nonlinear Operator
%Fundamental field
ck1 = cos(kappa1*vg1*dt2); sk1 = sin(kappa1*vg1*dt2);
Phif1 = angle(Af1); Phib1 = angle(Ab1);
%Third-harmonic field
ck3 = cos(kappa3*vg3*dt2); sk3 = sin(kappa3*vg3*dt2);
Phif3 = angle(Af3); Phib3 = angle(Ab3);
for jj = 1:tt
    %exp(Ldt/2)
    A1f1 = ifft2(Uf1.*fft2(Af1)); A1b1 = ifft2(Ub1.*fft2(Ab1));
    A1f3 = ifft2(Uf3.*fft2(Af3)); A1b3 = ifft2(Ub3.*fft2(Ab3));
    %exp(Kdt/2)
    A2f1 = Ddelta1.*(ck1.*A1f1+1i*sk1.*A1b1); A2b1 = Ddelta1.*(ck1.*A1b1+1i*sk1.*A1f1);
    A2f3 = Ddelta3.*(ck3.*A1f3+1i*sk3.*A1b3); A2b3 = Ddelta3.*(ck3.*A1b3+1i*sk3.*A1f3);
    %exp(Ndt)
     A3f1 = A2f1.*exp((1i*(chi3.*(3*g10*(abs(Af1).^2 + 2*abs(Ab1).^2 + 2*abs(Af3).^2 + 2*abs(Ab3).^2))
     + 3*g1n1*(Af1.*conj(Ab1)) + 3*g1n3*(2*Af3.*conj(Ab3))))*vg1*dt)
     + ((1i*chi3.*(3*g11*(Ab3.*(conj(Ab1).^2)) + 6*g1n1*(Af3.*conj(Af1).*conj(Ab1))
     + 6*g12*(Ab3.*conj(Af1).*conj(Ab1)) +3*g1n2*(Af3.*(conj(Ab1).^2))
     + 3*g13*(Ab3.*(conj(Af1).^2))))*vg1*dt)
     + A2b1.*(1i*(chi3.*(3*g11*(2*abs(Af1).^2 + abs(Ab1).^2 + 2*abs(Af3).^2 + 2*abs(Ab3).^2))
     + 3*g12*(Ab1.*conj(Af1)) + 3*g13*(2*Ab3.*conj(Af3))))*vg1*dt;
     A3b1 = A2b1.*exp((1i*(chi3.*(3*g10*(2*abs(Af1).^2 + abs(Ab1).^2 + 2*abs(Af3).^2 + 2*abs(Ab3).^2))
     + 3*g11*(Ab1.*conj(Af1)) +3*g13*(2*Ab3.*conj(Af3))))*vg1*dt)
     + ((1i*chi3.*(3*g1n1*(Af3.*(conj(Af1).^2)) + 6*g11*(Ab3.*conj(Af1).*conj(Ab1))
     + 6*g1n2.*(Af3.*conj(Af1).*conj(Ab1))
     + 3*g12.*(Ab3.*(conj(Af1).^2)) + 3*g1n3.*(Af3.*(conj(Ab1).^2))))*vg1*dt)
     + A2f1.*(1i*(chi3.*(3*g1n1*(abs(Af1).^2 + 2*abs(Ab1).^2 + 2*abs(Af3).^2 + 2*abs(Ab3).^2))
     + 3*g12*(Af1.*conj(Ab1)) + 3*g1n3*(2*Af3.*conj(Ab3))))*vg1*dt;
```

```
A3f3 = A2f3.*exp((1i*(chi3.*(3*g30*(2*abs(Af1).^2 + 2*abs(Ab1).^2 + abs(Af3).^2+2*abs(Ab3).^2))
+ 3*g31*(2*Ab1.*conj(Af1)) + 3*g3n1*(2*Af1.*conj(Ab1)) + 3*g32*(2*Ab1.*conj(Af1))
+ 3*g3n3*(Af3.*conj(Ab3))))*vg3*dt) + (1i*chi3.*(g30*((1/3)*(A2f1).^3)))*vg3*dt
+ ((1i*chi3.*(3*g31*((Af1.^2).*Ab1))))*vg3*dt
+ A2b3.*(1i*(chi3.*(3*g33*(2*abs(Af1).^2 + 2*abs(Ab1).^2 + 2*abs(Af3).^2+ abs(Ab3).^2))))*vg3*dt;
A3b3 = A2b3.*exp((1i*(chi3.*(3*g30*(2*abs(Af1).^2 + 2*abs(Ab1).^2 + 2*abs(Af3).^2 + abs(Ab3).^2)
+ 3*g3n1*(2*Af1.*conj(Ab1)) + 3*g31*(2*Ab1.*conj(Af1)) + 3*g3n2*(2*Af1.*conj(Ab1))
+ 3*g33*(Ab3.*conj(Af3)))))*vg3*dt) + (1i*chi3.*(g30*((1/3)*(A2b1).^3)))*vg3*dt
+ ((1i*chi3.*(3*g3n1*((Ab1.^2).*Af1))))*vg3*dt
+ A2f3.*(1i*(chi3.*(3*g3n3*(2*abs(Af1).^2 + 2*abs(Ab1).^2 + abs(Af3).^2 + 2*abs(Ab3).^2))))*vg3*dt;
%exp(Kdt/2)
A1f1 = Ddelta1.*(ck1.*A3f1+1i*sk1.*A3b1); A1b1 = Ddelta1.*(ck1.*A3b1+1i*sk1.*A3f1);
A1f3 = Ddelta3.*(ck3.*A3f3+1i*sk3.*A3b3); A1b3 = Ddelta3.*(ck3.*A3b3+1i*sk3.*A3f3);
%exp(Ldt/2)
Af1 = ifft2(Uf1.*fft2(A1f1)); Ab1 = ifft2(Ub1.*fft2(A1b1));
Af3 = ifft2(Uf3.*fft2(A1f3)); Ab3 = ifft2(Ub3.*fft2(A1b3));
%updating and capturing fields at the boundaries
Phif1 = angle(Af1); Phib1 = angle(Ab1);
Phif3 = angle(Af3); Phib3 = angle(Ab3);
%Register the conservation of the energy (first conservation law)
E(jj+1) = sum(sum((abs(Af1).^2 + abs(Ab1).^2 + abs(Af3).^2 + abs(Ab3).^2)))*(Z0/n);
end
%storing data
If1 = abs(Af1).^2; Ib1 = abs(Ab1).^2;
If3 = abs(Af3).^2; Ib3 = abs(Ab3).^2;
toc
```

Appendix F

Publications in international journals

[1] S. Wicharn, P. Buranasiri, C. Ruttanapun, and P. Jindajitawat, "Optical parametric amplification in one-dimensional photonic bandgap structures," *Appl. Opt.* **52**(25), p. 6090-6099 (2013).

[2] S. Wicharn and P. Buranasiri, "Third-harmonic pulse generation in one-dimensional photonic crystal structures," on process to publish in *J. Nanophotonics* **8**(1), p. 083893-1-083893-18 (2014).

Optical parametric amplification in one-dimensional photonic bandgap structures

Surawut Wicharn, Prathan Buranasiri,* Chesta Ruttanapun, and Phumin Jindajitawat

Physics Department, Faculty of Science, King Mongkut's Institute of Technology Ladkrabang, 1 Chalongkrung 1, Chalongkrung Road, Ladkrabang, Bangkok 10520, Thailand

*Corresponding author: kbpratha@kmitl.ac.th

Received 29 March 2013; revised 1 July 2013; accepted 25 July 2013; posted 31 July 2013 (Doc. ID 188007); published 22 August 2013

In this paper, optical parametric amplification based on the degenerate four-wave mixing principle in a one-dimensional photonic bandgap (PBG) structure has been numerically studied. First, the multiple scale method was introduced to derive a complete set of nonlinear coupled-mode equations for a finite structure with different inhomogeneous nonlinear coefficients than those used in previous works. This finite structure is composed of 680 dielectric layers, which are alternating half-wave/eight-wave films. The wavelengths of the pump, signal, and idler pulses have been determined from the transmission spectrum, which was illustrated by using the transfer matrix method. The parametric interaction of the pump, signal, and idler pulses inside PBG structure has been numerically simulated by using the split-step Fourier transform method. The results of the simulation have shown that the intensities of the signal and idler have exponential growth with respect to the number of layers in the medium. Meanwhile, pump wavevector detuning directly affects the intensities of both pulses due to a band-edge phase-matching condition that might be achieved from only one optimal detuning parameter. Moreover, both the amplification gain and the conversion efficiency of the idler pulse have been shown to be dependent on the bandwidth of the pump pulse spectrum. A very narrow pulse, with a bandwidth much less than the relevant transmission peak, enables the highest amplification and conversion efficiency in this medium because the most efficient phase-matched condition occurs in this situation. Finally, the conversion efficiency grows exponentially with input pump intensity for several input signal intensities. Furthermore, the maximum conversion efficiencies directly vary with input signal intensity. © 2013 Optical Society of America

OCIS codes: (190.4970) Parametric oscillators and amplifiers; (190.4410) Nonlinear optics, parametric processes.

http://dx.doi.org/10.1364/AO.52.006090

1. Introduction

Photonic bandgap (PBG) structures are artificial optical materials whose optical parameters, such as refractive index, linear susceptibility, and nonlinear susceptibility, are periodically modulated within these structures. PBG structures have played an important role in nonlinear optics applications, especially in improving conversion efficiency for harmonic generation and frequency mixing. The improving of conversion efficiency of second-harmonic generation was first theoretically studied by using the phase-matching condition of a two-dimensional PBG structure, which was proposed by Bloembergen and Sievers [1]. Van der Ziel and co-workers experimentally demonstrated the phase-matched condition for second-harmonic generation in this structure [2–4]. To simplify the theoretical analysis and fabrication process, many researchers have studied one-dimensional PBG structures. The nonlinear optical properties in PBG stacks have been widely studied and applied to many photonic devices, such as optical diodes [5], optical limiters [6,7],

1559-128X/13/256090-10$15.00/0

photonic band-edge lasers [8], coherent blue-light generators [9,10], and high-gain optical amplifiers for nonlinear frequency conversion [11]. Almost all applications have been based on resonance properties at the band edge of a PBG, which can be identified by the band-edge maxima in the transmission spectrum, where the high density of photon states confines the field and enhances nonlinear effects in this situation. Many previous works have shown that by using PBG stacks, the conversion efficiency may be improved more than using phase-matched nonlinear bulk or quasi-phase-matched (QPM) crystals [11].

This paper has been organized as follows. In Section 2, multiple-scale expansion with the band-edge phase-matching condition has been applied to derive a complete set of nonlinear coupled-mode equations (NCMEs) that correspond to optical parametric amplification (OPA) based on degenerate four-wave mixing (DFWM), in a finite PBG stack with nonlinear deep gratings. The NCMEs include higher-order nonlinear coefficients in comparison with NCMEs in previous OPA works [12]. In Section 3, a split-step Fourier transform method (SSFM) has been chosen to solve our NCMEs by setting an approximated solution in the symmetrized split-step formalism [13]. In this work, both a depleted pump beam and multiple reflections of counter-propagating beams inside the nonlinear PBG stack are considered. The initial pump and signal pulses are launched into the same side of the medium, as shown in Fig. 1. The pump field wavelength is tuned to the same wavelength at the photonic band edge, and the ensuing interaction leads to a strong desired nonlinear effect. Finally, in Section 4, the signal pulse amplification and idler pulse generation are investigated, and the amplified signal gain and the conversion efficiency of idler generation are explored.

2. Coupled-Mode Equations

In this section, a complete set of coupled-mode equations corresponding to parametric amplification based on DFWM in the third-order nonlinear PBG stack has been derived. The Maxwell equation with third-order nonlinear polarization in this PBG stack is given by

$$\frac{\partial^2 E(z,t)}{\partial z^2} - \frac{\hat{\varepsilon}(z,\omega)}{c^2}\frac{\partial^2 E(z,t)}{\partial t^2} = \frac{4\pi}{c^2}\frac{\partial^2 P_{\mathrm{NL}}(z,t)}{\partial t^2}. \quad (1)$$

The electric field (E), which depends on both longitudinal spatial variable (z) and time (t) is expressed as

$$E = \sum_{j=1}^{3} A_{j\pm} \exp[\pm i(k_j z \mp \omega_j t)] + \text{c.c.}, \quad (2)$$

where the subscripts ($\pm$) denote the forward- and backward-propagating of waves, and the pump, signal, and idler frequency components are represented by numbers 1, 2, and 3, respectively. Meanwhile, $\hat{\varepsilon}(z,\omega)$ is the dielectric function. Here, nonlinear susceptibility has been chosen as an inhomogeneous nonlinearity. Therefore, the nonlinear polarization has been written as:

$$P_{\mathrm{NL}}(z,t) = \mu\chi^{(3)}(z)E^3(z,t). \quad (3)$$

The multiple-scale method (MSM) has been used to derive the desired nonlinear coupled-mode equations, which are correspond to the parametric interaction of the light wave and the PBG stack. This procedure consists of expanding the space and time variables in a power series form. The multiple-scale perturbation variables (μ) have been introduced as $z = \sum_{n=0}^{\infty}\mu^n z_n$ and $t = \sum_{n=0}^{\infty}\mu^n t_n$, where $n = 0,1,2,\ldots$. Now, the second-order derivatives, with respect to these spatial and time variables, are

$$\frac{\partial^2}{\partial z^2} = \frac{\partial^2}{\partial z_0^2} + 2\mu\frac{\partial}{\partial z_0}\frac{\partial}{\partial z_1} + 2\mu^2\frac{\partial}{\partial z_0}\frac{\partial}{\partial z_2} + \cdots, \quad (4a)$$

$$\frac{\partial^2}{\partial t^2} = \frac{\partial^2}{\partial t_0^2} + 2\mu\frac{\partial}{\partial t_0}\frac{\partial}{\partial t_1} + 2\mu^2\frac{\partial}{\partial t_0}\frac{\partial}{\partial t_2} + \cdots. \quad (4b)$$

Similarly, the perturbed total electric field series is given by

$$E = E_0 + \mu E_1 + \mu^2 E_2 + \cdots, \quad (5)$$

where μ is a dimensionless parameter that will be chosen to unity after the perturbation analysis is carried out.

The dielectric function ($\hat{\varepsilon}$) and inhomogeneous third-order nonlinearity ($\chi^{(3)}$) are expanded in the Fourier series form as follows:

$$f(z) = \sum_{l=-\infty}^{\infty} F_l \exp(2\pi i l z/d), \quad (6)$$

where $F_l = (1/d)\int_0^d f(z)\exp(-2\pi i l z/d)\mathrm{d}z$ is represented as Fourier coefficients of $\hat{\varepsilon}$, and $\chi^{(3)}$. The periodic length of the PBG stack is d.

Finally, Eqs. (2)–(5) are substituted into Eq. (1) and group together the higher-order terms that include μ. Then, a new set of wave equations with nonlinear

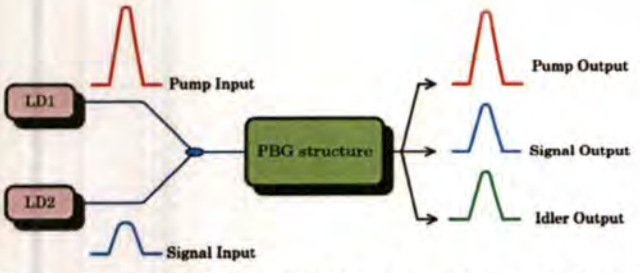

Fig. 1. Schematic of degenerate four-wave mixing with pulsed pump and signal inputs.

source terms is obtained. The nonlinear polarization term with E^3 is expanded and 28 terms are retained for the frequency components corresponding to our calculations. The 28 terms are combined with the Fourier components of the third-order nonlinearity. Finally, the band-edge phase-matching condition, which is written as

$$\frac{d}{\pi}\Delta k + 2\delta^{(1)} = \delta^{(2)} + \delta^{(3)}, \tag{7}$$

where $\Delta k = 2k_1 - k_2 - k_3$ is the wave vector mismatch, and then scaling the length and the field amplitudes as dimensionless variables such that

$$z = \frac{\pi}{d} z_1 \quad \text{and} \quad A_{j\pm} = N_0^{(j)} a_{j\pm} e^{\mp i \frac{\pi}{d}\delta^{(j)} z_1} \tag{8}$$

has been used.

The coupled equation for the forward- and backward-propagating waves of each frequency components is expressed as follows:

$$\begin{aligned}\frac{\partial a_{1+}}{\partial z} + \frac{d}{\pi v_g^{(1)}}\frac{\partial a_{1+}}{\partial t} - i\delta^{(1)} a_{1+} - i\kappa_1^{(1)} a_{1-} &= iN_0^{(1)}[(|a_{1+}|^2 + 2|a_{1-}|^2 + 2|a_{2+}|^2 + 2|a_{2+}|^2 \\ &\quad + 2|a_{3+}|^2 + 2|a_{3-}|^2)a_{1+} + 2a_{2+}a_{3+}a_{1+}^*] \\ &\quad + iN_1^{(1)}[(2|a_{1+}|^2 + |a_{1-}|^2 + 2|a_{2+}|^2 + 2|a_{2-}|^2 \\ &\quad + 2|a_{3+}|^2 + 2|a_{3-}|^2)a_{1-} + (2a_{2-}a_{2+}^* + 2a_{3-}a_{3+}^*)a_{1+}] \\ &\quad + iN_{-1}^{(1)}[a_{1+}a_{1-}^* + 2a_{2+}a_{2-}^* + 2a_{3+}a_{3-}^*]a_{1-} + iN_2^{(1)}[a_{1-}^2 a_{1+}^*],\end{aligned} \tag{9a}$$

$$\begin{aligned}-\frac{\partial a_{1-}}{\partial z} + \frac{d}{\pi v_g^{(1)}}\frac{\partial a_{1-}}{\partial t} - i\delta^{(1)} a_{1-} - i\kappa_{-1}^{(1)} a_{1+} &= iN_0^{(1)}[(2|a_{1+}|^2 + |a_{1-}|^2 + 2|a_{2+}|^2 + 2|a_{2-}|^2 \\ &\quad + 2|a_{3+}|^2 + 2|a_{3-}|^2)a_{1-} + 2a_{2-}a_{3-}a_{1-}^*] \\ &\quad + iN_{-1}^{(1)}[(|a_{1+}|^2 + 2|a_{1-}|^2 + 2|a_{2+}|^2 + 2|a_{2-}|^2 \\ &\quad + 2|a_{3+}|^2 + 2|a_{3-}|^2)a_{1+} + (2a_{2+}a_{2-}^* + 2a_{3+}a_{3-}^*)a_{1-}] \\ &\quad + iN_1^{(1)}[a_{1-}a_{1+}^* + 2a_{2-}a_{2+}^* + 2a_{3-}a_{3+}^*]a_{1-} + iN_{-2}^{(1)}[a_{1+}^2 a_{1-}^*],\end{aligned} \tag{9b}$$

$$\begin{aligned}\frac{\partial a_{2+}}{\partial z} + \frac{d}{\pi v_g^{(2)}}\frac{\partial a_{2+}}{\partial t} - i\delta^{(2)} a_{2+} - i\kappa_1^{(2)} a_{2-} &= iN_0^{(2)}[(2|a_{1+}|^2 + 2|a_{1-}|^2 + |a_{2+}|^2 + 2|a_{2-}|^2 + 2|a_{3+}|^2 \\ &\quad + 2|a_{3-}|^2)a_{2+} + 2a_{1+}^2 a_{3+}^*] \\ &\quad + iN_1^{(2)}[(2|a_{1+}|^2 + 2|a_{1-}|^2 + 2|a_{2+}|^2 + |a_{2-}|^2 + 2|a_{3+}|^2 + 2|a_{3-}|^2)a_{2-} \\ &\quad + (2a_{1-}a_{1+}^* + 2a_{3-}a_{3+}^*)a_{2+}] \\ &\quad + iN_{-1}^{(2)}[2a_{1+}a_{1-}^* + a_{2+}a_{2-}^* + 2a_{3+}a_{3-}^*]a_{2+} + iN_2^{(2)}[a_{2-}^2 a_{2+}^*],\end{aligned} \tag{9c}$$

$$\begin{aligned}-\frac{\partial a_{2-}}{\partial z} + \frac{d}{\pi v_g^{(2)}}\frac{\partial a_{2-}}{\partial t} - i\delta^{(2)} a_{2-} - i\kappa_{-1}^{(2)} a_{2+} &= iN_0^{(2)}[(2|a_{1+}|^2 + 2|a_{1-}|^2 + 2|a_{2+}|^2 + |a_{2-}|^2 + 2|a_{3+}|^2 \\ &\quad + 2|a_{3-}|^2)a_{2-} + 2a_{1-}^2 a_{3-}^*] \\ &\quad + iN_{-1}^{(2)}[(2|a_{1+}|^2 + 2|a_{1-}|^2 + |a_{2+}|^2 + 2|a_{2-}|^2 + 2|a_{3+}|^2 + 2|a_{3-}|^2)a_{2+} \\ &\quad + (2a_{1+}a_{1-}^* + 2a_{3+}a_{3-}^*)a_{2-}] \\ &\quad + iN_1^{(2)}[2a_{1-}a_{1+}^* + a_{2-}a_{2+}^* + 2a_{3-}a_{3+}^*]a_{2-} + iN_{-2}^{(2)}[a_{2+}^2 a_{2-}^*],\end{aligned} \tag{9d}$$

$$\frac{\partial a_{3+}}{\partial z}+\frac{d}{\pi v_g^{(3)}}\frac{\partial a_{3+}}{\partial t}-i\delta^{(3)}a_{3+}-i\kappa_1^{(3)}a_{3-}$$
$$=iN_0^{(3)}[(2|a_{1+}|^2+2|a_{1-}|^2+2|a_{2+}|^2+2|a_{2-}|^2+2|a_{3+}|^2+|a_{3-}|^2)a_{3+}+2a_{1+}^2a_{2+}^*]$$
$$+iN_1^{(3)}[(2|a_{1+}|^2+2|a_{1-}|^2+2|a_{2+}|^2+2|a_{2-}|^2+2|a_{3+}|^2+|a_{3-}|^2)a_{3-}+(2a_{1-}a_{1+}^*+2a_{2-}a_{2+}^*)a_{3+}]$$
$$+iN_{-1}^{(3)}[2a_{1+}a_{1-}^*+2a_{2+}a_{2-}^*+a_{3+}a_{3-}^*]a_{3+}$$
$$+iN_2^{(3)}[a_{3-}^2a_{3+}^*]. \tag{9e}$$

$$-\frac{\partial a_{3-}}{\partial z}+\frac{d}{\pi v_g^{(3)}}\frac{\partial a_{3-}}{\partial t}-i\delta^{(3)}a_{3-}-i\kappa_{-1}^{(3)}a_{3+}$$
$$=iN_0^{(3)}[(2|a_{1+}|^2+2|a_{1-}|^2+2|a_{2+}|^2+2|a_{2-}|^2+2|a_{3+}|^2+|a_{3-}|^2)a_{3-}+2a_{1-}^2a_{2-}^*]$$
$$+iN_{-1}^{(3)}[(2|a_{1+}|^2+2|a_{1-}|^2+2|a_{2+}|^2+2|a_{2-}|^2+|a_{3+}|^2+2|a_{3-}|^2)a_{3+}+(2a_{1+}a_{1-}^*+2a_{2+}a_{2-}^*)a_{3-}]$$
$$+iN_1^{(3)}[2a_{1-}a_{1+}^*+2a_{2-}a_{2+}^*+a_{3-}a_{3+}^*]a_{3-}$$
$$+iN_{-2}^{(3)}[a_{3+}^2a_{3-}^*], \tag{9f}$$

where $v_g^{(j)}=\partial\omega_j/\partial k_j$ is the group velocity, $\delta^{(j)}=[\pi/d-k_j]$ is the wave number detuning from the center of the band gap, $\kappa_{\pm1}^{(j)}=(\omega_j^2/2k_jc^2)\hat{\varepsilon}_{\pm1}(\omega_j)$ is the coupling coefficients, $N_0^{(j)}=(2\pi\omega_j^2/k_jc^2)\chi_0^{(3)}$ is the zeroth-order Fourier coefficient of the cubic nonlinearity function, and $N_{\pm1}^{(j)}=(2\pi\omega_j^2/k_jc^2)\chi_{\pm1}^{(3)}$ and $N_{\pm2}^{(j)}=(2\pi\omega_j^2/k_jc^2)\chi_{\pm2}^{(3)}$ are the first- and second-order Fourier coefficients of the cubic nonlinearity function, respectively. Since this structure has been created by two dielectric components, the nonlinear effect strength depends on the difference between the cubic nonlinearity of two dielectric layers. Meanwhile, the magnitudes of each Fourier coefficient depend on the symmetry of the structured lattice and are based on the beginning value of $\chi^{(3)}$ for any chosen material.

3. Numerical Computations

A. Boundary Conditions

In this section, a numerical method is proposed for solving the NCMEs that were derived in previous section. First, appropriate boundary conditions that correspond to the parametric interaction process have been applied to two ends of the sample stack with length L:

$$E_{f\text{pump}}(0,t)=a_{1+}(0,t),$$
$$E_{f\text{signal}}(0,t)=a_{2+}(0,t),$$
$$E_b(L,t)=0. \tag{10}$$

In this case, the pump and signal pulses have been launched on the left-hand side of sample stack only and all other field amplitudes are zero.

B. Split-Step Fourier Transform Method

Previous works have used the analytical method to find the solutions for parametric interaction for special cases, i.e., no pump depletion or weak grating structures [12,14]. Similarly, the slowly varying envelope in the time approximation had been used to solve the NCMEs for deep grating structures. However, these methods cannot be used to find the general solution. In this research, the SSFM has been chosen to solve the general solutions of Eqs. (9) by using the boundary conditions in Eq. (10). Equations (9) have been rewritten in matrix form as

$$\frac{1}{v_g}\frac{\partial \mathbf{A}}{\partial t}=(\mathbf{D}+\mathbf{K}+\mathbf{N})\mathbf{A}, \tag{11}$$

where $\mathbf{A}$ is a matrix of the amplitudes of interacting waves inside a PBG stack.

To approach the general solution, the approximated solution has been split into two steps, which are the linear and nonlinear solutions, for each time increment (Δt) step. Thus, the general solution of Eq. (11) can be expressed in the symmetrized split-step operator form [13]

$$\mathbf{A}(t+\Delta t)=\exp\left(v_g\frac{\Delta t}{2}\mathbf{D}\right)\exp\left(v_g\frac{\Delta t}{2}\mathbf{K}\right)\times\exp(v_g\Delta t\mathbf{N})\exp\left(v_g\frac{\Delta t}{2}\mathbf{K}\right)\times\exp\left(v_g\frac{\Delta t}{2}\mathbf{D}\right)\mathbf{A}(t). \tag{12}$$

The linear step deals with propagation ($\mathbf{D}$) and coupling ($\mathbf{K}$) operators, which have been used in a computing loop. The $\mathbf{D}$ operator, which contains the spatial derivative, the linear absorption coefficients, and the detuning parameters, has been solved by using the fast Fourier transform (FFT) algorithm. The $\mathbf{K}$ operator contains the coupling coefficients. Meanwhile, the nonlinear solution deals with the $\mathbf{N}$ operator, which can be expressed in a 6×6 matrix form that includes the diagonal and off-diagonal components that are dependent on theamplitude of the field. The nonlinear solution has been handled in real space, but due to the complication of $\mathbf{N}$ operator matrix, an exponential form has been used in the diagonal part and the off-diagonal part of the nonlinear solution, which has been approximated by using a first-order difference form. Therefore, the nonlinear solution has been expressed as a summation of diagonal part and the off-diagonal part solutions as follows [15]:

$$\exp(v_g\Delta t\mathbf{N})\approx\exp(v_g\Delta t\mathbf{N}_d)+v_g\Delta t\mathbf{N}_o. \tag{13}$$

This approximation has given good convergence solutions in most cases. Meanwhile, the incremental

time step has affected the computational accuracy because good accuracy in computing has been obtained from choosing a small step size. Moreover, the accuracy of the computation has been verified by checking the conservation of energy at each time step. For this work, the errors of energy conservation should not exceed 1%. Energy conservation errors begin to occur when the stack is composed of more than approximately 890 dielectric layers. . The elements of amplitude matrix (**A**) and the propagating (**D**), coupling (**K**), and nonlinear (**N**) operators are shown in Appendix A.

4. Simulation Results

The calculation of the amplified signal and the generated idler pulse amplitudes produced during the OPA process in a finite PBG stack is a more complicated problem that requires numerical methods. Our method is based on the SSFM algorithm. This method had been demonstrated to be efficient for analyzing nonlinear optical effects involving short laser pulses in photonic crystals [16]. For our goal of OPA analysis, a SSFM algorithm has been implemented for a medium with third-order nonlinearity. These simulation results show that the maximum efficiency of OPA has been achieved for a PBG stack with a half-wave/eight-wave stack formation, so that the thicknesses of two dielectric layers are $a = \lambda_0/2n_a = 351$ nm and $b = \lambda_0/8n_b = 100$ nm when these optical parameters are assumed to be refractive indices of $n_a = 2.12$ and $n_b = 1.85$ and a reference wavelength of $\lambda_0 = 1.489$ nm. In addition, the third-order nonlinear susceptibilities for each layer are $\chi_a^{(3)} = 3 \times 10^{-19}$ and $\chi_b^{(3)} = 4 \times 10^{-20}$ m^2/V^2.

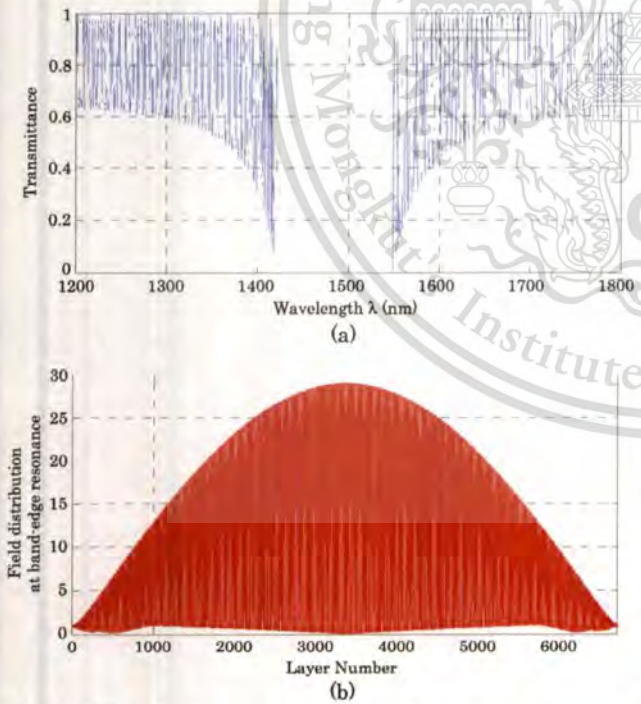

Fig. 2. (a) Transmission spectrum of a PBG stack composed of 680 dielectric layers. (b) Electric field distributions (of $\lambda_1 = 1,550$ nm) inside the PBG stack when band-edge resonance is satisfied.

Then, transmission spectrum of the considered PBG stack has been calculated by using the transfer matrix method (TMM) [17] and the calculated results are illustrated as Fig. 2(a). Furthermore, the wavelength at the edge in the right-hand side of the PBG is especially interesting because maximum resonance occurs at this position, and it is called "band-edge resonance." The local electric field of the band-edge wavelength distribution inside the PBG stack is shown in Fig. 2(b). From previous literature, the density of photon modes was high at the band-edge position [18,19], and then it is possible to enhance the nonlinear effect in the PBG stack [19]. Therefore, in this simulation, the wavelength of the signal field has been continuously tuned to the value around the bandedge (1550 nm) to obtain the idler pulse. Therefore, the signal wavelength is chosen to be 1555 nm and, consequently, the idler wavelength must be 1545 nm.

In our SSFM simulation, the NCMEs have been solved by stepping forward in the time domain. Initial Gaussian pump and signal pulses have been launched into the PBG stack from outside the medium:

$$a_{1+}(z,0) = a_{10}\exp[-(z-L_c)^2/\sigma_1^2],$$
$$a_{2+}(z,0) = a_{20}\exp[-(z-L_c)^2/\sigma_2^2]. \quad (14)$$

The pulse width has been calculated by using the root-mean-square width (σ) formula [17]. Therefore, the bandwidth of the pump and signal pulses is $\sigma_1 = \sigma_2 = 0.16$ μm and the initial position of pulse center (L_c) has been set (from the left-hand side of PBG stack) to be larger than its pulse width, as shown in Fig. 3(a). Therefore, there is no overlap of the leading edge of the pulse on the stack. The dimensionless distance in the z axis spans from -20π to 20π (actual distance is between −3.14 and 3.14 mm). Here, the total time steps in this simulation are 400 and the increment of each step is $\Delta t = 0.1$.

The group velocity of each frequency component (pump, signal, and idler pulses) can be determined by using the TMM [20], similar to the calculations for the transmission spectrum, and their values are determined to be $0.496c$, $0.507c$, and $0.497c$, respectively, where c is light speed in vacuum.

Figure 3 shows a snapshot of signal pulse amplification and idler pulse generation under OPA in a nonlinear PBG stack when structure length L is about 68 μm and the input intensity of the pump wavelength is 4.5 GW/cm^2 and of the signal wavelength is 0.011 GW/cm^2. The rectangular black bar in each figure denotes a nonlinear PBG stack. Each snapshot has been immediately captured, when the total time steps have been 0, 200, or 400, respectively.

The nonlinear interaction of the input pump pulse and the signal pulse inside a PBG stack has created an idler pulse with a different frequency and

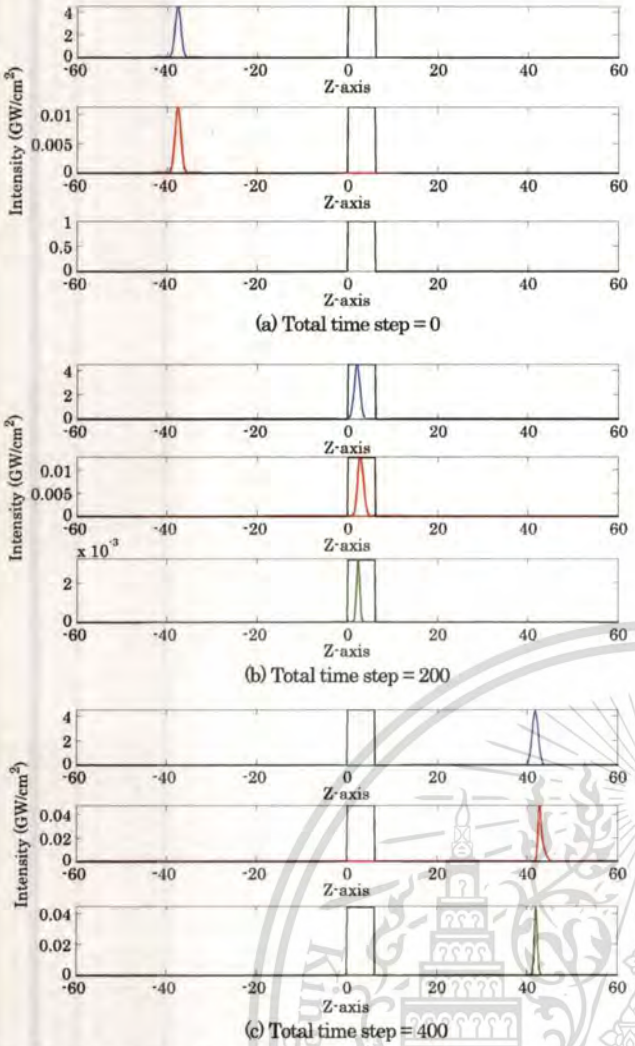

Fig. 3. Snapshot of the OPA process in a nonlinear PBG stack (black bar) where the pump, signal, and idler pulses are represented by the blue (top plot in each set), red (middle), and green (bottom) lines, respectively. In this simulation, we determined that the normalized input pump and signal intensities are 4.500 and 0.011 GW/cm^2, while stack length L is about 154 μm. Figures 3(a)–3(c) are immediately captured when total time are 0, 200, and 400, respectively.

co-propagating with the pump and signal pulses, while the signal pulse has been amplified, corresponding to the OPA effect. In our numerical results, backward-propagating pulses have low intensities such that the intensities of these backward-propagating pulses of pump, signal, and idler are 0.006, 0.0025, and 0.0015 GW/cm^2, respectively, and they are greatly distorted. Therefore, the propagation of backward pulses has not been shown in Fig. 3. For this example, since the group velocity of each frequency component is different, the signal pulse is noticed as the leading pulse because it has the largest group velocity. The slowest pulse is the pump pulse because the wavelength of this pulse was chosen at the band-edge position in Fig. 2(a). Consequently, the effective refractive index, due to this wavelength, of our structure has a large value, and the group velocity has been reduced [20]. Then the slow-light effect has been noticed. However, the wavelengths of the signal and idler components are not at a transmission maximum, so their group velocities are larger than the group velocity of the pump pulse. In addition, the pulses have been simultaneously compressed because of the slow-light effect near the band edge, as previously mentioned.

The amplification of the signal pulse and generation of the idler pulse have been explained by using the OPA theory, since, in the DFWM phenomenon, the energy of the input pump pulse loses energy to the signal and idler beams [21]. Therefore, energy conservation is satisfied. Our computing algorithm has used the energy conservation to check the correction of each computing loop, also. The strength of the OPA effect has been enhanced by increasing the number of pair layers in the stack. Consequently, the magnitudes of both the forward-propagating signal and the idler pulse amplitude are increased, as shown in Fig. 4.

Figure 4 shows that the amplitudes of both the amplified signal and the generated idler pulses have experienced monotonic growth and that, asymptotically, each pulse experiences exponential growth. The signal pulse retains its initial phase and is simply amplified by the nonlinear interaction, whereas the generated idler pulse has a phase that depends on both the pump and signal pulses.

Next, the effect of output intensity of the signal and idler pulses and wave-vector detuning between the wave vector of the pump pulse and the grating wave vector are shown in Fig. 5. The maximum intensity of the amplified signal [Fig. 5(a)] and the generated idler [Fig. 5(b)] pulses are obtained when the optimal wave-vector detuning of the pump pulse ($\delta^{(1)}$) is 0.1462. Both the output signal and the idler intensities were decreased by decreasing or increasing the pump wave-vector detuning, by changing the wavelength of the pump pulse (λ_1) or the periodic length of the structure (d), because this detuning parameter has been linked directly to the band-edge phase-matching condition [as in Eq. (7)].

Here, the signal gain (G_s), which is calculated by using the ratio of forward-propagating output and input signal power, can be expressed as the following [21,22]:

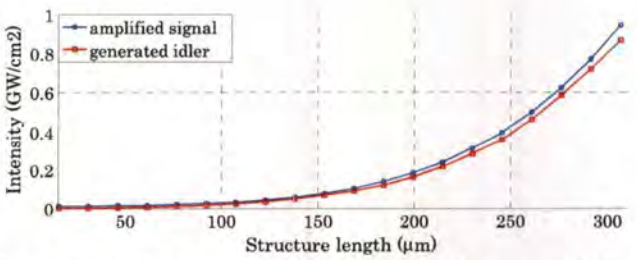

Fig. 4. Amplified signal pulse (blue line) and the generated idler pulse intensities (red line) with respect to structure length.

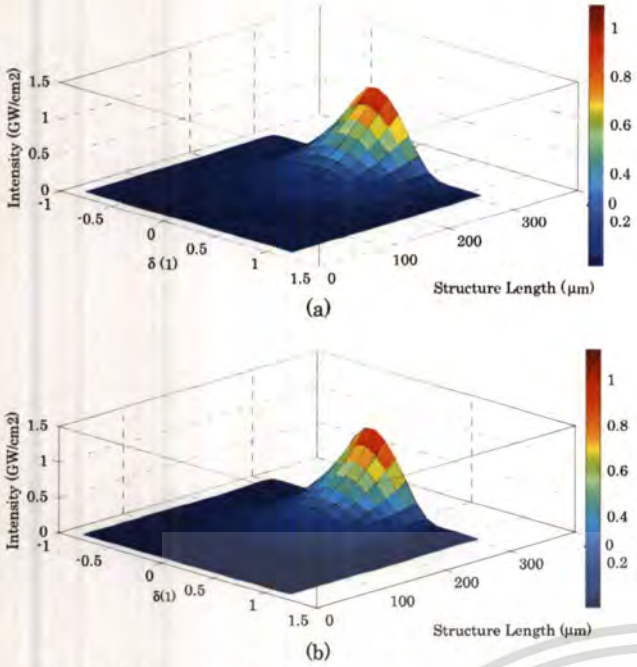

Fig. 5. Output intensities of the (a) signal and (b) idler pulses, which both depend on pump wave-vector detuning and total structure length (L).

$$G_s = \frac{P_{2+}(L)}{P_{2+}(0)} = \frac{|a_{2+}(L)|^2}{|a_{2+}(0)|^2}. \tag{15}$$

The conversion efficiency for idler pulse generation can be determined by the ratio of the generated idler power to the input pump power and can be expressed as the following [21–23]:

$$\eta = \frac{P_{3+}(L)}{P_{1+}(0)} = \frac{|a_{3+}(L)|^2}{|a_{1+}(0)|^2}. \tag{16}$$

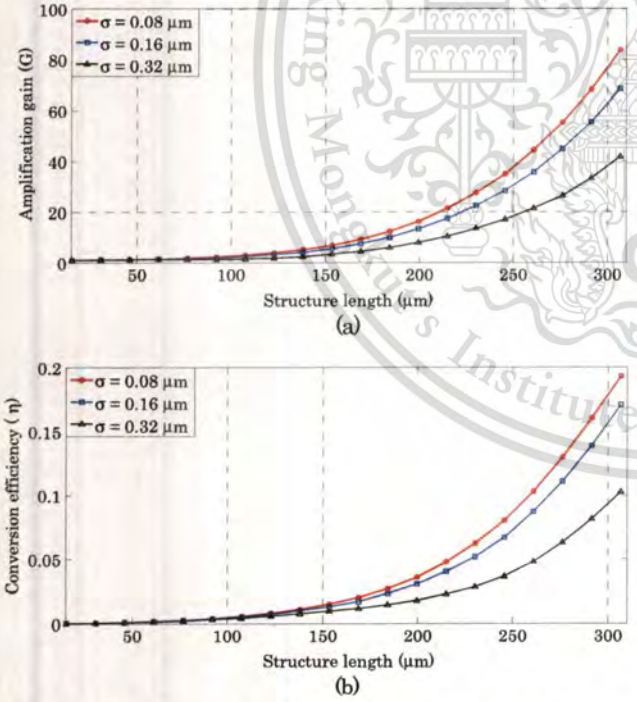

Fig. 6. (a) Amplification gain of the signal pulse when the pulse widths are 0.08 (red line), 0.16 (blue line), and 0.32 (black line) μm, with respect to the number of layer pairs. (b) Conversion efficiency of idler pulse generation when the pulse widths are 0.08 (red line), 0.16 (blue line), and 0.32 (black line) μm with respect to the number of layer pairs.

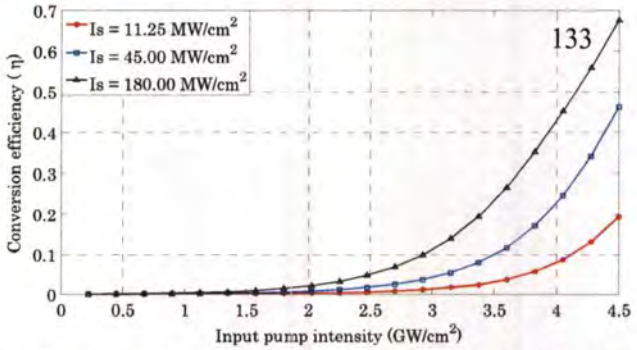

Fig. 7. Conversion efficiency of idler pulse generation for a PBG stack with respect to input pump intensity when input signal intensity is 11.25 (red), 45.00 (blue), and 180.00 (black) MW/cm^2 with medium length of 307 μm.

The signal gain illustration has been shown in Fig. 6(a) when pulse widths of the signal pulse are 0.08, 0.16, and 0.32 μm and the intensities of the input pump and signal pulses are 4.50 and 0.0112 GW/cm^2, respectively. Similarly, conversion efficiency for idler pulse generation can be illustrated as shown in Fig. 6(b) with the same initial conditions.

The relationship between signal gain and conversion efficiency of idler pulse and number of layers (medium length) have been shown in Fig. 6. The signal gain and conversion efficiency have exponential growth with medium length. When the periodic structure lengths are larger than 138 μm, both gain and conversion efficiency for each pulse width has been obviously separated and continued to exponentially increase. The effects of broadening the input pump pulse on both gain and conversion efficiency has been investigated as well. As shown in Fig. 6, both gain and conversion efficiency is reduced when the pulse width of the input pulses is large. In our calculations, the pump pulse width was varied at 0.08, 0.16, and 0.32 μm but the pulse width of the signal pulse was fixed at 0.08 μm. From calculated results, we found that both gain and conversion efficiency fell when the input pump pulse changed from a narrow pulse regime to a broad pulse regime because a narrow pulse could propagate through the PBG stack without noticeable changes in its waveform. Thus, the desired phase matching condition could be achieved in this short pulse regime more than in broad pulse regimes [9].

The conversion efficiency can be enhanced by the intensity of the pump pulse. Figure 7 shows the conversion efficiency for several sets of input pump and signal intensities. From the figure, there are two interesting aspects. First, there is the same threshold input pump intensity for several input signal intensities, which leads to the maximum conversion efficiency. The threshold input pump intensity is

1.62 GW/cm^2 when input signal intensities are 11.25, 45.00, and 180.00 MW/cm^2. Finally, the conversion efficiency is increasing with the input pump intensity and the input signal intensities. The maximum conversion efficiencies in these cases are 19.24%, 46.15%, and 67.52% when the number of layers in the stack is about 680 (307 μm).

5. Conclusions

In this work, the OPA effect in a PBG stack, with third-order nonlinearity under pump depletion and multireflection conditions, has been investigated. First, our PBG stack has been designed by optimizing two types of layer materials and their thicknesses. A half-wave/eighth-wave stack has been found to be an efficient structure to achieve maximum frequency conversion efficiency and transmission spectrum of this stack, as presented in Section 2. Then a complete set of NCMEs in nonlinear deep gratings, which corresponds to the OPA effect, has been derived by using the MSM procedure under the phase-matching condition. After that, the SSFM has been proposed to solve these six NCMEs with appropriate boundary conditions. In our simulation, input Gaussian-shaped pump and signal pulses have been initially launched into only the left-hand side of the PBG stack with input intensities 4.50 GW/cm^2 (pump) and 11.2 MW/cm^2 (signal). The input pump wavelength has been tuned first to the lower band edge of the transmission spectrum to achieve a maximum nonlinear effect, while the input signal wavelength has been tuned near the band edge. Simulation results show that idler pulses can be generated by gaining energy from the input pump and signal fields, while the signal field can be immediately amplified under this nonlinear interaction.

Next the signal gain and conversion efficiency of idler generation were calculated directly and both exponentially increased with the number of layers. The maximum gain of about 83.5 can be achieved when the PBG stack is composed of 680 layers (~307 μm). Furthermore, gain and conversion efficiency have been shown to be dependent on pulse width of the input pump pulse, since the phase-matching condition can be achieved for the short pulse regime more than for the long pulse regime. Finally, the input normalized pump and signal intensities have been found to directly affect to the conversion efficiency. As the calculated results show, threshold intensity for several input signal amplitudes is 1.62 GW/cm^2 and it achieves the maximum efficiency (19.24%, 46.15%, and 67.52%) when the input pump intensity increases to 4.5 GW/cm^2. Finally, the results suggest that the nonlinear PBG stack can possibly be designed to serve as a high gain optical amplifier or an efficient frequency down-converter with compact size, low price, and an uncomplicated fabrication process.

Appendix A

The matrix of the pulse amplitude, which contains the amplitude of the pump, signal, and idler pulses in the forward and backward directions is shown as the following equation:

$$\mathbf{A} = \begin{bmatrix} a_{1+} & a_{1-} & a_{2+} & a_{2-} & a_{3+} & a_{3-} \end{bmatrix}^{\mathrm{T}}. \tag{A1}$$

In the split-step algorithm, the linear and nonlinear parameters have been defined as linear and nonlinear operators. The linear operator is split into two operators, such as the propagating and coupling operators, and their matrix elements are shown as the following:

$$\mathbf{D} = \begin{bmatrix} -\frac{\partial}{\partial z} + i\delta^{(1)} & 0 & 0 & 0 & 0 & 0 \\ 0 & \frac{\partial}{\partial z} + i\delta^{(1)} & 0 & 0 & 0 & 0 \\ 0 & 0 & -\frac{\partial}{\partial z} + i\delta^{(2)} & 0 & 0 & 0 \\ 0 & 0 & 0 & \frac{\partial}{\partial z} + i\delta^{(2)} & 0 & 0 \\ 0 & 0 & 0 & 0 & -\frac{\partial}{\partial z} + i\delta^{(3)} & 0 \\ 0 & 0 & 0 & 0 & 0 & \frac{\partial}{\partial z} + i\delta^{(3)} \end{bmatrix}, \tag{A2}$$

The intensity of signal and idler pulses has exponential growth with an increasing number of layers. Meanwhile, these intensities have been directly affected by pump wave-vector detuning because the band-edge phase-matching condition could be achieved by determining the optimal detuning parameter. From our simulated results, the output intensities would be decreased by increasing and decreasing of the detuning parameter from the optimal value (0.1462).

$$\mathbf{K} = \begin{bmatrix} 0 & i\kappa_{+1}^{(1)} & 0 & 0 & 0 & 0 \\ i\kappa_{-1}^{(1)} & 0 & 0 & 0 & 0 & 0 \\ 0 & 0 & 0 & i\kappa_{+1}^{(2)} & 0 & 0 \\ 0 & 0 & i\kappa_{-1}^{(2)} & 0 & 0 & 0 \\ 0 & 0 & 0 & 0 & 0 & i\kappa_{+1}^{(3)} \\ 0 & 0 & 0 & 0 & i\kappa_{-1}^{(3)} & 0 \end{bmatrix}. \tag{A3}$$

Finally, the nonlinear operator, which includes diagonal and off-diagonal elements, can be written in

matrix form as propagating and coupling operators, as shown in the following:

$$\mathbf{N} = \begin{bmatrix} N_{11} & N_{12} & 0 & 0 & 0 & 0 \\ N_{21} & N_{22} & 0 & 0 & 0 & 0 \\ 0 & 0 & N_{33} & N_{34} & 0 & 0 \\ 0 & 0 & N_{43} & N_{44} & 0 & 0 \\ 0 & 0 & 0 & 0 & N_{55} & N_{56} \\ 0 & 0 & 0 & 0 & N_{65} & N_{66} \end{bmatrix}, \quad \text{(A4)}$$

where the diagonal matrix elements are

$$N_{11} = i\Gamma_0^{(1)}\Big[|a_{1+}|^2 + 2|a_{1-}|^2 + 2|a_{2+}|^2 + 2|a_{2-}|^2 + 2|a_{3+}|^2 + 2|a_{3-}|^2 + 2a_{2-}a_{3+}\frac{a_{1+}^*}{a_{1+}}\Big] + i\Gamma_1^{(1)}[2a_{2-}a_{2+}^* + 2a_{3-}a_{3+}^*] + i\Gamma_{-1}^{(1)}[a_{1+}a_{1-}^* + 2a_{2+}a_{2-}^* + 2a_{3+}a_{3-}^*], \quad \text{(A4.1)}$$

$$N_{22} = i\Gamma_0^{(1)}\Big[2|a_{1+}|^2 + |a_{1-}|^2 + 2|a_{2+}|^2 + 2|a_{2-}|^2 + 2|a_{3+}|^2 + 2|a_{3-}|^2 + 2a_{2-}a_{3-}\frac{a_{1-}^*}{a_{1-}}\Big] + i\Gamma_{-1}^{(1)}[2a_{2+}a_{2-}^* + 2a_{3+}a_{3-}^*] + i\Gamma_1^{(1)}[a_{1-}a_{1+}^* + 2a_{2-}a_{2+}^* + 2a_{3-}a_{3+}^*], \quad \text{(A4.2)}$$

$$N_{33} = i\Gamma_0^{(2)}\Big[2|a_{1+}|^2 + 2|a_{1-}|^2 + |a_{2+}|^2 + 2|a_{2-}|^2 + 2|a_{3+}|^2 + 2|a_{3-}|^2 + 2a_{1+}^2\frac{a_{3+}^*}{a_{3+}}\Big] + i\Gamma_1^{(2)}[2a_{1-}a_{1+}^* + 2a_{3-}a_{3+}^*] + i\Gamma_{-1}^{(2)}[2a_{1+}a_{1-}^* + a_{2+}a_{2-}^* + 2a_{3+}a_{3-}^*], \quad \text{(A4.3)}$$

$$N_{44} = i\Gamma_0^{(2)}\Big[2|a_{1+}|^2 + 2|a_{1-}|^2 + 2|a_{2+}|^2 + |a_{2-}|^2 + 2|a_{3+}|^2 + 2|a_{3-}|^2 + 2a_{1-}^2\frac{a_{3-}^*}{a_{3-}}\Big] + i\Gamma_{-1}^{(2)}[2a_{1+}a_{1-}^* + 2a_{3+}a_{3-}^*] + i\Gamma_1^{(2)}[2a_{1-}a_{1+}^* + a_{2-}a_{2+}^* + 2a_{3-}a_{3+}^*], \quad \text{(A4.4)}$$

$$N_{55} = i\Gamma_0^{(3)}\Big[2|a_{1+}|^2 + 2|a_{1-}|^2 + 2|a_{2+}|^2 + 2|a_{2-}|^2 + |a_{3+}|^2 + 2|a_{3-}|^2 + 2a_{1+}^2\frac{a_{2+}^*}{a_{2+}}\Big] + i\Gamma_1^{(3)}[2a_{1-}a_{1+}^* + 2a_{2-}a_{2+}^*] + i\Gamma_{-1}^{(3)}[2a_{1+}a_{1-}^* + 2a_{2+}a_{2-}^* + a_{3+}a_{3-}^*], \quad \text{(A4.5)}$$

$$N_{66} = i\Gamma_0^{(3)}\Big[2|a_{1+}|^2 + 2|a_{1-}|^2 + 2|a_{2+}|^2 + 2|a_{2-}|^2 + 2|a_{3+}|^2 + |a_{3-}|^2 + 2a_{1-}^2\frac{a_{2-}^*}{a_{2-}}\Big] + i\Gamma_{-1}^{(3)}[2a_{1+}a_{1-}^* + 2a_{2+}a_{2-}^*] + i\Gamma_1^{(3)}[2a_{1-}a_{1+}^* + 2a_{2-}a_{2+}^* + a_{3-}a_{3+}^*]. \quad \text{(A4.6)}$$

The off-diagonal matrix elements are

$$N_{12} = i\Gamma_1^{(1)}[2|a_{1+}|^2 + |a_{1-}|^2 + 2|a_{2+}|^2 + 2|a_{2-}|^2 + 2|a_{3+}|^2 + 2|a_{3-}|^2] + i\Gamma_2^{(1)}[a_{1-}a_{1+}^*], \quad \text{(A4.7)}$$

$$N_{21} = i\Gamma_{-1}^{(1)}[|a_{1+}|^2 + 2|a_{1-}|^2 + 2|a_{2+}|^2 + 2|a_{2-}|^2 + 2|a_{3+}|^2 + 2|a_{3-}|^2] + i\Gamma_{-2}^{(1)}[a_{1+}a_{1-}^*], \quad \text{(A4.8)}$$

$$N_{34} = i\Gamma_1^{(2)}[2|a_{1+}|^2 + 2|a_{1-}|^2 + 2|a_{2+}|^2 + |a_{2-}|^2 + 2|a_{3+}|^2 + 2|a_{3-}|^2] + i\Gamma_2^{(2)}[a_{2-}a_{2+}^*], \quad \text{(A4.9)}$$

$$N_{43} = i\Gamma_{-1}^{(2)}[2|a_{1+}|^2 + 2|a_{1-}|^2 + |a_{2+}|^2 + 2|a_{2-}|^2 + 2|a_{3+}|^2 + 2|a_{3-}|^2] + i\Gamma_{-2}^{(2)}[a_{2+}a_{2-}^*], \quad \text{(A4.10)}$$

$$N_{56} = i\Gamma_1^{(3)}[2|a_{1+}|^2 + 2|a_{1-}|^2 + 2|a_{2+}|^2 + 2|a_{2-}|^2 + 2|a_{3+}|^2 + |a_{3-}|^2] + i\Gamma_2^{(3)}[a_{3-}a_{3+}^*], \quad \text{(A4.11)}$$

$$N_{65} = i\Gamma_{-1}^{(3)}[2|a_{1+}|^2 + 2|a_{1-}|^2 + 2|a_{2+}|^2 + 2|a_{2-}|^2 + |a_{3+}|^2 + 2|a_{3-}|^2] + i\Gamma_{-2}^{(3)}[a_{3+}a_{3-}^*]. \quad \text{(A4.12)}$$

References

1. N. Bloembergen and A. J. Sievers, "Nonlinear optical properties of periodic laminar structures," Appl. Phys. Lett. **17**, 483–485 (1970).
2. J. P. van der Ziel and M. Ilegems, "Optical second harmonic generation in periodic multilayer GaAs-$Al_{0.3}Ga_{0.7}As$ structures," Appl. Phys. Lett. **28**, 437–439 (1976).
3. J. P. van der Ziel and M. Ilegems, "Second harmonic generation in a thin AlAs-GaAs multilayer structure with wave propagation in the plane of the layers," Appl. Phys. Lett. **29**, 200–202 (1976).
4. J. P. van der Ziel, M. Ilegems, P. W. Foy, and R. M. Mikulyak, "Phase-matched second harmonic generation in a periodic GaAs waveguide," Appl. Phys. Lett. **29**, 775–777 (1976).
5. M. Scalora, J. P. Dowling, M. J. Bloemer, and C. M. Bowden, "The photonic band edge optical diode," J. Appl. Phys. **76**, 2023–2026 (1994).
6. M. Scalora, J. P. Dowling, C. M. Bowden, and M. J. Bloemer, "Optical limiting and switching of ultrashort pulses in nonlinear photonic band gap materials," Phys. Rev. Lett. **73**, 1368–1371 (1994).

7. B. Y. Soon, J. W. Haus, M. Scalora, and C. Sibilia, "One-dimensional photonic crystal optical limiter," Opt. Express **11**, 2007–2018 (2003).
8. J. P. Dowling, M. Scalora, M. J. Bloemer, and C. M. Bowden, "The photonic band edge laser: a new approach to gain enhancement," J. Appl. Phys. **75**, 1896–1899 (1994).
9. A. V. Tarasishin, S. A. Magnitskii, and A. M. Zheltikov, "Matching phase and group velocities in second-harmonic generation in finite one-dimensional photonic band-gap structures," Laser Phys. **11**, 31–38 (2001).
10. A. V. Balakin, V. A. Bushuev, B. I. Mantsyzov, I. A. Ozheredov, E. V. Petrov, and A. P. Shkurinov, "Enhancement of sum frequency generation near the photonic band gap edge under quasi phase matching conditions," Phys. Rev. E **63**, 046609 (2001).
11. M. Centini, M. Scalora, C. Sibilia, M. Bertolotti, M. J. Bloemer, C. M. Bowden, and J. W. Haus, "Efficient nonlinear infrared parametric generation on one-dimensional photonic band gap structures," Opt. Commun. **189**, 135–142 (2001).
12. M. J. Steel and C. M. de Sterke, "Continuous-wave parametric amplification in Bragg grating," J. Opt. Soc. Am. B **12**, 2445–2452 (1995).
13. Z. Toroker and M. Horowitz, "Optimized split-step method for modeling nonlinear pulse propagation in fiber Bragg gratings," J. Opt. Soc. Am. B **25**, 448–457 (2008).
14. M. J. Steel and C. M. de Sterke, "Bragg-assisted parametric amplification of short optical pulses," Opt. Lett. **21**, 420–422 (1996).
15. J. W. Haus, B. Y. Soon, M. Scalora, C. Sibilia, and I. V. Mel'nikov, "Coupled-mode equations for Kerr media with periodically modulated linear and nonlinear coefficients," J. Opt. Soc. Am. B **19**, 2282–2291 (2002).
16. M. Scalora and M. E. Crenshaw, "A beam propagation method that handles reflections," Opt. Commun. **108**, 191–196 (1994).
17. M. Weiner, *Ultrafast Optics* (Wiley, 2009).
18. M. Centini, C. Sibilia, M. Scalora, G. D'Aguanno, M. Bertolotti, M. J. Bloemer, C. M. Bowden, and L. Nefedov, "Dispersive properties of finite, one-dimensional photonic band gap structures: applications to nonlinear quadratic interactions," Phys. Rev. E **60**, 4891–4898 (1999).
19. J. W. Haus, P. Powers, P. Bojja, M. Torres-Cisneros, M. Scalora, M. J. Bloemer, N. Akozbek, and M. A. Meneses-Nava, "Enhanced tunable terahertz generation in photonic band-gap structures," Laser Phys. **14**, 1–8 (2004).
20. J. W. Haus, "Photonic band gap structure," in *The Handbook of Nanotechnology: Nanometer Structures—Theory, Modeling, and Simulation*, A. Lakhtakia, ed. (Prentice-Hall, 2004), pp. 45–108.
21. M. E. Marhic, *Fiber Optical Parametric Amplifiers, Oscillators, and Related Devices* (Cambridge University, 2008).
22. G. P. Agrawal, *Nonlinear Fiber Optics*, 2nd ed. (Academic, 1995).
23. Z. Wang, H. Liu, N. Huang, Q. Sun, and J. Wen, "Efficient terahertz-wave generation via four-wave mixing in silicon membrane waveguides," Opt. Express **20**, 8920–8928 (2012).

Journal of
Nanophotonics

DigitalLibrary.org/jnp

Third-harmonic pulse generation in one-dimensional photonic crystal structures

Surawut Wicharn
Prathan Buranasiri

SPIE

Third-harmonic pulse generation in one-dimensional photonic crystal structures

Surawut Wicharn and Prathan Buranasiri
King Mongkut's Institute of Technology Ladkrabang, Faculty of Science, Department of Physics, Chalongkrung 1, Chalongkrung Road, Ladkrabang, Bangkok 10520, Thailand
kbpratha@kmitl.ac.th

Abstract. Enhanced third-harmonic generation in a one-dimensional photonic crystal doped with third-order nonlinear medium was numerically investigated using the multiple-scale method and the split-step Fourier transform. The optimal fundamental frequency for third-harmonic wave generation was determined from the transmission spectrum. The third-harmonic pulse intensities grow, depending on the structure thickness and the fundamental-frequency detuning parameter, which determines the band-edge phase matching condition. Furthermore, the total energy output of third-harmonic pulses, depending on the fundamental-frequency pulse width, may be more than 1000 times the energy produced by a phase-matched bulk medium. A narrow pulse with bandwidth less than the band-edge transmission peak enables high conversion efficiency. The maximum conversion efficiency of the forward component may be 12 to 13 orders of magnitude greater than that of the backward component. © *2014 Society of Photo-Optical Instrumentation Engineers (SPIE)* [DOI: 10.1117/1.JNP.8.083893]

Keywords: photonic crystal; third-harmonic generation; multiple-scale method; split-step Fourier transform; band-edge phase matching.

Paper 13097SS received Sep. 22, 2013; revised manuscript received Dec. 4, 2013; accepted for publication Dec. 23, 2013; published online Jan. 29, 2014.

1 Introduction

Since photonic crystals were introduced more than a quarter century ago, they have played an important role by introducing new concepts to develop optics and photonics applications.[1,2] Especially, the simple one-dimensional photonic crystals (1D-PCs) have been theoretically and experimentally studied in many topics over the past few years as a prototype system that can be extended to describe the same or similar effects in higher-dimensional structures. The 1D-PCs have been used to design a compact device for supporting a large bandwidth. The 1D-PCs consist of periodic dielectric stacks or periodically patterned waveguides that offer simplicity in fabrication over higher-dimensional periodic structures. In addition, the nonlinear effects in these layered structures have been investigated and analyzed to reveal a wide variety of optical phenomena as well. The potential nonlinear device applications, which are based on 1-D nonlinear systems, are optical diodes,[3] optical limiters,[4] coherent blue-light generators,[5] high-gain optical parametric amplifiers,[6] and optical true-time delay line.[7] Improving the efficiency of nonlinear frequency conversion. i.e., frequency up- and down-conversion,[8,9] second-harmonic generation,[10–15] and third-harmonic generation,[16] is a traditional problem of nonlinear optics. The design of 1D-PCs for nonlinear frequency conversion leads to higher conversion efficiency, more compact structures, and lower input power requirements.

The phase matching technique, which is a key factor for nonlinear wave mixing by periodic structures, was first discussed by Armstrong et al.[17] and Bloembergen and Sievers.[18] One of the popular phase-matching techniques for nonlinear optics is quasi-phase matching.[6,17,18,19] The quasi-phase matching in periodic structure would be efficient when the periodic length of the structure is on the order of the coherence length; for this length scale, periodically varying the nonlinear coefficient is important. If the periodic length of the structure is chosen to be on the order of a wavelength, the linear properties of the medium become important and can be

0091-3286/2014/$25.00 © 2014 SPIE

managed to reduce the phase mismatch arising in the nonlinear frequency conversion processes. This phase-matching technique is called "the band-edge phase-matching";[11] it is different from other phase matching techniques, since it depends on structure modifications on the order of the wavelength. In band-edge phase-matching, the fundamental frequency (FF) wavelength is chosen to be near the band-edge of the longest wavelength photonic band-gap of the structure to efficiently promote frequency conversion.

Recently, the enhancement of the third-harmonic generation in 1D-PCs using cascaded nonlinear processes in structures with a second-order nonlinearity or three-wave mixing has been a research area of intense interest. For example, the cascaded process in nonlinear 1D-PC has been based on combining and balancing geometrical and material dispersion;[20] it does not require any complicated material processing, such as poling, e.g., in periodically poled lithium niobate. The cascaded process is also efficient at concurrently achieving second- and third-harmonic generations. In this PC structure, the maximum conversion efficiency of TH waves could be around 40%.

The enhancement of the third-harmonic generation in the 1D-PC with third-order nonlinearity (based on four-wave mixing) has also been explored, but so far no complete study has appeared.[21] So, this paper has been devoted to an analysis of the third-harmonic generation in 1D-PC with high-index contrast and also proposed the different mathematical models by using the perturbation method. By the way, there are no cascaded nonlinearities in this system, since the bulk $\chi^{(2)}$ is zero. Furthermore, it has shown how to enhance the third-harmonic generation conversion efficiency by using the advantage of PC structure geometry, which has been used to solve the phase-matching problem. The basic period length of the 1D-PC is on the order of the fundamental harmonic wavelength. The novelty of this paper is in the derivation of a new set of coupled-mode equations (CMEs) including higher-order nonlinear coefficients for third-harmonic generation. These equations are complete and extend treatments in previous publications on third-harmonic generation in periodic structures.

The multiple-scale method (MSM), a kind of perturbation method, is used as a tool for our investigation. The MSM is adopted for higher-order perturbation problems that have several time and length scales. This would be done by expanding the independent variables in terms of an expansion parameter. These new coordinates are considered independent of each other. Thus, a single problem is simplified by being broken down into several processes, each occurring at a difference scale and each being independently treated. The advantage of this method over other perturbation techniques is its ability to seek a uniform perturbation expansion by using the systematic elimination of secularly growing forcing terms that enter at the higher perturbation orders.[11,22]

The CMEs derived from this method include higher-order nonlinear coefficients, which differ from equations in other TH generation works. The details of the MSM are shown in Sec. 2. In Sec. 3, a split-step Fourier method (SSFM) is chosen to solve our CMEs by setting approximated solution in the split-step operators. The SSFM is based on separating the propagation operator into linear and nonlinear operators. Each operator has a simple solution. In any small section of the medium, the propagation has been calculated for each of the operators separately. The error in the solution of the split-step method is due to the noncommutability of two operators. Moreover, the solution of the nonlinear operator is separated from the linear operator because of its complexity.

In Sec. 4, we investigate the optical properties of the 120-alternating dielectric layers structure with quarter-wave thickness by calculating and analyzing the photonic band gap of our 1D-PC. There are a number of methods that have been used to calculate and analyze the photonic band gap, such as plane-wave expansion method,[23] finite-element method (FEM),[24] finite-difference time-domain method,[25] and transfer-matrix method (TMM).[26,27,28] Among the numerical techniques that have been used so far for analyzing band gap, the finite-difference time domain is perhaps the most accurate, although it suffers from huge computational requirements in both memory and time that limit its range of practical applicability in the design of actual structures.[28] Similarly, the commercial software based on FEM such as a COMSOL is a good option to analyze the band-gap of 1D-PCs.[24] Of course, these techniques require a considerable investment in both time and/or money. A simple, inexpensive, and accurate approach to solve these problems is the TMM algorithms. TMM is used to calculate the transmission and reflection spectrum and to analyze the local field in the 1D-PCs because matrix multiplication is computationally convenient with a personal computer. TMM is robust and could be deployed to investigate optical properties in multilayered thin-film stacks like 1D-PCs.

In Sec. 5, we discussed about the band-edge phase-matching technique, which is an appropriate phase-matching technique and is also widely used for nonlinear frequency conversion in periodic structures.[11] In a PC structure, this technique can adjust the geometry to the material dispersion to eliminate the phase mismatch across the structure.

Finally, in Sec. 6, both pump depletion and multiple reflections of counter-propagating beams inside the 1D-PC structure are explored as well. For our initial condition, the FF pump pulse is outside the 1D-PC and launched toward the left side of the structure. The FF wavelength is tuned to the wavelength at lower band edge of the principle band gap, for achieving band-edge phase-matching and ensuing interaction leads to a strong nonlinear effect. The TH pulse generation in the forward and backward directions is calculated. Furthermore, the total TH energy output is dependent on the FF pulse width, and the TH conversion efficiency is dependent on FF pulse intensity; these quantities have also been calculated.

2 Multiple-Scale Method

A kind of perturbation theory, such as the MSM is used to derive a complete set of CMEs valid for electromagnetic wave propagation in nonlinear periodic medium. First, the CMEs have been derived by considering the 1-D case of nonlinear wave equation for the total field as

$$\frac{\partial^2 E}{\partial z^2} + \mu \nabla_{\perp}^2 E - \frac{1}{c^2}\frac{\partial^2 D_L}{\partial t^2} = \frac{4\pi}{c^2}\frac{\partial^2 P_{\mathrm{NL}}}{\partial t^2}, \tag{1}$$

where $\nabla_{\perp}^2$ is the transverse Laplacian operator, E is the electric field, and in this context, the dimensionless parameter μ is a parameter that multiplies a perturbing contribution and will be set to unity after the end of analysis. D_L is the linear electric displacement, which is related to the electric field by following this relation:

$$D_L(x, y, z, t) = \int_{-\infty}^{t} \varepsilon(x, y, z, t - t')E(x, y, z, t')\mathrm{d}t'. \tag{2}$$

Here, the function $\varepsilon(x, y, z, t)$ is the dielectric function of considering medium and it is periodic in z. Before deriving the coupled equations, the dielectric function could be rewritten in the Fourier transform relation as

$$\varepsilon(x, y, z, t) = \int \hat{\varepsilon}(x, y, z, \omega)e^{-i\omega t}\mathrm{d}\omega. \tag{3}$$

The function $\hat{\varepsilon}(x, y, z, \omega)$ is Fourier transform coefficient of dielectric function and it is complex function, i.e., $\hat{\varepsilon}(\omega) = \hat{\varepsilon}_r(\omega) + i\mu\hat{\varepsilon}_i(\omega)$. Its real and imaginary parts are denoted by the subscripts r and i, respectively. The real part of the dielectric function is of order unity and the imaginary part is considered to be weak. By using the Taylor series, Eq. (2) can be expressed in a local form,

$$D_L(x, y, z, t) = \hat{\varepsilon}\left(x, y, z, i\frac{\partial}{\partial t}\right)E(x, y, z, t), \tag{4}$$

where $i\partial/\partial t = \omega$. The expression in Eq. (4) is very suitable to the MSM given below. Now, the Fourier transform coefficient of dielectric function is considered again, and the first-order expansion of dielectric function of this periodic structure can be expressed in the form

$$\hat{\varepsilon}\left(x, y, z_0, i\frac{\partial}{\partial t}\right) = \hat{\varepsilon}_r\left(i\frac{\partial}{\partial t_0}\right) + i\mu\hat{\varepsilon}_i\left(i\frac{\partial}{\partial t_0}\right) + \mu\hat{\varepsilon}_r'\left(i\frac{\partial}{\partial t_0}\right)i\frac{\partial}{\partial t_1} + \mu \sum_{\substack{\ell = -\infty \\ \ell \neq 0}}^{+\infty} \Delta\hat{\varepsilon}_\ell e^{i\left(\frac{2\pi\ell}{\Lambda}z\right)}. \tag{5}$$

$\Delta\varepsilon_1$ is the amplitude of spatially dielectric modulation. The prime parameter denotes a derivative respect to the frequency. Meanwhile, P_{NL} is the nonlinear polarization, which is a third-order nonlinearity for our case

$$P_{\mathrm{NL}} = \mu\chi^{(3)}E^3. \tag{6}$$

Then, $\chi^{(3)}$ is an inhomogeneous third-order nonlinear susceptibility function, which can control the third-harmonic generation. Similarly, the third-order nonlinear susceptibility for periodic medium can be expanded in Fourier series as

$$\chi^{(3)}(x,y,z,\omega) = \sum_{\ell=-\infty}^{+\infty} \chi_\ell^{(3)} e^{i\left(\frac{2\pi\ell}{\Lambda}z\right)}. \tag{7}$$

Here, Λ is the periodic length of a unit cell of 1D-PC structure.

In the MSM, the space and time coordinates are expanded in a power series of a small parameter that we denote as μ: $z_n = \mu^n z_0$ and $t_n = \mu^n t_0$. In this context, the expansion of our analysis is limited at the first-order perturbation theory. So, the second derivative of space and time is

$$\frac{\partial^2}{\partial z^2} = \frac{\partial^2}{\partial z_0^2} + 2\mu\frac{\partial}{\partial z_0}\frac{\partial}{\partial z_1} + \mu^2\left(2\frac{\partial}{\partial z_0}\frac{\partial}{\partial z_2} + \frac{\partial^2}{\partial z_1^2}\right) + \ldots, \tag{8}$$

$$\frac{\partial^2}{\partial t^2} = \frac{\partial^2}{\partial t_0^2} + 2\mu\frac{\partial}{\partial t_0}\frac{\partial}{\partial t_1} + \mu^2\left(2\frac{\partial}{\partial t_0}\frac{\partial}{\partial t_2} + \frac{\partial^2}{\partial t_1^2}\right) + \ldots. \tag{9}$$

By assuming weak transverse effect for the fast scale ($x = x_0$ and $y = y_0$), an important note is that $\partial^2/\partial x^2$ and $\partial^2/\partial y^2$ have not been expanded. Similarly, the electric field is also expanded in powers of the perturbation parameter as

$$E = E_0 + \mu E_1 + \mu^2 E_2 + \ldots. \tag{10}$$

After that, all of the parameters with first-order expansion have been substituted into Eq. (1). Then, the terms with parameter μ^0 are grouped together. Now, $O(\mu^0)$ term equation is obtained as

$$L_0 E_0 = \left[\frac{\partial^2}{\partial z_0^2} - \frac{1}{c^2}\frac{\partial^2}{\partial t_0^2}\hat{\epsilon}_r\left(i\frac{\partial}{\partial t_0}\right)\right]E_0 = 0. \tag{11}$$

This equation is classical wave equation with no nonlinear source term. The solution of this equation is a plane-wave solution with FF frequency and TH frequency and it is expressed as

$$\begin{aligned} E_0 = {} & (1/\sqrt{k_1})A_{f1}(x,y,z_1,t_1)e^{i(k_1 z_0 - \omega t_0)} + (1/\sqrt{k_1})A_{b1}(x,y,z_1,t_1)e^{-i(k_1 z_0 + \omega t_0)} \\ & + (1/\sqrt{k_3/3})A_{f3}(x,y,z_1,t_1)e^{i(k_3 z_0 - 3\omega t_0)} + (1/\sqrt{k_3/3})A_{b3}(x,y,z_1,t_1)e^{-i(k_3 z_0 + 3\omega t_0)} + \text{c.c.} \end{aligned} \tag{12}$$

where the wave vectors (k_1, k_3) are obtained from the chromatic dispersion properties of bulk medium, so that $k_1^2 = \omega^2\hat{\epsilon}_r(\omega)/c^2$ and $k_3^2 = (3\omega)^2\hat{\epsilon}_r(3\omega)/c^2$. In this analysis, the phase mismatch is also treated as small, $\mu\Delta k = k_3 - 3k_1$. Note that $\mu\Delta k z_0 = \Delta k z_1$. Thus the first-order perturbation, the four-wave process is obtained where cubic nonlinearities dominate. The field amplitudes of both FF and TH fields depend on the slower scale parameter (z_1, t_1) and the rapid variations of the field appear as fundamental waves (A_{f1}, A_{b1}), and third-harmonic waves (A_{f3}, A_{b3}) are treated as order unity functions, which multiply the plane-wave solutions.

Next, the term with μ parameter have been grouped and obtained the $O(\mu)$ term equation as follows:

$$L_0E_1=\left[2\frac{\partial}{\partial z_0}\frac{\partial}{\partial z_1}-\frac{i}{c^2}\hat{\varepsilon}_i\left(i\frac{\partial}{\partial t_0}\right)\frac{\partial^2}{\partial t_0^2}-\frac{2}{c^2}\hat{\varepsilon}_r\left(i\frac{\partial}{\partial t_0}\right)\frac{\partial}{\partial t_0}\frac{\partial}{\partial t_1}-\frac{i}{c^2}\hat{\varepsilon}_r'\left(i\frac{\partial}{\partial t_0}\right)\frac{\partial^2}{\partial t_0^2}\frac{\partial}{\partial t_1}\right.$$
$$\left.-\frac{1}{c^2}\sum_{\substack{\ell=-\infty\\ \ell\neq 0}}^{\ell=+\infty}\Delta\hat{\varepsilon}_\ell\frac{\partial^2}{\partial t_0^2}e^{i\ell\frac{2\pi}{\Lambda}z_0}\right]E_0=\frac{4\pi}{c^2}\frac{\partial^2}{\partial t_0^2}\sum_{\ell=-\infty}^{\ell=+\infty}\chi_\ell^{(3)}e^{i\ell\frac{2\pi}{\Lambda}z_0}E_0^3. \tag{13}$$

The value of Λ have been chosen to the value closed to one-half of FF wavelength. The deviation from this condition is $2\mu\delta=2\pi/\Lambda-2k_1$ and note that $2\mu\delta z_0=2\delta z_1$. Then Eq. (11) is substituted into Eq. (12) to obtain the CMEs for the FF and TH components. The compact set of coupled equations is simplified by scaling the length: $z_1\rightarrow(\pi/\Lambda)z$ and the field amplitudes: $a_{f1}=N_0^{(1)}A_{f1}e^{-i\pi\delta_1 z_1/\Lambda}$, $a_{b1}=N_0^{(1)}A_{b1}e^{-i\pi\delta_1 z_1/\Lambda}$ and $a_{f3}=N_0^{(3)}A_{f3}e^{-i\pi\delta_3 z_1/\Lambda}$, $a_{b3}=N_0^{(3)}A_{b3}e^{-i\pi\delta_3 z_1/\Lambda}$. Here, the detuning parameters are $\delta_1=(\Lambda/\pi)\delta$ and $\delta_3=(\Lambda/\pi)\Delta k-3\delta_1$. The scaled-form of CMEs for the FF components are

$$\frac{\partial a_{f1}}{\partial z}-\frac{i}{F_1}\nabla_\perp^2a_{f1}+\frac{\Lambda}{\pi v_{g1}}\frac{\partial a_{f1}}{\partial t}+\frac{\alpha_1}{2}a_{f1}+i\delta_1a_{f1}-i\kappa_1a_{b1}$$
$$=iN_0^{(1)}[|a_{f1}|^2+2|a_{b1}|^2+2|a_{f3}|^2+2|a_{b3}|^2]a_{f1}+iN_1^{(1)}[(2|a_{f1}|^2+|a_{b1}|^2+2|a_{f3}|^2$$
$$+2|a_{b3}|^2)a_{b1}+a_{b1}^{*2}a_{b3}]+iN_{-1}^{(1)}[a_{f1}^2a_{b1}^*+2a_{f1}^*a_{b1}^*a_{f3}]+iN_2^{(1)}[a_{b1}^2a_{f1}^*+2a_{f1}^*a_{b1}^*a_{b3}]$$
$$+iN_{-2}^{(1)}[a_{b1}^{*2}a_{f3}]+iN_3^{(1)}[2a_{f1}a_{f3}^*a_{b3}+a_{f1}^{*2}a_{b3}]+iN_{-3}^{(1)}[2a_{f1}a_{f3}a_{b3}^*], \tag{14}$$

$$-\frac{\partial a_{b1}}{\partial z}-\frac{i}{F_1}\nabla_\perp^2a_{b1}+\frac{\Lambda}{\pi v_{g1}}\frac{\partial a_{b1}}{\partial t}+\frac{\alpha_1}{2}a_{b1}+i\delta_1a_{b1}-i\kappa_{-1}a_{f1}$$
$$=iN_0^{(1)}[2|a_{f1}|^2+|a_{b1}|^2+2|a_{f3}|^2+2|a_{b3}|^2]a_{b1}+iN_{-1}^{(1)}[(|a_{f1}|^2+2|a_{b1}|^2+2|a_{f3}|^2$$
$$+2|a_{b3}|^2)a_{f1}+a_{f1}^{*2}a_{f3}]+iN_1^{(1)}[a_{b1}^2a_{f1}^*+2a_{f1}^*a_{b1}^*a_{b3}]+iN_{-2}^{(1)}[a_{f1}^2a_{b1}^*+2a_{f1}^*a_{b1}^*a_{f3}]$$
$$+iN_2^{(1)}[a_{f1}^{*2}a_{b3}]+iN_{-3}^{(1)}[2a_{b1}a_{f1}a_{b3}^*+a_{b1}^{*2}a_{f3}]+iN_3^{(1)}[2a_{b1}a_{b3}a_{f3}^*] \tag{15}$$

and the scaled-form of CMEs for the TH components are

$$\frac{\partial a_{f3}}{\partial z}-\frac{i}{F_3}\nabla_\perp^2a_{f3}+\frac{\Lambda}{\pi v_{g3}}\frac{\partial a_{f3}}{\partial t}+\frac{\alpha_3}{2}a_{f3}+i\delta_3a_{f3}-i\kappa_3a_{b3}$$
$$=iN_0^{(3)}\left[(2|a_{f1}|^2+2|a_{b1}|^2+|a_{f3}|^2+2|a_{b3}|^2)a_{f3}+\frac{1}{3}a_{f1}^3\right]+iN_1^{(3)}[a_{f1}^2a_{b1}+2a_{b1}a_{f3}a_{f1}^*]$$
$$+iN_{-1}^{(3)}[2a_{f1}a_{f3}a_{b1}^*]+iN_2^{(3)}[2a_{b1}a_{b3}a_{f1}^*]+iN_3^{(3)}[2|a_{f1}|^2+2|a_{b1}|^2+2|a_{f3}|^2$$
$$+|a_{b3}|^2]a_{b3}+iN_{-3}^{(3)}[a_{f3}^2a_{b3}^*], \tag{16}$$

$$-\frac{\partial a_{b3}}{\partial z}-\frac{i}{F_3}\nabla_\perp^2a_{b3}+\frac{\Lambda}{\pi v_{g3}}\frac{\partial a_{b3}}{\partial t}+\frac{\alpha_3}{2}a_{b3}-i\delta_3a_{b3}-i\kappa_{-3}a_{f3}$$
$$=iN_0^{(3)}\left[(2|a_{f1}|^2+2|a_{b1}|^2+2|a_{f3}|^2+|a_{b3}|^2)a_{b3}+\frac{1}{3}a_{b1}^3\right]+iN_{-1}^{(3)}[a_{b1}^2a_{f1}+2a_{f1}a_{b3}a_{b1}^*]$$
$$+iN_1^{(3)}[2a_{b1}a_{b3}a_{f1}^*]+iN_{-2}^{(3)}[2a_{f1}a_{f3}a_{b1}^*]+iN_{-3}^{(3)}[2|a_{f1}|^2+2|a_{b1}|^2$$
$$+|a_{f3}|^2+2|a_{b3}|^2]a_{f3}+iN_3^{(3)}[a_{b3}^2a_{f3}^*], \tag{17}$$

where the group velocity of the FF and TH components is defined as $v_{g1}=\partial\omega/\partial k_1$ and $v_{g3}=\partial(3\omega)/\partial k_3$, the diffraction parameter of FF and TH components is $F_1=2k_1$ and $F_3=2k_3$, and the normalized absorption for both components is $\alpha_1=(\Lambda/\pi)(\omega^2/k_1c^2)\hat{\varepsilon}_i(\omega)$ and

$\alpha_3 = (\Lambda/\pi)(9\omega^2/k_3c^2)\hat{\varepsilon}_i(3\omega)$. The normalized coupling coefficient of grating for FF and TH frequencies is $\kappa_{\pm 1} = (\Lambda/\pi)\Delta\hat{\varepsilon}\omega^2/(2k_1c^2)$ and $\kappa_{\pm 3} = (\Lambda/\pi)\Delta\hat{\varepsilon}(3\omega)^2/(2k_3c^2)$. Finally, the nonlinear coefficient for each frequency components is $N_\ell^{(1)} = (\Lambda/\pi)6\pi\omega^2\chi_\ell^{(3)}/(k_1^3c^2)$ and $N_\ell^{(3)} = (\Lambda/\pi)6\pi(3\omega)^2\chi_\ell^{(3)}/(k_3^3c^2)$, where ℓ is 0, ± 1, ± 2, and ± 3. In a two component, alternated dielectric formation, the Fourier coefficients of nonlinearity for both frequencies are dependent on the underlying symmetry of the lattice and based on a specific choice of the materials. For instance, the first layer may be the highest dielectric constant material. For this work, the above coupled equations were derived under the assumption that grating dispersion is used to compensate chromatic dispersion.

3 Numerical Calculation for CMEs

In previous publications, the analytical method was used to find solutions for harmonic generation in special cases, i.e., no pump depletion or weak grating structures.[29,30] Similarly, the slowly varying envelope in time approximation has been used to solve the CMEs for strong periodic structure.[6,7] However, these methods cannot be used to find the general solution. In this study, the SSFM has been chosen to solve the general solutions of CMES as shown in Eq. (13) and the absorption terms are neglected.[31] To implement the SSFM for solving the coupled equations, Eq. (13) is presented in the matrix form[22,32] as

$$\frac{1}{v_g}\frac{\partial U}{\partial t} = (\hat{D} + \hat{K} + \hat{N})U, \tag{18}$$

where U is a matrix of amplitudes of FF and TH waves in both forward- and backward-propagating direction. According to Eq. (14), the linear operator consists of the propagating operator ($\hat{D}$) and the operator ($\hat{K}$) coupling forward- and backward waves. These two operators describe the linear propagation of optical pulses in 1D-PC structures. The nonlinear operator ($\hat{N}$) describes the nonlinear interactions between the multiple frequency waves in the structure. To determine the general solution, the approximated solution is split into two steps, which is the linear and nonlinear solutions, for each time increment (Δt) step. Thus, the general solution of Eq. (14) can be expressed in the symmetrized split-step operator form[32] as

$$U(t+\Delta t) = \exp\left(v_g\frac{\Delta t}{2}\hat{D}\right)\exp\left(v_g\frac{\Delta t}{2}\hat{K}\right)\exp(v_g\Delta t\hat{N})\exp\left(v_g\frac{\Delta t}{2}\hat{K}\right)\exp\left(v_g\frac{\Delta t}{2}\hat{D}\right)U(t). \tag{19}$$

The linear step deals with propagating ($\hat{D}$) and coupling ($\hat{K}$) operators, which have been used in the computation loop. The $\hat{D}$ operator, which contains the spatial derivatives and the detuning parameters, has been solved by using a fast Fourier transform algorithm. The $\hat{K}$ operator contains the coupling coefficients. Meanwhile, the nonlinear solution is found using the $\hat{N}$ operator, which is expressed in a 4×4 matrix form including diagonal and off-diagonal components that depend on the fields. The nonlinear solution is handled in real space. But due to the complexity of the $\hat{N}$ operator matrix, an exponential form has been used in the diagonal part, and meanwhile the off-diagonal part has been approximated by using a first-order difference form. Therefore, the nonlinear solution has been expressed in summation of diagonal part and off-diagonal part solutions[22] as follows:

$$\exp(v_g\Delta t\hat{N}) \approx \exp(v_g\Delta t\hat{N}_d) + v_g\Delta t\hat{N}_{\text{od}}. \tag{20}$$

This approximation gives a good convergent solution in most of the cases. Meanwhile, the incremental time step determines the computational accuracy because a good accuracy in computing is obtained from choosing a sufficiently small step size. Moreover, the accuracy of the computation has been verified by checking the conservation of energy at each time step. For this study, the errors of the energy conservation did not exceed 1%. The matrix elements of amplitude

matrix (U), propagating ($\hat{D}$), coupling ($\hat{K}$), and nonlinear ($\hat{N}$) operators are presented in the Appendix.

4 Model

In our model, we consider the following simple 1D-PC. The structure is composed of 120 dielectric layers (total structure length is about 22 μm for a reference wavelength of 1480 nm), which are alternating quarter-wave stacks, and the refractive index alternates between a high and a low value, $n_a = 2.12$ and $n_b = 1.85$. In addition, the third-order nonlinear susceptibility for each layer is $\chi_a^{(3)} = 3 \times 10^{-19}$ and $\chi_b^{(3)} = 4 \times 10^{-20}$ m^2/V^2. Then, for a reference wavelength λ_0, thickness of high-index and low-index layers is $a = \lambda_0/4n_a = 175$ nm and $b = \lambda_0/4n_b = 200$ nm, respectively. A transmission spectrum of this crystal is shown in Fig. 1, where we plot this spectrum by using TMM.[26,27] This figure suggests that this choice of material parameters causes the position of the second-order band-gap to be removed from the first-order band-gap by a factor of 3.

In this case, we tune the FF wavelength to the first long-wavelength band-edge transmission peak to avoid taking material dispersion into account. The forward and backward TH generation can occur and their wavelengths have been found well away from the second long-wavelength band-edge as indicated in Fig. 1. So, the wavelength of FF and TH signals is 1550 and 517 nm, respectively. The FF wavelength should not be chosen in photonic band-gap region because the PC structure would not allow the wavelength in this region propagating through the structure. This is a basic important property of PC structure. In this case, it is impossible to build the nonlinear effect like TH generation in the PC structure since all of the energy of FF wavelength is reflected at the band-gap and does not penetrate into the structure. Furthermore, the structure group index can be defined from the transmission spectrum in Fig. 1 as $n_g = cdk/d\omega$[12,26] and can be depended on the index contrast and the number of periods. In this calculation, the group indices of FF (1550 nm) and TH (517 nm) components are 2.152 and 1.933, respectively. In addition, we are dealing with the pulse propagation through the 1D-PC, so the spectral bandwidth of femtosecond pump or FF pulse should be narrower than the bandwidth of the first transmission resonance (10 nm) where the FF wavelength is tuned.[12] So, the pulse width that corresponds to the bandwidth of the band-edge resonance peak (10 nm) is 800 fs. The condition that the bandwidth of pulse equal to bandwidth of band-edge resonance peak can be called "quasi-monochromatic."[10] In this case, the pulse dispersion in the structure can be avoided and also good nonlinear frequency conversion is obtained.

In Fig. 1, the calculations demonstrate that the band structure, transmission spectrum, and other physical quantities are strongly influenced by the number of periods, layer thickness, and material dispersion.[27] For example, increasing (or decreasing) the number of layers sharpens

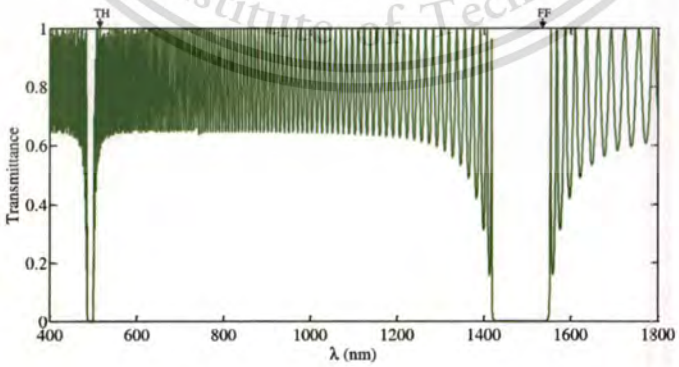

Fig. 1 Transmission spectrum for a 60-period quarter-wave stack. The indices are $n_a = 2.12$ and $n_b = 1.85$, and no dispersion is assumed. Tuning the FF at the first-lower band-edge causes the TH signal to be tuned away from the second-lower band-edge. The spectrum bandwidth of a femtosecond pump pulse is narrower than the long-wavelength band-edge peak bandwidth of principle band-gap where the pump is tuned.

the band edges and increases (or decreases) the number of transmission resonances between gaps, causing an effective shift of each resonance. Changing the thickness of dielectric layer from the quarter-wave or half-wave formations causes wavelength shifts in the position of the band gaps and transmission resonances. When this shifting of band gaps is coupled with material dispersion, a structure with the optimal properties may be realized.

In Fig. 2(a), we plot the FF field intensity ($|E|^2$), which is defined by the ratio of the field amplitude in the last layer and the incident filed amplitude, inside the structure, at the instant peak of 800-fs pulse width at a wavelength of 1550 nm reaches to the structure. This intensity is enhanced compared to its peak value outside the structure. Figure 2(b), on the other hand, represents the TH field intensity quasi-standing wave pattern at the same time as Fig. 2(a) with three peaks. The three peaks overlap to a large extent inside the high-index layers, and the fields can propagate in this configuration for the duration of the pump pulse. This mode overlap, combined with the group velocity reduction for the three fields, allows efficient energy exchange between the FF and TH signals. Moreover, the field intensity can be enhanced by increasing the number of periods (N) due to the field intensity; it is asymptotically proportional to N_2. Thus, the nonlinear effect is enhanced with respect to structure length.[26]

5 Band-Edge Phase-Matching

To approach the efficient TH generation, a phase-matching condition should be satisfied. An advantage of the periodic structure is its ease of satisfying the phase-matching condition by applying combinations of effective linear optical parameters that differ from the parameters of each bulk material. The enhancement of harmonic generation is obtained by carefully choosing these two parameters (δ, κ). The coupling coefficient (κ) can improve the energy coupling between forward- and backward-propagating waves that occur in periodic structure. Meanwhile, the detuning parameters (δ_1, δ_3) play an important role in satisfying phase-matching condition in periodic structure. In nonlinear bulk medium, the phase-matching condition could be obtained when phase-mismatch $\Delta k = 0$ but this situation is very difficult to obtain, especially for the third-harmonic wave. Thus, the periodic structure can compensate the nonzero phase mismatch by choosing an optimum value of δ_1 and then getting the maximum intensity of TH waves. The relationship between δ_1 and δ_3 is shown as

$$\delta_3 = \frac{\Lambda}{\pi}\Delta k - 3\delta_1 = 0. \tag{21}$$

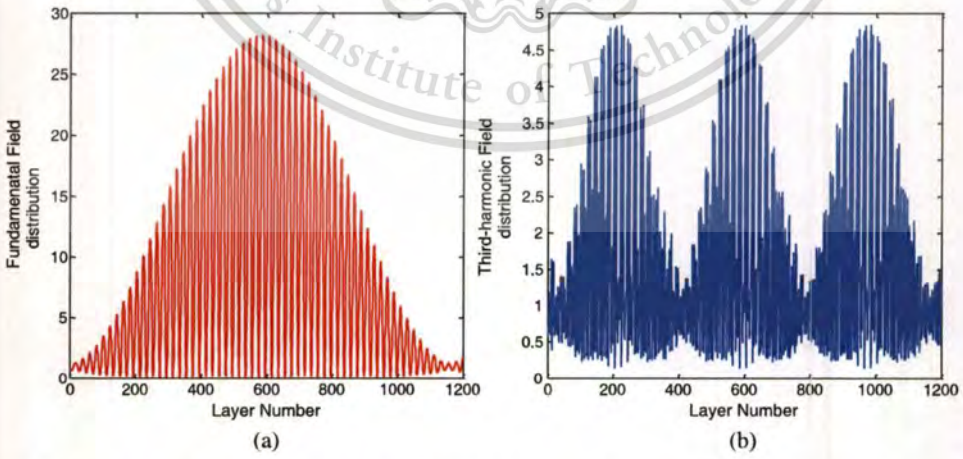

Fig. 2 (a) The fundamental field distribution inside the structure which has wavelength at the first lower band-edge position (1550 nm). (b) The third-harmonic (TH) field distribution inside the structure with three maxima inside, in contrast to the fundamental field single peak, is due to the fact that the wavelength of TH signal is 1/3 time to the fundamental signal wavelength.

The phase matching is obtained by choosing δ_1 to offset nonzero phase-mismatch Δk arising from nonlinear wave mixing. Finally, δ_3 has been found approaching zero and this condition is called band-edge phase-matching because the optimal detuning parameters can be obtained from wavelength at the band-edge of the photonic band-gap. The alternate form of phase matching can be changed to

$$n(3\omega) - n(\omega) = \frac{\pi c}{\omega \Lambda}\delta_1, \tag{22}$$

where $n(\omega)$ and $n(3\omega)$ are effective refractive indices of the 1D-PC structure at the fundamental-frequency and the third-harmonic frequency, respectively.

6 Numerical Results and Discussion

In this section, the CMEs are solved by applying the numerical method which is described in Sec. 3. The fields are stepped forward in time to solve the equations of pulse motion. The longitudinal or transverse dimensions of the pulse are either considered in the model. Here, the boundary conditions at the opposite ends of our 1D-PC are

$$\begin{aligned} a_{f1}(x, y, z = 0, t) &= F(x, y, t), \quad a_{b1}(x, y, z = L, t) = 0, \\ a_{f3}(x, y, z = 0, t) &= a_{b3}(x, y, z = L, t) = 0. \end{aligned} \tag{23}$$

In this condition, the initial pulses incident on both ends of the 1D-PC should not be considered. The function $F(x, y, t)$ is the input FF pulse applied to our medium. An initial FF pulse with Gaussian shape is launched toward the 1D-PC structure from outside the medium as

$$F(x, y, z, 0) = a_0 \exp[-(z - L_c)^2/\sigma_z^2] \exp[-x^2/\sigma_x^2], \tag{24}$$

where L_c is the initial position of FF pulse in longitudinal direction, which is sufficiently far from the medium and the tail of the initial pulse is not appreciable inside our medium. The normalized longitudinal width (σ_z) of FF pulse is about 1.00 and the normalized transverse width (σ_x) is also about $\pi/4$.

Figure 3 shows that the initial FF 800-fs-pulse with Gaussian shape is located outside the 1D-PC, corresponding to the boundary and the initial conditions in Eqs. (19) and (20). In the figure, the 1D-PC structure is represented by the light-blue stripe that located near the origin and the scaled structure length is about 4.7 (actual length is about 22 μm). The initial FF pump pulse is

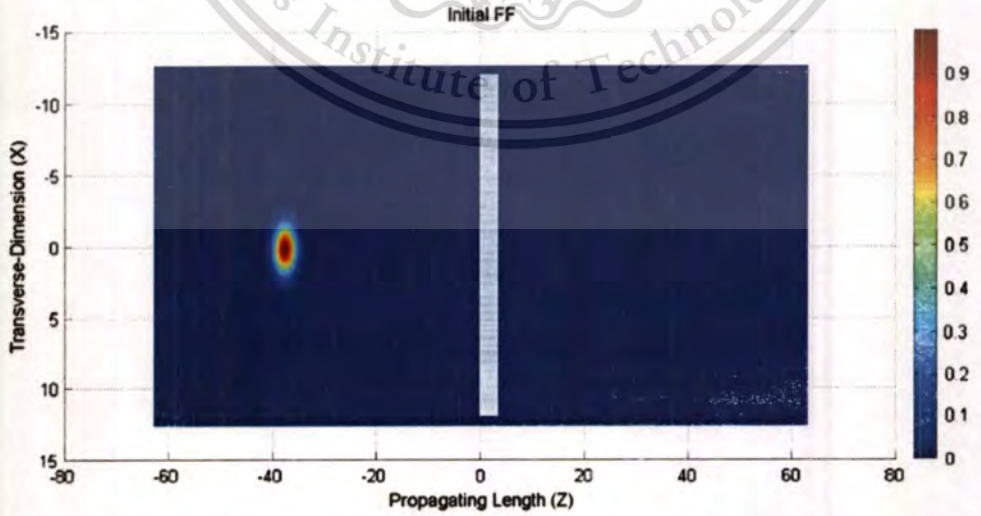

Fig. 3 The initial FF pulse with Gaussian-shape (incident pump pulse) is set following the boundary and the initial conditions as mentioned in Eqs. (19) and (20).

incident from the left as shown in Fig. 3, note that the structure scatters output FF pulses and emits TH pulses significantly in both directions, as shown in Figs. 4(a), 4(b), 5(a) and 5(b), respectively. The intensity of FF pulse in the forward-direction is decreased after passing through the structure because of energy transferring between the frequency components and conversion to reflected energy. The backward FF pulse is generated from the multireflection inside multi-layered structure as our 1D-PC and its intensity is much lower than the forward FF pulse due to the choice of transmission maximum for the central FF wavelength which results in a low forward–backward conversion efficiency. Figure 5 shows the TH pulses at a time snapshot after the FF pulse has propagated through the 1D-PC. Meanwhile, the TH pulses are generated since energy transfer from FF pulse to TH pulses.

Since the 1D-PC in this work consists of dielectric layers with a third-order nonlinearity, which has an optical constant that characterizes the strength of the optical nonlinearity. This optical constant is also responsible for an intensity-independent nonlinear refractive index, e.g., self-phase modulation or self-focusing effect. The nonlinear index can also directly be applied to convert FF pulse energy to TH pulse energy in the model. It varies from material to material and therefore is expanded in a Fourier series expansion form in the CMEs. The

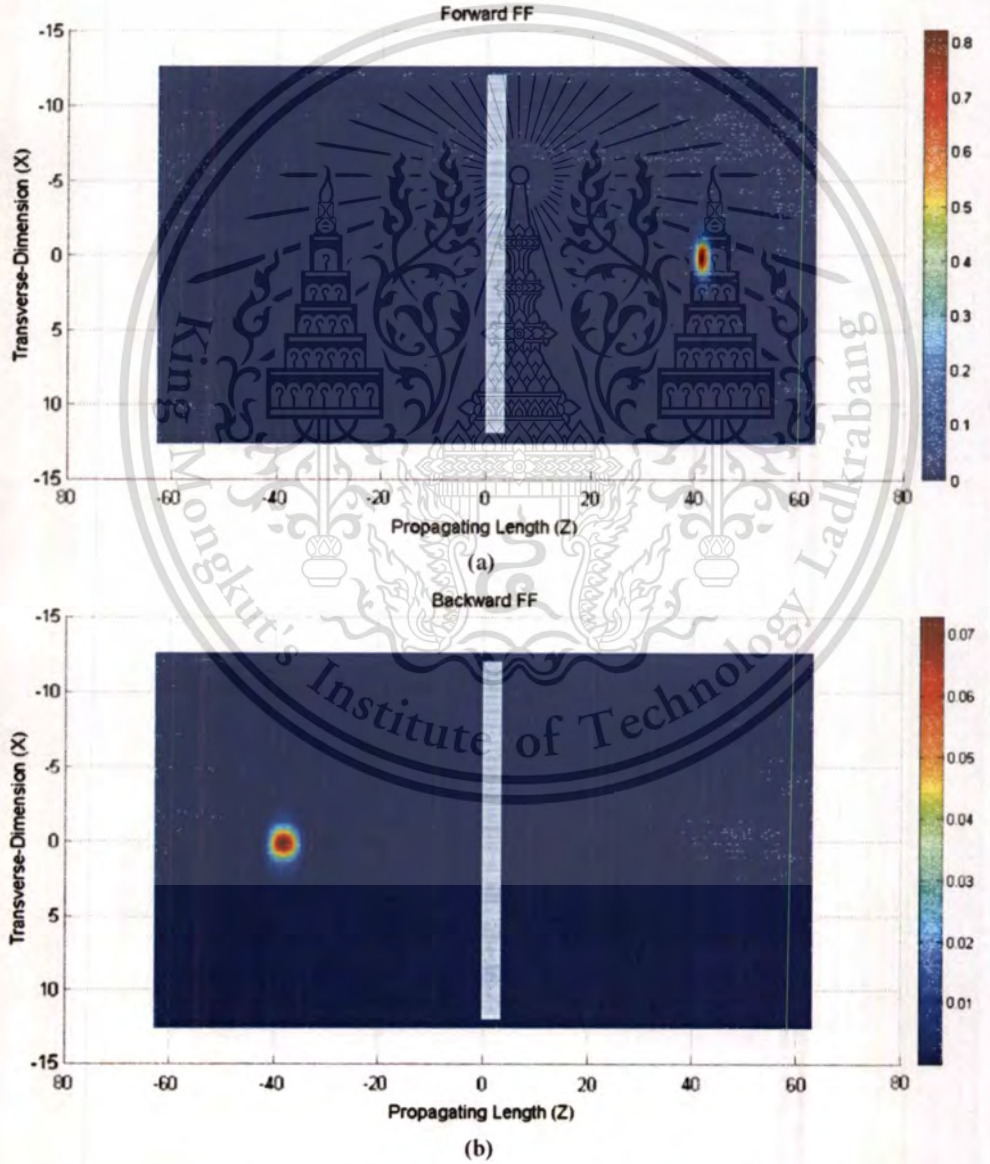

Fig. 4 (a) The scattered forward and (b) backward FF pulses propagate out from the 1D-PC. The amplitudes have been normalized with nonlinear coefficient and amplitude of the initial FF pulse.

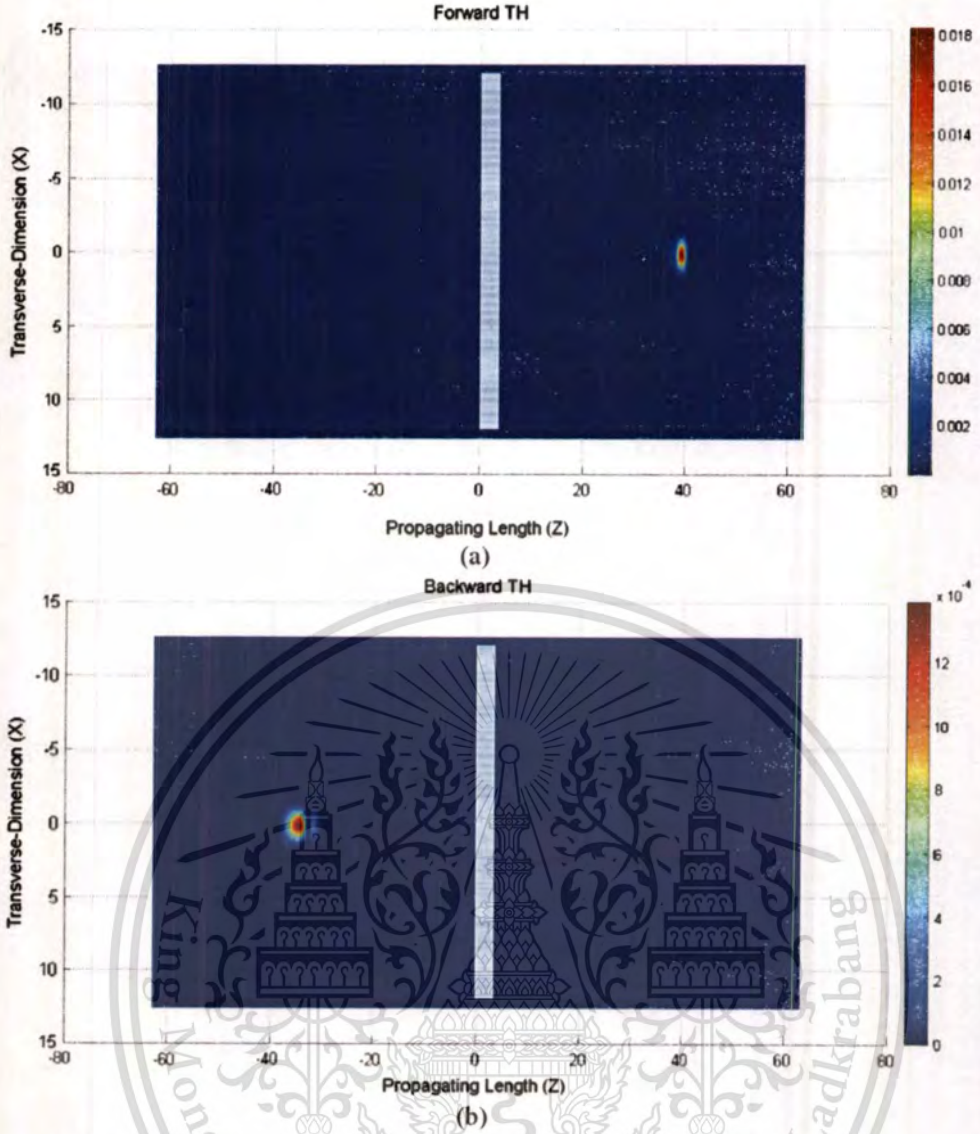

Fig. 5 (a) The spontaneously generated forward and (b) backward TH pulses. The amplitudes have been normalized with nonlinear coefficient and amplitude of initial FF pulse.

transmitted FF and TH pulses in Figs. 4(a) and 5(b) are focused due to the self-focusing effect. But the reflected FF and TH pulses in the backward direction are spread out along propagating direction due to the Fabry–Perot like resonance in the structure as shown in Figs. 4(b) and 5(b), respectively. Note that the set of CMEs containing the zeroth-order and higher-order Fourier components of the nonlinear coefficients is dependent on the amplitude (or intensity) of fundamental pulses. So, when the high intensity fundamental pulse interacts with the nonlinearity of PC structure, then the amplitude of higher-order Fourier components contributes to third-harmonic generation. Consequently, the desired nonlinear effect, i.e., third-harmonic generation, should be strengthened and then the amplitudes of third-harmonic pulse should be further amplified due to these terms. Therefore, the conversion efficiency of this effect has been directly increased following the increased nonlinearity of PC structure.

The wavelength for the FF pulse is tuned to the first lower band-edge transmission maximum in Fig. 1, where the group velocity for this frequency component is slowed to 0.492c. The slow light effect occurred because the dispersion of the effective index of 1D-PC at the band edge is large as described above in Sec. 4.[26] Therefore, the longitudinal walk-off between the FF and TH pulses occurs because of the change in the group velocities near the first and second band edge of photonic band gap, the group velocity of TH pulse is 0.466c, which is close to the FF pulse group

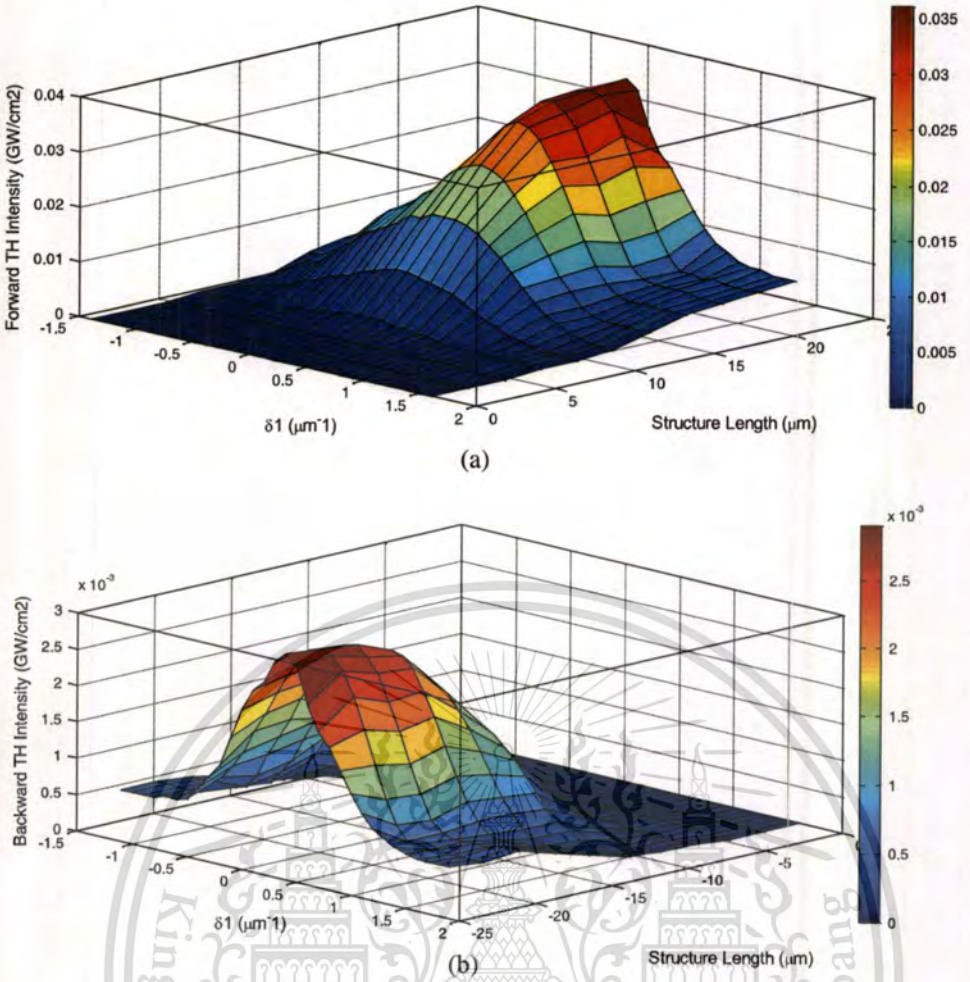

Fig. 6 (a) The forward TH intensities relate to the structure length and the pump detuning parameter. (b) The backward TH intensities relate to the structure length and the pump detuning parameter.

velocity mentioned above. Therefore, the FF pulses will lead the TH pulses as shown in Figs. 4(a), 4(b), 5(a), and 5(b).

The effect of the pump detuning parameter (δ_1) on the output intensity of forward and backward TH pulses is illustrated in Figs. 6(a) and 6(b), respectively. The maximum intensities of both pulses are obtained when optimal detuning parameter of pump FF pulse is 0.0046 to satisfy the band-edge phase-matching for TH generation in the structure. Both output forward and backward TH intensities are decreased by decreasing or increasing of pump detuning parameter from its band-edge transmission maximum by changing wavelength of the pump pulse or the periodic length of structure (Λ), which directly affects the detuning parameter for band-edge phase matching [as Eq. (17)].

In Fig. 7, the total-energy output (both forward and backward components) is plotted as a function of incident pulse width for a 60-period, 22-μm-thick 1D-PC (straight line), and 22-μm bulk medium (dashed line). For clarity, the graph is plotted on a logarithmic scale. The figure shows that the total energy output becomes 1000 times greater for the 1D-PC when compared to a phase-matched bulk medium of the same length[33] when pulse width approaches 800 fs. For very short pulses, the energy conversion grows rapidly and then slowly increases only when the pulse width approaches 800 fs for both cases as shown in Fig. 7. The rapid increase of the TH field intensity as the incident pulse width increases, and its subsequent saturation when frequency bandwidth of the pulse begins to be less than band-edge resonance bandwidth is responsible for this phenomenon. When the pulse frequency bandwidth is less than the transmission

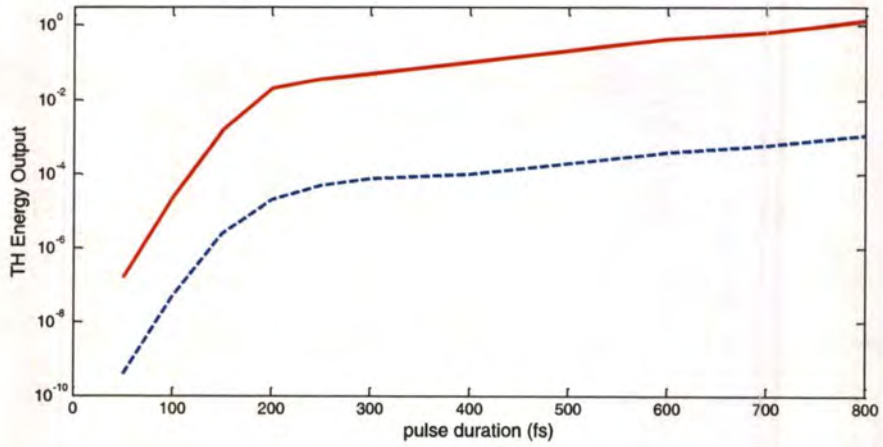

Fig. 7 The comparison between the total TH energy output from the 1D-PC (straight line) and from the phase-matched bulk medium (dashed line), as a function of pulse width. The vertical axis is represented in logarithmic scale. The pulse width is given in units of femtosecond (fs). The output energy from 1D-PC is greater than the output energy from bulk medium about 1000 times when the incident pulse width approaches 800 fs.

resonance bandwidth, the quasi-monochromatic limit is reached. In both regimes, the amplitude of the generated TH pulses is increasing with increasing incident pulse width.

Figure 8 plots the conversion efficiency with respect to the power of pump field FF for a pulse of 800-fs duration. The conversion efficiencies are defined as the ratio between the final forward TH intensity and the total initial pump intensity, and final backward TH intensity and the total initial pump intensity, respectively. Figure 8 shows that for this 1D-PC, the conversion efficiency achieved is 1.8% for forward TH component and to 0.14% for backward TH component when the incident FF pump intensity is 2 GW/cm^2, yielding a TH intensity of approximately 36 and 2.8 MW/cm^3, respectively. This figure also shows that the conversion efficiency becomes about 10 times greater for forward-TH pulse than for backward-TH pulse when input FF intensity approaches 2 GW/cm^2. As we previously mentioned in Sec. 4, the higher conversion efficiencies can be obtained by increasing structure length or number of periods (N), since it increases proportional to N^2 due to the field enhancement inside the structure. Furthermore, according to the set of CMEs containing with the zeroth-order and higher-order Fourier nonlinear components

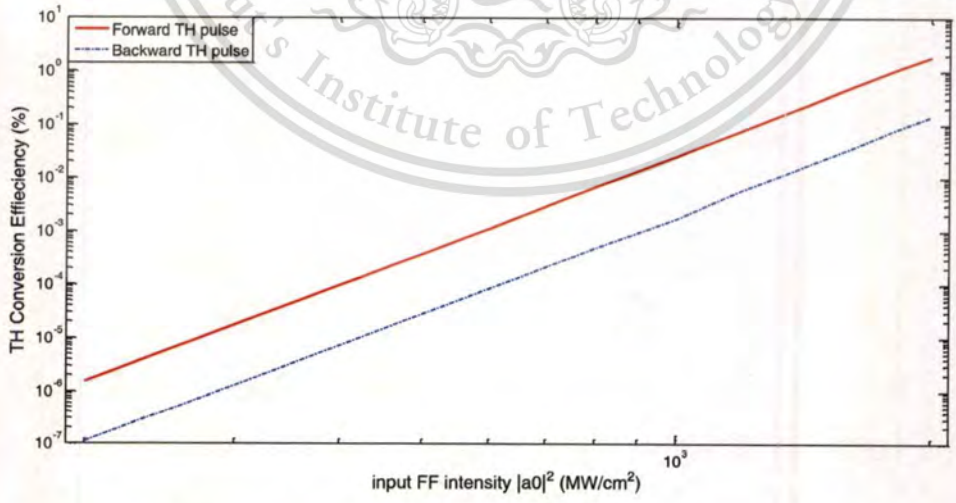

Fig. 8 The TH conversion efficiency respect to the incident FF pump pulse intensity for forward- and backward-propagating TH pulses. Our calculations show that the conversion efficiency is increasing proportional to the amount of pump passes inside the structure. The maxima of conversion efficiency is achieved when the FF pulse intensity reach to 2 GW/cm^2.

which depend on the amplitude (or intensity) of the FF pulse, the action of the high-intensity FF pulse through the nonlinearity of 1D-PC is to further amplify the third-harmonic wave. Consequently, all nonlinear effects, like third-harmonic generation, can be strengthened and the conversion efficiency is directly increased through the additional nonlinear contributions in the 1D-PC.

7 Conclusions

In summary, third-harmonic generation in 1D-PCs, which has $\chi^{(3)}$ response, has been numerically investigated. To model TH generation in the structure, a complete group of CMEs, which correspond to TH generating effect, has been derived by using the MSM. Strong TH enhancement is found for band-edge phase-matching condition. A split-step Fourier-transform has been adopted to solve these four CMEs with appropriate boundary condition. In this study, our 1D-PC has been composed of 120 dielectric layers, which are alternating two types of quarter-wave films. So, the total length of this finite structure is about 22 μm. The transmission spectrum of the TMM designed structure has two photonic band gaps; the second band-gap center wavelength position is shifted to a shorter wavelength from the first band-gap center wavelength by a factor of 3.

In the modeling, the input FF (pump) pulse has a Gaussian shape and it is initially launched toward the left-hand side of 1D-PC with a peak intensity of 2 GW/cm^2. The input FF wavelength is chosen at the lower frequency band-edge of the first band-gap about 1550 nm (to enhance nonlinear effect in the structure). Consequently, the wavelength of TH pulse is about 517 nm. In addition, the spectrum bandwidth of FF pulse should be less than or equal to the spectrum bandwidth of lower band-edge peak (~10 nm) to avoid pulse dispersion in the structure and reflection of the FF pulse energy; this condition will guarantee that efficient TH generation occurs. For our model, the pulse width of the FF pulse, which has the desired spectral bandwidth, is 800 fs.

The simulation results show that the TH pulses in forward and backward direction can be emitted from the structure by gaining energy from input FF field under the nonlinear interaction. The output forward TH longitudinal component is focused since the self-focusing effect occurred in the intensity-dependent index material and the backward TH longitudinal component is spread along propagating direction because of Fabry–Perot like effect in the structure. The transverse components of both directional TH pulses are not changed since the transverse dimension is not sensitive to the periodicity of the structure. Meanwhile, the intensities of forward and backward TH pulses have been directly affected by pump detuning parameter because the band-edge phase matching condition could be achieved by determining the optimal detuning parameter.

From our simulated results, the output TH intensities is decreased by increasing and decreasing of detuning parameter from its optimal value (0.0046). Furthermore, the total-energy output of TH pulses is also depended on the pulse width of FF pulse. The total-energy output is 1000 times greater for the 1D-PC than that of phase-matched bulk medium when pulse width approaches 800-fs. The third-harmonic energy output grows rapidly when FF pulse width is initially small and then approaches 800 fs and then more increases for longer pulse widths. The energy saturates because pulse width corresponds to a spectral width that is smaller than the spectral width of the band-edge transmission peak; in other words, the quasi-monochromatic limit is reached. TH conversion efficiencies are calculated directly and both are increased with input FF intensity. The maximum conversion efficiencies are about 1.8% for forward TH component and 0.14% for backward TH component, which can be achieved when the input intensity is reached to 2 GW/cm^2. Finally, the results suggest that the 1D-PC can be possibly designed to be a highly efficient TH generator with compact size, cheap price, and an uncomplicated fabrication process.

Appendix

The matrix of pulse amplitude, which contains amplitude of each FF and TH pulses in forward- and backward-direction has been shown as

$$U = [a_{f1} \quad a_{b1} \quad a_{f3} \quad a_{b3}]^T. \tag{25}$$

In split-step operator formation, the linear and nonlinear parameters are defined as linear and nonlinear operators. The linear operator is split into two operators such as propagating and coupling operators and their matrix elements have been shown as follows:

$$\hat{D} = \begin{bmatrix} -\frac{\partial}{\partial z} + \frac{i}{F_1}\nabla_\perp^2 + i\delta_1 & 0 & 0 & 0 \\ 0 & \frac{\partial}{\partial z} + \frac{i}{F_1}\nabla_\perp^2 + i\delta_1 & 0 & 0 \\ 0 & 0 & -\frac{\partial}{\partial z} + \frac{i}{F_3}\nabla_\perp^2 + i\delta_3 & 0 \\ 0 & 0 & 0 & \frac{\partial}{\partial z} + \frac{i}{F_3}\nabla_\perp^2 + i\delta_3 \end{bmatrix} \tag{26}$$

$$\hat{K} = \begin{bmatrix} 0 & i\kappa_{+1} & 0 & 0 \\ i\kappa_{-1} & 0 & 0 & 0 \\ 0 & 0 & 0 & i\kappa_{+3} \\ 0 & 0 & i\kappa_{-3} & 0 \end{bmatrix} \tag{27}$$

Finally, the nonlinear operator, which includes diagonal and off-diagonal elements, is written in matrix form as propagating and coupling operators as

$$\hat{N} = \begin{bmatrix} N_{11} & N_{12} & 0 & 0 \\ N_{21} & N_{22} & 0 & 0 \\ 0 & 0 & N_{33} & N_{34} \\ 0 & 0 & N_{43} & N_{44} \end{bmatrix}, \tag{28}$$

where the diagonal matrix elements are

$$N_{11} = iN_0^{(1)}[|a_{f1}|^2 + 2|a_{b1}|^2 + 2|a_{f3}|^2 + 2|a_{b3}|^2] + iN_{-1}^{(1)}\left[a_{f1}a_{b1}^* + \frac{2a_{f1}^*a_{b1}^*a_{f3}}{a_{f1}}\right] + iN_{-2}^{(1)}\left[\frac{a_{b1}^{*2}a_{f3}}{a_{f1}}\right] + iN_3^{(1)}\left[2a_{f3}^*a_{b3} + \frac{a_{f1}^{*2}a_{b3}}{a_{f1}}\right] + iN_{-3}^{(1)}[2a_{f3}a_{b3}^*] \tag{29}$$

$$N_{22} = iN_0^{(1)}[2|a_{f1}|^2 + |a_{b1}|^2 + 2|a_{f3}|^2 + 2|a_{b3}|^2] + iN_1^{(1)}\left[a_{b1}a_{f1}^* + \frac{2a_{f1}^*a_{b1}^*a_{b3}}{a_{b1}}\right] + iN_2^{(1)}\left[\frac{a_{f1}^{*2}a_{b3}}{a_{b1}}\right] + iN_{-3}^{(1)}\left[2a_{f1}a_{b3}^* + \frac{a_{b1}^{*2}a_{f3}}{a_{b1}}\right] + iN_3^{(1)}[2a_{b3}a_{f3}^*] \tag{30}$$

$$N_{33} = iN_0^{(3)}\left[(2|a_{f1}|^2 + 2|a_{b1}|^2 + |a_{f3}|^2 + 2|a_{b3}|^2) + \frac{1}{3}\frac{a_{f1}^3}{a_{f3}}\right] + iN_1^{(3)}\left[\frac{a_{f1}^2a_{b1}}{a_{f3}} + 2a_{b1}a_{f1}^*\right] + iN_{-1}^{(3)}[2a_{f1}a_{b1}^*] + iN_{-3}^{(3)}[a_{f3}a_{b3}^*] \tag{31}$$

$$N_{44} = iN_0^{(3)}\left[(2|a_{f1}|^2 + 2|a_{b1}|^2 + 2|a_{f3}|^2 + |a_{b3}|^2) + \frac{1}{3}\frac{a_{b1}^3}{a_{b3}}\right] + iN_{-1}^{(3)}\left[\frac{a_{b1}^2a_{f1}}{a_{b3}} + 2a_{f1}a_{b1}^*\right] + iN_1^{(3)}[2a_{b1}a_{f1}^*] + iN_3^{(3)}[a_{b3}a_{f3}^*] \tag{32}$$

And off-diagonal matrix elements are

$$N_{12} = iN_1^{(1)}\left[(2|a_{f1}|^2 + |a_{b1}|^2 + 2|a_{f3}|^2 + 2|a_{b3}|^2) + \frac{a_{b1}^{*2}a_{b3}}{a_{b1}}\right] + iN_2^{(1)}\left[a_{b1}a_{f1}^* + \frac{2a_{f1}^*a_{b1}^*a_{b3}}{a_{b1}}\right], \tag{33}$$

$$N_{21} = iN_{-1}^{(1)}\left[(|a_{f1}|^2 + 2|a_{b1}|^2 + 2|a_{f3}|^2 + 2|a_{b3}|^2) + \frac{a_{f1}^{*2}a_{f3}}{a_{f1}}\right] + iN_{-2}^{(1)}\left[a_{f1}a_{b1}^{*} + \frac{2a_{f1}^{*}a_{b1}^{*}a_{f3}}{a_{f1}}\right], \tag{34}$$

$$N_{34} = iN_{2}^{(1)}[2a_{b1}a_{f1}^{*}] + iN_{3}^{(3)}[2|a_{f1}|^2 + 2|a_{b1}|^2 + 2|a_{f3}|^2 + |a_{b3}|^2], \tag{35}$$

$$N_{43} = iN_{-2}^{(1)}[2a_{f1}a_{b1}^{*}] + iN_{-3}^{(2)}[2|a_{f1}|^2 + 2|a_{b1}|^2 + |a_{f3}|^2 + 2|a_{b3}|^2]. \tag{36}$$

Acknowledgments

This research is partially supported by Science Achievement Scholarship of Thailand.

References

1. E. Yablonovitch, "Inhibited spontaneous emission in solid-state physics and electronics," *Phys. Rev. Lett.* **58**(20), 2059–2062 (1987), http://dx.doi.org/10.1103/PhysRevLett.58.2059.
2. S. John, "Strong localization of photons in certain disordered dielectric superlattices," *Phys. Rev. Lett.* **58**(23), 2486–2489 (1987), http://dx.doi.org/10.1103/PhysRevLett.58.2486.
3. M. Scalora et al., "The photonic band edge optical diode," *J. Appl. Phys.* **76**(4), 2023–2026 (1994), http://dx.doi.org/10.1063/1.358512.
4. B. Y. Soon et al., "One-dimensional photonic crystal optical limiter," *Opt. Express* **11**(17), 2007–2018 (2003), http://dx.doi.org/10.1364/OE.11.002007.
5. A. V. Balakin et al., "Enhancement of sum frequency generation near the photonic band gap edge under quasi phase matching conditions," *Phys. Rev. E* **63**(4), 046609 (2001), http://dx.doi.org/10.1103/PhysRevE.63.046609.
6. M. Centini et al., "Efficient nonlinear infrared parametric generation on one-dimensional photonic band gap structures," *Opt. Commun.* **189**(1–3), 135–142 (2001), http://dx.doi.org/10.1016/S0030-4018(01)00994-4.
7. M. Scalora et al., "Ultrashort pulse propagation at the photonic band edge: large tunable group delay with minimal distortion and loss," *Phys. Rev. E* **54**(2), 1078–1081 (1996), http://dx.doi.org/10.1103/PhysRevE.54.R1078.
8. M. Scalora et al., "Choose your color from the photonic band edge: nonlinear frequency conversion," *Opt. Photon. News* **12**, 36–40 (2001), http://dx.doi.org/10.1364/OPN.12.4.000039.
9. M. J. A. de Dood, W. T. M. Irvine, and D. Bouwmeester, "Nonlinear photonic crystals as a source of entangled photons," *Phys. Rev. Lett.* **93**(4), 040504 (2004), http://dx.doi.org/10.1103/PhysRevLett.93.040504.
10. M. Scalora et al., "Pulsed second-harmonic generation in nonlinear, one-dimensional, periodic structures," *Phys. Rev. A* **56**(4), 3166–3174 (1997), http://dx.doi.org/10.1103/PhysRevA.56.3166.
11. J. W. Haus et al., "Enhanced second-harmonic generation in media with a weak periodicity," *Phys. Rev. A* **57**(3), 2120–2128 (1998), http://dx.doi.org/10.1103/PhysRevA.57.2120.
12. A. V. Tarasishin, S. A. Magmitskii, and A. M. Zheltikov, "Matching phase and group velocities in second-harmonic generation in finite one-dimensional photonic band-gap structures," *Laser Phys.* **11**(1), 31–38 (2001).
13. J. P. van der Ziel and M. Ilegems, "Optical second harmonic generation in periodic multilayer GaAs-Al0.3Ga0.7As structures," *Appl. Phys. Lett.* **28**(8), 437–439 (1976), http://dx.doi.org/10.1063/1.88789.
14. J. P. van der Ziel and M. Ilegems, "Second harmonic generation in a thin AlAs-GaAs multilayer structure with wave propagation in the plane of the layers," *Appl. Phys. Lett.* **29**(3), 200–202 (1976), http://dx.doi.org/10.1063/1.88992.

15. J. P. van der Ziel et al., "Phase-matched second harmonic generation in a periodic GaAs waveguide," *Appl. Phys. Lett.* **29**(12), 775–777 (1976), http://dx.doi.org/10.1063/1.88945.
16. M. G. Martemyanov, T. V. Dolgova, and A. A. Fedyanin, "Optical third-harmonic generation in one-dimensional photonic crystals and microcavities," *J. Exp. Theor. Phys.* **98**(3), 463–477 (2004), http://dx.doi.org/10.1134/1.1705697.
17. J. A. Armstrong et al., "Interactions between light waves in a nonlinear dielectric," *Phys. Rev.* **127**(6), 1918 (1962), http://dx.doi.org/10.1103/PhysRev.127.1918.
18. N. Bloembergen and A. J. Sievers, "Nonlinear optical properties of periodic laminar structures," *Appl. Phys. Lett.* **17**(11), 483–485 (1970), http://dx.doi.org/10.1063/1.1653278.
19. K. Tarnowski et al., "Quasi-phase-matched third harmonic generation in optical fibers using refractive-index gratings," *IEEE J. Quant. Electron.* **47**(5), 622–628 (2011), http://dx.doi.org/10.1109/JQE.2011.2107888.
20. M. Centini et al., "Simultaneously phase-matched enhanced second and third harmonic generation," *Phys. Rev. E* **64**(4), 046606 (2001), http://dx.doi.org/10.1103/PhysRevE.64.046606.
21. P. P. Markowicz et al., "Electrically switchable third-harmonic generation in photonic crystals," *J. Appl. Phys.* **97**(8), 083512 (2005), http://dx.doi.org/10.1063/1.1868081.
22. J. W. Haus et al., "Coupled-mode equations for Kerr media with periodically modulated linear and nonlinear coefficients," *J. Opt. Soc. Am. B* **19**(9), 2282–2291 (2002), http://dx.doi.org/10.1364/JOSAB.19.002282.
23. Z. X. Tang et al., "Optical properties of a square-lattice photonic crystal within the partial bandgap," *J. Opt. Soc. A* **24**(2), 379–384 (2007), http://dx.doi.org/10.1364/JOSAA.24.000379.
24. H. M. Lee and J. C. Wu, "Transmittance spectra in one-dimensional superconductor-dielectric photonic crystal," *J. Appl. Phys.* **107**(9), 09E149 (2010), http://dx.doi.org/10.1063/1.3362935.
25. M. Thevenot, A. Reineix, and B. Jecko, "FDTD approach for modelling PBG structures," *J. Opt. A: Pure Appl. Opt.* **1**(4), 495–500 (1999), http://dx.doi.org/10.1088/1464-4258/1/4/314.
26. M. Centini et al., "Dispersive properties of finite, one-dimensional photonic band gap structures: applications to nonlinear quadratic interactions," *Phys. Rev. E* **60**(4), 4891–4898 (1999), http://dx.doi.org/10.1103/PhysRevE.60.4891.
27. J. W. Haus, "Photonic band gap structure," Chapter 3 in *The Handbook of Nanotechnology: Nanometer Structures-Theory, Modeling, and Simulation*, pp. 45–108, A. Lakhtakia, Ed., Prentice-Hall, India (2004).
28. M. Skorobogatiy and J. Yang, *Fundamentals of Photonic Crystal Guiding*, pp. 59–63, Cambridge University Press, New York (2009).
29. M. J. Steel and C. M. de Sterke, "Continuous-wave parametric amplification in Bragg grating," *J. Opt. Soc. Am. B* **12**(12), 2445–2452 (1995), http://dx.doi.org/10.1364/JOSAB.12.002445.
30. M. J. Steel and C. M. de Sterke, "Bragg-assisted parametric amplification of short optical pulses," *Opt. Lett.* **21**(6), 420–422 (1996), http://dx.doi.org/10.1364/OL.21.000420.
31. M. Scalora et al., "Optical limiting and switching of ultrashort pulses in nonlinear photonic band- gap materials," *Phys. Rev. Lett.* **73**(10), 1368–1371 (1994), http://dx.doi.org/10.1103/PhysRevLett.73.1368.
32. Z. Toroker and M. Horowitz, "Optimized split-step method for modeling nonlinear pulse propagation in fiber Bragg gratings," *J. Opt. Soc. B* **25**(3), 448–457 (2008), http://dx.doi.org/10.1364/JOSAB.25.000448.
33. T. Schneider, *Nonlinear Optics in Telecommunications*, Springer-Verlag, Berlin Heidelberg (2004).

Surawut Wicharn received his BS degree with honors and his MS degree in applied physics from King Mongkut's Institute of Technology Ladkrabang, Thailand, in 2007 and 2010, respectively. He is currently working toward the PhD degree in applied physics at the same institute. His research areas have included photonic band-gap structures and modeling their nonlinear optical phenomena by using numerical methods.

Prathan Buranasiri received his BS degree in physics from Ramkhamhaeng University, Thailand. Then, he went to the United States to pursue his graduate degree and received his MSc in physics and PhD in electrical engineering from University of Alabama in Hunstville and University of Dayton, respectively. He is currently an instructor at the Department of Physics of King Mongkut's Institute of Technology Ladkrabang, Bangkok, Thailand. His recent research interests include nanophotonics, photorefractive materials, and fiber optic communication systems.

Author Biography

Name: Surawut Wicharn

Date of Birth: September 13, 1984

Address: 36/1 M.5, Wangluk sub-district, Srisamrong district, Sukhothai 64120

E-mail: kwsurawut@gmail.com

Education:

1988-1996 Srisamrong school, Sukhothai, Thailand

1997-2002 Sawan-anan Wittaya school, Sukhothai, Thailand

2003-2006 King Mongkut's Institute of Technology Ladkrabang, Bangkok, Thailand

B.Sc. Applied Physics, Major Scientific Instrument and Industrial

Thesis: Liquid Level Measurement Device

Advisor: Assoc. Prof. Sarai Lekcha-Um

GPA: 3.49 (2nd Class Honor)

2008-2009 King Mongkut's Institute of Technology Ladkrabang, Bangkok, Thailand

M.Sc. Applied Physics

Thesis: Metallo-Dielectric Photonic Band-Gap Structure Simulation using Transfer-Matrix Method

Advisor: Dr. Prathan Buranasiri

GPA: 3.77